Université de Montréal

Defining the Functions and Mechanisms of mRNA Targeting to the Mitotic Apparatus

par

Dhara Patel

Département de biologie moléculaire

Faculté de médecine

Thèse présentée en vue de l'obtention du grade de Philosophiae Doctor (Ph.D.)

en biologie moléculaire, option médecine cellulaire et moléculaire

Juillet 2022

Université de Montréal

Faculté de Médecine

Cette thèse intitulée

Defining the Functions and Mechanisms of mRNA Targeting to the Mitotic Apparatus

Présentée par

Dhara Patel

A été évaluée par un jury composé des personnes suivantes

Dr. David Hipfner
Président-rapporteur

Dr. Eric Lécuyer
Directeur de recherche

Dr. Maria Vera Ugalde
Membre du jury

Dr. François Dragon
Examinateur Externe

Dr. Gilles Hickson
Représentant du Doyen

RÉSUMÉ (FR)

La localisation des ARNm dans différents compartiments subcellulaires est conservée dans un large éventail d'espèces et de divers types cellulaires. Le trafic est médié par l'interaction entre les protéines de liaison à l'ARN (RBP) et l'ARNm. Les RBP reconnaissent les éléments cis-régulateurs de l'ARNm, également appelés éléments de localisation. Ceux-ci sont définis par leur séquence et/ou leurs caractéristiques structurelles résidant dans la molécule d'ARNm. La localisation des ARNm est essentielle pour la résolution subcellulaire et temporelle. De plus, les ARNm se sont avérés enrichis dans de nombreux compartiments cellulaires, notamment les mitochondries, l'appareil mitotique, et le réticulum endoplasmique. En outre, des études ont démontré que les RBP et les ARNm sont associés aux structures de l'appareil mitotique. Cependant, le rôle que joue la localisation de l'ARNm au cours de la mitose reste largement inexploré. Ma thèse de doctorat vise à comprendre comment le trafic d'ARNm est impliqué lors de la mitose.

La première partie de cette thèse porte sur l'interaction post-transcriptionnelle qui se produit entre les deux ARNm, *cen* et *ik2*. Les gènes qui se chevauchent sont une caractéristique frappante de la plupart des génomes. En fait, il a été constaté que le chevauchement des séquences génomiques module différents aspects de la régulation des gènes tels que l'empreinte génomique, la transcription, l'édition et la traduction de l'ARN. Cependant, la mesure dans laquelle cette organisation influence les événements réglementaires opérant au niveau post-transcriptionnel reste incertaine. En étudiant les gènes cen et ik2 de Drosophila melanogaster, qui sont transcrits de manière convergente avec des régions 3' non traduites qui se chevauchent, nous avons constaté que la liaison physique de ces gènes est un déterminant clé dans la co-localisation de leurs ARNm aux centrosomes cytoplasmiques. Le ciblage du transcrit *ik2* dépend de la présence et de l'association physique avec l'ARNm de *cen*, qui est le principal moteur de la co-localisation centrosomale. En interrogeant les ensembles de données de séquençage de fractionnement, nous constatons que les ARNm codés par des gènes qui se chevauchent en 3' sont plus souvent co-localisés par rapport aux paires de transcrits aléatoires. Ce travail suggère que les interactions post-transcriptionnelles des ARNm avec des

séquences complémentaires peuvent dicter leur destin de localisation dans le cytoplasme.

La deuxième partie de cette thèse consiste à étudier le rôle que jouent les RBP au cours de la mitose. Auparavant, les RBP se sont avérés être associés au fuseau et aux centrosomes. Cependant, leur rôle fonctionnel au niveau de ces structures reste à étudier. Grâce à un criblage par imagerie avec plus de 300 anticorps, nous avons identifié 30 RBP localisés dans les structures mitotiques des cellules HeLa. Ensuite, pour évaluer les rôles fonctionnels de ces RBP, nous avons utilisé l'interférence ARN (ARNi) pour évaluer si la fidélité du cycle cellulaire était compromise dans les cellules HeLa et les embryons de Drosophila melanogaster. Fait intéressant, nous avons identifié plusieurs candidats RBP pour lesquels le knockdown perturbe la mitose et la localisation de l'ARNm dans les cellules HeLa. De plus, la perte des orthologues a entraîné des défauts de développement chez l'embryon de mouche. Grâce à ce travail, nous avons démontré que les RBP sont impliquées pour assurer une mitose sans erreur.

En résumé, les travaux que j'ai menés mettent en lumière l'implication de la régulation post-transcriptionnelle au cours de la mitose. En définissant les fonctions et le mécanisme de localisation des ARNm en mitose, ce travail permettra de définir de nouvelles voies moléculaires impliquées dans la régulation de la mitose. Puisque la division cellulaire non contrôlée peut mener à des maladies tel le cancer, étudier le contrôle du cycle cellulaire sous cet angle « centré sur l'ARN » peut aider à développer de nouvelles approches thérapeutiques pour trouver des solutions aux problèmes de santé.

<u>Les mots-cles</u>

Localisation de l'ARN, Mitose, Protéines de Liaison à l'ARN, Régulation Post-Transcriptionnelle, Transcrit Naturel Antisens en Cis, Drosophile, Développement Embryonnaire

Translated by: Veneta Krasteva

ABSTRACT (EN)

The localization of mRNAs to different subcellular compartments is conserved in a wide range of species and diverse cell types. Trafficking is mediated by the interaction between RNA binding proteins (RBPs) and mRNA. RBPs recognize mRNA *cis regulatory motifs*, otherwise known as localization elements. These are defined by their sequence and/or structural features residing within the mRNA molecule. Localization of mRNAs is essential for subcellular and temporal resolution. Furthermore, mRNAs have been found to be enriched in many cellular compartments including the mitochondria, mitotic apparatus, and endoplasmic reticulum. Moreover, studies have demonstrated that RBPs and mRNAs are associated with mitotic apparatus structures. However, the role that mRNA localization plays during mitosis remains largely unexplored. My PhD thesis aims to understand how the trafficking of mRNAs is implicated during mitosis.

The first part of this thesis encompasses the post-transcriptional interaction that occurs between the two mRNAs, *cen* and *ik2*. Overlapping genes are a striking feature of most genomes. In fact, genomic sequence overlap has been found to modulate different aspects of gene regulation such as genomic imprinting, transcription, RNA editing and translation. However, the extent to which this organization influences regulatory events operating at the post-transcriptional level remains unclear. By studying the *cen* and *ik2* genes of *Drosophila melanogaster*, which are convergently transcribed with overlapping 3'untranslated regions, we found that the physical linkage of these genes is a key determinant in co-localizing their mRNAs to cytoplasmic centrosomes. Targeting of the *ik2* transcript is dependent on the presence and physical association with *cen* mRNA, which serves as the main driver of centrosomal colocalization. By interrogating global fractionation-sequencing datasets, we find that mRNAs encoded by 3'overlapping genes are more often co-localized as compared to random transcript pairs. This work suggests that post-transcriptional interactions of mRNAs with complementary sequences can dictate their localization fate in the cytoplasm.

The second part of this thesis involves investigating the role that RBPs play during mitosis. Previously, RBPs have been found to be associated with the spindle and

centrosomes. However, their functional role at these structures was yet to be investigated. Through an imaging screen with >300 antibodies, we identified 30 RBPs localized to mitotic structures in HeLa cells. Then, to assess the functional roles of these RBPs, we used RNA interference (RNAi) to assess whether cell cycle fidelity was compromised in HeLa cells and *Drosophila melanogaster* embryos. Interestingly, we identified several RBP candidates for which the knockdown disrupted mitosis and mRNA localization in HeLa cells. Furthermore, loss of the orthologs led to developmental defects in the fly embryo. Through this work, we demonstrated that RBPs are involved in ensuring an error-free mitosis.

In summary, the work that I have conducted sheds light on the involvement of post-transcriptional regulation during mitosis. By defining the functions and mechanism of mRNA localization in mitosis, this work will help define new molecular pathways involved in mitosis regulation. As uncontrolled cell division can lead to diseases such as cancer, studying cell cycle control from this 'RNA-centric' angle may help to develop new therapeutic approaches to find solutions to health problems.

Keywords

mRNA localization, Mitosis, RNA binding proteins, Post-transcriptional Regulation,Cis-Natural Antisense Transcripts, Drosophila, Embryonic development

List of Figures

Chapter 1

Chapter 2

Chapter 3

Chapter 4

List of Tables

Chapter 2

Chapter 3

List of Acronyms and Abbreviations

Abbreviation	Expanded Term
3'UTR	3 prime untranslated region
5'UTR	5 prime untranslated region
a tubulin	Alpha tubulin
Ago-2	Argonaute-2
AKAP1	A-kinase anchoring protein 1
AKAP450	A-kinase anchoring protein 450
ALS	Amyotrophic lateral sclerosis
APC/C	Anaphase-promoting complex
ARP2/3	Actin related protein 2/3
Ash1	DNA-binding transcription repressor ASH1
ASPM	Assembly factor for spindle microtubules
ATP	Adenosine 5'-triphosphate
AURKB	Aurora kinase B
β actin	Beta actin
β tubulin	Beta tubulin
Bcd	Bicoid
Bdnf	Brain derived neurotrophic factor
BicD	Bicaudal D
BLE	Bicoid localization element
C-NAP1	Centrosomal Nek2-associated protein 1
C9ORF72	C9orf72-SMCR8 complex subunit
CAK	CDK activating kinase
CamKII	Ca(2+)/Calmodulin-dependent protein kinase II
Cat2	Cationic amino acid transporter 2
CBs	Cajal bodies
CCDC86	Coiled-coil domain-containing protein 86
CCR4-NOT	Carbon catabolite 4-negative on TATA-less
CDC40	Cell division cycle 40
CDK	Cyclin dependent kinase
CDNA	Complementary DNA
CeFrac-Seq	Cell fractionation combined with RNA sequencing
Cen	Centrocortin
CEP152	Centrosomal protein 152
CEP192	Centrosomal protein 192
CEP250	Centrosomal protein 250
CIN	Chromosomal instability
Cis-NATs	Cis-natural antisense transcripts
Cp110	Centriolar coiled coil domain protein 110kDa

CPAP	Centromere protein J
CPC	Chromosomal passenger complex
CPEB1	Cytoplasmic polyadenylation element binding protein 1
CR	Coding region
CRM	Cis regualatory motif
D. melanogaster	Drosophila melanogaster
D. mojavensis	Drosophila mojavensis
D. simulans	Drosophila simulans
D. virilis	Drosophila virilis
Dazl	Deleted in azoospermia-like
DC	Dyskeratosis congenita
Dhc	Dynein heavy chain
DM1	Myotonic dystrophy type 1
DM2	Myotonic dystrophy type 2
dsRBD	double stranded RBD
dT	deoxythymine
E.coli	Escherichia coli
Eg5	Kinesin family member 11 L homeolog
Endoplasmic Reticulum	ER
FISH	Fluorescence in situ hybridization
FMR1	Fragile X mesenger ribonucleoprotein 1
Ftz	Fushi tarazu
FXR1	FMR1 autosomal homolog 1
FXR2	FMR1 autosomal homolog 2
γ tubulin	Gamma tubulin
γ-TuRCs	g Tubulin ring complex
GFP	Green fluorescent protein
Grk	Gurken
HNRNPUL1	Heterogeneous nuclear ribonucleoprotein U like 1
hpRNA	Hairpin RNA
Hsp83	Heat shock protein 83
IF	Immunofluorescence
Ik2	I-kappaB kinase e
INCENP	Inner centromere protein
KH	K-homology
LARP1	LA Ribonucleoprotein 1
LARP6	LA Ribonucleoprotein 6
LE	Localization element
LIGR-seq	LIGation of interacting RNA followed by high throughput Sequencing

MCAK	Kinesin family member 2C
mRNA	messenger RNA
MZT	Maternal-to-zygotic
NET1	Neuroepithelial cell transforming 1
NGV	Nanos-Gal4-VP16
OFD1	OFD1 centriole and centriolar satellite protein
OreR	*Oregon R*
Osk	Oskar
PARIS	Psoralen Analysis of RNA Interactions and Structures
PAZ	Piwi/Argonaute/Zwille
PCM	Pericentriolar matrix
PCNT	Pericentrin
PLK1	Polo-like kinase 1
PLK4	Polo-like kinase 4
POC5	POC5 centriolar protein
PPIL4	Peptidylprolyl isomerase like 4
PUF60	Poly(U) binding splicing factor 60
Puro-PLA	Puromycin-labelling with proximity ligation assay
qRT-PCR	Quantitiatve real-time polymerase chain reaction
RAB13	Rab13, member ras oncogene family
RAD21	RAD21 cohesin complex component
RBD	RNA binding domain
RBMX2	RNA binding motif protein X-linked 2
RBP	RNA binding protein
RIP	RNA immunoprecipitation
RISC	RNA-induced silencing complex
RNAi	RNA interference
RNP	Ribonucleoprotein
RPS3	Ribosomal protein S3
RRM	RNA recognition motif
Run	Runt
SAC	Spindle assembly checkpoint
Sak	Sak kinase
Sas-4	Spindle assembly abnormal 4
SAS-6	Spindle assembly abnormal 6
SD	Standard deviation
SEM	Standard error of the mean
SF1	Splicing factor 1
SF3A3	Splicing factor 3a subunit 3
SMA	Spinal muscular atrophy

smFISH	single molecule FISH
smiFISH-IF	single molecule inexpensive FISH combined with immunfluorescence
SPLASH	Sequencing of Psoralen crosslinked, Ligated, and Selected Hybrids
SSB	Small RNA binding exonuclease protection factor Ia
STIL	STIL centriolar assembly protein
Stress Granule	SG
TARP	Talipes equinovarus syndrome
TDP-43	Tar DNA-Binding Protein 43
UAS	Upstream activating sequence
Ube3a	Ubiquitin protein ligase E3A
UTR	Untranslated region
UV	Ultraviolet
Vg1	growth differentiation factor 1 S homeolog
WDR43	WD repeat domain 43
Wg	Wingless
Xpat	Xenopus primordial germ cell associated transcript
XPO1	Exportin 1
Xrhamm	receptor for hyaluronic-acid-mediated motility
ZNF622	Zinc finger protein 622

For my mom, dad, and sister.

Acknowledgments

First and foremost, I would like to thank my lab supervisor **Dr. Eric Lecuyer**. Thank you for making me part of the team and all your support throughout these years. I was able to grow as a scientist and learned to think critically and work independently. I appreciate all your positivity, even when things were not going as planned. It allowed me to redirect and stay motivated. Also, thank you for making the lab a fun place to work and planning so many activities! My deepest thanks and gratitude for your mentorship and patience.

This thesis was truly a group effort. I would like to acknowledge the wonderful people who constantly supported me and gave me their feedback: **EJ**, **Veneta**, **Farah**, **Sahar**, **Ashley**, and **Judy**. Thank you! This would not have been possible without you!

I would like to thank all the members of the Lecuyer Laboratory, former and present. I have been lucky to have been working with a supportive and wonderful group of people. **Andy**, thank you for your guidance. You gave me all the tools I needed to succeed when I first joined the lab. I am very grateful for everything you have taught me. **Veneta**, thank you for all your positivity, even when I felt demotivated! Your constant smiles and encouragement really helped push me to where I am today. **EJ**, thank you for your guidance and constructive feedback. Your passion and positive mindset are the qualities that I will always look up to and be inspired by. I am immensely grateful to have worked alongside with you. **Juan Carlos**, **Easin**, and **Judy**, my lunch buddies for life. **Juan Carlos**, we have been part of each other's journey since the beginning. Thank you for always being there to talk and for the constant support. I really appreciated it. **Judy**, thank you for your kindness and always being there for me. I am always rooting for you! **Sahar**, thank you for always supporting me through ups and downs as well as rooting for me since day one. **Ashley**, thank you for creating so many fun memories in the lab! From running to our fun lunches and trips to Second Cup! You will always be my matcha buddy. **Lynda**, thank you for always cheering me up and being a wonderful friend. **Sam**, thank you for your encouragement! Additionally, I would like to thank my fantastic co-authors: **Julie**, **Felix**, **Catherine**, **Philip**, **EJ**, **Ashley**, **Dr. Mathieu Blanchette**, **Sulin**, **Andy**, **Sam**, **Juan Carlos**, and **Philippe**.

I would also like to thank the dedicated individuals responsible for the core facilities at the IRCM, particularly **Dominic Filion** (microscopy) and **Eric Massicotte**, and **Julie Lord** (flow cytometry). A special thanks goes out to **Dominic** for all his patience and help throughout these years.

Additionally, I would like to thank my committee members: **Dr. David Hipfner**, **Dr. William Tsang**, and **Dr. Sebastien Carreno**. Thank you for all your helpful advice and feedback throughout these years. I would like to express my gratitude for **Dr. David Hipfner**. You have been following my scientific journey since I was a master's student. Thank you for all your support throughout these years. I am extremely grateful.

I would also like to take the opportunity to thank the Academic Affairs Department at the IRCM: **Sebastien Sabbagh**, **Myrna Khuon**, and **Virginie Leduc**. A special appreciation goes to **Sebastien Sabbagh** for all his encouragement. Additionally, I would like to thank **Lucie Yan Lu** at the Molecular Biology Department at UdeM.

I would like to thank my family: my **mom**, **sister**, and **dad**.
Mom, thank you for everything. You will always be the strongest person I know. Thank you for all your sacrifices and constant encouragement. I would not be where I am without you.
Gangi, thank you for all your support and always listening to me.

Farah, thank you for always supporting me and always seeing the positive in every situation. You have been a constant throughout this journey, and I am forever grateful for all the memories that we have made. We experienced so much together- the good and the bad. Thank you for always pushing me even when I thought I reached the bottom. Thank you for everything from the bottom of my heart. My PhD experience would not have been the same without you.

Ibani, you have been an amazing friend and been there for me through ups and downs. Thanks for all the positivity, laughter, and constant support! It means the world!

Tom, I am immensely grateful for having you in my life. Your friendship, words of encouragement, and positive mindset are deeply appreciated.

Sweetie, thank you for supporting me throughout this journey! You have been so amazing, and I don't know how I would have done it without you. Even though we were always 400 miles away, I never felt the distance.

Krupa and **Monika**, thank you for all your support throughout these years!

Aurelie, thank you for your constant support and listening to me (even though it can be for several hours). I am extremely grateful to have you in my life.

Mathieu, thank you for always brightening up my days and being there to talk to. I am extremely grateful to have you in my life.

Simsim, thank you for everything and being such a wonderful friend. I don't know what I would have done without you. From having scientific discussions to talking about very random stuff, I am so glad to have you in my life!

I would also like to thank my undergraduate supervisor, **Dr. Karen Schindler** for sparking my interest in conducting research.

Brent, our paths kept on crossing throughout these years. Thank you for everything.

I would also like to thank all the wonderful friends and family who have constantly supported me: **Xavier**, **Shirley**, **Susan**, **Evangeline**, **Alan**, **Fay**, **Evelyn**, **Carolina**, **Rachna**, **Michael**, **Mehrnoush, Lena, Lalu**, **Janvi**, **Girishkaka**, and **Anakaki**. Thank you all for being part of my journey!

I would like to thank my dog, **Kiki**. You will always be the sweetest yet sassiest chihuahua on the planet.

Lastly, I would like to thank the **Universe** for making the stars align and providing me with the opportunity to write a chapter of my life in Montreal. I was provided with the right challenges that helped me grow as a person and learn more about myself. I was able to meet the most amazing people and formed deep connections that transcended anything I've ever felt before. The experiences that I have accumulated throughout this journey shapes the person that I am today. Thank you. **YOU did it!**

"The Universe knows the perfect timing for all those things you want and will find, through the crack of least resistance, the best way to deliver it to you."
-Esther Hicks

\

Table of Contents

Chapter 1 Introduction

1.1 Mitosis

Mitosis is a highly coordinated and essential life process that is required for the accurate segregation of the cell's DNA. It is the driving force in the growth and development of an organism, cell renewal, and asexual reproduction. The end result is two identical daughter cells. Execution of the events that occur during mitosis must be conducted properly in order to avoid detrimental consequences for the cell. In fact, dysregulation of mitosis can lead to diseases such as cancer. Therefore, having a thorough understanding of this process is quite important to find potential therapeutics in the future. There has been extensive research conducted on understanding the underlying mechanisms involved in mitosis regulation. The precision of this process is carried out by many key players and their disruption can lead to cell catastrophe. Although many aspects in deciphering mitosis have been unraveled, some are yet to be investigated. Understanding how mRNA localization influences fidelity during mitosis is an aspect that is yet to be further explored. Over the years, remarkable work has been conducted on understanding how mRNA is involved in regulating mitosis. This portion of the thesis chapter will be focused on the cell cycle, mitosis, and its regulation.

1.1.1 The Cell Cycle

Mitosis is a small part of the cell cycle. The cell cycle is made up of four distinct stages: G1 phase, S phase, G2 phase, and M phase (**Figure 1.1**). Tight control and coordination of events during the cell cycle is required to produce two identical daughter cells. The G1, S, and G2 phases are all part of interphase, while mitosis and cytokinesis make up the M phase [1]. Cells that enter G0 phase are quiescent and non-proliferating, and this cellular commitment is determined during G1 phase [2, 3]. During the G1 and G2 phase, the gap phases, the cell prepares for DNA replication and mitosis [4]. During interphase, an appropriate amount of cellular constituents and DNA is made for the newly synthesized daughter cells [5]. Whereas in M phase, the cell undergoes nuclear and cellular division during mitosis and cytokinesis respectively. In addition, the M phase is considered to be the shortest phase of the cell cycle. Transitioning from one phase to the next is highly regulated by oscillation activities from the cyclin dependent kinases (CDKs) [2].

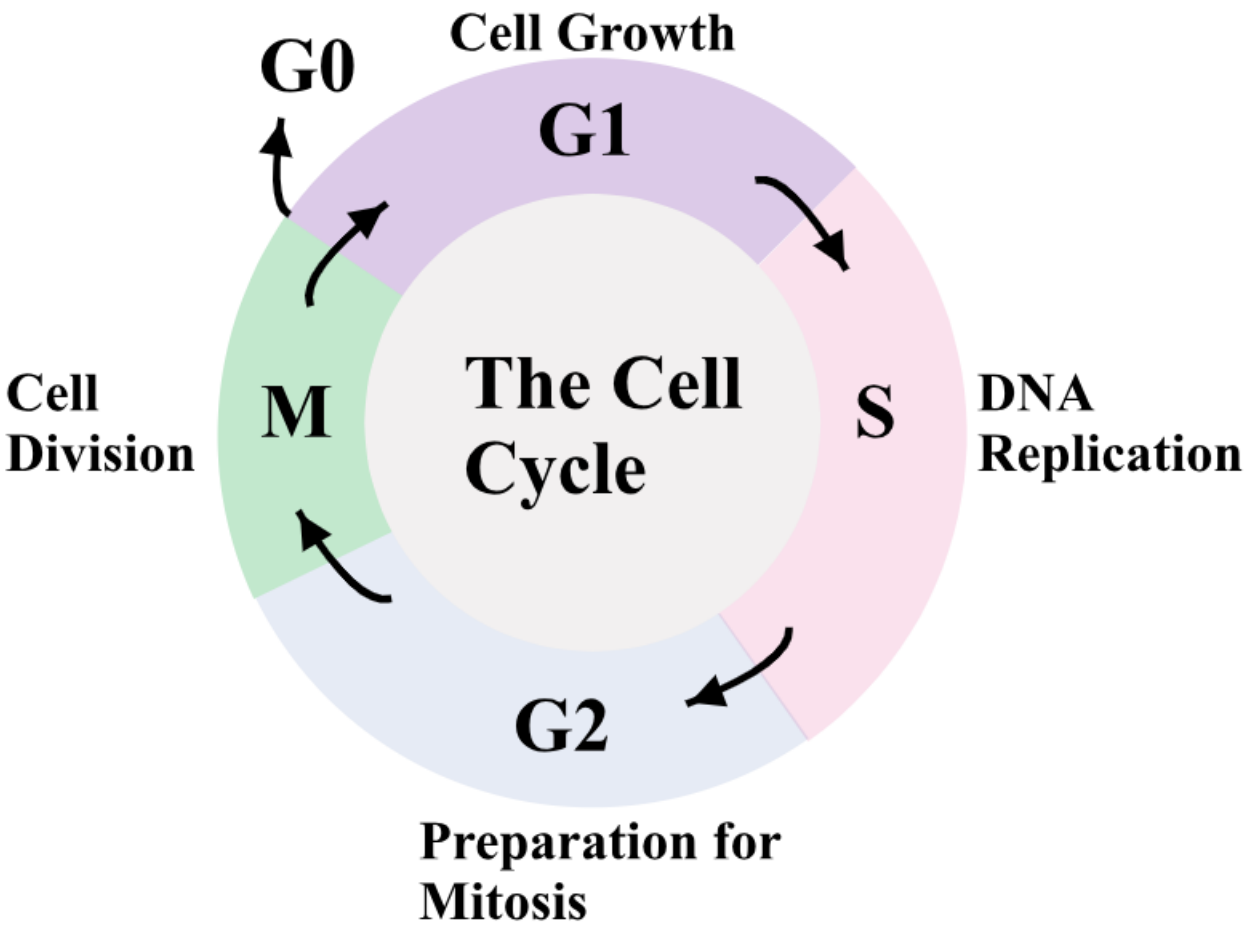

Figure 1.1 The cell cycle. The cell cycle is divided into four stages: G1, S, G2, and M phases. Interphase consists of G1, S, and G2 phases, while M the phase comprises of mitosis and cytokinesis. During interphase, the cell grows, replicates its DNA, and prepares for mitosis. The cell can also enter G0 where it is in a non-dividing, quiescent state. Nuclear division followed by cell division occurs in mitosis and cytokinesis respectively.

1.1.2 Cell Cycle Control

The key regulatory proteins responsible for the precise and orderly transitions that occur during the cell cycle are CDKs [2]. CDKs are a group of serine/threonine kinases that are activated at particular points of the cell cycle, by their regulatory subunits called cyclins [1, 2]. The activation of CDKs' catalytic subunit leads to the phosphorylation of selected proteins [2]. To date, there have been 20 identified CDKs and 29 cyclins in humans, many of which play an active role in cell cycle regulation [6]. Additionally, other CDKs and cyclins are involved in regulating transcription and splicing [6] There are 4 CDKs (CDK1, CDK2, CDK4, and CDK6) as well as 10 cyclins (Class A-, B-, D-, and E-) that are involved in the progression of the cell cycle [7]. Interestingly, many of the CDKs are dispensable as shown by knockout studies in mice [8-10]. However, CDK1, which serves as the key regulator, is required for the cell cycle [11].

Cyclins work in coordination with CDKs, by forming a dimer complex through interaction with the PSTAIRE motif present in CDKs [12]. Binding of the cyclins with CDKs results in conformational changes that lead to the activation of different CDKs, an interaction required for enzymatic activity [2, 12]. While the protein levels of the CDKs are stable throughout the cell cycle, the cyclin levels rise and fall [2]. Moreover, cyclins regulate the activity of CDKs through their synthesis and destruction at specific points of the cell cycle [7]. For example, during the entry to G1 phase, cyclins D1, D2, and D3 bind to CDK4 and CDK6 [2]. Whereas, transitioning from G1 phase to S phase requires the interaction between cyclin E and CDK2 and Cyclin A binds to CDK2 during S phase [2, 8]. Entry into mitosis requires cyclin A binding to CDK1 and its completion is driven by the interaction of Cyclin B with CDK1 [2, 8]. While cyclins are crucial for the activation of CDKs, phosphorylation of CDK1 by CDK activating kinase (CAK), composed of CDK7-Cyclin H, leads to its full activation [2, 12]. Lastly, inactivation of CDKs occurs through the proteolytic destruction of cyclins by the anaphase-promoting complex (APC/C) at the end of mitosis [13-15]. Cyclin degradation is required for mitotic exit as its prevention results in mitotic arrest and elongated spindles [16].

1.1.3 Cell Cycle Checkpoints

Checkpoints exist to prevent the progression of unhealthy cells within the cell cycle. In cases where there are errors, the cell undergoes an arrest to allow for repair [17]. The G1/S checkpoint, also known as the restriction point, inhibits cells exhibiting DNA damage from entering S phase [18]. Notably, advancement through this checkpoint marks the irreversible commitment to the cell cycle [19]. Additionally, an intra-S phase checkpoint exists to stall DNA replication in the presence of errors and prevent further initiation of replication origin firing [20]. Before entry into mitosis, the G2/M checkpoint ensures that cells with accumulated damage do not progress [20]. Lastly, the mitotic checkpoint, also known as the spindle assembly checkpoint (SAC) prevents premature chromosome segregation [17]. The SAC will be explained in further detail in **Section 1.1.5**. In conclusion, these checkpoints are essential to halt the passing down of errors to daughter cells. These errors can contribute to genomic instability, which can consequently lead to cancer [20].

1.1.4 Key Steps During Mitosis in Eukaryotes

Mitosis can be divided into the following stages: prophase, prometaphase, metaphase, anaphase, telophase, and cytokinesis (**Figure 1.2)**. The correct events must take place in a timely and coordinated manner to ensure an error-free mitosis. In this section, I will go over the key events that take place during these phases.

Before the onset of mitosis, the duplicated chromosomes remain in close association with each other to form sister chromatids during DNA replication[21]. Following DNA replication, the establishment of sister chromatid cohesion occurs, which is essentially the physical interaction between the two chromatids that lasts until anaphase [21]. During prophase, the nuclear chromatin starts to become compact and individualizes to form chromosomes [5]. Condensin, a large pentameric complex, governs mitotic chromosome condensation [22, 23]. Upon compaction, transcriptional activity becomes inhibited and the displacement of transcription factors from the mitotic chromatin occurs [24]. Furthermore, disassembly of the nuclear envelope ensues [5]. The

centrosomes begin to move to opposite poles, while nucleating microtubules extending radially resulting in the onset of spindle formation [25].

Prometaphase is the longest stage of mitosis [26] The presence of a disassembled nuclear envelope marks the beginning of prometaphase and the presence of aligned chromosomes at the spindle equators marks the end [26]. Early on, the microtubule network restructures to form the mitotic spindle [26]. To maintain fidelity during cell division, the equal separation of sister chromatids must occur. This is dependent on the interactions that occur between the chromosomes and microtubules, influencing the ability to form a bipolar spindle [27]. The spindle microtubules and chromosomes begin to form attachments mediated by the kinetochores [26, 28]. Kinetochores consist of a large multiprotein structure that are assembled on the centromere [29]. Upon nuclear envelope break down, single microtubules capture the kinetochores through a search and capture mechanism [26]. This is done by the fluctuating growth and retraction of microtubules when searching for the kinetochore in the nuclear space [26]. If there are improper microtubule-kinetochore attachments, the SAC becomes activated, and the cell stalls until the errors are corrected [5]. Following the attachment of the mitotic spindle to the chromosomes, the chromosomes start to move towards the equatorial plane also known as the metaphase plate [5]. Eventually, all of the chromosomes are congressed and are correctly lined up at the spindle equator [5]. The correct positioning of the chromosomes is essential to allow for proper chromosome segregation during anaphase.

In anaphase, the sister chromatids physically separate from one another [5]. The chromosomes move towards opposite poles with action from the microtubules [5]. With the segregation of the sister chromatids into two individualized nuclei, telophase and cytokinesis follow towards the end of mitosis. During telophase, the nuclear envelope begins to reassemble simultaneously with chromosome segregation [5]. Lastly in cytokinesis, the chromosomes are partitioned into two separate cells [30]. This process heavily relies on the microtubules and actin, which are core components of the cytoskeleton [30].

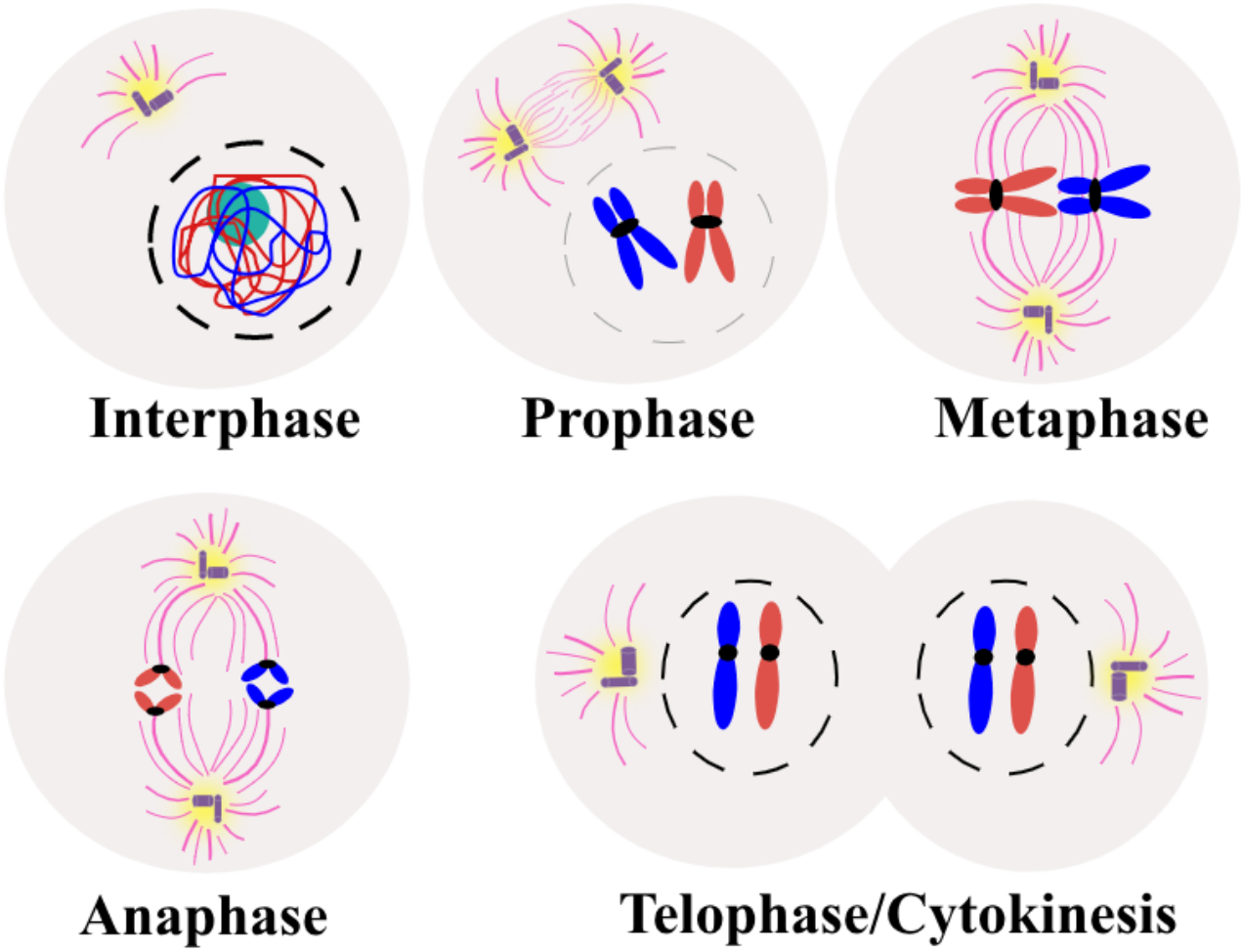

Figure 1.2 A schematic depicting the different stages of mitosis. Before the onset of mitosis, the cell grows and the DNA replicates in interphase. Mitosis consists of the following phases: prophase, metaphase, anaphase, and telophase. In prophase, the chromosomes begin to condense, and the centrosomes start moving towards opposite poles while emanating microtubules. During metaphase, the chromosomes migrate towards the center. Throughout anaphase, the chromosomes segregate. Finally, partitioning of the chromosomes into separate cells occurs during telophase and cytokinesis.

1.1.5 Spindle Assembly Checkpoint and the Chromosomal Passenger Complex

To ensure faithful segregation during mitosis, cells utilize the chromosomal passenger complex and the spindle assembly checkpoint (SAC), which is also known as the mitotic checkpoint) [31-34]. These two mechanisms work in coordination with each other. The SAC is responsible for regulating the transition from metaphase to anaphase by delaying the separation of the sister chromatids in the presence of erroneous kinetochore-microtubule attachments [34]. Proper functioning of the SAC is vital to prevent precocious chromosome segregation [33]. Hence, the anaphase promoting complex/cyclosome (APC/C) is inhibited when components of the SAC localize to the unattached kinetochores [35]. Furthermore, the CPC serves as a surveillance mechanism to ensure an orderly mitotic exit and transition into interphase [32]. It exhibits dynamic localization throughout mitosis to the inner centromeres upon mitotic entry and then translocates to the equatorial plane during the metaphase to anaphase transition [32]. During early mitosis, its localization to the centromeres is required for removal of erroneous microtubule-kinetochore attachments through its activation of the SAC [31, 32]. Towards the end of mitosis, the CPC prevents cytokinesis completion with the presence of lagging chromosomes [36]. These safeguard mechanisms are essential in preventing mitotic errors that can lead to dire consequences for the cell.

1.1.6 Mitotic Errors and Cancer

Cancer cells surpass the regulatory checkpoints that prevent a cell with mitotic defects to continue progressing throughout mitosis [17]. Consequently, this results in daughter cells comprising of an abnormal number of chromosomes, leading to aneuploidy [17]. Exhibiting aneuploidy during meiosis and development can serve to be lethal, while the presence of abnormal number of chromosomes in somatic cells has been linked to aging and cancer [35]. In fact, approximately 70% of human tumors exhibit aneuploidy [37]. Aneuploidy is often a result of chromosomal instability, an occurrence where the chromosomes mis-segregate at increased rates, consequently leading to an abnormal number of chromosomes [38]. The sources of these errors can be due to an impaired spindle assembly checkpoint (SAC), cohesion defects, merotelic attachments, and tetraploidy, often leading to detrimental consequences [35]. Impaired spindle assembly

checkpoint and cohesion defects make up just a small number of cases in chromosomal instability, while merotelic attachments, centrosome amplification, and tetraploidy make up a higher proportion [35]. Further details will be provided on centrosome amplification and cancer in **Section 1.2.2**.

As abnormalities during mitosis are a hallmark of cancer, directing therapeutics towards anti-mitotic agents serves as an approach to treating cancer [17]. Treatments involving agents targeting microtubules, CDKs, PLK1, and the Aurora kinases have been tested in the clinical setting [17]. However, not all therapeutic agents showed promising clinical results [17]. For instance, agents that target PLK1 and the Aurora kinases show a poor success rate due to their activity primarily during mitosis [17]. Cancer cells actively divide less frequently, once every few months to a year [17]. Therefore, damage to the cell will not occur in the absence of mitosis with mitosis-specific agents [39]. Currently, agents targeting the microtubule still serve to be the most common, as they work by promoting apoptosis in cancer cells during interphase and mitosis [17, 39, 40]. Albeit successful, their inability to discriminate between a normal cell and a cancerous cell still serves to be problematic [17]. Emerging therapeutic strategies in the future will involve using agents against proteins involved in the regulation of centrosomes, thereby targeting the genomic instability that is particular to cancer cells [17].

1.2 The Centrosome

The centrosome is an organelle that was discovered over 100 years. In 1876, Edouard van Beneden discovered the centrosome and Theodor Boveri gave it the name “centrosome” [41]. Boveri and van Beneden independently noticed that the centrosome appeared to be the main organizer of the cell during division [42]. Boveri conducted an experiment that involved using double fertilization to result in dispermic sea urchin eggs, which subsequently led to a multipolar mitosis and multiple centrosomes [43]. These observations led him to believe that tumors may be a result of these increased number of centrosomes [43]. Around the same time, Gino Galeotti and David von Hansemann saw that abnormal mitoses were prevalent in cancer cells [44]. These early observations have set the stage for the current research that exists today on centrosomes.

The centrosome is the main microtubule organizing center in animal cells during mitosis and it is responsible for microtubule nucleation and organization. It is involved in the regulation of cell motility, polarity, and migration during interphase [45]. The centrosome can play different roles in the cell that extends beyond their microtubule organizing capabilities such as being involved in signaling, stress response, and the transitioning of the cell cycle [46]. Understanding the centrosome is important because defects in this structure have been implicated in multiple cancers and diseases [47].

The centrosome consists of two centrioles, a mother and daughter centriole, that are positioned orthogonally and surrounded by an electron dense pericentriolar matrix (PCM) [45]. Centrioles are made up of nine triplets of microtubules assembled into a cylindrical barrel structure [45, 48]. The mother centriole has distal and subdistal appendages that are involved in the anchoring of the microtubules [45]. During the onset of mitosis, the inner layer of the PCM increases in size [47, 49]. Comprising of hundreds of proteins, the PCM primarily serves a role in microtubule nucleation [50, 51]. An important complex of proteins involved in nucleation is the γ tubulin ring complex (γ-TuRC) that serve as a template for the microtubules to emanate from [52]. The γ-TuRCs are composed of approximately 10-14 γ-tubulin as well as other proteins [52]. In addition to the γ-TuRCs, pericentrin (PCNT), and AKAP450 are coiled-coil proteins that are involved in the docking of key proteins involved in microtubule nucleation [53].

Although centrosomes are the cell's main microtubule organizing center, there have been several examples that have shown that they can be dispensable and the ability to form a bipolar spindle was still feasible. These examples have been shown in fly cells as well as cultured mammalian cells [54-56]. For instance, a mutation in Sas-4, a protein necessary for centriole replication, resulted in a lack of detectable centrioles in flies [54]. Closer examination of mitosis occurring in larval brains revealed that although mitosis was slowed down, bipolar spindles were able to be formed [54]. Additionally, the mutants underwent the normal development stages all the way up to the adult stage [54]. However, the flies died soon after they hatched because they were uncoordinated due to the lack of cilia [54]. Additionally, in BSC-1 cells, centrosomes were microsurgically removed

before S phase was completed, and bipolar spindles were formed [55]. However, the cells would arrest at G1 phase, revealing that the centrosome is required to transition from G1 phase to S phase [55]. Moreover, in the oocytes from many species including *Drosophila*, mice, and *Xenopus*, meiotic spindle is formed without the presence of centrosomes [57-59]. For instance, in mammalian oocytes a functional spindle is formed through mechanisms involving chromatin [60]. The organization of the microtubules is mediated by the chromatin and molecular motor proteins [56, 60]. Additionally, using laser irradiation to destroy centrosomes in CVG-2 cells still allows for a bipolar spindle to form, suggesting the utilization of a centrosome-independent pathway [56]. Although cell can form bipolar spindles in the absence of centrosomes, they are key players in the organization of microtubules. The centrosome is an organelle that has been implicated in many diseases, and further investigation of the role that it plays in diseases can bring a therapeutic perspective in treatments.

1.2.1 The Centrosome Cycle

The duplication of centrosomes occurs once per cycle in dividing cells in cooperation with the cell cycle. In quiescent cells, the centrioles can lead to the formation of cilia or flagella [61]. The key events that occur during the centrosome duplication process are: a) centriole disengagement b) procentriole nucleation c) assembly of centriole microtubules d) centriole elongation e) centrosome maturation f) centrosome separation [62]. During centriole disengagement, the mother and daughter centriole separate at the end of mitosis [62]. This is carried out by the serine/threonine protein kinase, PLK1 and SEPARASE [62, 63].

To ensure that centrosomes duplicate only once per cycle, the centrioles undergo centriole disengagement, a process that separates the mother and daughter centrioles at the end of mitosis [62]. After the centrioles are disengaged, a proteinaceous liner, also known as “centrosome cohesion”, physically links the two centrioles from interphase to early mitosis [62, 64, 65]. The centrosome cohesion is mediated by C-NAP/CEP250 [65]. During the G1/S transition, a procentriole is formed adjacent to the pre-existing centrioles [62]. The PLK4 protein kinase is known to be a key player involved in centriole duplication

[62, 66-68]. Then, CEP192 is involved in the recruitment of CEP152 and PLK4 to the centrioles [69, 70]. Then, CEP192 interacts with the cryptic polo box of PLK4, leading to the localization switch of PLK4 from enrichment at the centriole to the location of where the procentriole will form [69]. PLK4 recruits SAS-6 and STIL, proteins necessary for centriole assembly, to the mother centrioles [71-73]. SAS-6 is restricted only to the nascent procentrioles and is thought to form a complex with STIL [68, 74]. STIL has a direct interaction with CPAP [74]. This cascade of events occurring among the proteins is necessary to ensure proper procentriole formation.

The formation of the procentriole is marked by a 9-fold symmetrical cartwheel-like structure [75, 76]. Within the cartwheel, a central hub exists as well radial spokes that are rotated by 40° [77]. SAS-6 is highly involved in the assembly of the cartwheel structure. The homodimerization of SAS-6 leads to formation of oligomers, subsequently leading to a ring-like structure [62]. The establishment of the microtubule triplet involves CEP135 interacting with both SAS-6 and microtubules, forming the physical link [62, 74]. After the procentrioles form, the centrioles begin to elongate during S and G2 phase [62]. There are multiple factors involved in centriole elongation. CPAP is a key player that is involved in the stabilization of the cartwheel structure as well as the recruitment of microtubules during elongation [78-80]. The establishment of an interaction between STIL and CPAP while being in a complex is essential for centriole elongation [73, 74, 81, 82]. Phosphorylation of CPAP at S589 and S595 by PLK4 is necessary for procentriole formation and centriole elongation [83]. Elongation of the distal part of the centrioles occurs during the G2 phase [62]. This is done by POC5 and OFD1 proteins [84, 85]. CP110 is essential for the regulation of centriole length and is localized to the distal part of the centriole [68, 78].

During centrosome maturation, the ability for the centrosomes to nucleate microtubules gets enhanced through accumulation of γ-TuRCs and other maturation factors in late G2 phase [25]. In fact, the ability of the centrosomes to nucleate microtubules during mitosis increases 7-fold as compared to interphase [86]. The PCM is responsible for microtubule nucleation. CPAP is involved in the recruitment of PCM

protein around the centriole via its T complex protein 10 domain, the site where tethering occurs [87, 88]. Additionally, PLK1 is involved in the initiation of centrosome maturation by phosphorylation of target proteins [89]. After centrosome maturation and for the duration of mitosis, PLK1 activity is still required as suppression of its activity compromises the centrosome's structural integrity [90]. The last step of the cycle is centrosome separation. This occurs in two steps: a) dissolution of the proteinaceous linker b) separation of the centrosome [62]. The dissolution of the proteinaceous linker occurs during the transition of G2 to M when the protein kinase NEK2 phosphorylates C-NAP1/CEP250 and ROOTELIN [62]. After the dissolution of the linker, the centrosomes move to the opposite side of the spindle pole with the aid of the motor protein, EG5 [62]. EG5 generates enough force, allowing the centrosomes to separate [65]. This is a general overview of the centrosome cycle and the events that take place and some of the key players involved in ensuring its proper execution.

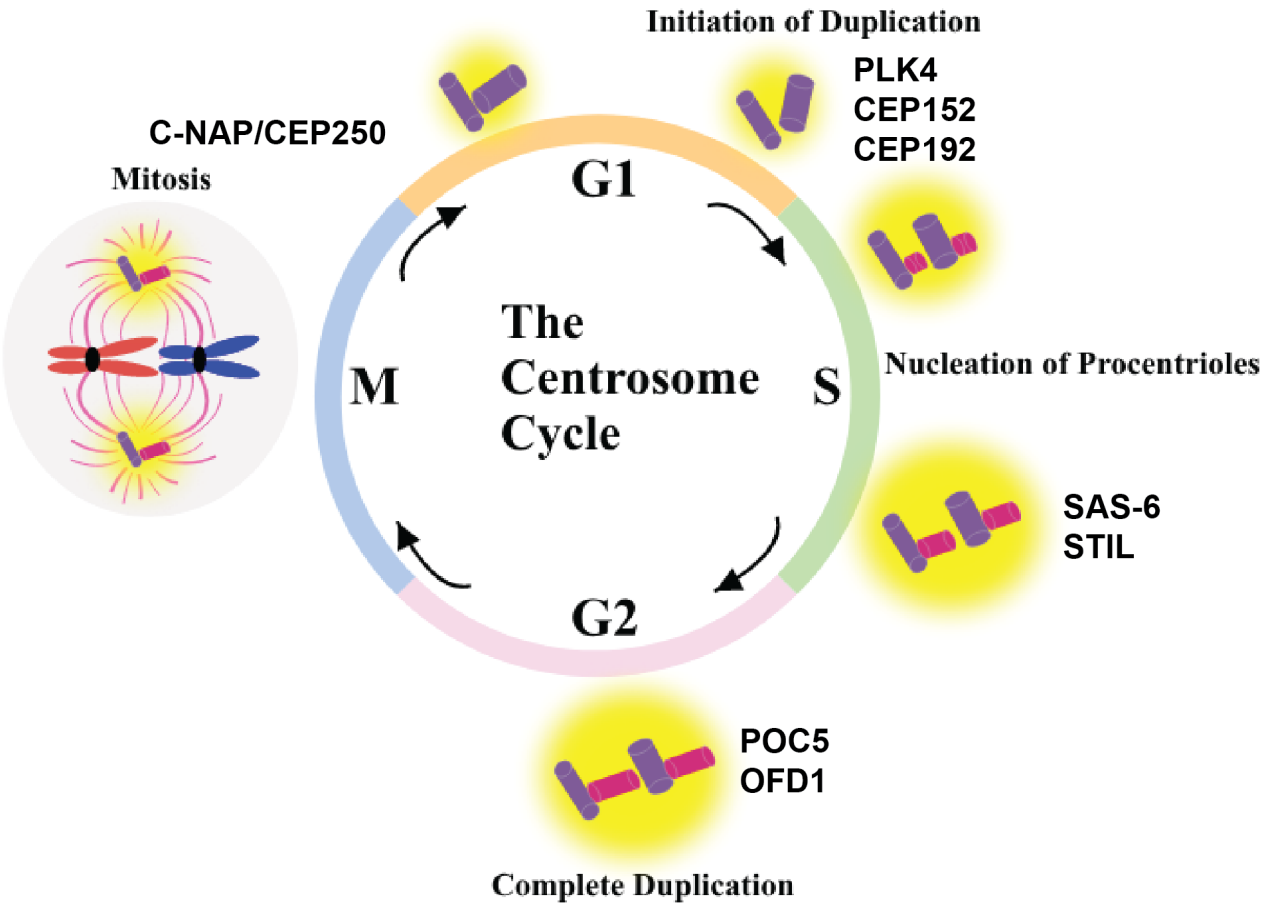

Figure 1.3 The centrosome cycle. The centrosome cycle is divided into four stages and is in sync with the cell cycle to ensure that duplication occurs only once. Onset of the centrosome cycle involves the procentrioles forming in close proximity to the pre-existing centrioles resulting in the transition into a cartwheel-like structure. After, the centriole pairs undergo maturation through accumulation of pericentriolar material. Lastly, the centrosomes separate after duplication is complete.

1.2.2 Centrosome Errors and Disease

Centrosome abnormalities have been linked to several pathologies. Dysfunction in centrosomes have been implicated in cancer, polycystic kidney syndrome, obesity, infertility, neurological disorders, and other diseases [91]. The abnormalities in centrosomes have been associated in a variety of diseases targeting different organs, further elucidating the important role it plays in the cell. The etiology of these pathologies is a result of the centrosome abnormalities and centrioles.

Centrosome abnormalities have been detected in many types of cancer including breast, urothelial, cervical, ovarian, testicular, gastrointestinal, pancreatic, lung, and neural cancer [92]. Additionally, these defects have been observed in hematological malignancies such as acute and chronic myeloid leukemia as well as Hodgkin's lymphoma [92]. Approximately 90% of the solid tumors are aneuploid, and many tumor cells exhibit chromosome instability (CIN) [93]. One of the leading causes of CIN is due to centrosome amplification [93]. Centrosome amplification can lead to aneuploidy in a two-step mechanism which involves the formation of a multipolar spindle and the maintenance of this error in the transition to a bipolar spindle [93]. The modification leads to abnormal kinetochore microtubule attachments, subsequently leading to chromosome segregation errors and aneuploidy [93]. There are two categories that centrosomal aberrations can be placed in: structural and numerical defects [44]. Examples of structural defects can include aberrations in the centriole structure and the PCM size and numerical defects include centrosome amplification [44].

Cancer cells have adapted mechanisms to continue to thrive and divide with multiple centrosomes, where loss of control would prove to be detrimental to the cell and affect cell viability. Some of these mechanisms include the activation of the centrosome, centrosome loss, and centrosome clustering [44]. The most prominent mechanism is centrosome clustering and this mechanism has been observed in many cell types [44, 94-97]. In regard to therapeutics, drugs targeting centrosome clustering can prove to be advantageous [98]. In BT-549 cells, a breast cancer cell line containing supernumerary centrosomes, a screening was conducted to search for molecules that impeded

centrosome clustering and led to mitotic arrest [98]. A compound called CCCI-01 was found to show selective toxicity to only the BT-549 cells as opposed to a normal mammary epithelial cell line [98]. Although there have been many links between centrosomes and tumors, it remains controversial whether centrosomes can induce the formation of tumors. It remains a question on whether the existence of multiple centrosomes that occur results in the development of cancer or if it plays a secondary role [99-101]. Although tumor cells with aberrations in centrosomes have abnormal chromosome numbers, there is no direct evidence that it is causal [99]. Supporting evidence that centrosome amplification can lead to tumorigenesis was seen in *Drosophila* [102]. Fly lines overexpressing Sak, the fly ortholog of PLK4, resulting in supernumerary centrosomes were used [102]. In the somatic cells of these flies, cell division was normally occuring with the centrosomes being clustered [102]. However, when larval brains containing supernumerary centrosomes were transplanted into wild-type flies via injection, it resulted in the formation of tumors [102]. Indeed, the relationship between cancer and centrosomes is quite complicated. However, ongoing research exploring their links can potentially open new possibilities when it comes to treatment.

Additionally, defects in the formation and function of cilia contribute to many diseases [103]. Cilia are projections from the cell surface that are comprised of microtubules and centrioles [104]. Centrioles make up basal bodies, which give rise to cilia and flagella [104]. Motile and nonmotile cilia are the two types of cilia that exist and are involved in different processes [105]. Motile cilia can be found in the epithelial cells while nonmotile cilia can be found in specialized sensory structures [105]. There are several diseases that can be attributed to defects in cilia. These diseases can be classified as ciliopathies and they include: Joubert syndrome, orofaciodigital syndrome, polycystic kidney disease, and renal dysplasia [103].

Abnormalities in centrosomes can also play a role in male fertility. A comparison in sperm motility revealed immotile sperm had a higher proportion of centriolar defects and absence of centrioles as opposed to motile sperm [106]. For instance, in patients who had defects in the centriolar protein, CEP135 played a role in male infertility [107].

Additionally, patients with globozoospermia, a condition that leads to a loss of a functional acrosome, exhibited reduced aster formation [107]. This abnormality can be linked to a defective centriole [107]. In conclusion, centrosomes have been implicated in a wide range of diseases from cancer to infertility. Therefore, understanding diseases in the context of centrosomes could be important in finding therapeutic solutions.

1.3 Mitotic Spindle

Mitosis is highly dependent on a properly functioning mitotic spindle to warrant a normal cell division. The mitotic spindle is primarily composed of microtubules, the major structural component, as well as a myriad of proteins [108]. Proteins found on the mitotic spindle include motor proteins and microtubule-associated proteins [109]. The motor proteins, dynein and kinesin are essential in regulating polymerization and microtubule length to facilitate the movement of chromosomes [108]. Notably, microtubule-associated proteins bind to microtubules and are involved in spindle assembly [110]. Together, these proteins aid in establishing a bipolar spindle [108]. The formation of microtubules is commenced by the γ-TuRCs [108]. Dimers of α and β tubulin polymerize to form microtubules and they are arranged to build protofilaments in a parallel manner [111]. In fact, 13 protofilaments make up the microtubule [111]. The α and β dimers are organized asymmetrically where one end of the microtubule has the β tubulin exposed and the opposite end has the α tubulin exposed, forming the plus and minus ends respectively [112]. Moreover, the rate of growth varies among the two ends where the plus end grows more rapidly therefore executing different functions for the microtubule ends [112].

Assembling of a bipolar spindle requires three types of microtubules: kinetochore microtubules, aster microtubules, and non-kinetochore microtubules [108]. Kinetochore microtubules are required for the attachment of chromosomes to the mitotic spindle while aster microtubules are involved in the positioning of the spindle [108]. The non-kinetochore microtubules give the spindle stability and the opposing sliding forces allow for the movement of the chromosomes to opposite poles [108]. In conclusion, many components are involved in the formation of a functional spindle.

1.3.1 Spindle defects

As the establishment of a bipolar spindle is a highly coordinated process, there are several defects that can result in a loss of bipolarity, consequently resulting in monopolar or multipolar spindles. Abnormalities in the spindle can be the result defects in motor proteins, centrosomes, spindle pole integrity, microtubule dynamics, and kinases [109, 113]. For instance, inhibition of the molecular motor protein Eg5 with treatment with monastrol results in monopolar spindles exhibiting unseparated centrosomes [114]. Typically, Eg5 is involved in centrosome separation through its sliding of microtubules of opposite polarity [114]. However, abolishment of Eg5 prevents this force consequently resulting in a monopolar spindle [114]. Additionally, interfering with the stability of the microtubules can lead to spindle defects [109]. For instance, overexpression of the microtubule destabilizing protein XKCM1 results in an increase in the frequency of monopolar and monoastral spindles [115]. Depletion CDK11, a protein kinase involved in centrosome maturation, leads to monopolar spindles [116]. Additionally, centrosome amplification and the loss of accurate kinetochore-microtubule attachments can lead to multipolar spindles[113]. In sum, there are multiple factors that lead to spindle defects.

1.4 RNAs are Associated with the Mitotic Apparatus

RNAs have been implicated in the regulation of mitosis. A hint that translational regulation was occurring at the mitotic apparatus was elicited by ribosomes being in close proximity with microtubules through classical electron microscopy experiments [117]. Furthermore, previous studies have reported that RNA is concomitant with proteins involved with the proper execution of mitosis [118, 119]. For example, RNA is required for stimulating the activity and localization of AURKB kinase and involved in the trafficking of SURVIVIN and INCENP, components of the chromosomal passenger complex [118-120]. In fact, treatment with RNase led to a half-fold decrease in the capability for AURKB to phosphorylate its protein target, MCAK [119]. Additionally, an effort to find mRNAs that were associating with microtubules identified a subset of mRNAs that were enriched, as depicted by microarrays performed on frog and human extracts [121]. The mRNAs that encoded proteins involved in mitosis and DNA replication were over-represented [121]. Due to the limitations of microarrays, a RNA-seq approach was later used to reveal the

microtubule-interacting transcriptome in frog extracts [122]. This study identified novel genes that were associating with the microtubules and implicated in mitosis [122]. In conclusion, these findings suggest that RNA plays a role during mitosis.

1.4.1 mRNA Localization and Mitosis

Localized mRNAs have been found to be associated with the mitotic apparatus structures including the centrosome and spindle [122-127]. The first discovery of a localized mRNA at these sites was found in syncytial-staged *Drosophila melanogaster* (*D. melanogaster*) embryos [128]. *Cyclin B* mRNA was delimited to the centrosomes [128]. Additionally, *xbub3* and *cyclin b1* were found to be enriched to the centrosomes and microtubules of *Xenopus* oocytes [124]. Screening approaches in *D. melanogaster* and human cell lines have also identified several candidates showing enrichment to the centrosomes, spindle, and astral microtubules [125, 127]. However, the significance of these mRNAs at these sites remains largely unknown. The next sections will delve into the current knowledge involving mRNA localization.

1.5 Overview of mRNA Localization

The trafficking of mRNAs to different parts of the cell is a mechanism that has been utilized to restrict transcripts to a particular subcellular compartment. Previously, this notion has been seen as a rare phenomenon. However, in recent years, there have been many examples of localized mRNAs that have emerged, highlighting its common occurrence in a diverse range of species and cell types. The significance of RNAs first came about in the study of development. It was suspected that cytoplasmic determinants were involved in the development of *Smittia* embryos [129]. Directing UV radiation to the anterior region of the cytoplasm of the egg resulted in an induction of an abnormal double abdomen phenotype, suggesting that there factors in the cytoplasm influencing its development [129]. To get a clearer picture of specific cytoplasmic determinants, treatment with different enzymes including RNase, trypsin, and DNAse I were used as an attempt to disrupt embryonic patterning [130]. Only RNase application resulted in a double abdomen phenotype, suggesting the involvement of RNA as a determinant of developmental progression [130]. These initial experiments showed that the cytoplasmic

determinants were involved in embryonic development, opening a new angle on the significance of RNA. These findings were later followed by the discovery of the first instance of a localized mRNA in ascidian during development [131]. *Actin* mRNA was enriched in different cytoplasmic regions including the myoplasm, ectoplasm, and endoplasm in eggs and embryos [131]. From revealing RNA as an important regulator of development to finding the first localized RNA, thus far there have been growing examples of its localization in diverse cell types and organisms.

1.5.1 The Conservation of mRNA Localization

Localized mRNAs have been found in a variety of species, cell types, and subcellular compartments. As mentioned earlier, the initial finding of subcellular trafficking of mRNAs was revealed by the *Actin* in the developing eggs and embryos in ascidians [131]. During this period, localized mRNAs were found in a diverse range of species. Some examples include: the concentration of *ASH mRNA* to the bud tip of the daughter cell to prevent mating type switch during anaphase in yeast, the enrichment of β *actin* to the cell protrusion of chicken myoblasts and fibroblasts, and the distribution of transcripts along the axes of developing eggs in fruit flies and frogs [132-139] (**Figure 1.4**). In addition to fungi and animals, localized mRNAs have also been found in plants, bacteria, and protists [140-145]. During differentiation in amoebas, the α and β *tubulin*, *flagellar calmodulin*, and *class I* mRNAs are localized at particular regions during the formation of the basal body [141]. Assessing the spatial distribution of mRNAs in *Escherichia coli* (*E.coli*) revealed that the localization of the mRNA was coincident of that of the protein [146]. There was a consensus that transcripts that were concentrated to the inner membrane had protein products that exhibited localization to the membrane, whereas cytoplasmic transcripts had protein products that were enriched in the cytoplasm [146]. Moreover, in rice endosperm cells, *prolamine* and *glutelin* mRNAs were found to be distributed to the endoplasmic reticulum [143]. These incidences of evidence of localized mRNAs in all kingdoms of life further emphasizes its importance as a widespread phenomenon that occur for cell function.

In fact, mRNA trafficking is important for proper function of many cell types including oocytes, cancer cells, neurons, and kidney cells [147-151]. Additionally, the localization of mRNAs in neuronal cells is important for its development and behavior as well as responding to external factors [150]. The coincidence of the mRNA and protein in neurons is essential for carrying out tasks that require a rapid increase in the concentration of proteins [150]. For instance, one study found that approximately 400 mRNAs exhibited localization to the dendrites of rat hippocampal neurons [151]. Moreover, the distribution of mRNAs leads to cell polarity during development. For instance, the localization of different maternal mRNAs has been found in oocytes and embryos including the *bicoid* (*bcd*), *gurken* (*grk*), and *oskar* (*osk*) in *Drosophila* as well as β *actin* and *deleted in azoospermia-like* (*Dazl*) in the mouse [132, 133, 148, 152]. These examples depict the versatility of dispersed mRNAs among diverse cell types.

The precise targeting of localized transcripts has been reported in different subcellular compartments including the pseudopodia, mitotic apparatus, mitochondria, dendrite, and endoplasmic reticulum [121, 122, 151, 153-155]. Fractionation studies in migrating fibroblasts showed several transcripts enriched to the cell extremities in response to stimuli in NIH/3T3 cells [155]. Additionally, yeast mRNAs that encode proteins that are subunits of ATP synthase biogenesis appeared to localize near the mitochondria, as revealed by strong punctuate structure in fluorescence in situ hybridization (FISH) experiments [153]. In another instance, the bound mRNA from the rough endoplasmic reticulum was isolated as part of a search for mRNAs that encode membrane and secreted proteins during fly embryogenesis [154]. A complementary DNA (cDNA) library was prepared downstream and was used to perform RNA in situ hybridization, revealing a variety of expression patterns in the embryo [154]. Overall, the discoveries of mRNA enrichment to different subcellular compartments/cell types conveys the prevalence of the mechanism.

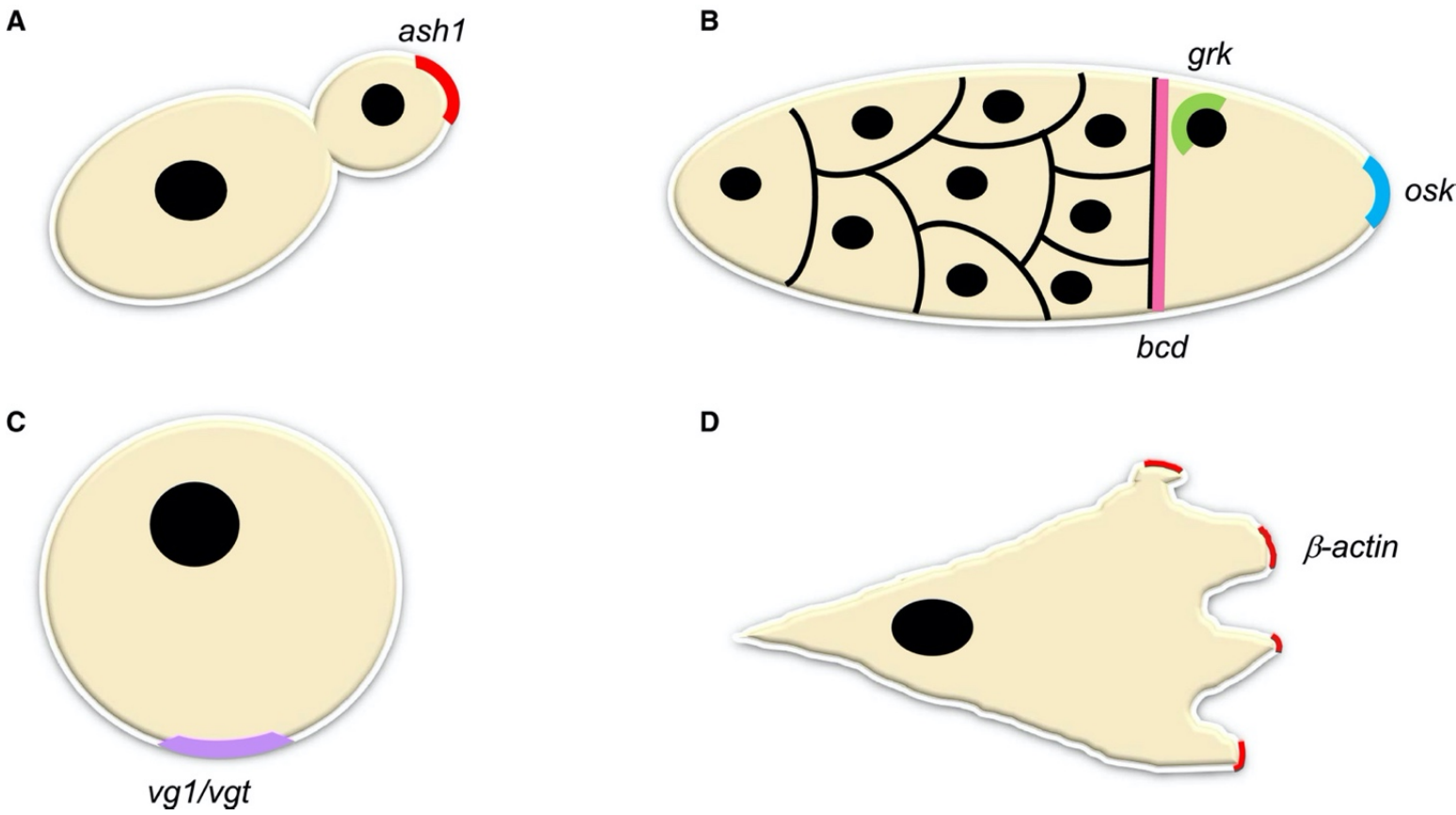

Figure 1.4 Targeting of mRNAs is a conserved process in a diverse range of species. Here are some examples of localized mRNAs. **(A)** *Ash1* mRNA is localized to the bud tip in yeast. **(B)** *Bcd* and *osk* mRNA are localized to the anterior and posterior respectively, while *grk* is enriched to the anterodorsal corner in the *Drosophila* oocyte. **(C)** *Vg1*/*vgt* mRNA is localized to the vegetal cortex in the Xenopus oocyte. **(D)** *β actin* mRNA is localized to the cell extremities of chicken fibroblasts.

Adapted from: Bovaird S, Patel D, Padilla JA, Lecuyer E. Biological functions, regulatory mechanisms, and disease relevance of RNA localization pathways. FEBS Lett. 2018;592(17):2948-72.

1.5.2 Advantages of Trafficking mRNAs

Although there are mechanisms that exist including the secretory and endocytic pathways for trafficking proteins to their final destination in the cells, there are several advantages in localizing RNAs [156]. First, the mRNA can be directed towards and enriched to its subcellular destination with precise timing, which can serve to be very beneficial for the cell [157]. The ability to localize mRNAs in a timely manner in response to extracellular signals and undergo local protein synthesis is crucial in cells, as highlighted in neuronal cells [158-162]. For example, tetanic stimulation leads to an increase in newly synthesized CAMKII protein to the distal part of the dendrites [160, 162]. CAMKII is involved in synaptic plasticity [160, 162]. Second, targeting a mRNA molecule is economical, considering that a single mRNA can undergo hundreds of rounds of translation [163]. This is beneficial bearing in mind that it is more efficient to localize transcripts and translate them locally rather than trafficking the newly synthesized proteins to the destination site [157, 164]. There have been several examples of mRNAs that undergo local translation. A large scale-screen to find genes that encoded subcellularly localized mRNAs in fly embryos showed several of striking examples of mRNAs and their respective proteins showing similar localization patterns [125]. Furthermore, a co-translational mechanism is required for the recruitment of PCNT to the centrosomes in HeLa cells [123]. Third, the delimiting of transcripts reduces the risks of mistargeting proteins and prevents them from going to areas of the cells where they can serve to be toxic [165]. For instance, MBP is rather sticky and its presence into unwanted areas of the cell can lead to aggregation [165]. Therefore, it is more beneficial to target its mRNA to the distal parts of the oligodendrocytes [165]. In a similar manner, the ectopic localization of *nos* to the anterior region leads to abnormal embryogenesis in flies, consequently resulting in the development of a second abdomen [166]. Fourth, targeting mRNAs of the same complex can result in more efficient complex assembly [167]. For example, the differentiation of amoebas into swimming flagellates required the co-localization of a group of mRNAs to the cell periphery [141]. In chicken fibroblasts, it has been shown that the mRNAs for the subunits of the Arp2/3 complex all colocalize to the cell protrusions [168]. Mathematical modeling have showed that within a cell, the proximity between the mRNAs determines the chances of protein interactions [167].

Therefore, having localized mRNAs would be favorable when forming complexes due to an increased rate of interactions [167] Lastly, localizing mRNAs can also have coding-independent functions. The *vegt* mRNA and *xlsirts* non-coding RNA serve to hold together the cytokeratin network of the vegetal cortex in frog oocytes [169]. The retention of *Cat2* transcripts in the cell nuclei of mouse hepatocytes is released during conditions of stress and is cleaved to form a protein-coding version that can be translated [170]. Another example is the zygotic mRNAs that are kept in the nuclei when treated with DNA damaging reagents, subsequently preventing the translation of these mRNAs [171]. Furthermore, *Ube3a* in mice hippocampal neurons was found to regulate miRNAs during neuronal development [172]. The examples mentioned emphasize the many reasons of why it is more beneficial to localize mRNAs to specific regions in the cell.

1.5.3 Mechanisms for Localizing mRNAs

A single mRNA molecule can exhibit two fates after transcription: it can be translated immediately, or it has the potential of being transported to its subcellular destination and be translated locally where it is required. There are *cis regulatory motifs (CRMs)* residing within the mRNA molecule that RNA binding proteins (RBPs) recognize. Together, the ribonucleoprotein complex (RNP) is transported out of the nucleus and into the cytoplasm where the RNA complex moves towards its final destination. The following mechanisms have emerged in trafficking mRNAs: 1) directed transport 2) cytoplasmic diffusion followed by trapping and 3) generalized degradation and local protection (**Figure 1.5**) [157, 173-175].

1.5.3.1 Directed Transport

The most common way to deliver mRNAs is by directed transport along cytoskeletal networks [157, 173, 174]. The RNP complex can be brought to its destination by utilizing the cytoskeletal networks: actin microfilaments and microtubules [175]. The network that is used is contingent on the distance the mRNA needs to travel [175]. Generally for shorter distances, the mRNA utilizes actin microfilaments for travel, whereas for longer distances, microtubules are employed [175]. For the transport of mRNA along microtubules, kinesin, kinesin-like, and dynein motor proteins are used, while for transport

along the actin microfilaments, the myosin-based motor proteins are utilized [175]. One of the earliest examples of a cytoskeletal network dependent pathway was the localization of *vg1* to the vegetal cortex during oogenesis in frogs [176]. Interestingly, the treatment of oocytes with nocodazole, a drug that depolymerizes microtubules, disrupted the translocation of *vg1* [176]. However, treatment with cytochalasin B, a drug that inhibits actin microfilament polymerization, did not affect the localization of *vg1* but interfered with its tight distribution [176]. These results suggest that both microtubules and actin microfilaments are involved in the localization of *vg1* [176]. On the other hand, in the fibroblast cells of chicken embryos, treatment with cytochalasin D, a drug that inhibits actin microfilament polymerization, disrupted the distribution of *Actin* to the periphery [177]. These findings suggest an actin microfilament dependent mechanism [177]. Looking into mRNAs such as *run, wg*, and *ftz* in the cellular blastoderm of fly embryos showed that the pre-injection of colcemid, a microtubule-depolymerizing dug, disrupted the apical localization of these mRNAs [178]. In addition, injecting an anti-dhc (dynein heavy chain) antibody affected the localization of the mRNAs, suggesting that dynein is the motor protein responsible for the proper distribution of the mRNAs [178]. Disruption of *par-1* in fly oocytes results in the disorganization of microtubules, subsequently perturbing the localization of *osk* to the posterior region of the oocyte [179]. Additionally, disrupting *rab11* expression in fly oocytes, which affects microtubule orientation results in abnormal *osk* localization [180]. Mutations in tropomyosin II, a motor protein that travels along the actin microfilaments, results in a loss of *osk* mRNA localization to the posterior part of the oocyte [181]. More recently, a study found that the recruitment of *pcnt* mRNA to the centrosomes is microtubule dependent with the aid of dynein motor proteins in HeLa cells [123]. Treatment with ciliobrevin D, an inhibitor of dynein, or nocodazole, a microtubule depolymerizing drug, both disrupted *pcnt* mRNA localization [123]. The examples mentioned above all elucidate the importance of the cytoskeletal system along with the respective motor proteins in localizing mRNAs.

1.5.3.2 Cytoplasmic Diffusion Followed by Trapping

The distribution of mRNAs can also occur by the diffusion of transcripts into the cytoplasm and becoming trapped at the anchor, subsequently leading to its enrichment

at a particular region [157, 173, 174]. The localization of *zorba* and *vg1* in zebrafish oocyte occur due to diffusion followed by entrapment at the animal pole in an actin and microtubule independent manner [182]. Additionally, *nanos* mRNA is localized by diffusion to the posterior part of the oocyte in flies [183]. Live imaging revealed that the displacement of *nanos* from the nurse cells to the posterior region is achieved by the diffusion of transcripts and entrapment of the mRNAs to the germ plasm, where the germ plasm serves to be an anchor [183]. *Xcat2*, *xlsirts,* and *xwnt11* in frog oocytes also undergo a similar mechanism [184, 185]. Taken together, these examples show that the entrapment of mRNAs is a mechanism utilized to localize mRNAs to a specific compartment.

1.5.3.3 Generalized Degradation and Local Protection

While undergoing localization, transcripts that do not have protection elements can be subjected to degradation [157, 173-175]. The concentration of *hsp83* mRNA to the posterior pole of fly embryos is achieved through this mechanism, as ones that do not reach the posterior pole are eliminated [186]. For instance, maternal effect mutations in genes that are components of the posterior polar granule leads to the degradation of *hsp83,* suggesting they serve a role in the protection of the mRNA [186]. Additionally, determinants located in the cis-acting elements of the mRNA determine whether it will be targeted for protection or degradation, as shown in both *nanos* and *hsp83* mRNAs [187, 188]. In the case of *nanos*, only 4% of it is localized to the posterior pole in the fly embryo while most of it remains scattered in the cytoplasm [189]. The decay of *nanos* is dependent on whether Osk protein prevents the binding of Smaug to the 3'UTR of *nanos* [189]. However, the binding of Smaug leads to the recruitment of the Ccr4-Not complex, which leads to deadenylation and eventual decay of *nanos* [189].

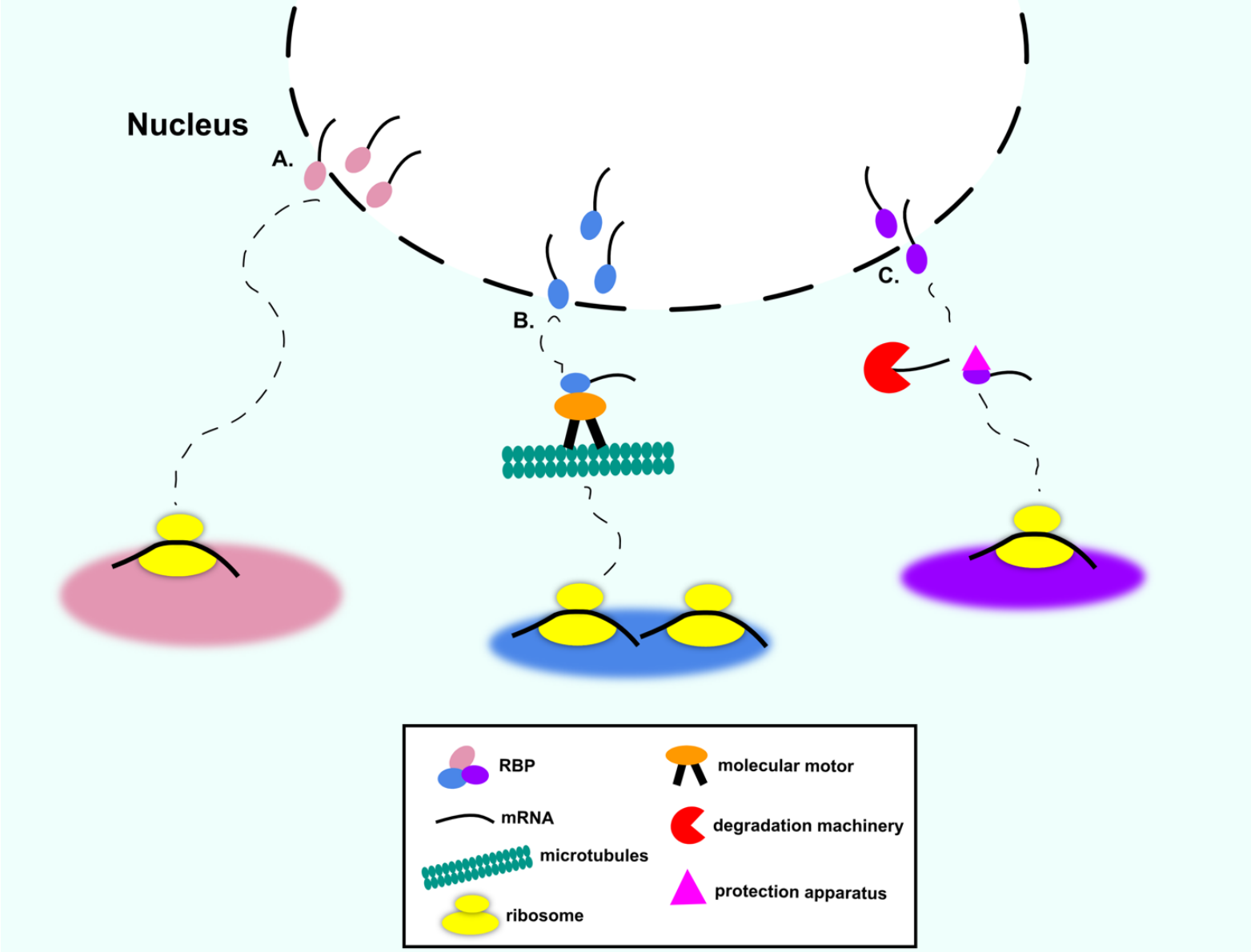

Figure 1.5: Mechanisms for mRNA localization. The mRNAs are trafficked to the subcellular destination with the aid of RNA binding proteins. These are three ways in which RNAs are transported. **(A)** Random diffusion with localized entrapment. **(B)** Transport along cytoskeletal networks. **(C)** Generalized degradation and localized protection.

1.5.4 mRNA localization Elements

The transport of mRNAs requires localization elements (LEs) that RBPs can bind to which determine the destination of the mRNA (**Figure 1.6**). This association subsequently leads to enrichment to a subcellular compartment (**Figure 1.6**). The LEs are usually found in the 3'UTR, but they can also reside in the coding region or in the 5'UTR [157]. The length of the LEs can range from a few to a several hundred of nucleotides [157, 190]. The LEs can be defined by the primary sequence as well as the second/ tertiary structures. There have been many LEs that have been revealed for several mRNAs.

One of the earliest defined LE was involved in localizing the *bcd* mRNA to the anterior region in fly oocytes and *β actin* to the cell periphery in chicken embryo fibroblast cells [191, 192]. By utilizing transgenes with deletions within the 3'UTR, several *bicoid localization elements* (*BLEs*) were revealed in *D. melanogaster* [134]. Interestingly, the *bcd* oligomerizes forming a stem-loop and this secondary structure is required for the RBP Staufen to bind to it and distribute it to the anterior pole [193]. Additionally, monitoring the β-galactosidase activity of different *β actin* chimeras revealed a 54-nucleotide and 43-nucleotide LE in chicken fibroblasts [191]. Targeting oligonucleotides against the identified LEs prevented the trafficking of *β actin* mRNA and affected the cell morphology [191]. In the case of *ASH1* in yeast, it contains four localization elements required to transport the transcript to the bud tip of the daughter cell [194]. The localization elements E1, E2A, and E2B reside in the coding sequence and E3 is in the 3'UTR [194]. The localization elements E1 and E3 can form stem-loop containing secondary structures, while mutations interfering with these structural features prevent the proper localization of *ash1* [194, 195]. Additionally, the targeting of *vg1* to the vegetal pole requires a 340-nucleotide sequence located in its 3'UTR in frog oocytes [196]. Similarly, *fatvg* also shows localization to the vegetal pole in frog oocytes, which is mediated by a 25-nucleotide sequence residing in its 3'UTR [197]. Even though *vg1* and *fatvg* exhibit a similar localization pattern, the sequences of the LEs were not conserved between the two mRNAs [197]. Furthermore, localizing *osk* during fly oogenesis requires its 3'UTR and different parts of this region were involved in distinct processes [198]. Mutations in these

regions led to defects including compromised movement to the oocyte, increased localization to the anterior region, and impaired concentration of transcripts [198]. Additionally, a 547-nucleotide sequence was found in the 3'UTR of *nanos* that was involved in its localization to the posterior region during fly oogenesis [199]. Remarkably, *D. melanogaster* and *D. virilis* both had conserved LEs in the 3'UTR of *nanos* mRNA [199]. The LEs that were mentioned are just a few of the increasing number of identified LEs as more research is conducted on understanding the elements that aid in governing mRNA localization.

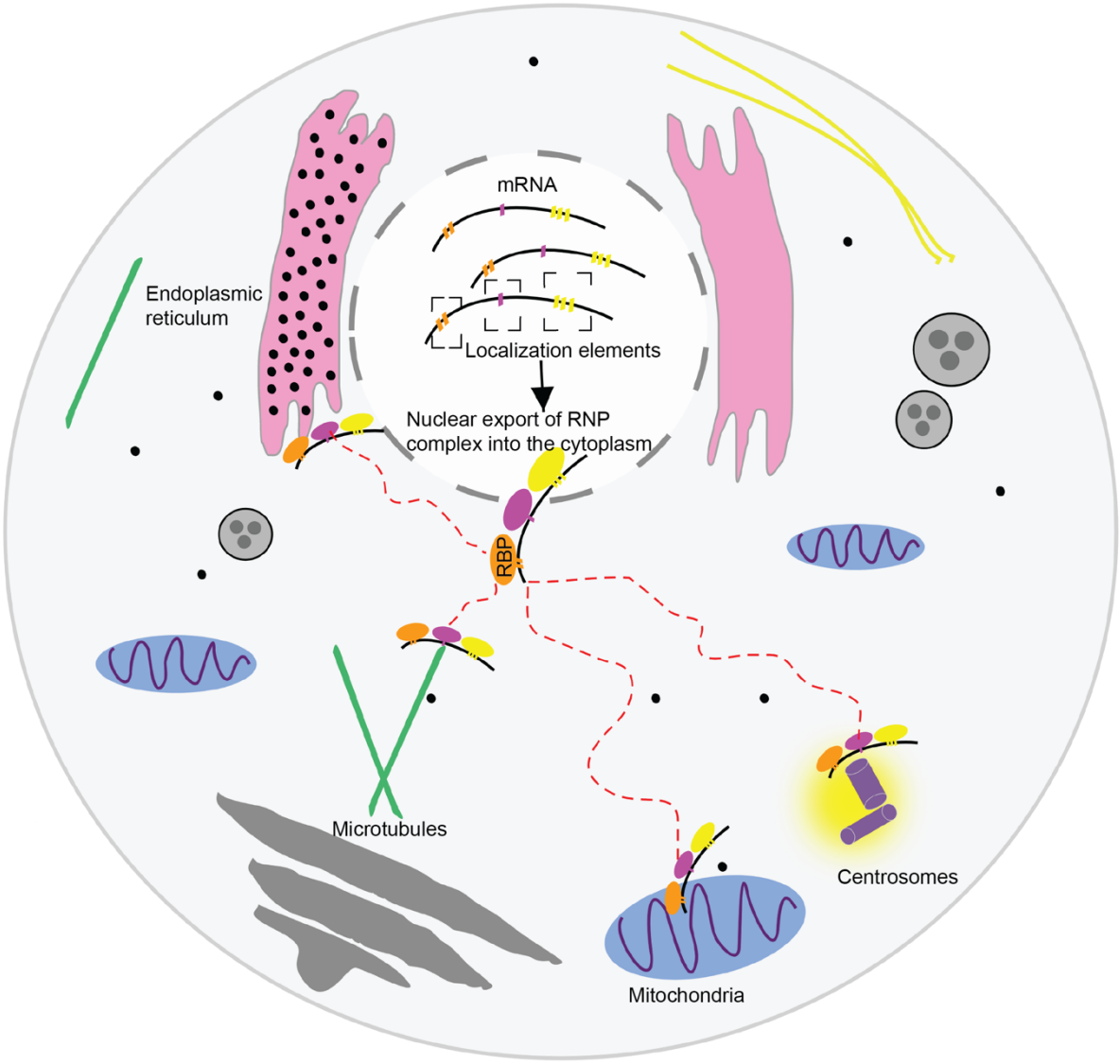

Figure 1.6 An overview of mRNA localization. mRNA localization is a mechanism used in cells to enrich transcripts to specific subcellular compartments. Within mRNA transcripts, localization elements exist that RBPs recognize. Together this ribonucleoprotein (RNP) complex is exported out of the nucleus and targeted to its final destination. There has been evidence of localized mRNAs to different structures including the mitochondria, microtubules, and centrosomes.

1.6 RNA Binding Proteins

RBPs are trans-acting factors involved in the post-transcriptional regulation of RNA metabolism. They have a myriad of roles including localization, translation, splicing, editing, and decay, essentially controlling all aspects of mRNA life cycle [170, 200, 201]. Additionally, these factors are evolutionarily conserved, making up approximately 3% to 11% of the total protein composition in the different kingdoms [202].

1.6.1 Identification of RNA Binding Proteins

Over the years, many methods have been utilized to capture the repertoire of RBPs that exist within the cell. Commonly used were techniques employing ultraviolet (UV) crosslinking combined with oligo(dT) purification [203-206]. In brief, UV crosslinking was used to preserve the interactions between the mRNA and RBP, and oligo(dT) beads were used to precipitate the complexes. To date, approximately 1500 proteins are classified as RBPs in humans [207]. Furthermore, a repertoire of RBPs have been identified in diverse species including *Saccharomyces cerevisiae, D. melanogaster,* and human cell lines [204-206, 208].

1.6.2 RNA Binding Domains

Interaction between the RBPs and LEs residing within the mRNA molecule is mediated by one or multiple RNA binding domains (RBDs), facilitating the recognition of the target RNA via its primary sequence or secondary/tertiary structures [200]. RBDs serve as the functional unit of the RBP. RBPs are subclassified by their RBDs, and some of the well-known RBD domains include RNA recognition motif (RRM), K-homology (KH), double stranded RBD (dsRBD), Piwi/Argonaute/Zwille (PAZ), and cold shock domains [200, 209]. The RRM is the most common among all, found in over 50% of RBPs [209]. The modular nature of the RBDs has many advantages such as the recognition of RNA with high accuracy, the ability to recognize multiple RNA sequences, and working as spacers to facilitate other RBD-RNA interactions [209]. Whereas many RBDs (KH,RRM) bind to single-stranded RNA by recognition of the primary sequence, others interact preferentially with double-stranded RNA (dsRBD) [210, 211].

1.7 RNA Binding Proteins and Localized mRNAs in the Context of Disease

The disruption of RNP complexes has been implicated in the context of disease [212]. An analysis conducted on 3470 RBPs showed that approximately one-third of the RBPs exhibited mutations in different diseases [212]. Some disorders correlated with alterations in ribonucleoprotein components include: dyskeratosis congenita (DC), fragile X syndrome, talipes equinovarus syndrome (TARP), spinal muscular atrophy (SMA), myotonic dystrophy type 1 and 2 (DM1 and DM2), amyotrophic lateral sclerosis (ALS), microcephalic osteodysplastic primordial dwarfism, and multisystem proteinopathies [212]. Diseases in the nervous system were highly corelated with mutations in RBPs [212]. Albeit the research is ongoing, there have been many discoveries bridging RBP and localized RNAs with different diseases. Therefore, understanding how the proper function of this multifaceted entity serves to ensure cell harmony is significant when it comes to the treatment of various types of pathologies.

1.7.1 Ribonucleoprotein Granules

To better understand the association of RNP complexes with disease, one needs to appreciate RNP granules that exist within all cells. RNP granules are higher order, membraneless structures residing in the nucleus and cytosol, composed of RNA-protein assemblies that are involved in different parts of RNA metabolism [213, 214]. There are several types of RNP granules found in the cell comprising of stress granules, Cajal bodies (CBs), paraspeckles, P-bodies, and neuronal granules [215]. Formation and maintenance of these entities is mediated by liquid-liquid phase separation (LLPS) [kitigawa216]. Granules are prone to responding to stress, thereby influencing its features, including function, morphology, and size [216]. For example, in moments of stress, structural alterations leading to the reorganization of CB factors occurs when subjected to UV-C irradiation [217, 218]. In other cases, specific RNP granules only exist in diseased cells, consequently disrupting cellular metabolism [216]. A particular one that will be mentioned more in the next section is the stress granule (SG), owing to its links to disease.

1.7.2 Stress Granules

Recently, SGs have garnered a lot of attention due to their strong association with disease, prominently in neurodegenerative diseases and cancer [215, 219, 220]. SGs are essentially RNPs composed of RBPs, non-RBP proteins, mRNAs, and accompanying initiation factors that did not undergo translation [215]. For instance, a screening conducted in human cells lines revealed several RBPs that were localized to stress granules upon exposure to arsenite treatment or heat shock [221]. During instances of cellular stress, the formation of stress granules arises as a result of impaired translation [215, 222, 223]. Moreover, they aid in coping and recovery, and their disassembly occurs when more favorable conditions transpire [215, 222]. Mutations in the SG pathway have been linked to disease, and a large number of the ones that were found were RBPs [215]. For instance, exhibiting mutations in TAR DNA-Binding Protein 43 (TDP-43) have been linked to neurodegenerative diseases including ALS [224]. In conclusion, RNP granules are implicated in disease, and it would be important to continue to explore how these complex structures function in the cell.

1.7.3 Aberrant Localization of mRNAs

RNAs have also been implicated in different pathologies. For example, an attempt to understand how cancer cells invade revealed that *RAB13* and *NET1* RNAs concentrate to the front part of the leader cells in spheroids of breast cancer cells [147]. Using antisense phosphorodiamidate morpholino oligonucleotides against *RAB13* and *NET1* RNAs impeded the ability to invade, emphasizing the importance of the enrichment of RNAs in the leader cell [147]. Similarly, another study utilized Boyden chamber-based method and reported several mRNAs being localized to the cell protrusions of the MDA-MB-231 cancer cell line [225]. In the case of *C9ORF72*, a repeat expansion in the non-coding region leads to the build-up of toxic nuclear RNA foci, accounting for many cases of familial ALS [219, 226, 227]. In short, disruption of both mRNAs and RBPs can lead to diseases.

1.8 mRNA Localization in the *Drosophila melanogaster*

A prevalent mechanism occurring during *D. melanogaster* development is mRNA localization. The cytoplasmic restriction of transcripts is essential to ensure the proper development of the fly. This process has been studied extensively in the oocyte and embryo. For instance, the body axes of the developing embryo are dictated by the localization events that occur during oogenesis [228, 229]. The main mRNAs that are involved in specifying the embryonic axes are *osk*, *nanos*, *bcd*, and *grk* [229]. Enrichment of these mRNAs to specific regions of the oocyte requires LEs that work in trans with different RNA binding proteins to get to the required compartment [229]. The localization of *bc*d to the anterior region of the oocyte and the localization of *osk* and nanos to the pole plasm of the posterior region of the oocyte are necessary in the establishment of the anterior-posterior axis [229]. *Grk* is localized to the anterodorsal corner of the oocyte and its localization is critical for patterning of the anterior-posterior axis as well as the dorsal-ventral axis [229]. Transport of *os*k, *bcd*, and *grk* mRNAs are mediated by the RBPs, Egl-l and Bic-d, using the dynein motor complex on the microtubule cytoskeleton [229]. The precise localization of these mRNAs is necessary for embryonic development. As aforementioned, ~70% -79% of transcripts showed subcellular localization in embryos, exhibiting many patterns, highlighting its common occurrence [125, 230]. Establishing cell polarity mediated by mRNA localization is essential during development and the *D. melanogaster* is a great model to utilize.

1.9 The *Drosophila Melanogaster* as a Model System

The *D. melanogaster* is a commonly used model system to understand gene function. Thomas Hunt Morgan popularized *Drosophila* research. Morgan and his colleagues initially started using *D. melanogaster* to understand the chromosomal theory of inheritance [231]. After 100 years, Morgan's work on *Drosophila* continues to carry on today where laboratories all around the world continue to use this model system to study all types of biological processes.

The *D. melanogaster* serves to be an excellent model to understand the function of different genes. Considering that 65% of the genes that cause disease in humans have

an ortholog in the fly as well as the similarity in tissue function in both systems allow the fly model to be a great system to implement when studying different kinds of pathologies [232, 233]. There have been assays developed in different systems including but not limited to the cardiovascular and nervous system [233]. For example, the cardiac cycle in the fly also includes the diastolic and systolic periods like mammals, thus making it a solid model to study and conduct assays to gain further insight into the cardiovascular system [233]. Additionally, multiple screens have been conducted using the fly model to study different biological processes including metastasis, mRNA localization, and the auditory response [125, 234-246]. For example, a screen conducted in the eye imaginal discs of larvae searched for genes that promoted metastatic behavior by assessing if localized tumors spread to other tissues after gene inactivation or in the presence of a mutation [237]. Indeed, they found that $Ras^{V12}/scrib^{-/-}$ resulted in metastatic behavior, thus giving further insight into genes that are involved in the regulation of metastasis [237].

The *D. melanogaster* originates from the Sub-Saharan region of Africa [247]. To date, approximately over 2000 different species of *Drosophila* were discovered [248]. The generation time of the *D. melanogaster* is relatively short, taking approximately 9-10 days for the fertilized eggs to reach adult stage at 25°C and 19 days at 18°C [249]. Embryogenesis, as well as the first and second instar larva stages last approximately 24 hours, while the third instar larva stage lasts 48 hours [249]. Then, the larva undergoes metamorphosis and stays in the pupal case for 4-5 days [249]. During this stage, most of the tissue from the embryonic and larval tissues is destroyed and the 19 imaginal discs give rise to adult structures such as the wings [249]. After, the adult flies hatch from the pupae and reach sexual maturity in approximately 8-12 hours [249]. This cycle is then repeated once again. Further details regarding the development of the Drosophila will be mentioned in sections **1.9.2-1.9.4**. Having a short generation time, a compact genome of approximately 13000 protein-coding genes, a high percentage of orthologous genes to humans, low cost, the diversity of diseases that can be studied, and the ease at which they can be cultured in the lab alludes the *D. melanogaster* to be a popular and practical model system to use [249].

1.9.1 The *Gal4/UAS* System

The ability to alter gene expression is important in understanding the function of the gene. The *Gal4/UAS* system in *Drosophila* is a powerful technique that has been utilized to result in targeted gene expression and is cell and tissue-specific [250]. Before this system was employed, there were other approaches that were used to regulate gene expression. The two other techniques that were widely applied were inducible heat shock promoters and transcriptional regulatory sequences from specific promoters [250]. Although these techniques served the purpose of regulating gene expression, there were several drawbacks that had to be addressed. In the case of inducible heat shock promoters, they resulted in phenocopies, rendering the mutant phenotypes to be indiscernible [251, 252]. The latter technique allowed for targeted gene expression, but toxicity from the gene product prevented the formation of stable lines to work with [253-255].

Because of the caveats mentioned, this allowed for a more practical approach to emerge in manipulating gene expression. The *GAL4/UAS* system utilizes two fly strains: a strain with a tissue-specific promoter and a strain carrying a specific gene of interest (**Figure 1.7**) [250]. Since the two fly strains are separate, the parental lines are sustainable [250]. Therefore, genes can be activated in a tissue-specific manner to understand their functions. This system takes advantage of Gal4 and an Upstream Activating Sequence (UAS). Gal4 is a transcriptional activator found in yeast, and it can activate gene expression from enhancers [250, 256]. The Gal4 gene is placed under the control of a native promoter which controls the expression of the GAL4 protein and remains restricted to specific cells and tissues [250]. Additionally, there is a line containing the enhancer known as the Upstream Activating Sequence (UAS), that consists of five GAL4 binding sites [250]. The gene of interest is subcloned behind the UAS [250]. When the two fly lines are crossed, the Gal4 will initiate the transcription of the target genes by binding to the UAS [256-258]. The resulting progeny will have restricted expression to where Gal4 is expressed, therefore mediating targeted gene expression [250].

To induce gene knockdown using the *Gal4/UAS* system, RNA interference (RNAi) is used. RNAi is conserved among different species and has been used as a natural defense mechanism against foreign genetic material [259]. This gene regulatory mechanism was first discovered in *Caenorhabditis elegans* (*C.elegans*) as a way to promote gene silencing [260]. In *Drosophila*, transgenes encoding a double stranded RNA (dsRNA) that are complementary to the endogenous gene are located downstream of the UAS, consequently resulting in progeny that have undergone gene knockdown delimited to a specific compartment when crossed to a fly expressing Gal4 [261].

The transcription of the hairpin dsRNA results in a complex forming that consists of Dicer-2 and R2D2, subsequently leading to the cleavage of the RNAs into short 21-nucleotide long fragments [261]. The Hsc70/Hsp90 complex are then involved in the recruitment of the siRNAs into Argonaute-2 (Ago-2), a major protein involved in the RNA-induced silencing complex (RISC) [262]. Ago-2 is then responsible for the unwinding of the siRNA duplex by the cleavage of the passenger strand, subsequently leading to its removal and degradation [261]. This leads to the formation of the active RISC complex which is associated with the guide strand [261, 263]. Together, this complex is guided towards the complementary RNA resulting in its cleavage and silencing [263].

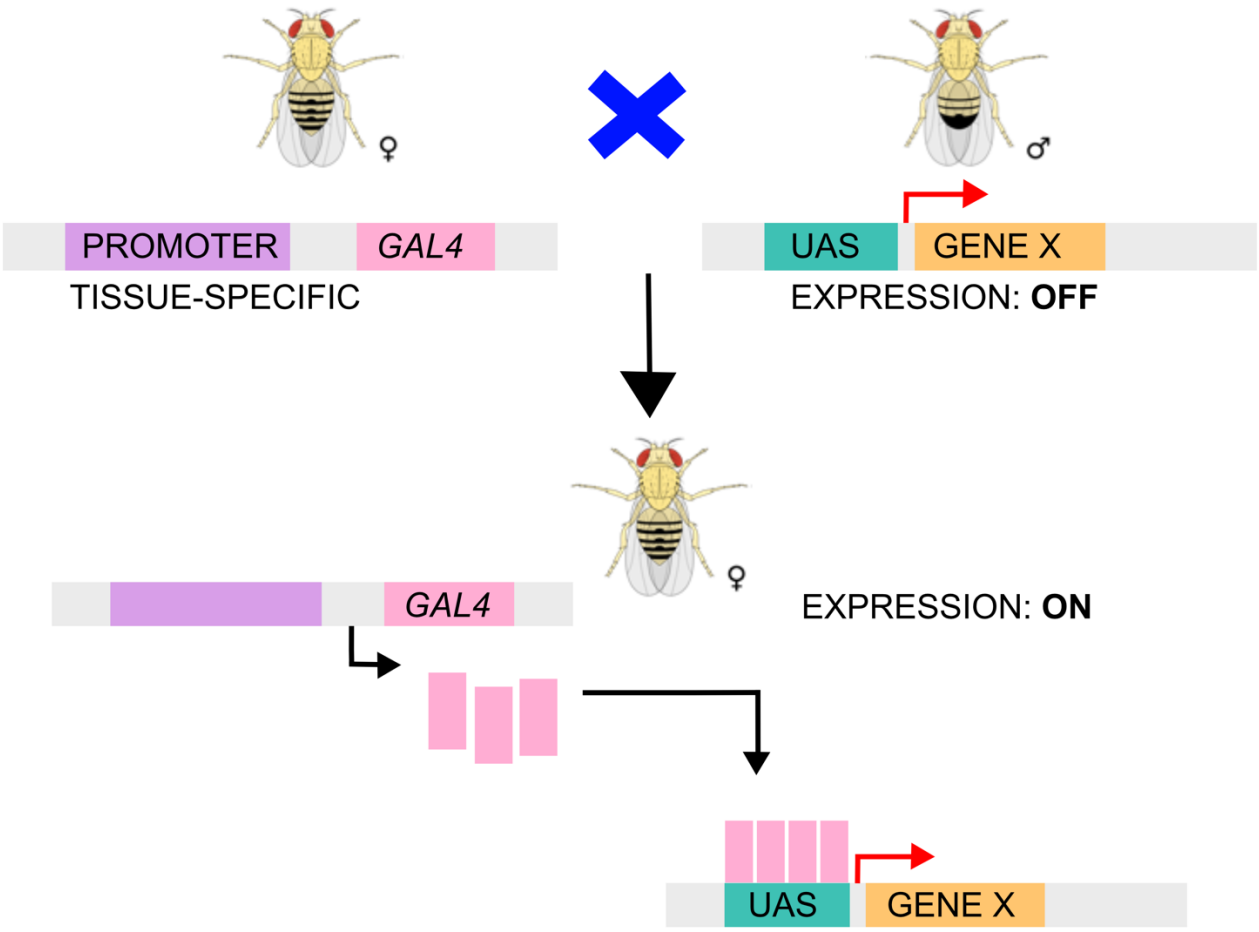

Figure 1.7 Overview of the *GAL4*/*UAS* System. The *GAL4-UAS* system is used for targeted gene expression in the *Drosophila melanogaster*. To utilize this system, two parental lines are employed. The female fly carries *GAL4* driver under the control of a tissue-specific promoter. In our studies, we used *nanos-gal4* to induce expression in the female germline. The male fly carries the *UAS* sequence with the transgenes encoding short hairpin RNAs located downstream. Performing the cross results in progeny exhibiting a loss of expression in the female germline for the gene of interest.

1.9.2 Oogenesis

During oogenesis, the formation of eggs occurs from the germ cells [264]. The process of oogenesis takes approximately 1 week and consists of 14 stages [264] The female *Drosophila* has two ovaries, and it is considered to be the largest organ in the female [264]. Each ovary consists of approximately 16-20 ovarioles [265, 266]. An ovariole, the functional unit, is made up of germ cells and somatic cells, and is formed during larval development [264].The germarium is located in the anterior region of the ovariole and serves as the basic unit for the production of the egg chambers, a multicellular entity that encapsulates the oocyte [264, 267]. Located at the anterior tip of the germarium, approximately 2-3 germline cells divide asymmetrically resulting in a new stem cell and cystoblast [264]. The cystoblast then divides four times, via mitosis with incomplete cytokinesis, producing a cluster of 16 cystocytes [264]. This results in a cyst containing 16 cells, where one of the 16 cells will be selected and differentiated into an oocyte, while the rest of the cells will form the polyploid nurse cells [264, 268]. The remaining nurse cells play a role in nourishing the oocyte by providing it maternal mRNAs and cytoplasmic components [229, 264]. Following the formation of the cyst, follicle cells migrate and surround the cystoblast [264]. The egg chambers bud off from the germarium and mature as they go down the ovariole, where the most mature eggs that have the potential to be fertilized are then located in the posterior end of the germarium [264].

1.9.2.1 Stages of Oogenesis

Located in the anterior extremity of the ovary, the germarium is divided into four regions (1, 2A, 2A, and 3) [269]. In these regions, the cysts form. In region 1, the germline stem cells and dividing cysts are present [269]. In region 2B, one of the cells becomes an oocyte while the remaining become the accompanying nurse cells [269]. In region 3, the cyst exhibits a rounder structure, and it becomes ready to bud off [270]. The region 3 portion of the germarium, consisting of the follicle cells and cyst is considered a stage one egg chamber. Stages 2-7I occur for approximately 2 days, and during this time the egg chamber grows [270]. The oocyte nucleus becomes repressed while the nurse cells undergo replication and form polyploid nuclei [270]. Follicle cells no longer divide after stage 5, and they start to replicate their DNA to form polyploid nuclei [270]. At the onset

of stage 8, the oocyte starts to acquire a large mass of yolk, which is required for nourishing the potential embryo with nutrients [270]. In stages 10 and 11, nurse cell dumping occurs where there is a breakdown of these cells and the cytoplasm is released into the oocyte, increasing its volume [271]. After dumping, the nurse cells undergo apoptosis [271, 272].

1.9.2.2 Oocyte Selection

Oocyte selection is dependent on the localization of cytoplasmic determinants, movement of the centrioles into the oocyte, and the organization of the microtubules [273, 274]. The fusome, an organelle that connects the 16 cells of the cyst via the ring canal, gives the first signal for oocyte selection [273, 275]. Two of the cells will have four ring canals, also known as pro-oocytes, and these two cells will enter prophase of meiosis I [276]. On the other hand, the cell that does not differentiate into an oocyte will revert back to a nurse cell [276]. Mainly asymmetric distribution of the fusome occurs during cystoblast division, as early as the first cystoblast division and continues until the 16-cell syncytium is formed [273]. Two of the major players involved in oocyte selection and formation of the fusome are the genes, dynein heavy chain and lis-1 [273, 277-279]. The fusome and microtubules closely associate with each other as the microtubules are necessary for the proper formation of the fusome [273]. Once the fusome is formed, it aids in organizing the microtubule cytoskeleton, which is essential for the transport of cytoplasmic determinants [273]. The determinants are involved in determining which cell will differentiate to form the oocyte [273]. In addition to the fusome, centriole clustering and restricted meiosis are involved in influencing oocyte selection [273]. The progression of meiosis occurs only in one cell, where Egl and BicD are involved in concentrating the “meiosis entry factors” into the selected cell [276]. Furthermore, centriole clustering occurs in the selected oocyte [274, 280-282]. All the cells within the cyst have centrioles within region 2A of the germarium, however, in region 2B, the centrioles migrate from the nurse cells through the ring canals and are enriched into one of the pro-oocytes [274, 280-282]. The events that have been mentioned are necessary in choosing the cell that will differentiate into an oocyte.

1.9.3 Spermatogenesis

The testis is involved in the production of the sperm in *Drosophila* throughout the life of the fly, and spermatogenesis occurs immediately after meiosis [283]. Stem cells are responsible for the maintaining spermatogenesis, where a few of them divide asymmetrically once every 24 hours [284]. Asymmetric division of the stem cells results in two cells: a gonialblast and a cell that preserves the stem cell features [284]. The gonialblast, which is also known as the daughter cell, will go on to differentiate into mature sperm that has the potential to take part in the fertilization process [284]. Within the germline, the gonialblast undergoes 4 rounds of mitosis and 2 rounds of meiosis, resulting in 64 haploid spermatids that are interconnected [283, 284]. Lastly, the spermatids exhibit maturation and elongation, a process known as spermiogenesis, to form sperm and are trafficked to the seminal vesicle [283, 284]. Following elongation, the nuclei undergo a transformation in the nuclear shape, where the nuclei become thinner and the chromatin undergoes condensation [283]. Finally, the mature sperm undergo individualization, where actin cones form around the nuclei in the spermatid cyst [283]. Each sperm cell will be encapsulated within its own plasma membrane [283]. After the formation of mature sperm, they are trafficked and stored in the seminal vesicle until they are required for fertilization [283, 284].

1.9.4 Embryogenesis

Embryogenesis in *D. melanogaster* has been extensively studied and has provided a lot of insight into the development of other organisms. It occurs relatively quickly, lasting approximately a day [249]. After fertilization, the embryo undergoes a series of 13 rapid and synchronous nuclear divisions without cellular division resulting in a massive cytoplasm called the syncytium [285]. Synchronization of the nuclear cycles is governed by the mitotic waves of Cdk1 activity [286]. The first 13 nuclear divisions last approximately 8-10 minutes and gradually slow down to 18 minutes [286, 287]. Due to a lack of gap phases and short S phases, the first 13 nuclear cycles occur rather quickly and take a total of approximately 2 to 2.5 hours [288]. The nuclei migrate from the interior of the embryo to the periphery during nuclear cycle 8 [285]. After the completion of 13 nuclear divisions, nuclear division stops and cellularization occurs, leading to the

formation of a cell membrane surrounding the nuclei during interphase of stage 14 [285, 289]. These cells are involved in gastrulation, a process where invagination of cells occur to produce different germ layers such as the mesoderm and endoderm [285]. During the onset of gastrulation, the mid blastula transition occurs where gap phases start to appear. Transcriptional waves occur in the embryo, where the mRNAs that are enriched support its development, including ones that are involved in establishing a body plan [290].

During the earlier nuclear divisions, the embryo remains transcriptionally silent and solely relies on loaded maternal mRNAs and proteins that are deposited in the egg during oogenesis [288, 290-293]. At this time, the embryo undergoes maternal-to-zygotic transition (MZT), spanning the first 13 nuclear cycles [287]. The slow eradication of maternal transcripts and activation of the zygotic genome occurs during MZT [290]. Zygotic gene activation occurs (ZGA) within 30 minutes after fertilization [125]. During nuclear cycles 9 and 14, a minor and major wave of zygotic genome activation occurs [287]. Initially, the egg activation is involved in the destabilization of a subset of maternal mRNAs, accounting for 20% of transcripts while zygotic transcription is involved in the degradation of another 15% [290, 294]. By the end of the MZT, approximately 35% of the maternal transcripts are eliminated [290]. Upon activation of zygotic genes, additional maternal transcripts undergo destabilization and degradation [290, 295]. In conclusion, embryogenesis in the *D. melanogaster* is a highly coordinated process.

1.10 A Summary of Major Findings from the Literature Leading to my Ph.D. Project

Since mitosis is a highly coordinated process, the precise targeting of RNA and proteins to the mitotic apparatus is essential for an error-free cell division. While many studies have established the key protein constituents involved in mitosis, a lot remains unknown about their mRNA counterparts [296]. Nevertheless, it has been established since the 1950s that RNAs are components of the mitotic apparatus and that microtubules are in close contact with ribosomes [117, 297]. To date, there have been several experimental approaches including proteomic, biochemical, and imaging that have unraveled the mRNAs and RBPs interacting with centrosomes and microtubules [121,

122, 125, 298-301]. For instance, RBPs and mRNAs have been found to be purified in extracts from mitotic spindles and centrosomes [299-301]. In a recent proteomics survey of proteins associated with the spindle purified from HeLa cells, it was found that close to 10% contained nucleic acid binding domains, including RBPs [301]. Similarly, imaging efforts have revealed numerous mRNAs and RBPs being colocalized to the centrosome and microtubules [122, 125, 127, 298]. Though countless examples of RNP constituents found at these structures hint that RNAs are indeed a component of the mitotic apparatus, their functional relevance and mechanisms remain primarily unknown. Based on the supporting evidence, **we hypothesized that the proper localization of the components of the ribonucleoprotein complexes is important for the regulation of mitosis and that interfering with the process will result in mitotic defects.**

Aims

This thesis centers around the implication of localized mRNAs in the regulation of mitosis. Thus, we set out to answer the following questions:

Q1 What are the mechanisms of mitosis regulation due to localized mRNAs?

Q2 What are the functional roles of localizing RBPs to the mitotic apparatus?

We addressed the following aims to answer Q1 in Chapter 2:

Aim I Determine if the physical linkage of the genes, cen and ik2 influences centrosomal targeting

Aim II Dissect the localization determinants in *cen* and *ik2* mRNAs

Aim III Elucidate the mechanism for targeting cen and ik2 mRNAs to the centrosomes

We addressed the following aims to answer Q2 in Chapter 3:

Aim I Identify RBPs that are localized to the mitotic apparatus structures

Aim II Perform systematic RNAi to determine which RBPs have mitotic functions

Aim III Assess the impact of localized mRNAs in mitosis regulation

Together, these data identify a distinct mechanism for centrosomal targeting and provide insight into the functions of RBPs during mitosis.

Chapter 2 Inter-dependent centrosomal co-localization of the *cen* and *ik2* *cis*-natural antisense mRNAs in *Drosophila*

Inter-dependent Centrosomal Co-localization of the *cen* and *ik2* *cis*-Natural Antisense mRNAs in *Drosophila*

*Julie Bergalet[1], ***Dhara Patel[2]**, Félix Legendre[2], Catherine Lapointe[1], Louis Philip Benoit Bouvrette[2], Ashley Chin[3], Mathieu Blanchette[4], Eunjeong Kwon[1], Eric Lécuyer[5]

[1] Institut de Recherches Cliniques de Montréal (IRCM), Montréal, QC, Canada.
[2] Institut de Recherches Cliniques de Montréal (IRCM), Montréal, QC, Canada; Département de Biochimie et Médecine Moléculaire and Programme de Biologie Moléculaire, Université de Montréal, Montréal, QC, Canada.
[3] Institut de Recherches Cliniques de Montréal (IRCM), Montréal, QC, Canada; Division of Experimental Medicine, McGill University, Montréal, QC, Canada.
[4] School of Computer Science, McGill University, Montréal, QC, Canada.
[5] Institut de Recherches Cliniques de Montréal (IRCM), Montréal, QC, Canada; Département de Biochimie et Médecine Moléculaire and Programme de Biologie Moléculaire, Université de Montréal, Montréal, QC, Canada; Division of Experimental Medicine, McGill University, Montréal, QC, Canada.

***Bergalet J and Patel D contributed equally to the manuscript.**

Note: A version of Chapter 2 has been published in the following manuscript: Bergalet J*, Patel D*, Legendre F, Lapointe C, Benoit Bouvrette LP, Chin A, et al. Inter-dependent Centrosomal Co-localization of the *cen* and *ik2* cis-Natural Antisense mRNAs in Drosophila. Cell Rep. 2020;30(10):3339-52 e6.

2.1 Contributions of the Authors

Figure 2.1**:** Eric Lecuyer

Figure 2.2: Dhara Patel

Figure 2.3: Dhara Patel and Julie Bergalet

Figure 2.4: Felix Legendre, Catherine Lapointe, and Julie Bergalet

Figure 2.5: Catherine Lapointe, Felix Legendre, Eunjeong Kwon, and Julie Bergalet

Figure 2.6: Dhara Patel and Ashley Chin

Figure 2.7: Louis Philip Benoit Bouvrette and Julie Bergalet

Supplemental Figure 2.1: Eric Lecuyer

Supplemental Figure 2.2: Dhara Patel

Supplemental Figure 2.3: Julie Bergalet

Supplemental Figure 2.4: Louis Philip Benoit Bouvrette

Eric Lecuyer, **Dhara Patel**, Julie Begalet, Felix Legendre, Mathieu Blanchette, Catherine Lapointe, Eunjeong Kwon, Louis Philip Benoit Bouvrette, and Ashley Chin designed the project and planned the experiments

Dhara Patel, Julie Bergalet, Felix Legendre, Catherine Lapointe, Eunjeong Kwon, Ashley Chin, and Eric Lecuyer carried out the experiments.

Louis Philip Benoit Bouvrette performed the bioinformatics analysis.

Dhara Patel, Julie Bergalet, and Eunjeong Kwon analyzed the results.

Eric Lecuyer, Felix Legendre, and Julie Bergalet made the figures and wrote the manuscript.

2.2 Summary

Overlapping genes are a striking feature of most genomes, but the extent to which this organization influences regulatory events operating at the post-transcriptional level is unclear. Studying the *cen* and *ik2* genes of *Drosophila melanogaster*, which are convergently transcribed as *cis*-natural antisense transcripts (*cis*-NATs) with overlapping 3'UTRs, we found that their encoded mRNAs strikingly co-localize to centrosomes. These transcripts physically interact in a 3'UTR-dependent manner and the targeting of *ik2* requires its 3'UTR sequence and the presence of *cen* mRNA, which serves as the main driver of centrosomal co-localization. The *cen* transcript undergoes localized translation in proximity to centrosomes and its localization is perturbed by polysome-disrupting drugs. By interrogating global fractionation-sequencing datasets generated from *Drosophila* and human cellular models, we find that RNAs expressed as *cis*-NATs tend to co-localize to specific subcellular fractions. This work suggests that post-transcriptional interactions between RNAs with complementary sequences can dictate their localization fate in the cytoplasm.

2.3 Highlights

- The *cen* and *ik2* mRNAs, *cis*-NATs encoded by 3'overlapping genes in *D. melanogaster*, co-localize to peri-centrosomal structures in the cytoplasm.
- Loss of *cen* mRNA disrupts the centrosomal targeting of *ik2*, revealing a co-dependency in their cytoplasmic localization fate.
- Centrosomal localization requires the coding region sequence of *cen* and the 3'UTR of *ik2*, with the 3'UTRs of these transcripts mediating their physical association.
- *Cen* mRNA undergoes localized translation at level of centrosomes and its localization requires active translation and intact polysomes.
- Analysis of subcellular transcriptomic datasets reveals that *cis*-NAT transcript pairs tend to co-localize within the same subcellular fraction.

2.4 Graphical Abstract

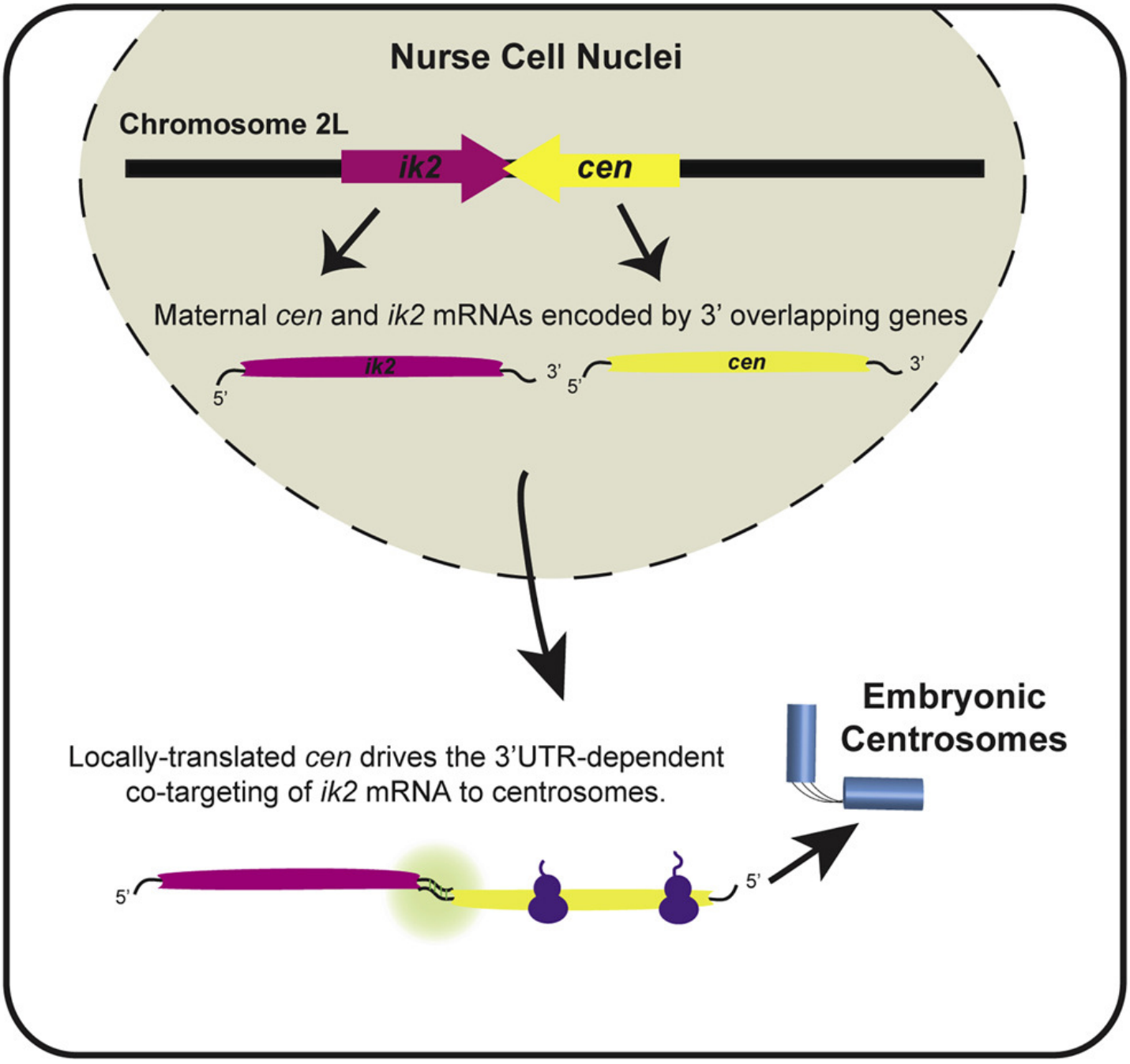

2.5 Introduction

Overlapping genes, defined as genes that share physical linkage within the same genomic locus, are a common feature of viral, prokaryotic and eukaryotic genomes [302]. Such genetic units can be sub-classified based on their relative transcriptional orientation (convergent, divergent or embedded) and the length of their sequence overlap [303]. Genome and transcriptome sequencing efforts in diverse species have identified large collections of *cis*-natural antisense transcripts (*cis*-NATs) encoded by overlapping gene pairs, either coding or non-coding [304-309]. Indeed, convergent antisense transcription of protein coding genes is frequently observed across the yeast (>60%) and human (>30%) genomes [310, 311]. Moreover, genomic sequence overlap has been found to modulate different aspects of gene regulation [312, 313] , including genomic imprinting [314], transcription [315-320], RNA editing [321-323], RNA stability [324-326], and translation [327, 328].

The subcellular localization of RNA molecules is an important aspect of post-transcriptional gene regulation, which involves the precise targeting of transcripts to specific regions of the cell [157, 329, 330]. RNA localization is a widespread regulatory mechanism, observed in species ranging from bacteria to humans, with functional roles in biological processes such as cell motility, embryonic axis establishment and asymmetric cell division [157, 173]. Moreover, high-throughput subcellular transcriptomic studies, either using fluorescent *in situ* hybridization (FISH), cell fractionation combined with RNA sequencing (CeFra-seq) or recent proximity-dependent RNA labeling methodologies, have revealed the high prevalence of RNA localization [125, 331-333]. For example, mRNAs are often targeted to precise organelles and subcellular structures in developing *Drosophila* embryos [125].

The process of RNA localization is generally governed by *cis*-regulatory elements residing within the RNA molecule, which are recognized by *trans*-acting RNA Binding Proteins (RBPs) that help specify the transport route [157, 329]. While *trans* interactions between RNA molecules are also likely to influence intracellular RNA trafficking, this paradigm remains poorly explored. In the present study, we characterize an example of

two centrosomally localized mRNAs, *centrocortin (cen)* and *IκB kinase like-2* (*ik2*), which are encoded by 3' overlapping genes in *Drosophila melanogaster*. We find that the localization of these transcripts is inter-dependent, with *cen* mRNA serving to recruit *ik2* to centrosomes in a 3'UTR dependent manner. Our results thus reveal a mechanism of cytoplasmic mRNA targeting, mediated by the *trans*-interactions of distinct mRNA species.

2.6 Experimental Procedures

2.6.1 *Drosophila* stocks

Oregon-R (*OreR*) flies were used as wild-type for all experiments. *Nanos-Gal4-VP16* (NGV), Cen^{f04787}, *Cen-RNAi-TRIP* and *Ik2-RNAi-TRIP* stocks were obtained from the Bloomington *Drosophila* Stock Center (BDSC). *D. Simulans*, *D. Virilis* and *D. Mojavensis* flies were purchased from the *Drosophila* Species Stock Center. GFP-fusion transgenes were generated as described below. Embryos were collected 4 h after egg laying for *D. Melanogaster* and *D. Simulans* flies. Due to longer development times, embryos were collected at 7 h after egg laying for *D. Virilis* and *D. Mojavensis* flies.

2.6.2 Plasmid Construction

To produce GFP fusion constructs, the sequences of *cen* and *ik2* were amplified by PCR using *Drosophila* Gene Collection bacterial cDNA clones (ik2= SD10041; cen= LD41224) or *OreR* genomic DNA as template. The *cen* or *ik2* CR+3'UTR, CR or 3'UTR segments, or the truncated versions of the *ik2* 3'UTR, were amplified by PCR with primers indicated in **Table S1**. Purified PCR fragments were digested using the restriction sites indicated in the corresponding primer sequences and ligated into the base pGem4-GFP vector (sequence available upon request), in order to generate in-frame fusion cassettes with the GFP coding region in 5' to the *cen* or *ik2* sequences. Expression and transgenesis vectors were constructed by sub-cloning the GFP-fusion cassettes into the pUASP-attB plasmid using the restriction enzymes KpnI or EcoRI/KpnI. All plasmid constructs were verified by sequencing.

2.6.3 *Drosophila* Transgenesis

Column purified pUASP-attB constructs were further cleaned via Na^+ acetate/ethanol precipitation and resuspended in water at a concentration of 500ng/μL. DNA preparations were diluted in 10X injection buffer (1.5M NaCl, 200mM Hepes) and injected into the PBac-attP-3B syncytial stage embryos using a Leica DMIL microinjection microscope. Given that the pUASP-attB transgenesis vector carries a *white* allele to confer red eye color, the resulting flies were crossed with W118 flies (white eyes) to select the transgenic progeny, which were then balanced with the Ly/TM3 Drosophila stocks. Transgene expression was induced by crossing pUASP transgenic flies to the NGV driver line [334].

2.6.4 Embryo Viability Tests

The hatching frequency of *OreR*, *cen*^{f04787}, *cen-RNAi*, and *ik2-RNAi* embryos was determined by counting the number of embryos that hatched on apple juice plates at 25°C of a three day time frame. Three independent experiments were conducted, each of which had two replicate plates contained 120 embryos each.

2.6.5 RT-qPCR

Total RNA was isolated from homogenized embryos using TRIzol reagent according to manufacturer's protocol (Life Technologies, Inc). Complementary DNA was generated using random hexamers, oligo dT and MMLV reverse transcriptase (Invitrogen) using 500ng of total RNA from each sample. Quantitative PCR (qPCR) analysis was performed with gene-specific primer pairs (**Table S2**), using the Power up™ SYBR® green Master Mix (Applied Biosystems) on an ABI ViiA7 instrument (Life Technologies, Inc). Each reaction was carried out in duplicates and three independent experiments were run. RPL32, RPL23, or RPL49 were used as an internal control.

2.6.6 Probe Synthesis For FISH

DNA templates to synthesize RNA probes were obtained from PCR amplification from the *Drosophila* Gene collection cDNA clones (cen= LD41224, ik2= SD10041). For *Simulans*, *Virilis,* and *Mojavensis* flies, templates were made by PCR amplification from

cDNA prepared from embryo total RNA samples. The GFP probe template was produced by PCR amplification of the GFP sequence. All probe templates were designed to be flanked by T7, T3 or SP6 promoter sequences, using the PCR primers listed in the **Table S3**. Each amplified DNA template was gel purified using Qiagen extraction kits and ethanol precipitated. From these templates, antisense RNA probes were synthesized by *in vitro* transcription in the presence of Dig-UTP nucleotide labeling mix with T7, T3 or SP6 RNA polymerases at 37°C for 4-12h. Transcription reactions were subsequently precipitated, dosed and stored at -80°C.

2.6.7 Immunofluorescence and FISH

Embryos were harvested from population cages, and processed for IF and FISH as described previously [125]. Briefly, embryos were harvested, dechorionated with 3% bleach, fixed with 4% paraformaldehyde (PFA) in a 25% PBS and 75% heptane mixture for 20 min, transferred to a 50:50 methanol:heptane mixture to crack vitelline membranes, then stored in methanol at -20°C.

For IF using cen-N-terminal (Dilution 1/25) or γ tubulin (Dilution 1/25) antibody, stored embryos were rehydrated into PBT (1X PBS, 0.1% Triton-X), they were then saturated with PBT + 2% BSA (PBTB) for 1h and incubated with appropriate primary antibodies overnight at 4°C on a nutator. After 5 washes with PBTB, samples were incubated with appropriate species-specific secondary antibodies for 2h at room temperature (RT), followed by an additional series of PBTB washes. The DAPI staining was performed during the last PBTB washes, after which the samples were mounted in a DABCO solution (2.5% DABCO, 70% Glycerol, 1X PBS).

For the Ik2 antibody, a tyramide amplification protocol was adapted from Perkin Elmer. The embryos were washed with PBT for 5 min each time on a nutator. Next, the embryos were blocked with PBTB for 1 h on a nutator. Next, the Ik2 antibody (Dilution 1/5) was diluted in PBTB and the embryos were incubated at 4°C overnight on a nutator. The next day, the embryos were washed with PBTB for 5 min each time on a nutator. The HRP conjugate antibody (Dilution 1/100) was diluted in PBTB for 1.5 hours. Next the

embryos were washed with PBTB for 5 min each time on a nutator. Next, the embryos were washed once with PBT and PBS respectively for 5 min on a nutator. Next, the embryos were incubated with the Cy3 tyramide antibody (Dilution 1/50). The embryos were incubated for 1.5 h. Next, the embryos were washed 6 times with PBS for 5 min each time on a nutator. The embryos were counterstained with DAPI (dilution 1/1000) during the first wash. Lastly, the samples were mounted with DABCO.

For FISH, embryos were rehydrated with successive washes of methanol, methanol:PBT (50:50) and PBT. After another 4% PFA fixation, the embryos were washed 3 times with PBT and incubated with 3 µg/mL of Proteinase K in PBT for 10min at RT and 1h on ice. Proteinase K was removed and embryos were rinsed twice with 2 mg/mL of glycine and 3 times with PBT. Embryos were fixed again with 4% PFA, rinsed 3 times with PBST and once with PBT:hybridization solution (50:50). In parallel, 100 µL per sample of hybridization (Hyb) solution (50% Formamide, 5× SSC, 0.1% Tween-20, 100 µg/mL Heparin and 100 µg/mL salmon sperm DNA) was boiled at 85°C for 5 min and then cool on ice for 5 min. Washes were removed and embryos were pre-hybridized with the boiled Hyb Solution at 56°C for 2h in a bead bath. For each sample, ~100ng of probe were diluted in 100µL of Hyb solution and boiled at 80°C for 3 min. After 2h, the pre-hyb was replaced with the probe solution and the samples were incubated overnight at 56°C in a bead bath. The next day, samples were successively washed with Hyb solution, Hyb:PBT (75:50,50:50, 25:75) and PBT in the bead bath. Embryos were then saturated with PBT + 1% non-fat dry milk (PBTM) for 15 min with shaking on a nutator and incubated with a biotinylated mouse Anti-Dig antibody (Dilution 1/400) for 2h in PBTM. After 5 x 8min washes, the embryos were then incubated on a nutator at RT with streptavidin-HRP reagent (Dilution 1/100) in PBTM for 2h. Finally, following several PBTM washes, the samples were incubated with Tyramide-Cy3 (Dilution 1/50) from the TSA Kits (Perkin Almer) for 2h, prior to washing them in PBT and their storage in DABCO mounting solution.

For single molecule FISH, the embryos were processed as described above, consistent with recommendations from a recently published protocol [335]. The main

difference was the inclusion of custom fluorescently-labelled Stellaris tiling oligonucleotide DNA probes (**Table S4**) targeting *cen* and *ik2* mRNAs, which were designed using the Stellaris Probe Designer tool, and used at a final concentration of 1-2μM respectively in smFISH hybridization solution (2X SSC, 10% formamide, 10% dextran sulfate, 100 μg/mL salmon sperm DNA, 100 μg/mL *E.coli* tRNA, 2mM BSA, and 2mM VRC). The embryos underwent one wash in methanol, two washes in a 1:1 mixture of methanol and PBT and two washes in PBT respectively for 5 min on a nutator. Next, the embryos were fixed with a final concentration of 3.7% formaldehyde in PBS on a nutator for 20 min. The embryos were washed three times with PBT on a nutator for 2 min each time. Next, proteinase K (3μg/mL) was added to the samples and incubated for 13 min at RT, inverting the tubes frequently. Next, the samples were placed on ice for 1 h, and the samples were inverted every 15 min. The embryos were washed twice with glycine (2mg/mL) for 2 min each time on a nutator to inactivate the proteinase K. The embryos were washed with PBT for 2 min each time on a nutator. Next, the embryos were again fixed with a final concentration of 3.7% formaldehyde on a nutator for 20 min. Next, the embryos were washed 5 times with PBT on a nutator for 2 min. Next, the samples were incubated in prehybridization solution (10% formamide and 2x SSC) for 10 min. Lastly, the embryos were placed in hybridization solution. After overnight hybridization of embryos at 37°C, the samples were washed with pre-hybridization buffer for 15 min twice at 37°C. Lastly, the samples were washed twice with PBS for 1 h on a nutator followed by DAPI staining. The samples were mounted with DABCO mounting solution. For smFISH experiments on ovary specimens, we followed recently detailed procedures [336]. Briefly, ovaries were dissected from well-fed females in PBS, followed by a fixation consisting of 3.7% formaldehyde in PBS containing 0.1% DEPC and 1% DMSO on the nutator at RT for 1 h. The specimens were then rinsed three times in PBS for 5 min each time on a nutator at RT and dehydrated in dilutions successive PBS:ethanol solutions at 1:3, 1:1, 3:1 and 100% ethanol, with subsequent storage at -20°C.

For RNA-protein co-stainings, IF was performed before the FISH procedure, as previously described [171]. After rehydration, embryos were saturated for 20 min at RT with PBT containing 50 μg/mL Heparin and 250 μg/mL tRNA. All the antibodies

incubations and washes were performed in presence of RNaseOUT (Invitrogen). After IF, the fluorescent signal was fixed for 20 min on a nutator at RT with a PBT solution containing 10% PFA, then the embryos were washed with PBT and used for the FISH procedure.

2.6.8 Microscopy

Samples were imaged on a Leica DM5500B microscope (Leica Microsystems, Canada) equipped with a QImaging Exi Aqua camera (QImaging), on a Zeiss LSM700 confocal microscope or on a Zeiss Elyra super resolution microscope (Carl Zeiss Canada Ltd). Images were collected on the Zeiss LSM700 confocal laser-scanning microscope or on the Leica DM5500B microscope. Figures were constructed using Photoshop and Illustrator (Adobe Systems Inc).

2.6.9 Drug Treatments

Staged 0-4h *OreR* embryos were collected and treated with harringtonine or emetine dihydrochloride diluted in Robb's solution to a final concentration of 100μM. Following dechorionation, the embryos were placed into a 1:1 mixture of heptane and Robb's solution with the appropriate drug or an equivalent volume of vehicle DMSO. The embryos were incubated on a nutating mixer at RT for 15 min, after which they were fixed by addition of formaldehyde to a 3.7% final concentration while shaking on a vortex mixer for 15min at the lowest setting and processed as described above for storage in methanol at -20°C until further use. FISH analyses were then conducted as detailed above.

2.6.10 Puro-PLA and Immunostaining

Puro-PLA was performed essentially as previously described [337], with several modifications tailored to *Drosophila* embryos. To begin, embryos were harvested and dechorionated, as detailed above, and were transferred to a 1:1 heptane and Robb's solution mixture containing appropriate protein synthesis inhibitor compounds. To conduct puromycylation, 50μg/mL of puromycin was added to the heptane:Robb's solution mixture, contrasted to a 'no puro' control sample processed in parallel, both of which were incubated for 5min on a nutator at room temperature. For the anisomycin

control, embryos were first pretreated with 100μM of anisomycin for 15min in the heptane:Robb's solution mixture, prior to the addition for puromycin for an addition 5min. The embryos were then immediately fixed by addition of PFA to a 4% final concentration for 20min on a vortex at the lowest setting, transferred to a 1:1 methanol:heptane mixture and vigorously shaken for 30sec to crack the vitelline membranes, washed and stored in methanol until further use. Upon retrieval from storage, the embryos were rehydrated and washed 3x in PBT, incubated in Duolink blocking solution for 1h at 37°C and then incubated with rabbit anti-Cen [338] and mouse anti-puromycin (Millipore) antibodies for 1.5h in Duolink antibody diluent (Sigma) at room temperature. Following 2x 5min washes with Duolink wash buffer, anti-rabbit PLAplus and anti-mouse PLAminus probes (Sigma) were added (diluted 1:40 in Duolink antibody diluent) and incubated at 37°C for 1h. Following 2x 5min washes, the Duolink Detection reagents Orange (Sigma) were added for the ligation and amplification steps of the PLA, according to company recommendations, with the amplification step running overnight at 37°C. Upon completion of Puro-PLA, embryos were immune-labelled with donkey anti-rabbit Alexa Fluor 488 secondary antibody (Invitrogen) for 1h in PBTB. Embryos were subsequently stained with DAPI (Invitrogen) and washed 3 x 30min with PBT,and mounted in DABCO mounting medium. Samples images were captured using the Zeiss LSM 700 confocal microscope with a 40x oil objective and a pinhole setting of 1AU.

2.6.11 RNA Capture Experiments

For *in vitro* RNA interaction experiments, the CR+3'UTR or CR alone (3'UTR truncated) versions of *cen* and *ik2* mRNAs were synthesized by *in vitro* transcription using T7 RNA polymerase (NEB). To make DNA templates, *GFP-cen-CR+3'UTR* or *GFP-cen-CR* pGem4 fusion plasmids, or non-GFP fused expression vectors for *ik2-CR+3'UTR* or *ik2-CR* were used. The *in vitro* transcriptions of GFP-cen RNAs were performed with of Biotin-16-UTP (Roche) containing NTP mix, to generated biotinylated mRNA products, whereas the *ik2* RNA variants were synthesized with regular NTPs. For the binding assays, 0.5ug of each appropriate *in vitro* transcribed RNA species were mixed and incubated in 50uL of dimerization buffer (50mM cacodylate, 300mM KCl, 5mM $MgCl_2$, and 0.1U/uL RNaseOUT) for 30min. Psoralen (40μg/mL, Sigma) was then added to the

RNA binding reactions and incubated for 15min on ice in the dark. The samples were then transferred to a 96-well plate on an icy tray and UV cross-linked at 365nm for 15min in a Stratalinker apparatus (Analytik Jena, Upland CA, USA). The samples were then mixed with streptavidin magnetic beads for 15min at RT. To avoid the nonspecific binding, 1mg/mL of tRNA and 5µg/mL of sheered salmon sperm DNA were added to the buffer. Bound RNAs were eluted with a 95% formamide /10mM EDTA buffer at 90°C for 5min, and input and pull downed RNAs were subjected to RT-qPCR analysis.

For RNA capture experiments on embryo extracts, staged 0-4h embryos were collected and lysed by douncing in 250µL of lysis buffer (50mM Tris-HCl pH 7.5, 1mM EDTA, 150mM KCl, 0.5 % Triton X-100, 0.1 U/µL RNaseOUT and protease inhibitors). After two centrifugations at 10,000 rpm for 10 min at 4°C, 100µg of cleared lysate was used for each pull-down. Samples were completed up to 200µl with lysis buffer and 100µl of hybridization buffer (500mM NaCl, 1% SDS, 100mM Tris-HCl pH 7.0, 10mM EDTA, 15% formamide with fresh 1mM DTT, 0.1 U/µL RNaseOUT and protease inhibitors) containing 100 pmol of biotinylated probe was added. Reactions were incubated for 4h at 37°C with rotation before being mixed with BSA- and tRNA-saturated streptavidin magnetic beads (Invitrogen) for 1h at 37°C. Supernatant was removed and beads were washed 4 times with washing buffer (2x SSC, 0.5% SDS, 1mM DTT). Bound RNAs were eluted with 500µL of TRIzol, purified and subjected to RT-qPCR analysis.

2.6.12 Phenotypic counts and RNA expression levels

For the quantifications of RNA expression levels and embryo phenotypic counts, statistical tests were performed using PRISM software (Graphpad). P-values are indicated in each graph and the statistical tests used are indicated in the figure legends.

2.6.13 smFISH Analysis

Analysis on smFISH samples image stacks was performed using IMARIS (Oxford Instruments). Surface masks were created for *cen* particles and spot masks were created for *ik2* particles due to the nature of their shapes respectively. For the *ik2* particle, we set the threshold for the estimated XY diameter to 0.2µM. For both of the mRNA particles,

thresholds were adjusted accordingly to avoid picking up background. Analysis was conducted on all Z-stack slices that encompassed all *cen* particles. After setting the thresholds, the volume of individual *ik2* and *cen* particles, and the number of *ik2* particles that are co-localized with particular *cen* particles, was outputted. Based on these data, we were able to perform calculations on the percentage of co-localizing particles for each mRNA. To control for random co-localization events, we shuffled the *cen* and *ik2* channels from different images and repeated the co-localization analysis.

2.6.14 Analysis of overlapping genes and CeFra-seq data

Transcripts encoded as *cis*-NATs with overlapping sequences in either their 3'UTR, 5'UTR or within gene bodies were retrieved via the UCSC table browser, by selecting for the gene and gene prediction group, Ensembl gene track and filtering for the positive or negative strand into two custom tracks and extracting their intersection. Transcriptomic data for subcellular fractions of *Drosophila* DM-D17-c3 and K562 cells, which were recently characterized [331, 339], were retrieved from the ENCODE portal (https://www.encodeproject.org/) under the experiment ID numbers: ENCSR283YJX (D17-Cytosol-PA); ENCSR053CWY (D17-Membrane-PA); ENCSR622ROA (D17-Cyto-insoluble-PA); ENCSR384ZXD (K562-Cytosol-PA); ENCSR596ACL (K562-Membrane-PA); ENCSR594NJP (K562-Cyto-Insoluble-PA). The distance measurement between two RNAs was derived by summing the absolute values of the differences between their read enrichment scores within each cytoplasmic fraction. For example, assuming transcripts A and B, the $distance = |Ins(A) - Ins(B)| + |Cyt(A) - Cyt(B)| + |Mem(A) - Mem(B)|$. These values range from 0 (perfect co-localisation) to 2 (perfectly asymmetric). For each type of *cis*-NAT classes that were analyzed, while comparative analyses on randomly selected RNA pairs were conducted to assess background distance values.

2.7 Results

2.7.1 The *cen* and *ik2* mRNAs, encoded by 3'overlapping genes, co-localize to centrosomes

In a previous FISH-based screen for localized mRNAs in *Drosophila*, ~30 transcripts were found to localize to structures of the mitotic apparatus (e.g. centrosomes,

astral microtubules and mitotic spindles) and were collectively enriched for functions related to cell division processes [125]. Among these transcripts, the *cen* mRNA, which encodes a coiled-coil domain protein orthologous to human Cerebellar degeneration related-2 [340], shows a striking localization to peri-centrosomal foci and astral microtubule (MT) networks in syncytial stage embryos at different phases of mitosis (**Figure 2.1A**). During interphase, *cen* concentrates within prominent foci in the cortical cytoplasm in close proximity to the centrosomal marker Centrosomin (CNN) (**Supplemental Figure 2.1A**). Cen protein has been reported to exhibit a similar peri-centrosomal localization, while *cen* loss of function leads to mitotic defects (e.g. multipolar spindles) and perturbed actin organization at cleavage furrows in fly embryos [338]. The mRNA encoding Ik2, a protein kinase implicated in cytoskeleton organization [341, 342], was also found to exhibit a centrosome-like pattern in syncytial stage embryos (**Supplemental Figure 2.1B**) and co-labeling of *ik2* and *cen* mRNA by FISH revealed a co-localization of both transcripts within prominent centrosomal foci (**Figure 2.1B**). During late syncytial nuclear divisions, both *cen* and *ik2* mRNAs, as well as their encoded proteins, also tend to display an asymmetric centrosomal localization to one of the two replicated centrosomes (**Figures 2.1C-D**). Intriguingly, the *cen* and *ik2* genes are organized in a tail-to-tail configuration at the same locus on chromosome 2L in *D. melanogaster*, overlapping on opposite DNA strands by 390 nucleotides (nts) at their 3' ends, according to the BDGP-R5/dm3 assembly, or by 59 nts as described in the more recent BDGP-R6 /dm6 assembly **(Figure 2.1C)**. Thus, these distinct mRNAs species, which are expressed as *cis*-NATs, exhibit a striking co-localization to a common cytoplasmic destination.

To assess more clearly the degree of co-localization of *cen* and *ik2* mRNAs, we next performed single-molecule FISH (smFISH) combined with high-resolution structured illumination microscopy (SIM) on syncytial blastoderm embryos (**Figure 2.2A**). Hybridizations were performed with mixtures of 20-nt tiling DNA oligonucleotide probes (48 per transcript) complementary to *cen* (Quasar 670-labelled) or *ik2* mRNAs (Quasar 570-labelled). The cortical cytoplasm of labelled embryos was then imaged as Z-stacks taken at 0.18 µm steps, followed by quantitative image analysis using Imaris software,

which revealed the distribution features of both transcripts. Indeed, *ik2* mRNA formed numerous small foci with consistent size that likely corresponding to individual mRNA molecules (**Figure 2.2A-A''**), ~20% of which co-localized with *cen* mRNA structures (**Figure 2.2B**). By contrast, *cen* mRNA localized within larger, but less numerous, structures of broader volumetric size range (i.e. from 0.025 to 2.3 μm^3), from small particles of similar size to *ik2* mRNA foci, which we attribute to single *cen* mRNA molecules, to larger clusters, ~60% of which were co-localized with *ik2* mRNA foci (**Figure 2.2A-B**). Using the smaller *cen* particles as a reference, we calculated that the larger *cen* aggregates have a volume corresponding to ~20.6 ± 14.3 *cen* molecules. To control for signal co-localization due to chance, comparative analyses were performed on shuffled image sets, which revealed a low level of signal overlap of ~1-2% (**Figure 2.2B**). Finally, as shown in **Figure 2.22C**, we noted a robust correlation between the size of *cen* mRNA clusters and the number of associated *ik2* molecules, whereas shuffled images showed no correlation.

The cytoplasmic pools of *ik2* and *cen* mRNAs appear to be of maternal origin, since neither transcript exhibits the nuclear nascent RNA foci pattern typically observed for zygotically-expressed genes in early embryogenesis. To assess whether these mRNAs are co-localized during their synthesis in oogenesis, we next performed smFISH co-labelling on dissected ovaries, followed by confocal microscopy. This analysis revealed that *cen* and *ik2* mRNAs co-localize at several sites within developing egg chambers (**Figure 2.2D**). Indeed, both transcripts are enriched and co-localized within transcript foci localized in the periphery of ovarian nurse cell nuclei (**Figure 2.2D'**) and within the cytoplasm of stage 8 oocytes (**Figure 2.2D**). Of note, both mRNAs also co-localize within cloudy structures in the nurse cell cytoplasm, a pattern reminiscent of the distribution noted for mitochondria in previous studies [343, 344]. Altogether, these results reveal that the *cen* and *ik2* mRNAs, which are expressed as *cis*-NATs, exhibit a striking co-localization at different stages of development and in different subcellular compartments, from the time of their synthesis in nurse cell nuclei. Their centrosomal co-localization in embryos suggests that the antisense genomic organization of these genes may influence

the downstream cytoplasmic localization properties of their encoded mRNAs, a hypothesis that we explored further.

2.7.2 Centrosomal targeting of *ik2* mRNA is dependent on the presence of *cen* mRNA

To assess whether the centrosomal targeting of *cen* and *ik2* transcripts is inter-dependent, we next evaluated the impact of perturbing either gene on the localization behaviour of both mRNAs. To evaluate the consequences of *cen* perturbation, we analyzed : *i)* homozygous cen^{f04787} mutant embryos, which harbour a coding region transposon insertion that disrupts *cen* mRNA expression [338], and *ii)* embryos in which *cen* mRNA was depleted by RNA interference (RNAi) via inducible expression of a *cen*-targeting hairpin RNA (hpRNA) in the female germline with the Gal4-UAS system [250], using the *nanos-Gal4-VP16* (*NGV*) driver [334]. Because *ik2* mutations disrupt oogenesis and prevent embryo harvesting [345], an hpRNA-mediated RNAi strategy was also used to disrupt *ik2* expression. As shown in **Figure 2.3A**, RT-qPCR analysis of cen^{f04787}, *cen-RNAi* or *ik2-RNAi* embryos revealed a selective and near complete loss of *cen* or *ik2* mRNA expression, respectively, without affecting expression of the neighbouring gene.

Phenotypically, disruption of *cen* or *ik2* strongly impaired viability, as assessed by measuring embryo-hatching frequencies (**Figure 2.3B**). Moreover, these specimens displayed a variety of abnormalities (**Supplemental Figure 2.2**), with a majority of mutant embryos exhibiting mitotic (e.g. aberrant mitotic figures, multipolar spindles, asynchronous mitoses) and morphological defects (e.g. abnormal yolk nuclei, enhanced nuclear fallout and misshapen embryos) (**Figure 2.3C**). Strikingly, in addition to confirming a loss of *cen* mRNA expression, FISH analysis of *cen*-deficient embryos revealed a disruption in the centrosomal localization of *ik2* mRNA, which became diffusely localized to the yolk region of the embryo (**Figure 2.3Di-ii**). By contrast, while we observed a disruption in the expression and centrosomal targeting of *ik2* mRNA in *ik2-RNAi* embryos, the localization of *cen* mRNA was normal in these samples (**Figure 2.3Diii**). Consistent with the observed effects on mRNA localization features, perturbation of *cen* also disrupted the centrosomal-like patterns of Cen and Ik2 proteins (**Figure 2.3E**).

We conclude that centrosomal targeting of *ik2* mRNA depends on the presence of the *cen* transcript, suggesting that *cen* mRNA is the main driver of this co-localization

2.7.3 Evolutionary conservation of *cen* and *ik2* localization in different *Drosophila* species

We next investigated the evolutionary conservation of *cen* and *ik2* mRNA localization properties across *Drosophila* species. Inspection of the genomic sequences of various drosophilids reveals a physical linkage of *cen* and *ik2* orthologs in species closely related to *D. melanogaster (D.mel)*, such as *D. simulans (D.sim)*, while these genes are on different chromosomes in more distant relatives, such as *D. mojavensis (D.moj)* and *D. virilis (D.vir)* (**Figure 2.4A-B**). Notably, orthologs of the genes neighbouring the *cen*/*ik2* locus in *D. mel*, namely *CG31678*, *CG2617* and *hr38*, are associated with *ik2* in *D. moj* and *D. vir*, but not with *cen* (**Figure 2.4B**). The expression levels of *cen* and *ik2* mRNAs in early stage embryos were comparable across species, as assessed by RT-qPCR analysis (**Fig. 2.4C**). As shown in **Fig. 2.4D** (upper panels), the peri-centrosomal foci localization of *cen* orthologs is clearly observed in *D. sim* and *D. moj*, while the *D.vir* ortholog shows an apically-enriched microtubule-like pattern that is reminiscent of, but more diffuse than *cen* in *D.mel*. By contrast, *ik2* targeting centrosome-like foci is observed in *D. sim*, where the *cen* and *ik2* genes are linked, but not in *D. moj* and *D. vir*, in which they are separated (**Fig 2.4D**, lower panels). These results suggest that the *cen* mRNA harbours conserved determinants for centrosomal localization and that the capacity of *ik2* mRNA to target to centrosomes was acquired evolutionarily following association of the *cen* gene with the *ik2* locus.

2.7.4 Sequence determinants of *cen* and *ik2* mRNA localization

To delimit the regions of *cen* and *ik2* mRNAs required for peri-centrosomal targeting, we next conducted *in vivo* structure-function analyses through site-specific transgenesis [346]. Transgenes were constructed in which the *GFP* mRNA coding sequence was fused in 5' to the coding region + 3'UTR (CR+3'UTR), coding region alone (CR) or the 3'UTR of either *cen* or *ik2* mRNAs. These transgenic GFP fusion cassettes were then placed under control of a UAS promoter, enabling us to induce their expression

in the female germline by crossing them to the *NGV* driver line (**Fig. 2.5A-B**). All transgenes were inserted in the same genomic landing site on chromosome 3L, at cytological position 65B2, and they were all efficiently expressed as assessed by RT-qPCR (**Supplemental Figure 2.3A-C**). FISH analysis of transgenic *GFP-Cen* fusion mRNAs, using a *GFP* sequence probe, revealed the robust centrosomal targeting of the *GFP-cen-CR+3'UTR* and *GFP-Cen-CR* transcripts, but not of *GFP-Cen-3'UTR* for which the localization was similar to *GFP* mRNA (**Figure 2.5Ai-ii**). These results indicate that *cen* localization to centrosomes is independent of its 3'UTR, but rather relies on determinants present in its coding region.

By contrast, FISH of *GFP-ik2* transcripts revealed that its centrosomal localization is dictated by its 3'UTR sequence, whereas its coding region is dispensable **(Figure 2.5Aiii**). Refined sequence truncation analyses, starting from the longer *ik2* 3'UTR sequence initially described in the BDGP genomic Release 5, identified a 114 nt region important for the centrosomal targeting of transgenic *GFP* fusion mRNA (**Figure 2.5B**). This sequence spans the region of overlap between *cen* and *ik2* transcripts in the shorter 3'UTR sequence defined in the BDGP genome Release 6 (**Supplemental Figure 2.3D**). Inspection of the *ik2* 3'UTRs of *Drosophila* orthologues reveals a close sequence conservation in *D. melanogaster* and *D. simulans*, in particular within the regions of antisense complementary with the *cen* 3'UTR, but a high sequence divergence in *D. mojavensis* and *D. virilis* (**Supplemental Figure 4**). Since *ik2* requires the presence of *cen* mRNA for its localization, our data suggest that the 3'UTR overlapping segment likely mediates base pairing interactions that allow co-targeting with *cen* mRNA. Moreover, since this co-targeting can occur in *trans*, i.e. with a *GFP-ik2-3'UTR* mRNA expressed from a different chromosome, we also conclude that genomic proximity of *cen* and *ik2* genes is not required for their co-localization, but rather the evolutionary acquisition of sequence complementarity is likely to be critical.

2.7.5 The *cen* and *ik2* mRNAs physically associate *in vitro* and *in vivo*

The requirement of *cen* expression for proper *ik2* mRNA targeting suggests that these transcripts may physically associate to enable their co-localization. We first sought

to assess whether *cen* and *ik2* mRNAs can interact *in vitro* and whether this interaction could be mediated by their complementary 3'UTR sequences (**Figure 2.5C**). For this, we synthesized versions of *cen* and *ik2* mRNAs bearing the coding region and 3'UTR (*Cen/Ik2-CR+3'UTR*) or coding region alone (*Cen/Ik2-CR*) of each transcript, with the *cen* variants having been labelled with biotin-UTP. After incubating biotinylated *Cen-CR+3'UTR* or *Cen-CR* transcripts with non-biotinylated *Ik2-CR+3'UTR* or *Ik2-CR* in dimerization buffer, psoralen was then added to the reactions followed by UV irradiation at 365 nm to cross-link RNA-RNA complexes. The samples were then purified on streptavidin beads and subjected to RT-qPCR analysis using *ik2* coding region primers. This analysis revealed that the *Cen-CR+3'UTR* mRNA was able to interact and co-purify the *Ik2-CR+3'UTR* transcript, but not *Ik2-CR* (**Figure 2.5C**). By contrast, pull-downs conducted with *Cen-CR* led to a similar low-level co-purification of *Ik2-CR+3'UTR* or *Ik2-CR*. These results reveal that *cen* and *ik2* mRNAs can interact physically *in vitro* in a manner dependent on their 3'UTR sequences.

To test whether these mRNAs could associate physically in a more *in vivo* setting, we next performed RNA pull-down assays using wildtype fly embryo extracts. For this, biotinylated antisense RNA probes, either complementary to endogenously expressed *ik2 or cen* mRNAs, or a *GFP* probe used as a negative control, were incubated with OreR whole-embryo lysates. Labelled probes were then captured with streptavidin beads and associated RNAs identified by RT-qPCR. As shown in **Figure 2.5D**, both *ik2* and *cen* mRNAs were efficiently captured in their respective pull-downs. Moreover, we observed that *cen* mRNA was robustly retained in *ik2* capture samples and vice-versa, that *ik2* mRNA was captured in *cen* pulldowns, although to a much weaker extent. In contrast, control transcripts such as *cyclin B*, another known mitotic mRNA, were not selectively captured with either the *cen* or *ik2* probes. These results indicate that *ik2* and *cen* mRNAs can also physically associate *in vivo* in fly embryos.

To assess whether the 3'UTR-mediated interaction of *cen* and *ik2* mRNAs is functionally important *in vivo*, we next performed genetic complementation assays in which the *GFP-cen-CR+3'UTR* or *GFP-cen+CR* mRNAs, or *GFP* as a negative control,

were expressed in a *cen*^{f04787} (i.e. *cen* $^{-/-}$) mutant background (**Figure 2.5E-F**). Strikingly, immuno-FISH assays to detect *cen* or *ik2* mRNAs in conjunction with the γ-Tubulin centriolar marker revealed that expression of *GFP-cen-CR+3'UTR* rescued the localization of endogenous *ik2* mRNA to peri-centrosomal foci in the embryonic apical cytoplasm (**Figure 2.5E**), as well as the mitotic and morphological defects associated with *cen* loss of function (**Figure 2.5F**). By contrast, *GFP-cen-CR* transgenic mRNA was unable to rescue *ik2* mRNA localization defects in *cen* $^{-/-}$ embryos and displayed a weaker capacity to rescue embryonic phenotypes (**Figure 2.5E-F**). We conclude that the 3'UTR-mediated centrosomal co-targeting of *ik2* and *cen* mRNAs is functionally important *in vivo*.

2.7.6 *cen* mRNA is locally translated at the level of centrosomes and requires intact polysomes to maintain its localization

We next investigated whether centrosomally localized mRNAs undergo localized translation in *Drosophila* embryos. To address this question, we adapted the puromycin-labelling with proximity-ligation assay (Puro-PLA) strategy in fly embryos, a method previously utilized to study localized translation in mammalian neuronal cells [337, 347]. The method first involves treating embryos for a short time (5min) with puromycin, which labels nascent peptide chains, leading to translation termination and the release of truncated proteins, followed by immediate fixation to preserve tissue integrity and the precise localization of molecules (**Figure 2.6A**). Immuno-labelling is then performed with an anti-puromycin antibody, which recognizes puromycylated proteins, and a second antibody targeting a protein of interest. Samples are then labelled with species-specific secondary antibodies that are conjugated to specific oligonucleotide probes that, when located in close proximity, can be hybridized to circle-forming oligonucleotides to allow rolling circle amplification and fluorescence labelling of the amplified product (**Figure 2.6A**). The availability of a rabbit anti-Cen antibody [338], enabled us to implement the Puro-PLA procedure for this protein in syncytial blastoderm stage embryos. As shown in **Figure 2.6Bi**, the Cen/Puro-PLA approach revealed the presence of newly synthesized Cen protein in bright centrosome-like foci within the embryonic cortex. Through addition of a fluorescently labelled anti-rabbit secondary antibody to our completed Cen/Puro-PLA reactions, we were also able to visualize residual Cen protein signal by IF. While the

signals observed for Cen/Puro-PLA versus Cen-IF were generally non overlapping, which we attribute to the competition between secondary antibodies for the same epitopes, several Cen/Puro-PLA foci showed a striking co-localization with Cen-labelled structures (**Figure 2.6Bi**, arrowheads). To confirm labeling specificity, several negative control samples were run in parallel, including: staining of non-puromycin treated embryos (**Figure 2.6Bii**), puromycin-treated embryos that were processed in the absence of Cen antibody (**Figure 2.6Biii**), and embryos that were pre-treated with anisomycin, a translation inhibitor that blocks peptidyl transferase activity within ribosomes, prior to puromycin exposure (**Figure 2.6Biv**). All of these controls showed a loss of Cen/Puro-PLA foci, demonstrating the specificity of the bright centrosome-like PLA signal observed in test specimens (**Figure 2.6Bi**).

Next, we sought to test whether the centrosomal localization of *cen* mRNA is dependent on intact translating polysomes by treating embryos with translation inhibitors. To address this question, we performed FISH analyses on embryos treated with emetine, which stalls translation during elongation and stabilizes polysomes, or with harringtonine, a polysome disruptor that blocks the initiation step of translation [123, 348]. While emetine induced morphological aberrations in a small subset of embryos, the centrosomal localization pattern of *cen* mRNA was similar to untreated or vehicle (DMSO) treated embryos, both during interphase and in mitosis (**Figure 2.6C**). By contrast, exposure to harringtonine led to a marked disruption of *cen* mRNA localization, which became diffusely distributed in the cytoplasm (**Figure 2.6C**). We conclude that the *cen* mRNA can undergo localized translation at the level of centrosomes and that its localization is dependent on the maintenance of intact polysomes, similar to recent observations for centrosomally-localized *pericentrin* (*PCNT*) mRNA in HeLa cells [123].

2.7.7 *Cis*-NATs tend to co-localize in the same subcellular compartment in *Drosophila* and human cells

Finally, we sought to evaluate whether the co-targeting behaviour observed for *cen* and *ik2* may also extend to other transcripts encoded by genes with genomic sequence overlap. To assess if RNAs encoded by overlapping genes have a tendency to co-localize

in the same subcellular compartment, we took advantage of our recently published CeFra-seq datasets, in which we defined the transcriptomic signatures of nuclear, cytosolic, membrane (endomembrane) and cytoplasmic insoluble (cytoskeletal) compartments of fractionated *Drosophila* DM-D17-c3 cells and human K562 cells, via RNA sequencing (**Figure 2.7A**) [331, 339]. From these datasets, we analyzed the cytoplasmic compartment distribution properties of pairs of *cis*-NATs, across all RNA biotypes, for which the genes are arranged either with a 3'End (tail-to-tail), 5'End (head-to-head) or a fully (embedded) overlapping configuration (**Figure 2.7B**). The number of RNA pairs ranged from 100-1391, depending on the type of *cis*-NAT and the species (**Figure 2.7C**). For each RNA pair, we defined a localization distance measure, which conveys the steady-state relative distribution properties of a given pair of RNAs (**Figure 2.7C),**

$$distance\ for\ RNAs\ A\ and\ B = |Ins(A) - Ins(B)| + |Cyt(A) - Cyt(B)| + |Mem(A) - Mem(B)|\ ,$$

by summing up their differences in fraction-specific FPKM expression levels [i.e. ranging from 0 (highly similar) to 2 (highly divergent)]. For each class of *cis*-NAT, we analyzed the distribution of distance scores of all *cis*-NAT pairs, compared to control pairs of an equal number of random RNAs from non-overlapping genes (**Figure 2.7C**). These analyses revealed that, in *Drosophila* D17 cells, transcripts from 3'overlapping or embedded genes exhibit a significantly smaller distance compared to controls. In comparison, interrogation of CeFra-seq data of human K562 cells revealed a highly significant shorter distribution of distance scores for all *cis*-NAT classes. Finally, as an alternative strategy to assess the co-localization behaviour of cis-NATs, we took advantage of recently published datasets by Fazal et al., who developed an ascorbate peroxidase (APEX)-based RNA proximity labeling method, designated APEX-seq, to define subcellular compartment enriched transcriptomes in HEK293T cells [332]. Our analyses of the organelle-specific RNA populations defined by APEX-seq revealed tha*t cis*-NATs with overlapping 3'UTRs are enriched within the 'nuclear' and 'nucleolar' subcellular transcriptomes compared to transcripts encoded by non-overlapping genes located with 10kb of each other (p-value$<$0.05, Fisher exact test). Altogether, our analyses of subcellular transcriptomic datasets generated via orthogonal methodologies indicate that *cis*-NATs tend to co-localize to specific subcellular compartments in human and fly cellular models.

2.8 Discussion

Despite the realization that overlapping transcriptional units represent a pervasive feature of genomes, the biological and mechanistic significance of this organization remains incompletely understood. For instance, while NATs have been found to modulate gene expression at the transcriptional level [319, 320], they can also impact post-transcriptional regulation, notably through the formation of double-stranded RNA leading to RNA masking, RNA interference or RNA editing [313, 349-351]. We report here a post-transcriptional function of NATs in mRNA subcellular localization. Indeed, we show that the *cen* and *ik2* mRNAs, two NATs expressed in *Drosophila melanogaster*, are tightly co-localized to centrosomes in the cytoplasm. We further demonstrate that the centrosomal localization of *ik2* is strictly dependent on *cen* mRNA and requires the 3'UTR overlapping region, which mediates their physical association (as modeled in **Fig. 7D**). More generally, our analyses of subcellular transcriptomics datasets, either based on biochemical cell fractionation or proximity labeling, suggest that the co-localization of *cis*-NATs is a common occurrence in *Drosophila* and human cells.

While several studies have shown that convergent transcription of NATs can lead to inhibitory interactions due to transcriptional interference [320, 352], our findings reveal an alternative scenario in which NATs can impose selectivity in downstream RNA subcellular localization behaviour. Early *Drosophila* embryogenesis may offer a favourable environment for such a regulatory mechanism, considering the diverse RNA populations they contain of either maternal or zygotic origin. The *cen* and *ik2* transcripts undergo co-localization as maternally-provided transcripts in syncytial-stage embryos, after being transcribed from polyploid nurse cells prior to their deposition in the maturing oocyte. While their 3'-overlapping sequence is important for centrosomal targeting of *ik2* mRNA, our transgenic reporter assays revealed that a *gfp-ik2-3'UTR* reporter mRNA can undergo proper localization when expressed in *trans* from a different chromosome landing site. These results are consistent with a previous study in yeast, showing that transcriptional interference mediated by 3'overlapping transcripts could also occur in *trans* [320]. Our findings thus suggest that, in addition to NATs, transcripts containing complementary sequences to other cellular RNAs may influence their subcellular localization properties. Interestingly, emergent methods used to define RNA-RNA

interactomes have shown that *trans*-interactions between mRNA molecules are prevalent in eukaryotic cells [353-356], which may profoundly influence post-transcriptional gene regulation, including RNA subcellular localization.

The number of RNA molecules that are present within RNA transport granules has remained a question of debate. While some studies support the concept that messenger ribonucleoprotein (mRNP) granules contain single mRNA molecules [357, 358], others have reported examples where such granules may contain multiple mRNA species [359]. Previous studies have revealed a role for RNA-RNA interactions in localization control. Indeed, the *bicoid* and *oskar* mRNAs have been shown to localize as homo-dimers in *Drosophila* embryos and oocytes, respectively [193, 360]. Our results define an alternate mechanism of transcript co-targeting mediated by hetero-duplexing of distinct mRNA species, a process that is required to allow centrosomal targeting of *ik2* mRNA in a *cen*-dependent manner. While our data indicate that *cen* and *ik2* co-localize at different subcellular locations during oogenesis and embryogenesis, it is unclear whether this involves a mechanism of co-transport within mobile RNP granules or whether their observed centrosomal co-targeting involves *ik2* mRNA capture by pre-localized *cen* transcripts. It is also unclear whether *cen* and *ik2* centrosomal co-targeting is dependent on direct RNA-RNA interactions between these transcripts or whether their association is mediated by specific protein interactors. Future experiments will aim to clarify these different possibilities.

Several studies in different organisms have characterized mRNAs that are specifically localized to mitotic structures [121, 122, 124, 125, 361-366], leading to different models of the potential functional roles of this process. For example, work in *Ilyanassa* embryos showed that the asymmetric localization of mRNAs to centrosomes provides an elegant mechanism to drive the selective inheritance of specific transcripts between daughter cells during embryonic cleavage divisions [363, 365]. Other mitotic transcripts encode proteins with mitotic related functions [124, 125, 364], implying that they may fulfill more active roles in cell division regulation via localized translation [124]. The possibility of localized translation at the level of the mitotic apparatus is supported by

various lines of evidence, including traditional electron microscopy approaches that revealed the presence of ribosome like particles in proximity to the mitotic spindle and centrosomes[117, 367], as well as more recent transcriptomic and mass spectrometry based approaches that co-purified various RNAs and RNA binding proteins with mitotic structures [121, 299, 368]. Our observations that *cen* and *ik2* mRNAs, as well as their encoded proteins, display peri-centrosomal targeting, combined with our Puro-PLA results, suggest that they undergo localized translation. This would be consistent with the established role of Cen in regulating mitotic spindle and cleavage furrow function [338]. While Ik2 (also known as I-KappaB Kinase Epsilon/IKK-E) has been implicated in various biological processes in *Drosophila*, including cytoskeleton regulation during oogenesis, endosome shuttling and dendritic pruning [341, 342, 345, 369, 370], our work uncovers a role of Ik2 in mitotic regulation, which we speculate may have evolved through the localization properties of its mRNA. Taken together, our findings reveal a mechanism of co-dependent localization of two mRNA species which has been acquired during evolution via genomic sequence reorganisation, leading to a potential acquisition of protein function. Understanding the spatial and temporal dynamics of the translation of centrosomal mRNAs will be an important area of future research.

2.9 Data and Software Availability

Transcriptomic data for subcellular fractions of *Drosophila* DM-D17-c3 and human K562 cells were retrieved from the ENCODE portal (https://www.encodeproject.org/).

2.10 Lead Contact and Materials Availability

Further information and requests for resources and reagents should be directed to and will be fulfilled by the Lead Contact, Eric Lecuyer (eric.lecuyer@ircm.qc.ca).

2.11 Acknowledgments

We thank the Bloomington *Drosophila* Stock Center, the *Drosophila* Species Stock Center, Timothy Megraw, Shigeo Hayashi and Carole Iampietro for fly stocks and antibodies. We thank Dominic Filion for his assistance in microscopy and Odile Neyret, Myriam Rondeau and Agnes Dumont for their help with DNA/RNA sequencing. We thank

Anca Savulescu for advice on RNA pull-downs. We are grateful to Francois Robert, Martin Sauvageau, Nicole Francis and Jonathan Bergeman for helpful comments on the manuscript. J.B. was supported by postdoctoral scholarship from the Fonds de Recherches Québec Santé (FRQS), A.C. holds a Vanier Canada scholarship and E.L is a Senior FRQS research scholar. This work was supported by a grant to E.L. from the Canadian Institutes of Health Research (CIHR).

2.12 Declaration of Interests

The authors declare no competing interests.

2.13 Figures and Figure Legends

Figure 2.1

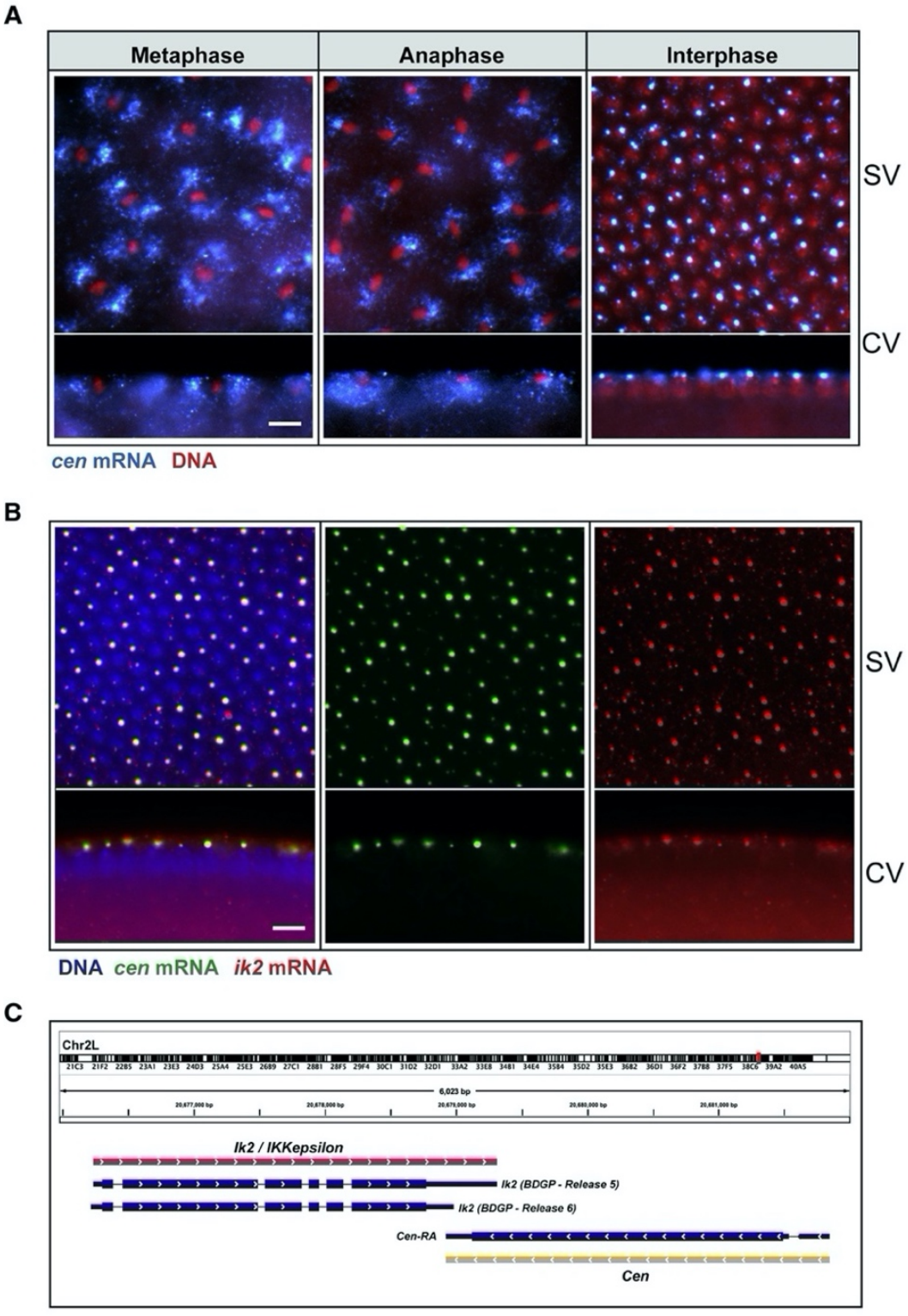

Figure 2.2

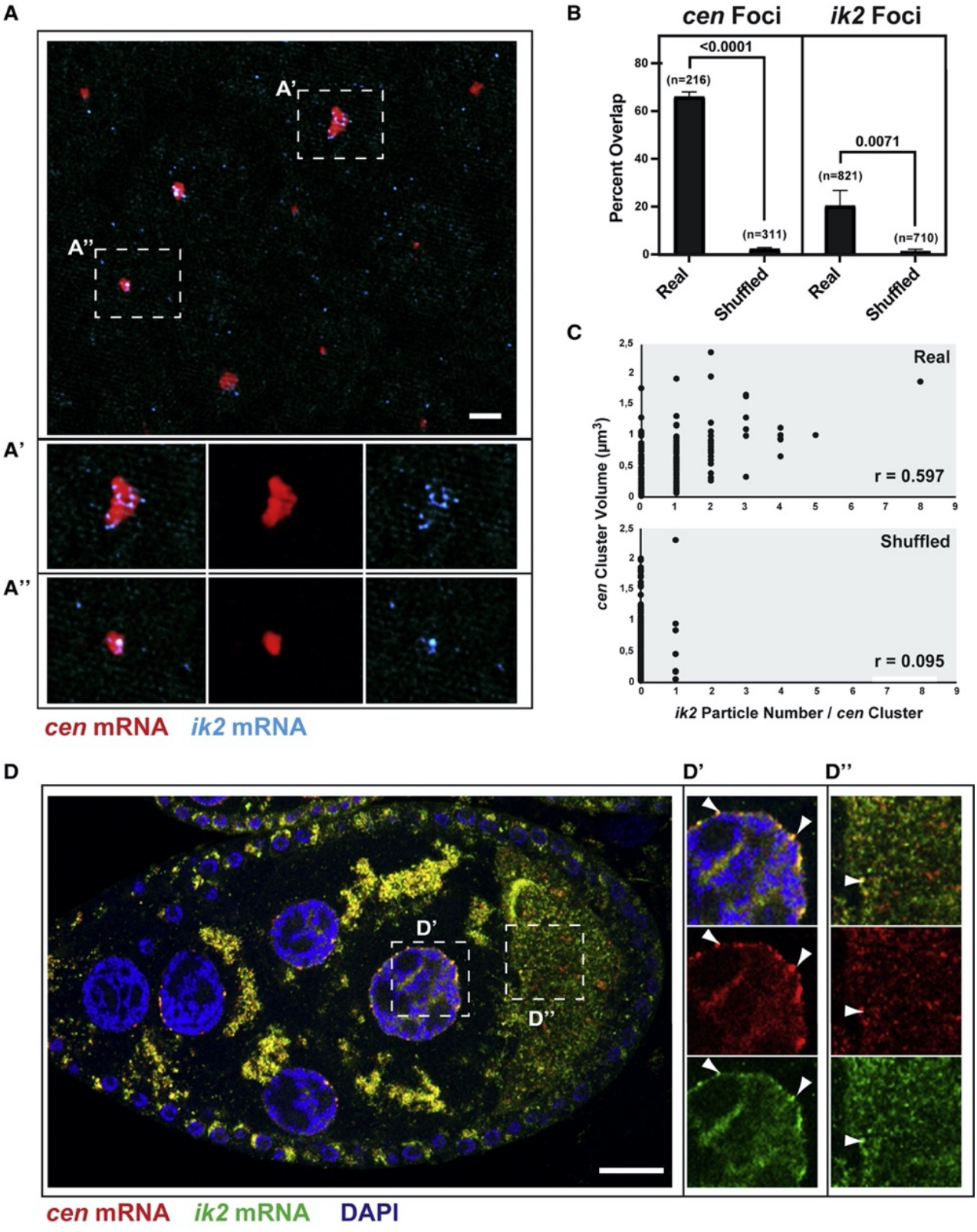
A
A'
A''
cen mRNA ik2 mRNA
B
cen Foci
ik2 Foci
<0.0001
(n=216)
(n=311)
0.0071
(n=821)
(n=710)
Percent Overlap
Real
Shuffled
C
Real
r = 0.597
Shuffled
r = 0.095
cen Cluster Volume (µm3)
ik2 Particle Number / cen Cluster
D
D'
D''
cen mRNA ik2 mRNA DAPI

Figure 2.3

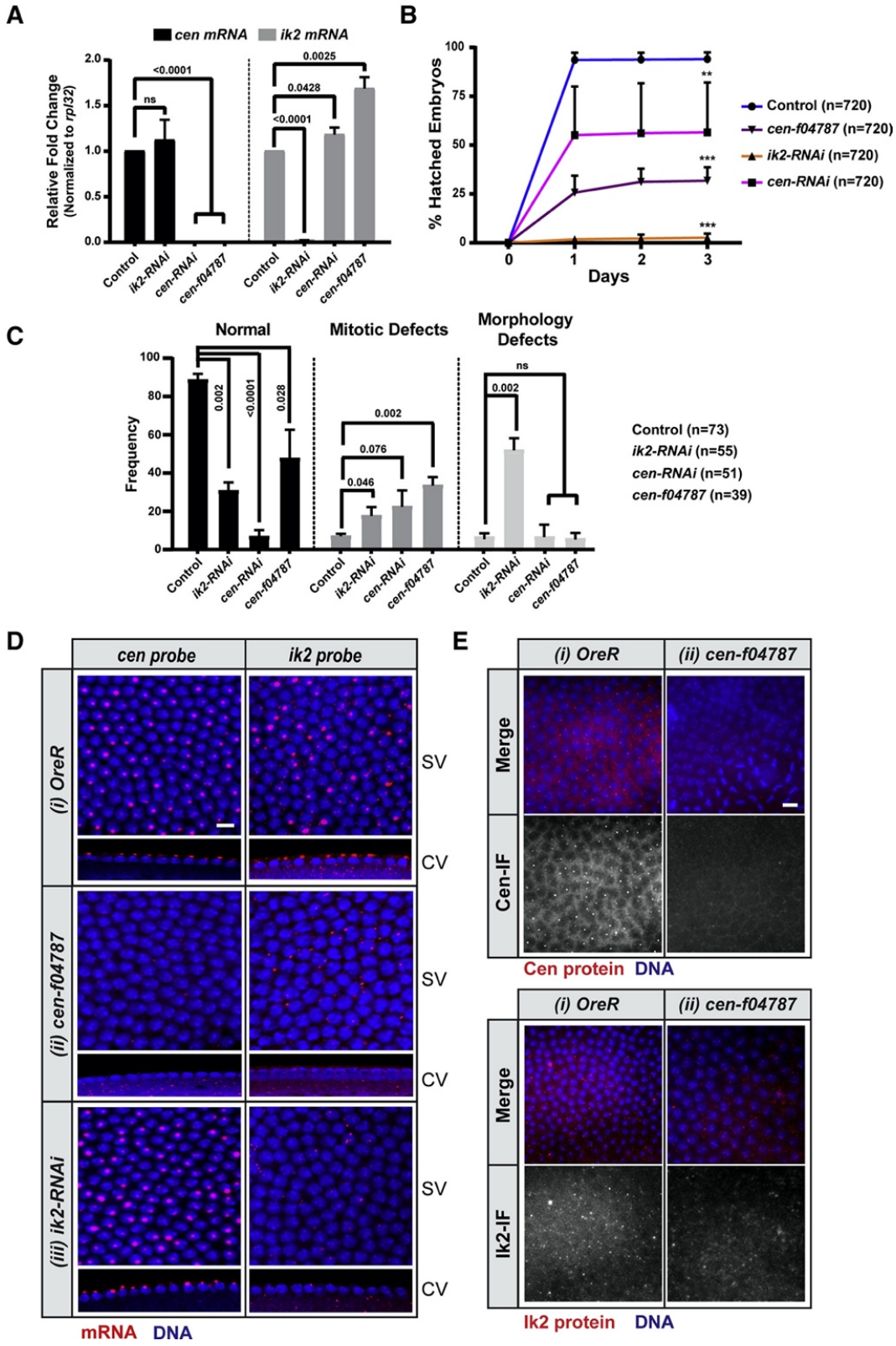
A
cen mRNA
ik2 mRNA
Relative Fold Change (Normalized to rpl32)
<0.0001
ns
0.0025
0.0428
<0.0001
Control
ik2-RNAi
cen-RNAi
cen-f04787
B
% Hatched Embryos
Days
Control (n=720)
cen-f04787 (n=720)
ik2-RNAi (n=720)
cen-RNAi (n=720)
C
Normal
Mitotic Defects
Morphology Defects
Frequency
0.002
<0.0001
0.028
0.076
0.046
Control (n=73)
ik2-RNAi (n=55)
cen-RNAi (n=51)
cen-f04787 (n=39)
D
cen probe
ik2 probe
(i) OreR
(ii) cen-f04787
(iii) ik2-RNAi
SV
CV
mRNA DNA
E
(i) OreR
(ii) cen-f04787
Merge
Cen-IF
Cen protein DNA
Ik2-IF
Ik2 protein DNA

Figure 2.4

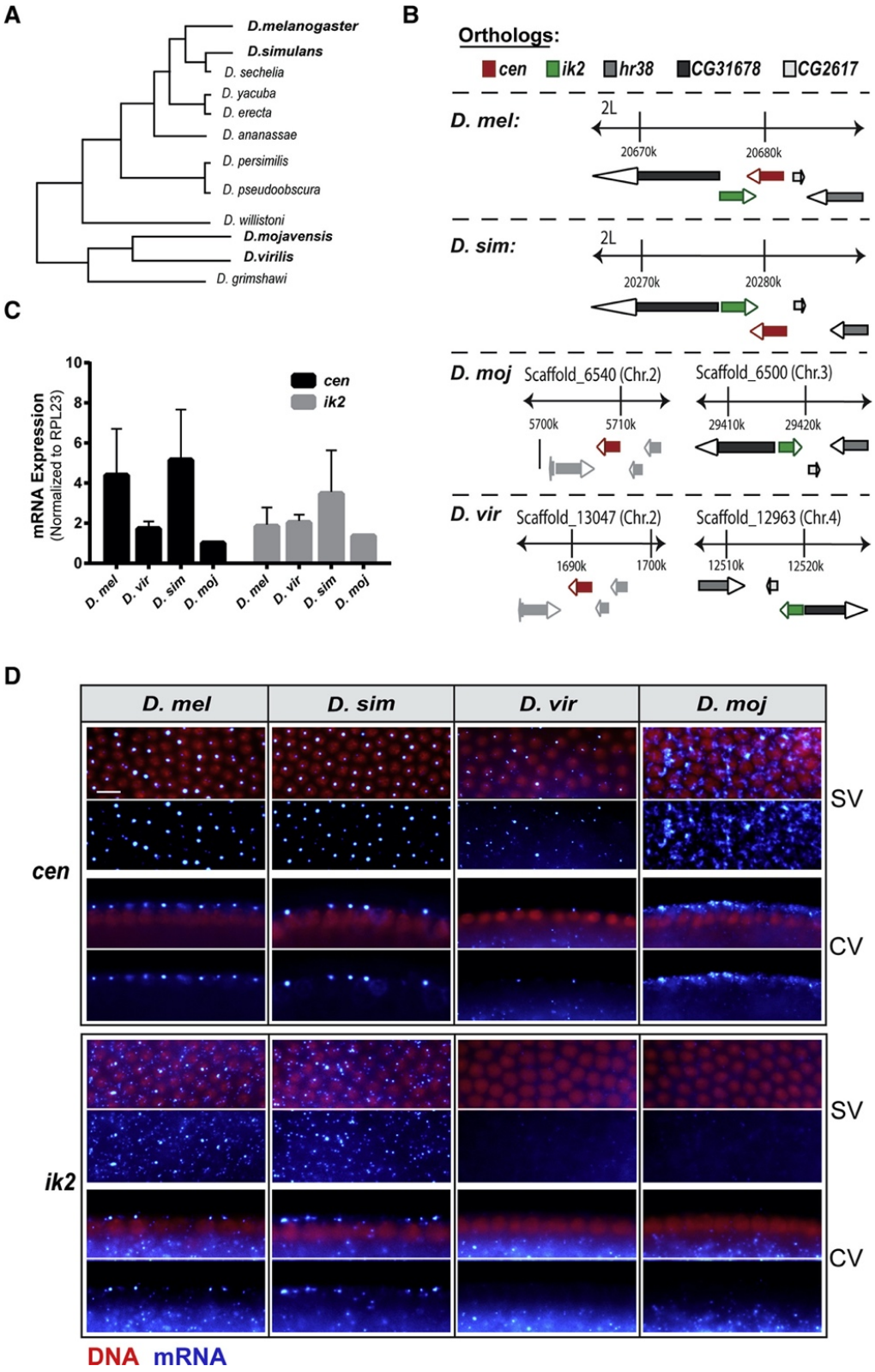
A
D.melanogaster
D.simulans
D. sechelia
D. yacuba
D. erecta
D. ananassae
D. persimilis
D. pseudoobscura
D. willistoni
D.mojavensis
D.virilis
D. grimshawi
B
Orthologs:
cen
ik2
hr38
CG31678
CG2617
D. mel:
2L
20670k
20680k
D. sim:
2L
20270k
20280k
D. moj
Scaffold_6540 (Chr.2)
5700k
5710k
Scaffold_6500 (Chr.3)
29410k
29420k
D. vir
Scaffold_13047 (Chr.2)
1690k
1700k
Scaffold_12963 (Chr.4)
12510k
12520k
C
mRNA Expression
(Normalized to RPL23)
cen
ik2
D. mel
D. vir
D. sim
D. moj
D
D. mel
D. sim
D. vir
D. moj
cen
ik2
SV
CV
SV
CV
DNA mRNA

Figure 2.5

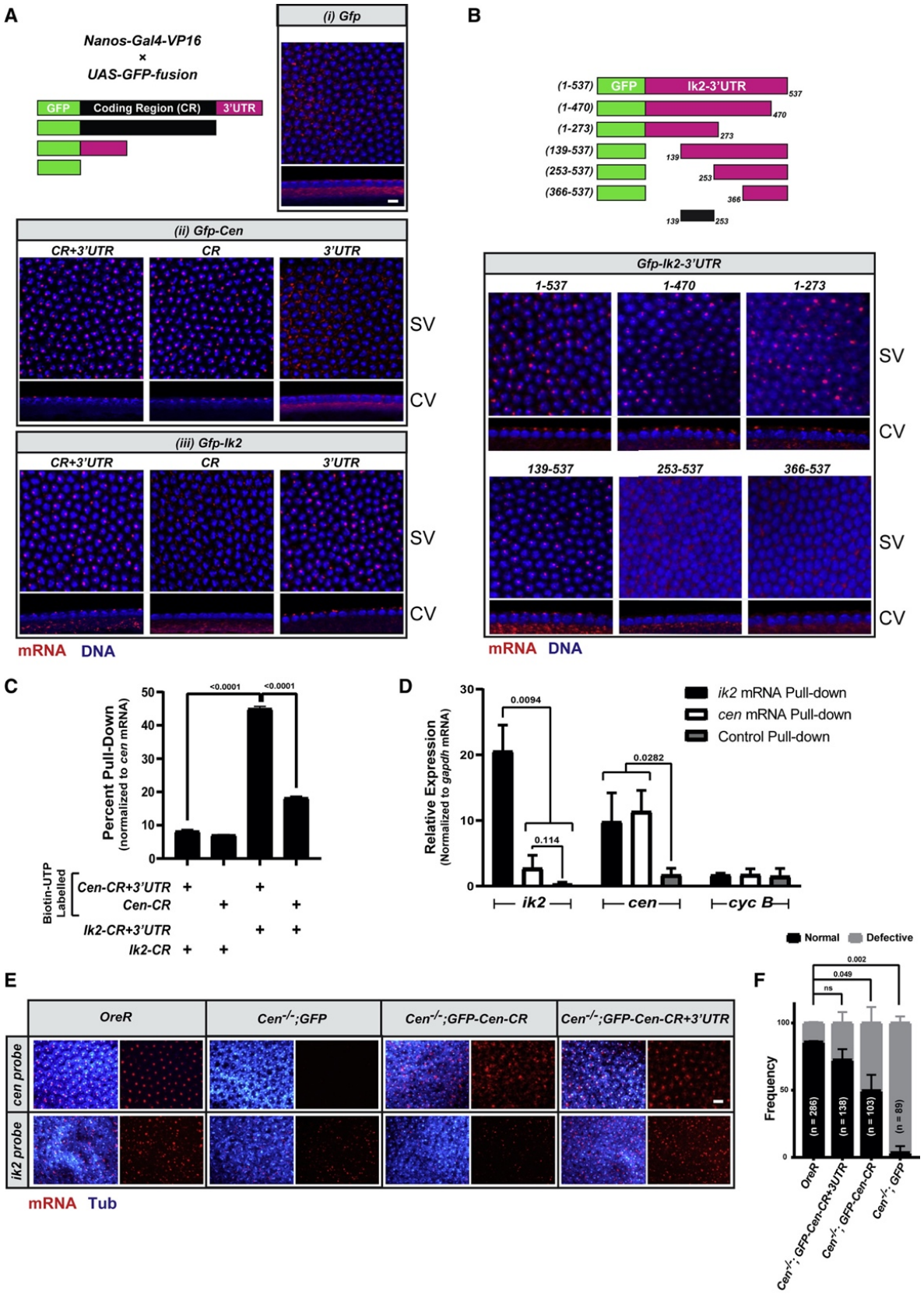
A
Nanos-Gal4-VP16
×
UAS-GFP-fusion
GFP
Coding Region (CR)
3'UTR
(i) Gfp
(ii) Gfp-Cen
CR+3'UTR
CR
3'UTR
SV
CV
(iii) Gfp-Ik2
CR+3'UTR
CR
3'UTR
SV
CV
mRNA DNA
B
(1-537) GFP Ik2-3'UTR 537
(1-470) 470
(1-273) 273
(139-537) 139
(253-537) 253
(366-537) 366
139 253
Gfp-Ik2-3'UTR
1-537
1-470
1-273
SV
CV
139-537
253-537
366-537
SV
CV
mRNA DNA
C
Percent Pull-Down
(normalized to cen mRNA)
<0.0001
<0.0001
Biotin-UTP Labelled
Cen-CR+3'UTR
Cen-CR
Ik2-CR+3'UTR
Ik2-CR
D
Relative Expression
(Normalized to gapdh mRNA)
ik2 mRNA Pull-down
cen mRNA Pull-down
Control Pull-down
0.0094
0.114
0.0282
ik2
cen
cyc B
E
OreR
Cen-/-;GFP
Cen-/-;GFP-Cen-CR
Cen-/-;GFP-Cen-CR+3'UTR
cen probe
ik2 probe
mRNA Tub
F
Normal
Defective
0.002
0.049
ns
Frequency
(n = 286)
(n = 138)
(n = 103)
(n = 89)
OreR
Cen-/-; GFP-Cen-CR+3UTR
Cen-/-; GFP-Cen-CR
Cen-/-; GFP

Figure 2.6

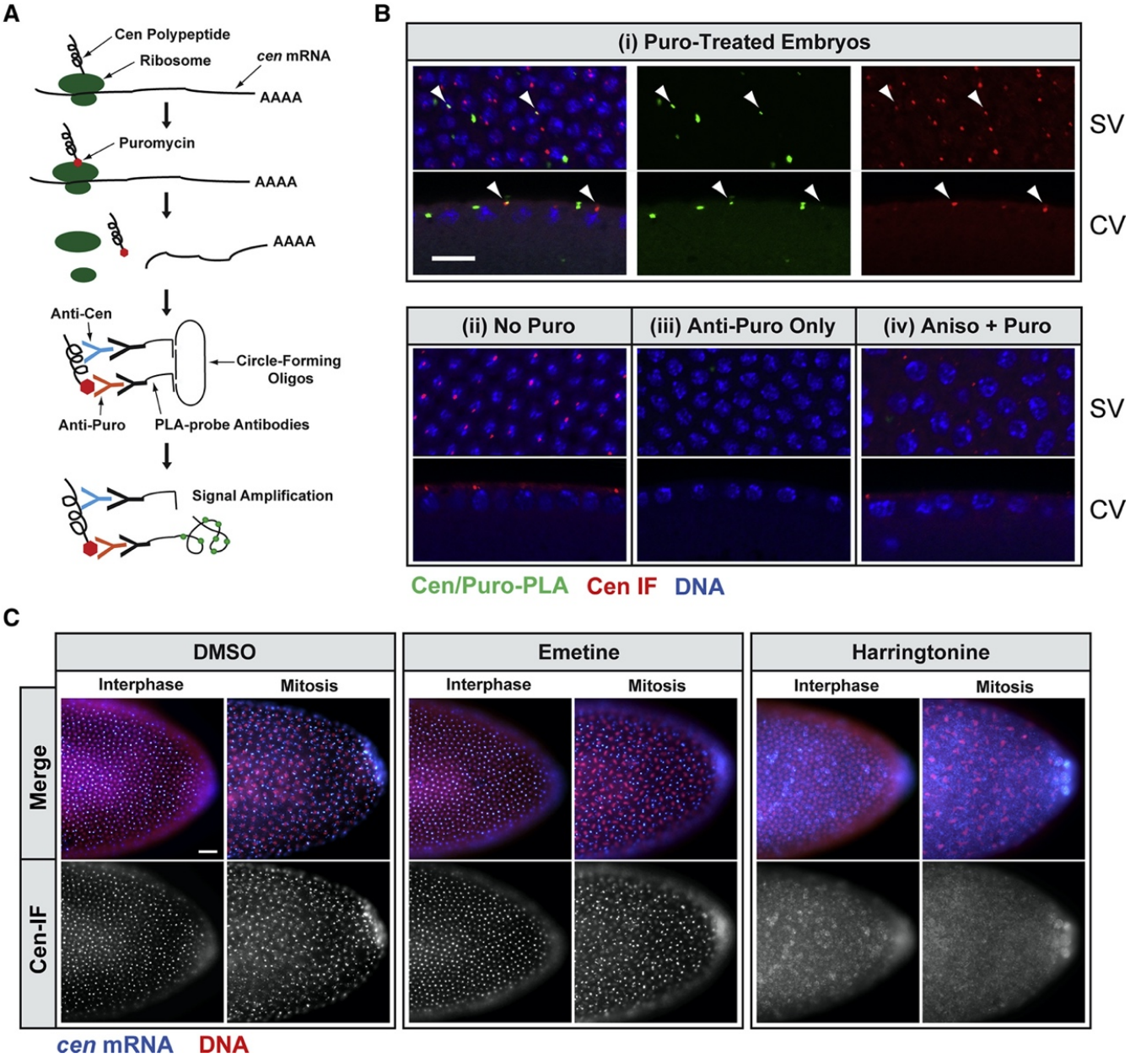
A
Cen Polypeptide
Ribosome
cen mRNA
AAAA
Puromycin
AAAA
AAAA
Anti-Cen
Circle-Forming Oligos
Anti-Puro
PLA-probe Antibodies
Signal Amplification
B
(i) Puro-Treated Embryos
SV
CV
(ii) No Puro
(iii) Anti-Puro Only
(iv) Aniso + Puro
SV
CV
Cen/Puro-PLA Cen IF DNA
C
DMSO
Emetine
Harringtonine
Interphase
Mitosis
Merge
Cen-IF
cen mRNA DNA

Figure 2.7

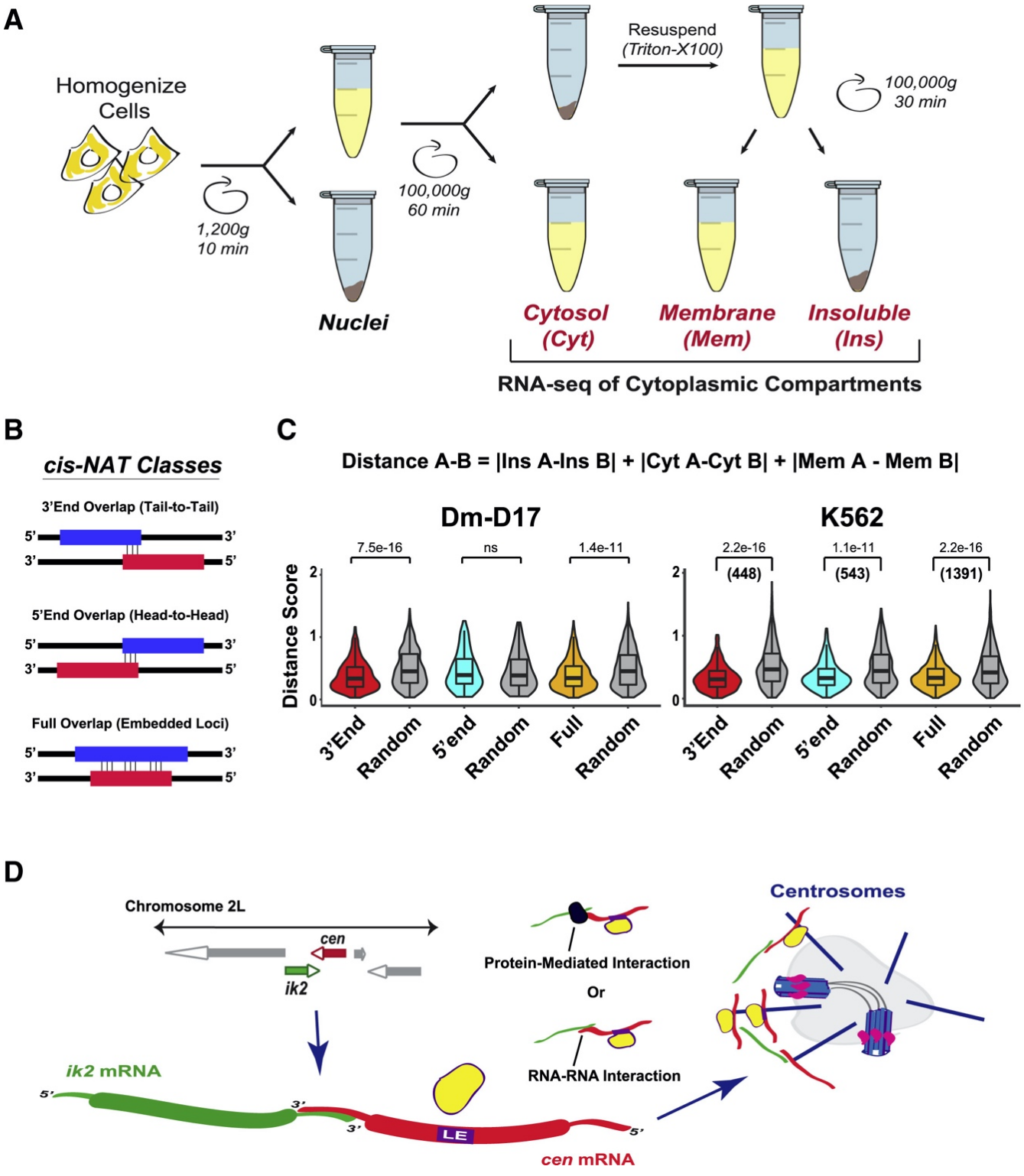
A
Homogenize Cells
1,200g
10 min
Nuclei
100,000g
60 min
Resuspend
(Triton-X100)
100,000g
30 min
Cytosol
(Cyt)
Membrane
(Mem)
Insoluble
(Ins)
RNA-seq of Cytoplasmic Compartments
B
cis-NAT Classes
3'End Overlap (Tail-to-Tail)
5'End Overlap (Head-to-Head)
Full Overlap (Embedded Loci)
C
Distance A-B = |Ins A-Ins B| + |Cyt A-Cyt B| + |Mem A - Mem B|
Dm-D17
K562
Distance Score
7.5e-16
ns
1.4e-11
2.2e-16
(448)
1.1e-11
(543)
2.2e-16
(1391)
3'End
Random
5'end
Full
D
Chromosome 2L
cen
ik2
ik2 mRNA
LE
cen mRNA
Protein-Mediated Interaction
Or
RNA-RNA Interaction
Centrosomes

Figure 2.1. The *Drosophila cen* and *ik2* mRNAs, encoded by 3'overlapping genes, localize to centrosomes and astral microtubules in developing embryos.

(A) FISH staining of wildtype (*OreR*) embryos showing that *cen* mRNA (blue) localizes to centrosomes and astral microtubules at different phases of the cell cycle. Red: DNA; SV: surface view; CV: cross-section view. Scale bar = 10 μm.

(B) Co-localization of *cen* (green) and *ik2* (red) mRNAs revealed by double FISH. Blue: DNA; SV: surface view; CV: cross-section view. Scale bar = 10 μm.

(C) Schematic representation of the *cen/ik2* locus, captured from the Integrated Genomics Viewer genome browser, revealing their tail-to-tail 3'overlapping arrange of the *cen* (pink) and *ik2* (orange) genes on chromosome 2L in *D. melanogaster*. For *ik2*, different isoforms with altered 3'UTR lengths were mapped in the BDGP genome sequence Releases 5 and 6, which respectively share 390 or 59 nt overlaps with the 3'UTR of *cen* mRNA.

Figure 2.2. Precise co-localization of *cen* and *ik2* mRNAs in syncytial embryos and oocytes.

(A) smFISH imaging of *cen* (red) and *ik2* (blue) mRNAs within the cortical cytoplasm of a syncytial blastoderm stage wildtype OreR embryo. **A'** and **A''** show magnified views of the regions outlined by the hatched boxes in A. Scale bar = 2 μm.

(B) Quantification of the percentage of overlap of *cen* and *ik2* mRNA signals, as assessed from the perspective of *cen* (left graph) or *ik2* (right graph) mRNA foci. To control for random co-localization events, comparative analyses were conducted on the original images and on sets of images for which the *cen* and *ik2* channels were shuffled. The number of *cen* and *ik2* particles analyzed in each condition is indicated by 'n'. Data are shown as mean ± SD. Statistical significance was assessed via unpaired t-tests using GraphPad Prism and p-values are indicated.

(C) The number of co-localizing *ik2* mRNA particles is strongly correlated with the size of *cen* clusters. The volume of *cen* mRNA clusters in μm^3 was plotted against the number

of co-localized *ik2* mRNA foci, either on the real experimental images (upper graph) or on shuffled image specimens (lower graph).

(D) smFISH for *cen* (red) and *ik2* (green) particles in dissected stage 8 wildtype ovaries. **D'** and **D''** show magnified views of the regions indicated by hatched boxes in **D**, which reveal signals associated with a nurse cell nucleus (**D'**) or within the oocyte cytoplasm (**D''**). Blue: DNA. Scale bar = 20 µm.

Figure 2.3. Centrosomal localization of *ik2* transcripts is dependent on the presence *cen* mRNA.

(A) Relative expression levels of *cen* and *ik2* mRNAs (normalized to *rpl32*) assessed by RT-qPCR in 0-4h control (*OreR*), ik2 RNAi, cen RNAi and cen^{f04787} embryos. Data indicate the mean ± SD from one experiment and are representative of at least three independent experiments. Statistical significance was assessed via unpaired t-tests, for which the p-values are indicated.

(B) Hatching frequency of control (*OreR*), ik2 RNAi, cen RNAi and cen^{f04787} embryos arrayed on apple juice agar plates counted over a 3 day time course. Data represent the average ± SD from three independent experiments for which 720 embryos of each genotype were analyzed. A two tailed t-test was used for statistics (**=$p<0.01$, ***=$p<0.001$).

(C) Phenotypic quantification of control (*OreR*), ik2 RNAi, cen RNAi and cen^{f04787} embryos. Syncytial blastoderm stage embryos were evaluated for their phenotypic features, classified according to whether they looked normal, or whether they presented mitotic or morphological defects. The number of embryos analyzed in each condition is indicate by 'n'. Statistical significance was assessed via unpaired t-tests, for which the p-values are indicated; n.s.: non-significant.

(D) FISH for *cen* and *ik2* mRNAs in ***(i)*** *OreR*, ***(ii)*** cen^{f04787} or ***(iii)*** *ik2 RNAi* embryos. Red: mRNAs; Blue: DNA; SV: surface view; CV: cross-section view. Scale bar = 10 µm.

(E) Immuno-fluorescence labelling of Cen and Ik2 proteins in ***(i)*** *OreR* and ***(ii)*** cen^{f04787} mutant embryos. Red: protein IF signal; Blue: DNA. Scale bar = 10 µm.

Figure 2.4. Localization of *cen* and *ik2* mRNA orthologues in different *Drosophila* species.

(A-B) Phylogenetic tree of *Drosophila* species (A) and organizational features of the *cen* (red) and *ik2* (green) loci, or of flanking genes, in the indicated species (B). Note that the *cen* and *ik2* genes are organized in a tail-to-tail configuration in *D. mel* and *D. sim*, while these genes are located at separate loci in *D. moj* and *D. vir*.

(C) Expression levels of *cen* and *ik2* mRNAs in the indicated fly species, as assessed by RT-qPCR. Data are normalized to *rpl23* mRNA levels and represent the mean ± standard error to the mean (SEM) of at least 3 independent experiments.

(D) FISH labelling of *cen* and *ik2* mRNA orthologues (blue) in syncytial blastoderm stage embryos of the indicated species. Note the centrosomal like pattern observed for *cen* mRNA in all species and for *ik2* mRNA in *D. mel* and *D. sim*. Red: DNA; SV: surface view; CV: cross-section view. Scale bar = 10 µm.

Figure 2.5. Mapping localization determinants of *cen* and *ik2* mRNAs.

(A) GFP-fusion reporter transgenes were constructed to map localization determinants of *cen* and *ik2* mRNAs. For these, the *GFP* sequence was inserted upstream of the coding region (CR) + 3'UTR, CR or 3'UTR of *cen* or *ik2* mRNAs (upper schematic). These UAS-promoter driven transgenes were maternally expressed by mating to the NGV Gal4 driver line. FISH analysis depicting the localization of the ***(i)*** GFP, ***(ii)*** *GFP-cen* or ***(iii)*** *GFP–ik2* reporter mRNAs expressed in transgenic embryos, detected with a *GFP* sequence probe*. Note that the centrosomal targeting of cen is dictated by its coding region, while ik2 targeting requires its 3'UTR.* Scale bar = 10 µm.

(B) GFP-fusion reporters used to test truncated forms of the *ik2* mRNA 3'UTR. Different truncated versions of the *ik2* 3'UTR were inserted downstream of the GFP coding sequence (upper schematic). FISH analyses reveal that the sequence lying between positions 139-253 is required for centrosomal localisation (lower panel). This region in depicted by the black-box in the upper panel. Red: mRNA; blue: DNA; SV: surface view; CV: cross-section view. **(C,D)** RT-qPCR analysis of *in vitro* and *in vivo* pull-down samples.

(C) *In vitro* transcribed *Cen-CR+3'UTR*, *Cen-CR* (both labeled with Biotin-UTP), *Ik2-CR+3'UTR*, *IK2-CR* mRNA were dimerized and pulled down on streptavidin beads. Results are presented as the relative *ik2* mRNA levels which is normalized to streptavidin/biotin captured *cen* RNA levels. Data represent the mean ± SD of three independent experiments. Statistical significance was assessed via unpaired t-tests, for which the p-values are indicated. **(D)** The result from *in vivo* pull-down samples from *OreR* whole embryo lysates conducted using biotinylated antisense RNA probes for *cen* and *ik2* mRNAs, or a *GFP* probe as a control. RT-qPCR analysis for *ik2*, *cen* or *cyclin B* (normalized to *gapdh*) mRNAs across pull-down samples. Note that *ik2* and *cen* mRNAs are enrichment in *ik2* or *cen* mRNA pull-downs, whereas negative controls *cyclin B* is not enriched. Data represent the mean ± SEM from across replicate experiments. Statistical significance was assessed via unpaired t-tests, p-values are indicated.

(E,F) Genetic complementation of cen^{f04787} ($cen^{-/-}$) mutant embryos with the *GFP*, *GFP-cen-CR* and *GFP-cen-CR+3'UTR* transgenes presented in (A) using the Gal4-UAS system. **(E)** Immuno-FISH analysis of embryos of the indicated genotypes was performed with *cen* or *ik2* probes (red) and with an antibody to γ-Tubulin (blue). Scale bar = 10 μm. **(F)** Quantification of embryonic phenotypes (normal or defective) from crosses presented in (E).

Figure 2.6. *cen* mRNA is locally translated at the level of centrosomes and intact polysomes are required to maintain its localization.

(**A-B**) Visualizing the local translation of Cen protein with the Puro-PLA assay and confocal microscopy. **(A)** Diagram showing the general principle of the Puro-PLA method to study the site of *de novo* protein synthesis. **(B)** Confocal imaging of the Cen-Puro-PLA (green) and Cen protein IF (red) signals. ***(i)*** Puro-treated samples show Cen synthesis *in situ*. As negative controls, ***(ii)*** no puromycin was used, ***(iii)*** protein-specific antibody was omitted (anti-puro only), and ***(iv)*** anisomycin treatment was performed prior to the addition of puromycin. Arrow heads indicate sites of coincident Cen-Puro-PLA and Cen immunofluorescence signals. Red: DNA; SV: surface view; CV: cross-section view. Scale bar = 10 μm.

(C) FISH performed on OreR embryos exposed to DMSO, emetine (100µM) or harringtonine (100µM) to visualize *cen* mRNA (blue) localization during interphase and in mitosis. Red: DNA. Scale bar = 25 µm.

Figure 2.7. Transcripts encoded by *cis*-NATs tend to co-localize in specific subcellular compartments.

(A) Schematic detailing the previously performed cell fractionation and RNA-seq (CeFra-seq) procedure [331]. *Drosophila* Dm-D17 and human K562 cells were fractionated into biochemically defined cytoplasmic compartments, including cytosol, membrane and cytoplasmic insoluble fractions, through hypotonic lysis and ultra-centrifugation steps. Each fraction was then subjected to RNA-seq, as described previously [331].

(B) Schematic representation of different *cis*-NAT classes, including those with tail-to tail (3'end), head-to-head (5'end) or full (embedded) overlap.

(C) A distance measurement score for all classes of *Drosophila* or human *cis*-NATs was calculated by summing the differences in fraction-specific RNA expression levels. This metric was used to evaluate the distance values of groups of RNAs encoded by genes with different overlapping arrangements. The violin plots convey the distance measure scores of pairs of RNAs encoded by genes with overlapping transcriptional units at the level of their 3'UTRs, 5'UTRs or through embedded exonic sequences, compared to control randomly shuffled mRNA pairs from non-overlapping genes. P-values were calculated with a Wilcoxon test and are indicated. **(D)** Model for the *cen-ik2* mRNA co-localization to centrosomes. Owing to the tail-to-tail configuration of their genes, maternally-expressed *cen* and *ik2* mRNAs interact through their 3'UTR, either via direct RNA-RNA interactions or through associated RNA binding proteins. The centrosomal co-localization of theses mRNAs, mediated by signals with the coding region of *cen*, may occur through co-transport or localized co-assembly. LE indicates potential cis-localization element residing within the coding region of *cen*.

2.14 Supplemental Figures and Figure Legends

Supplemental Figure 2.1

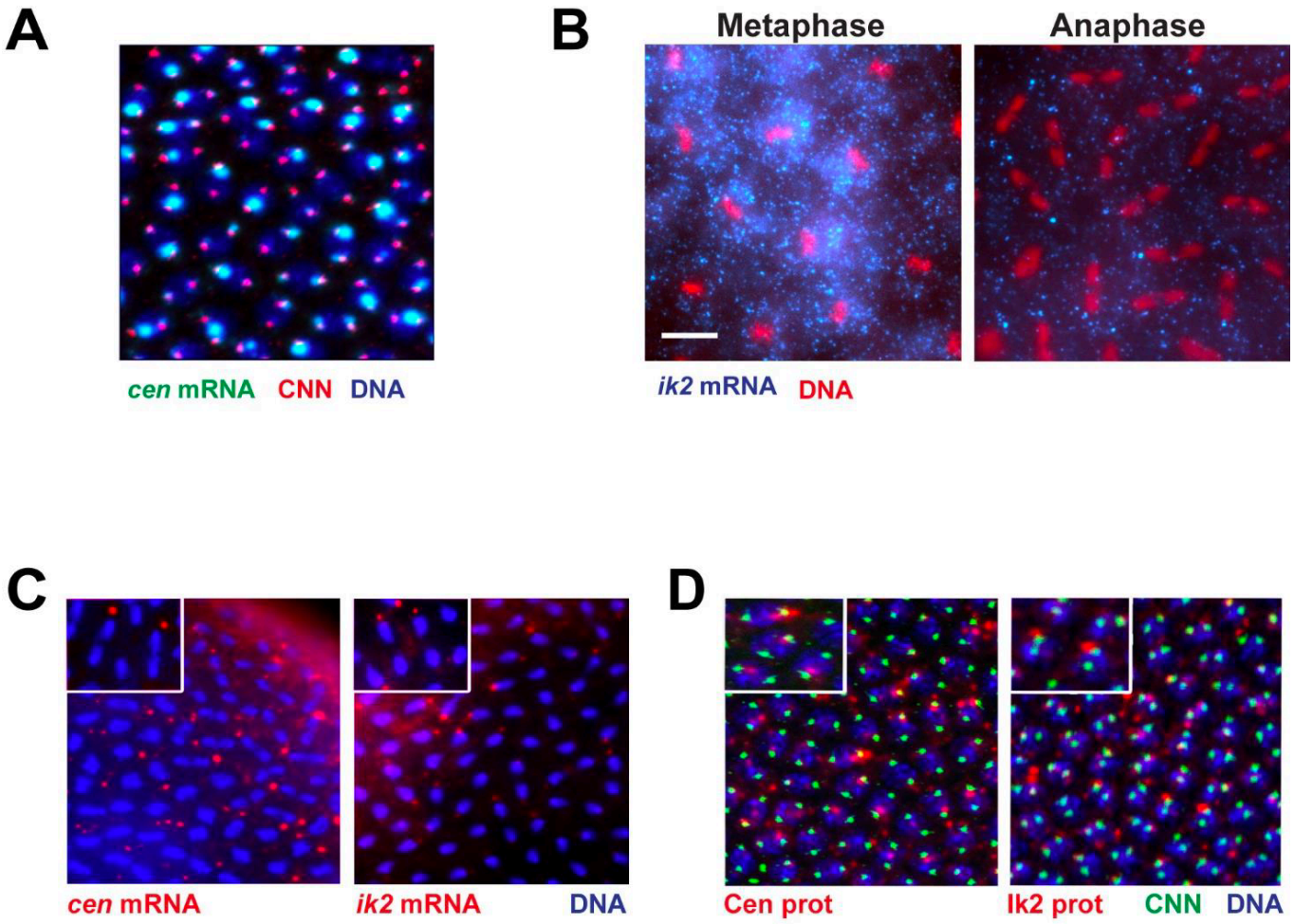

Supplemental Figure 2.2

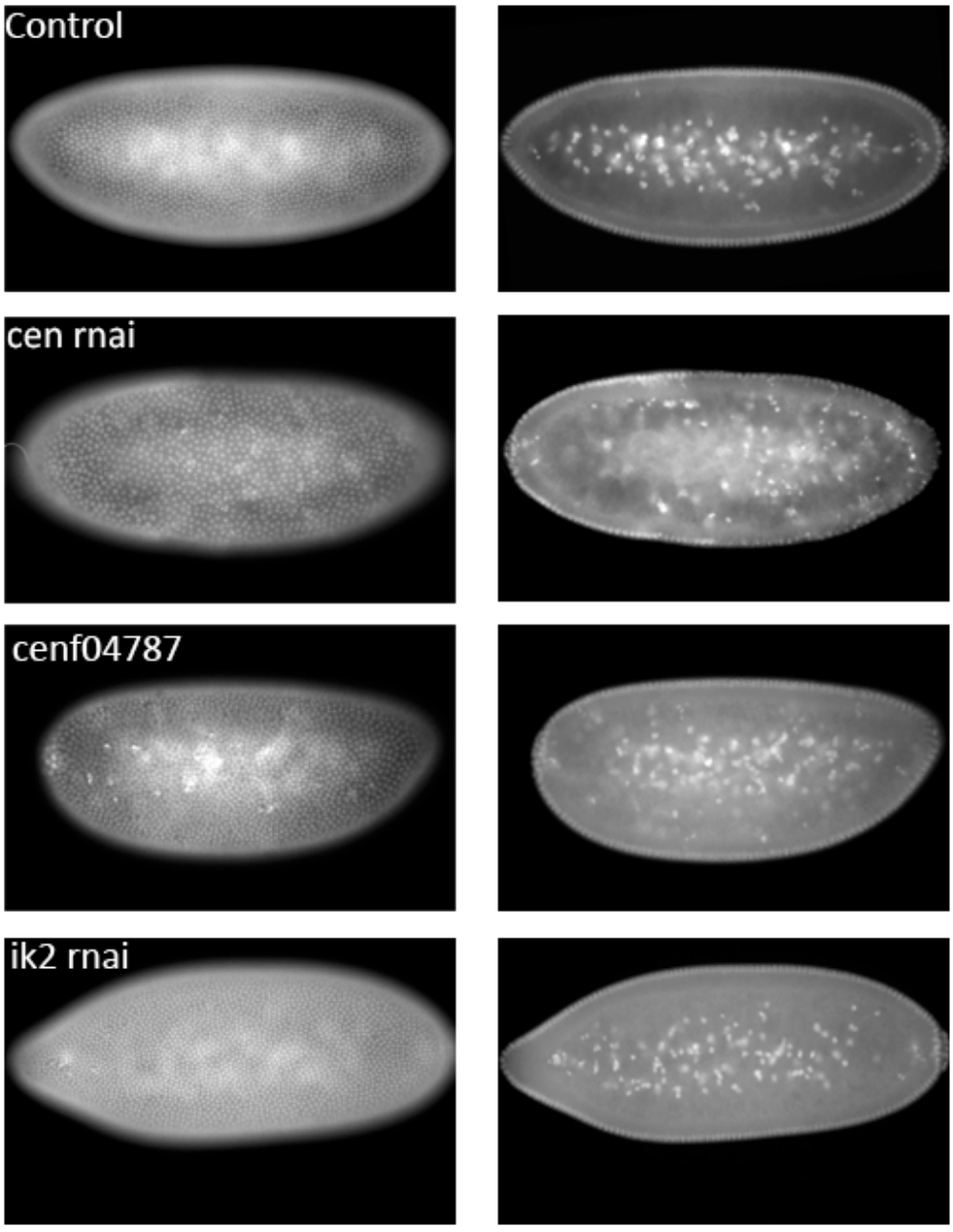

Supplemental Figure 2.3

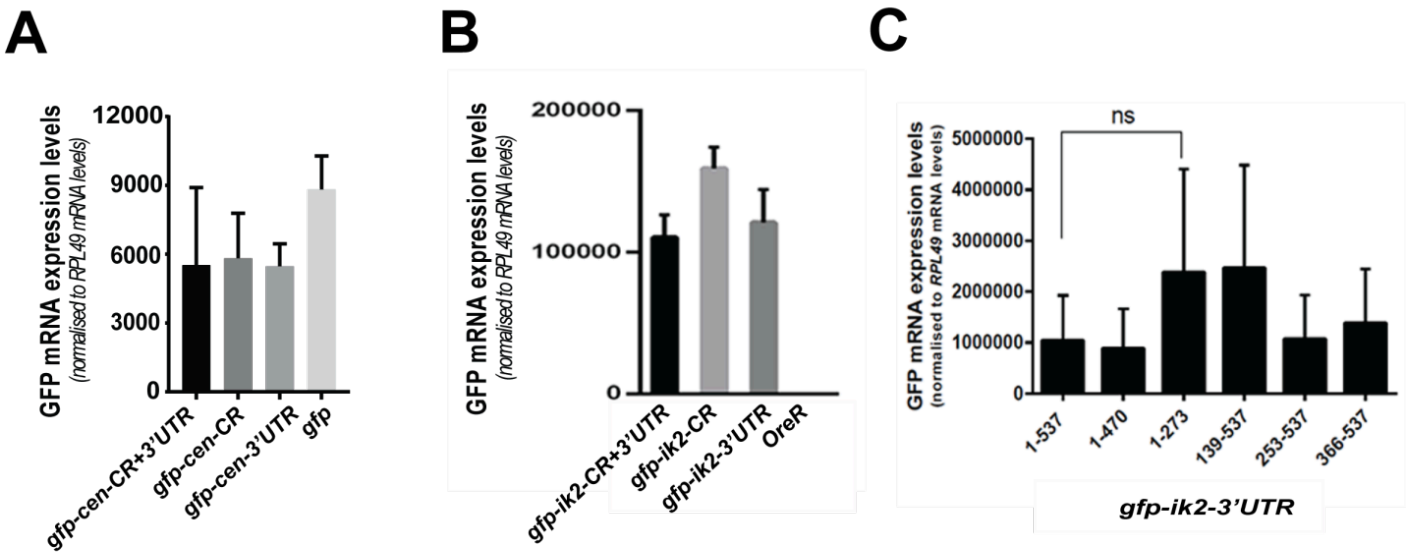

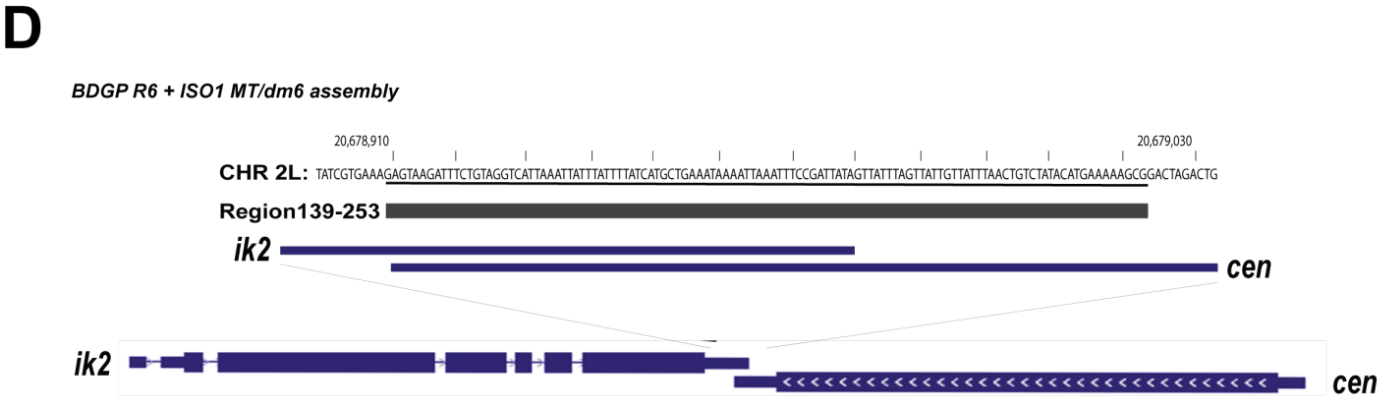

Supplemental Figure 2.4

A

	Predicted CDS Length (nt)	Predicted 3'UTR Length (nt)	Identity (%)		Gaps (%)	
			CDS	3'UTR	CDS	3'UTR
cen						
D. melanogaster	2374	199	NA	NA	NA	NA
D. simulans	2374	340	97.3	97.5	0.0	0.0
D. moravensis	2446	513	58.7	46.3	23.1	41.0
D. virilis	2443	577	58.6	44.6	21.4	42.4
ik2						
D. melanogaster	2164	208	NA	NA	NA	NA
D. simulans	2044	212	91.6	93.4	5.5	1.9
D. moravensis	2830	10	76	60.0	0.9	33.3
D. virilis	2026	59	77.1	42.7	1.9	49.4

B

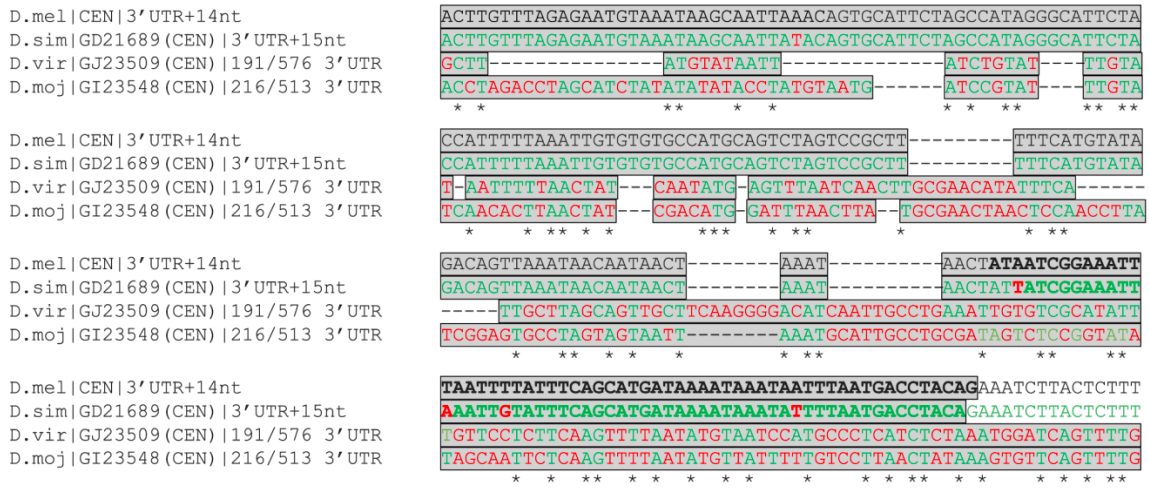

C

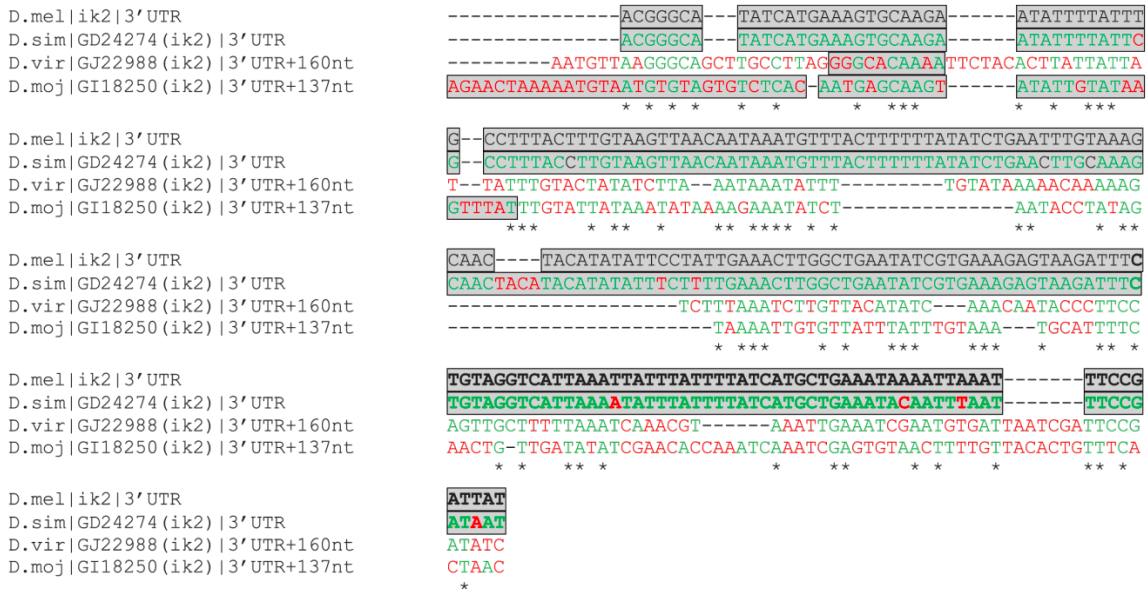

Supplemental Figure 2.1. *Cen* and *ik2* mRNAs exhibit mitotic localization patterns in Drosophila embryos. Related to Figure 2.1.

(A) Cen mRNA foci localize closely to a subset of structures define by the Centrosomin (CNN) protein. Immuno-FISH labelling performed on syncytial blastoderm stage embryos revealing *cen* mRNA (green) and CNN-GFP protein (red). Blue, DNA.

(B) FISH staining of wildtype (OreR) embryos showing that *ik2* mRNA (blue) exhibits a centrosomal localization pattern during mitosis. Red: DNA; SV: surface view; CV: cross-section view.

(C-D) Asymmetric localization of *cen* or *ik2* mRNAs **(C, red)**, or Cen and Ik2 proteins **(D, red)**, to one of the two replicated centrosomes during mitosis. Blue, DNA; Green, CNN.

Supplemental Figure 2.2. Phenotypic classes of mutant embryos. Related to Figure 2.3.

Microscopy images of DAPI stained Drosophila embryos. Examples of mitotic, yolk and morphological defects observed in cen-RNAi, cenf04787 and ik2-RNAi embryos.

Supplemental Figure 2.3. Expression levels of reporter *gfp-cen* and *gfp-ik2* mRNAs in transgenic flies. Related to Figure 2.5.

(A) Relative expression of gfp-cen fusion reporter mRNAs in the different transgenic embryos measured by RT-qPCR and normalized by *rpl49* mRNA. Data represent the mean ± SEM from at least 3 experiments.

(B) Relative expression of the reporter gfp-ik2 fusion mRNAs in the different transgenic embryos, as measured by RT-qPCR and normalized by rpl49 mRNAs. Wildtype (OreR) flies are used as a negative control for gfp expression. Data represent the mean ± SEM from at least 3 experiments.

(C) Relative expression of the truncated forms of the gfp-ik2-3'UTR mRNAs in the different transgenic embryos measured by RT-qPCR and normalized by rpl49 mRNA. Data represent the mean ± SEM from at least 3 experiments (ns: non significant p-value).

(D) Schematic representation of the region involved in the ik2 localization (black box), which includes the region of overlap with the cen 3'UTR according to the BDGP R6 + ISO1 MT/dm6 assembly.

Supplemental Figure 2.4. Sequence analysis of the *cen* and *ik2* mRNA orthologues. Related to Figure 2.5.

(A) Table showing the percent of identity and gaps for the coding sequence (CDS) and 3' UTR of the *cen* (red) and *ik2* (green) genes from *D. melanogaster, D. simulans, D. mojavensis,* and *D. virilis* calculated from a local alignment obtained with the Smith-Waterman algorithm, using default parameters. The predicted lengths from the annotations of both regions are shown.

(B,C) Multiple alignment, obtain by MUSCLE (Edgar, 2004), of the genomic region following the stop codon of the *cen* (B) and *ik2* (C) genes. Alignment was performed using additional nucleotides after the annotated 3'UTRs in order to have sequences of identical length. Nucleotides added after, or remaining from the truncation of the UTR, in order to achieve a better resolution of the overall alignment are noted in the text to the left of the alignments. Annotated 3'UTR sequences are highlighted in grey. Nucleotides from a pairwise alignment with *D. melanogaster* are colored in green for a match and red for a mismatch; hyphens represent indels. Stars indicate identical nucleotide alignment in all 4 species. The overlapping region of *cen* and *ik2* is marked in bold for *D. melanogaster* and *D. simulans*.

2.15 Tables

Table 2.1 Key Resources Table

REAGENT or RESOURCE	SOURCE	IDENTIFIER
Antibodies		
Biotinylated Mouse Anti-Dig	Jackson Immunoresearch	Cat# 200-062-156
Rabbit Anti-Cen N-terminus	Megraw, T.L laboratory	[338]
Mouse Anti-Ik2	Hayashi,S. laboratory	[341]
Rabbit Anti-γ-Tubulin	Sigma	Cat# T0950
Mouse Anti-Puromycin	Millipore	Cat# MABE343
Rabbit Anti-GFP	Abcam	Cat# 6556
Anti-Rabbit-Alexa488	Jackson Immunoresearch	Cat# 711-545-152
Anti-Rat-Cy5	Life technology	Cat# A10525
Anti-Mouse HRP	Jackson Immunoresearch	Cat# 715-035-150
Anti-Rabbit PLAplus	Sigma-Aldrich	Cat# DUO92002
Anti-Mouse PLAminus	Sigma-Aldrich	Cat# DUO92004
Chemicals		
Paraformaldehyde	Sigma-Aldrich	Cat# 252549
Trizol	Invitrogen	Cat# 15596026
Dynabeads M-270 Streptavidin	Invitrogen	Cat# 65305
Digoxigenin-11-UTP (DIG-UTP)	Roche	Cat# 11209256910
Biotin-16-UTP	Roche	Cat# 11388908910
NTPs	Promega	Cat# E601B, E602B, E603B, E604B
Streptavidin-HRP	Sigma-Aldrich	Cat# S911
Harringtonine	LKT Laboratories	Cat# H0169
Emetine Dihydrochloride	MilliporeSigma	Cat# 324693
Anisiomysin	Tocris	Cat# 1290
Puromycin	Sigma-Aldrich	Cat# P8833
Psoralen	Sigma-Aldrich	Cat# P8399
Critical commercial assays		
Power up SYBR Green Master Mix	Applied Biosystem	Cat# A25741
M-MLV Reverse Transcriptase	Invitrogen	Cat# 28025-013
T7 RNA polymerase	Invitrogen	Cat# 18033-019
T3 RNA polymerase	Thermo Scientific	Cat# EP0101
SP6 RNA polymerase	New England Biolabs	Cat# M02075
Tyramide Signal Amplification Kits-Alexa Fluor 488	Perkin Almer	Cat# T20932
Duolink detection kit	Sigma-Aldrich	Cat# DUO92007
Duolink wash reagents	Sigma-Aldrich	Cat# DUO82049
Deposited data		

Raw data files for RNA sequencing	ENCODE project : www.encodeproject.org/	**Dm-D17 Cells** : ENCSR283YJX (Cytosol-PA) ; ENCSR053CWY (Membrane-PA); ENCSR622ROA (Cyto-Insoluble-PA) **K562 Cells :** ENCSR384ZXD (Cytosol-PA); ENCSR596ACL (Membrane-PA); ENCSR594NJP (Cyto-Insoluble-PA).
Experimental models: organisms/strains		
Drosophila Simulans	Drosophila Species Stock Center	N/A
Drosophila Mojavensis	Drosophila Species Stock Center	N/A
Drosophila Virilis	Drosophila Species Stock Center	N/A
Drosophila Melanogaster Oregon R (OreR)	BDSC	N/A
PBac-attP-3B (VK00033)	BDSC	Cat# 24871
Cen^{f04787}	BDSC	Cat# F04787
Cen RNAi TRIP stock	BDSC	Cat# 43139
Ik2 RNAi TRIP stock	BDSC	Cat# 35266
Nanos-Gal4-VP16 (NGV)	BDSC	Cat# 4937
pUASP-Gfp	This paper	N/A
pUASP-Gfp-cenCR+3'UTR	This paper	N/A
pUASP-Gfp-cen-CR	This paper	N/A
pUASP-Gfp-cen-3'UTR	This paper	N/A
pUASP-Gfp-ik2CR+3'UTR	This paper	N/A
pUASP-Gfp-ik2-CR	This paper	N/A
pUASP-Gfp-ik2-3'UTR	This paper	N/A
pUASP-Gfp-ik2-3'UTR (1-537)	This paper	N/A
pUASP-Gfp-ik2-3'UTR (1-470)	This paper	N/A
pUASP-Gfp-ik2-3'UTR (1-273)	This paper	N/A
pUASP-Gfp-ik2-3'UTR (139-537)	This paper	N/A
pUASP-Gfp-ik2-3'UTR (253-537)	This paper	N/A
pUASP-Gfp-ik2-3'UTR (366-537)	This paper	N/A
Plasmids		
pGEM4	Promega Corporation	N/A
pUASP-attB	Howard Lipshitz	N/A
cDNA bank clones		
Cen cDNA	Drosophila Gene Collection	LD41224

Ik2 cDNA	Drosophila Gene Collection	SD10041
Software and algorithms		
Prism	Graphpad	
Zen lite	Zeiss	
Photoshop, Illustrator	Adobe Systems Inc.	
Imaris	Oxford Instruments	
Sequence-Based Reagents		
Please see **Table 2.2** for primers sequences used for transgenic flies	This paper	N/A
Please see **Table 2.4** for qPCR primer sequences	This paper	N/A
Please see **Table 2.3** for qPCR primer sequences used for Probes synthesis	This paper	N/A
Please see **Table 2.5** for primer sequences of Stellaris probes for *cen* and *ik2*.	This paper	N/A

Table 2.2 Plasmid Construction Primers

BamH1-Cen_Cod_Fw	ATTAGGATCCATGGAGGAATCCAATCACG
BamH1-Cen_Cod_Rv	ATTAGGATCCTTACTTTTGACGAAACTGATGATGATG
BamH1-Cen_3'UTR_Fw	ATTAGGATCCACTTGTTTAGAGAATGTAAAT
BamH1-Cen_3'UTR_Rv	ATTAGGATCCTTTCTGTAGGTCATTAAATTATTTA
BamH1-Ik2_Cod_Fw	ATTAGGATCCTGTTTGTCACAATCGAGAAG
EcoRI-Ik2_Cod_Rv	ATTAGAATTCCTAACTACTTTCCAGACTTCCG
BamH1-Ik2_3'UTR_Fw	ATTAGGATCCACGGGCATATCATGAAAG
EcoRI-Ik2_3'UTR_Rv	ATTAGAATTCGTCGAGTTTTATCATAACACGG
BamH1-Ik2_3UTR_139_Fw	ATTAGGATCCCGTAGGAGTAAGATTTCTGTAGG
EcoRI-Ik2_3UTR_156_Rv	ATTAGAATTCCCTACAGAAATCTTACTC
BamH1-Ik2_3UTR_253_Fw	ATTAGGATCCCGTAGGGACTAGACTGCATGGCA
EcoRI-Ik2_3UTR_270_Rv	ATTAGAATTCTGCCATGCAGTCTAGTCC
BamH1-Ik2_3UTR_366_Fw	ATTAGGATCCCGTAGGATGATGATGACTCTTGC
EcoRI-Ik2_3UTR_383_Rv	ATTAGAATTCGCAAGAGTCATCATCATC
BamH1-Ik2_3UTR_453_Fw	ATTAGGATCCCGTAGCCCGGCGCAAAACTTCGG
EcoRI-Ik2_3UTR_470_Rv	ATTAGAATTCCCGAAGTTTTGCGCCGGG

Table 2.3 Probe Synthesis Primers

POT2 Fw	AATGCAGGTTAACCTGGCTTATCG
POT2 Rv	AACGCGGCTACAATTAATACATAACC
SP6	ACGATTTAGGTGACACTATAGAA
T7	GTAATACGACTCACTATAGGGC
Moja_Vir_T3_Ik2_Fw	AATTAACCCTCACTAAAGGGAGAGCCGATGTGCAGATGCGCGA
Moja_Vir_T7_Ik2_Rv	TAATACGACTCACTATAGGGAGACAGTCGCGCACGTCTTTCTC
Moja_Vir_T3_Cen_Fw	AATTAACCCTCACTAAAGGGAGATGCGAGCCGGATGTGGATG
Moja_Vir_T7_Cen_Rv	TAATACGACTCACTATAGGGAGATCAGCACGGCGCAATACTTC
Cen_Cons_T3_Fw	AATTAACCCTCACTAAAGGGAGAAACCGAGTTTTCGGAATCAGA
Cen_Cons_T7_Rv	TAATACGACTCACTATAGGGAGATTCTTGAGCACTCCAAATAT
Ik2_Cons_T3_Fw	AATTAACCCTCACTAAAGGGAGACTGGTGACGCCTCTTCTAGC
Ik2_Cons_T7_Rv	TAATACGACTCACTATAGGGAGAAATACGCTCTCGGAAGTT
GFP_T3_Fw	AATTAACCCTCACTAAAGGGAGAGACGTAAACGGCCACAAGTT
GFP_T7_Rv	TAATACGACTCACTATAGGGAGATGTTCTGCTGGTAGTGGTCG

Table 2.4 RT-qPCR Primers

Cen_RT _Fw	AAGCGCGAACCACTCGAATA
Cen_RT _Rv	ATTCGATGCGATCTCCAGATG
Ik2_RT _Fw	GCGTGGACATCTTTACTTCCA
Ik2_RT _Rv	TGCATCTGCGAGATCACATC
Cen_RT_Vir_Fw	GATCTGTATGAACGCGCGG
Cen_RT_Vir_Rv	GCATTGTCTCGCGGTTCTTA
Cen_RT_Moj_Fw	TCCGTACAGTCACATGCGA
Cen_RT_Moj_Rv	CTTTGCCGCGTCCTTCTTG
Ik2_RT_Vir_Fw	CAAGCCCGGCAACATAATGA
Ik2_RT_Vir_Rv	CACCGCGCGTTCATACAG
Ik2_RT_Moj_Fw	TCCGTACAGTCACATGCGA
Ik2_RT_Moj_Rv	ACCGGCACATAGATGCTCC
RPL23_RT_Fw	AGGAAGAAGGTCATGCCTG
RPL23_RT_Rv	TATAGAGCTTGCATTGGATGC
RPL49_RT_Fw	ATGACCATCCGCCCAGCATAC
RPL49_RT_Rv	ATGTGGCGGGTGCGCTTGTTC
RPL23_RT_Vir/ Moj_Fw	CGTAAGCCGTTCAGAAGGAG
RPL23_RT_Vir/Moj_Rv	TGAATTGGGGAACTGTTGCT
GFP_RT_Fw	AGAACGGCATCAAGGTGAAC
GFP_RT_Rv	TGCTCAGGTAGTGGTTGTCG
CyclinB_RT_Fw	GGGCAGCAAGTTCCAGAAGA
CyclinB_RT_Rv	CCTTGGACCGCACTATTTCC
GAPDH_RT_Fw	ACCGAACTCGTTGTCGTACC
GAPDH_RT_Rv	TCAAGGCTAAGGTCGAGGAG

Table 2.5 Stellaris Probe Sequences

	cen probe	*ik2* probe
1	GAGCATGAACTGCGATACGT	GCATGTGACTGTAGGGATTA
2	CCTTAATCTTGTACTCCTTG	TCGCCAACAGCTTTACTATA
3	AGATGCAAGATCTCCAGTTC	ATGTTAAAGAGACTTCCGCC
4	GTCATCGCATTAATGTGCTT	TACGAGTTCTCAGGATCGTC
5	ACCTTAAGCCGTGAATCATT	CACAAGTGTTCCAAGACCAG
6	GATTCTTCTCCAGATTTAGC	AACTTCATTATGTTTCCGGG
7	CGTCTTAATCTGCTTCTTGT	AAGCTTGTATATGGTTTGCC
8	TCGCTCAGAAGTTGACTCAG	TTCTCTAGCAGCACCGAAAT
9	TCGAATGCTGCATCCTATAG	AGAGAGGCAAACGGCTGATT
10	GAATGCTGTGACTGGACACA	TGAAGATACTCTTCTGTGCC
11	GGAGAACTCAACACTCTGCT	GAACGATCGCTGGATTGACT
12	GCTATGGCCATAACATCTAG	CGACCACAAATCCACATTGG
13	CATGGTGGCATTACTGAAGG	AAAAGGCAGATTTCCGGTGG
14	CTGAGCAGCTTTACCAATTC	TTTTTCCTTCCACCAAAAGG
15	ACGTTTTAACACCTCCATTT	CAGAAGCCTTTTTGGTAGTG
16	GTTGTCTTGGATTATGGTCA	AACGTGGTGGACCATTCAAT
17	TTTCGTTAATATCCCTCAGG	CTCGAGAAGTCCAGCTAGAA
18	CTTCGTAGATTTCTTCGGTT	TCGAAAGACCAGGTCTTTTC
19	CTAGAGTTGGGATTGAGGTC	CGTCACCTCGTGGAAGAAAC
20	CCCGATAAGGATTTGGTTTG	ACATGAATGACACGCTTGCG
21	ACCAGAGCTTCATATTTCTC	TAGGAACACTTCCACCGAAC
22	CATCTGGATTGCTGGTGAAG	GCTCTCGGAAGTTGTCAATT
23	TCTGATTTTTTGCCTTGACT	CACCTCTGTTTGCAGGAAAA
24	CAGATTCCTTTGAGCTGTTA	CAAAAGGATCTGCTTCTCCA
25	CGCTTACGTGTTGAATCCAA	TTTAGCTATCGTTCGTGGAG
26	CGATGTAGTTTCTGATTCCG	TATTGGCTGATCTGTTGTGG
27	GCTAGTTTCATCCGAGAATC	AACATTGTTGTCGTCGTTGC
28	AAGGAAGTAACTCGGTCGCT	AGATCTAATTGCTGGGGCAA
29	TGAGATTCAATGGGGCTGAC	AGGGAACACTGGGAACTTGG
30	TGAGCACTCCAAATATCTCC	GTCGTTCTCCACTGAAACAT
31	TCTTCGTTATTATCAGCTGC	TAAAGATGTCCACGCGTCTT
32	TTTCTGTAATCTGTGCGTCG	TCCACTCCCTTCTTAATAAG
33	AAGTCATCTGGAGATTCCTC	GAGTTATTGTGGTCACTAGC
34	AACTGAGGATACGACGCTCT	TGCACCACATCTGCATAATC
35	ACTCGGACATTGCAATGGAC	CTCCATCAAAGTCGCTTTTG
36	AGATGTGTTTTTTGGCTGTC	AATGTTTGTGCATCTGCGAG
37	GTTTTGTTGGTTTCGGACAT	GGTCCATTGATCGTTAAGTT
38	AAGTGGATTGCGTTAGGGAC	CTTGCAAGGACACTTCTTTC
39	TCTCCCTTATGGGTTTATAA	CTTTCTACCAGATACTTGGC
40	GAGTGGAGTAAGTATCTGGC	GCATGAAACTGTTCGTCGTT
41	CGGTTAGATATTCGAGTGGT	GATCCACTTTAATCTTCTCC
42	TCGGTTCTTCTTCTTGATTC	TGTCGGATTTACGTTATCCA

43	CCCGGGAGTTAAACAATTCG	TTAAGGTAGACGGTCTGAGC
44	GTATCCGTACACATCTTTGA	CACGTCCTTCTCCAAAATTT
45	CCATTGAGCTCTATTACTCG	TTCCGTTCAACTTTCTTTCG

Chapter 3 Characterization of RNA Binding Protein Localization to the Mitotic Apparatus

Characterization of RNA Binding Protein Localization to the Mitotic Apparatus

Dhara Patel[1], Xiaofeng Wang[2], Sulin Oré Rodriguez[2], Eric Lécuyer[3]

[1] Institut de Recherches Cliniques de Montréal (IRCM), Montréal, QC, Canada; Département de Biochimie et Médecine Moléculaire and Programme de Biologie Moléculaire, Université de Montréal, Montréal, QC, Canada.

[2] Institut de Recherches Cliniques de Montréal (IRCM), Montréal, QC, Canada.

[3] Institut de Recherches Cliniques de Montréal (IRCM), Montréal, QC, Canada; Département de Biochimie et Médecine Moléculaire and Programme de Biologie Moléculaire, Université de Montréal, Montréal, QC, Canada; Division of Experimental Medicine, McGill University, Montréal, QC, Canada.

Note: A version of Chapter 3 will be used in a future publication.

3.1 Contributions of the Authors

Figure 3.1: Dhara Patel, Sulin Oré Rodriguez, Xiaofeng Wang

Figure 3.2: Dhara Patel

Figure 3.3: Dhara Patel

Figure 3.4: Dhara Patel

Figure 3.5: Dhara Patel

Figure 3.6: Dhara Patel

Supplemental Figure 3.1 Dhara Patel

Supplemental Figure 3.2 Dhara Patel

Dhara Patel and Eric Lecuyer designed the project and planned the experiments.

Dhara Patel, Sulin Oré Rodriguez, and Xiaofeng Wang carried out the experiments.

Dhara Patel analyzed the results.

Dhara Patel made the figures and wrote the manuscript.

3.2 Summary

The trafficking and localization of mRNA molecules is an exquisite mechanism to target proteins throughout the cell. This mechanism is mediated by interactions with RNA binding proteins (RBPs). Previous studies have identified both mRNAs and RBPs being localized to mitotic apparatus structures including centrosomes and the spindle, therefore we hypothesized that the RBP localization to the mitotic apparatus is involved in the local regulation of mitotic mRNAs. We implemented a combination of systematic imaging approaches and loss-of-function studies in human cells, as well as *in vivo* studies in flies to identify RBPs implicated in mitotic mRNA localization and cell division regulation. Through an imaging screen with approximately 300 RBP antibodies, we identified 30 RBPs localized to mitotic structures in HeLa cells and 6 RBP candidates for which the knockdown perturbs mitosis and mRNA localization. Similarly, loss of RBP orthologs in *Drosophila melanogaster* (*D. melanogaster*) embryos disrupted mitosis. Our studies highlight that RBPs are involved in post-transcriptional regulation during mitosis.

3.3 Introduction

RNA binding proteins are involved in the post-transcriptional regulation of mRNAs including polyadenylation, localization, alternative splicing, and degradation [371]. The malfunction of RBPs has been linked to cancer, neurological disorders, cardiovascular diseases, and diabetes [372]. To date, approximately 1500 proteins have been categorized as RBPs [207]. RBPs recognize and bind to the sequence and/or structural motifs in mRNAs via through their RNA binding domains (RBDs) [157, 173, 373]. Together, the ribonucleoprotein (RNP) complex, composed of mRNAs and RBPs undergoes nuclear export and becomes trafficked to a specific subcellular compartment [157, 173]. At the final site of localization, the mRNA has the potential to be locally translated [157, 173].

The partitioning of mRNAs into different subcellular compartments is important in processes such as establishing cell polarity and determining cell fate [133, 136, 166, 374-379]. Localized mRNAs have been found in structures including the mitochondria, centrosomes, spindle, and the endoplasmic reticulum [121-123, 127, 153, 154]. A

potential advantage of localized translation in contrast to transporting proteins is that a single mRNA can undergo several rounds of translation. Furthermore, there is spatial and temporal precision of the protein to the site where it is needed [157, 173, 175]. Strikingly, approximately 70% of genes in the *Drosophila melanogaster* (*D. melanogaster*) embryos encoded subcellularly localized mRNAs, including ones that were co-localized with mitotic apparatus structures [125]. In recent years, there have been several examples of mRNAs and RBPs that have been implicated in the context of mitosis [121-123, 125, 127]. Interestingly, a screening conducted in HeLa cells to look for transcripts localized to the centrosome identified 8 mRNAs that showed accumulation at the centrosomes [123]. Additionally, the loss of the RBP LARP1 resulted in a failure in the formation of a bipolar spindle [380]. Although there has been clear evidence of mRNAs and RBPs being associated with mitotic apparatus structures, the functional roles remain largely unexplored.

To further understand the roles that mRNAs and RBPs have in regulating mitosis, we first performed an imaging screen in HeLa cells with a validated collection of RBP antibodies, which identified a group of 30 RBPs that exhibit steady state co-localization with mitotic structures including centrosomes and the mitotic spindle. Subsequent loss-of-function (LOF) assays using siRNAs against the candidates revealed that depletion of several of these RBPs led to mitotic defects. Additionally, our results suggest that RBPs are involved in the localization of *Assembly Factor for Spindle Microtubules* (*ASPM)* mRNA*,* where loss of RBPs leads to defects in mRNA localization in HeLa cells. Complementary to our studies in human cells, we utilized the *D. melanogaster* model system and studied how the depletion of orthologous RBPs influenced the rapid mitotic divisions and viability in early fly embryos. We demonstrated that RBPs are indeed involved in the regulation of mitosis and cytoplasmic mRNA localization is implicated during mitosis.

3.4 Experimental Procedures

3.4.1 *Drosophila melanogaster* stocks

Oregon R (*OreR*) flies were used as wild-type for all experiments. *OreR*, *Nanos-Gal4*-VP16 (*NGV*), CG6695-*RNAi-TRIP*, *CG8549-RNAi-TRIP*, *CG13387-RNAi-TRIP*, *CG10466-RNAi-TRIP*, *CG6799-RNAi-TRIP*, *CG5808-RNAi-TRIP*, *CG7008-RNAi-TRIP*, *CG7946-RNAi-TRIP*, *CG12085-RNAi-TRIP*, and *CG31368-RNAi-TRIP* stocks were obtained from the Bloomington *Drosophila* Stock Center (BDSC). Embryos were collected 4 hours after egg laying.

3.4.2 Immunofluorescence and FISH on *D. Melanogaster* embryos

Embryos were harvested from population cages and collected 4 hours after laying. After harvesting, they were processed for IF and FISH as described previously [125] (**Refer to Sections 2.6.6 and 2.6.7**). For IF, embryos were stained with primary antibodies (α Tubulin, 1:50, rat; γ Tubulin, 1:50, rabbit) and secondary antibodies (FITC, 1:100, rat; CY3, 1:100, rabbit).

3.4.3 Embryo Viability Tests

The hatching frequency of *OreR*, *CG6695-RNAi-TRIP*, *CG8549-RNAi-TRIP*, *CG13387-RNAi-TRIP*, *CG10466-RNAi-TRIP*, *CG6799-RNAi-TRIP*, *CG5808-RNAi-TRIP*, *CG7008-RNAi-TRIP*, *CG7946-RNAi-TRIP*, *CG12085-RNAi-TRIP*, and *CG31368-RNAi-TRIP* embryos was determined by counting the number of embryos that hatched on apple juice plates. 120 embryos were arrayed on agar apple juice plates and the percentage of hatched embryos was noted each day for a 3-day time course at 25°C.

3.4.4 Cell culture

HeLa cells were maintained in Dulbeccos modified Eagle's medium (DMEM) containing 10% fetal bovine serum (FBS) and 1% penicillin/streptomycin (P/S) at 37°C in a humidified incubator with 5% carbon dioxide.

3.4.5 Transfections

Knockdowns were performed using Lipofectamine RNAi Max transfection reagent on HeLa cells. Plates were coated with Poly-L-Lysine according to the manufacturer's instructions. For IF and smiFISH-IF experiments, cells were seeded onto coverslips. 50nM of siRNA (**Refer to Table 3.5**) of the target gene was transfected. 2.5μL of Lipofectamine RNAiMAX was diluted in 100μL of OptiMEM and a mix containing a final concentration of 50nM of siRNA was diluted in 100μL of OptiMEM in a separate tube. Next, the components of the two tubes were mixed, and incubated for 10 minutes at room temperature. Lastly, 800μL of DMEM + 10% FBS was added to the tube making the final volume 1mL. The final mix was added to the cells. A Non-Targeting siRNA control was used for all experiments. The total incubation time was 48 hours, however after 24 hours, the cells were replenished with fresh DMEM + 10% FBS.

3.4.6 RNA Extraction, Precipitation, and cDNA Synthesis

HeLa cells were seeded on plates and the transfection procedure was carried out as mentioned previously. When cells were ready for harvesting, total RNA was isolated using TRIzol reagent according to the manufacturer's instructions.

Next the RNA underwent precipitation for purification. 0.1 volumes of 3M sodium acetate pH 5.2 and 2.5 volumes of cold 100% ethanol was added to each sample. The samples were precipitated at -80°C for 1 hour. Next, the samples were centrifuged at full speed at 4°C for 30 minutes. After, the pellet was centrifuged with 200μL of cold 75% ethanol for 10 minutes. This step was performed twice. Lastly, the samples were air dried for 10 minutes and resuspended in 25μL of 0.1% DEPC water.

Complementary DNA (cDNA) was generated using random hexamers, oligo dT, and M-MLV reverse transcriptase using 1μg of total RNA from each sample in line with the manufacturer's instructions.

3.4.7 Quantitative Real Time PCR (qRT-PCR)

Diluted 1/10 cDNA was used to perform qRT-PCR experiments. 1μL of diluted cDNA was added to each well. A master mix was made with 5μL of PowerUp™ SYBR® green Master Mix. 2μL of forward primer (5μM), and 2μL of reverse primer (5μM) per sample. The ABI ViiA7 instrument (Life Technologies, Inc) was used for detection of the amplified product. Each reaction was carried out in triplicates. The expression levels were normalized to *GAPDH* mRNA.

3.4.8 Immunofluorescence

HeLa cells were seeded on coverslips in plate and the transfection procedure was carried out as described previously. Cells were stained with PCNT, α Tubulin, and DAPI to visualize mitotic cells. Note, all solutions were made using PBS 1X unless otherwise stated. Cells were fixed with 3.7% formaldehyde for 20 minutes. After, the cells were washed with PBS three times for 5 minutes. The cells were subjected to permeabilization with 0.5% Triton-X for 5 minutes and washed 3 times with PBS for 5 minutes. Next, the cells were blocked with 0.1% Triton-X, 2% BSA for 10 minutes. Lastly, the primary antibodies (PCNT, 1:250, mouse; α Tubulin, 1:500, rat) were diluted in blocking solution and the cells were incubated overnight 4°C. The next day, the cells were washed 3 times with PBS for 5 minutes each time. The secondary antibody (CY3, 1:500, mouse; FITC, 1:500, rat) was diluted in 0.2% Tween-20, 2% BSA and the cells were incubated for 2 hours at room temperature in the dark. After the incubation period was over, the cells were washed with 0.2% Tween-20 three times for 5 minutes and 2 times with PBS for 5 minutes. Lastly, the coverslips were mounted using a mounting media containing DAPI.

3.4.9 Single Molecule Inexpensive FISH combined with IF (smiFISH-IF)

A. Probe preparation

Probe set: Each individual primer for the probe set was diluted in sterile water to a final concentration of 100μM. To make the probe set for each gene, 1μL of each primer was added to a microcentrifuge tube and diluted in sterile water to make a final concentration of 0.833μM.

B. FLAP preparation

The fluorescent FLAP was resuspended in sterile water to make a final concentration of 100μM.

Table 3.1 Synthesis of FLAP-Structured Duplexes

Synthesis of FLAP-structured duplexes	
Component	Volume per Reaction
Probe Set (0.833μM)	2μL
FLAP (100μM)	2.5μL
NEB 3 Buffer (10X)	1μL
Sterile Water	6.5μL

The reaction was placed on a heating block and underwent the following cycles:

1. 85°C for 3 minutes
2. 65°C for 3 minutes
3. 25°C for 5 minutes

C. Procedure

For the smiFISH-IF procedure, I adapted the protocol from [381]. To design the primers, the Oligostan script that was compatible with R was used to make *ASPM*, *β ACTIN*, and *GFP* probes against the mRNA. HeLa cells were seeded on coverslips in a plate and the transfection procedure was carried out as mentioned previously. Note, all solutions were made using sterile PBS 1X unless otherwise stated. When cells were ready to undergo smiFISH-IF, the cells were washed with PBS 3 times for 5 minutes. After, the cells were permeabilized for 15 minutes with 0.1% Triton-X and washed with PBS 3 times for 5 minutes. Primary antibody (ASPM, 1:1000, rabbit; α Tubulin, 1:500, rat) diluted in 0.1% Triton-X was added to the cells, incubating for 1 hour at room temperature. After the incubation, the cells were washed 3 times with 0.1% Triton-X for 5 minutes. Next, the cells were incubated with secondary antibody (CY3, 1:500, rabbit; FITC, 1:500, rat) diluted in 0.1% Triton-X for 2 hours at room temperature. After the incubation, the cells were washed 3 times with 0.1% Triton-X for 5 minutes. The cells were fixed again with 3.7% formaldehyde for 10 minutes and washed 3 times with sterile PBS for 5 minutes. Next, the cells were incubated in 15% formamide, SSC 1X buffer diluted in double distilled

water for 15 minutes at room temperature. During this incubation period, a hybridization mix consisting of two components: Mix 1 and Mix 2, was prepared.

Table 3.2 Preparation of Hybridization Solution

Preparation of Hybridization Solution	
Component	Volume per Reaction
Mix 1:	
SSC 20X	20μL
E.coli tRNA (8μg/μL)	17μL
Formamide (100%)	60μL
FLAP Structured Duplexes	8μL
Sterile Water	95μL
Mix 2:	
RNAse OUT (40U/μL)	4μL
Dextran Sulphate (40%)	100μL
Sterile Water	96μL

Mix 2 was vortexed thoroughly and then both mixes were combined and vortexed again. Hybridization mix was added to each well and incubated at 37°C overnight in a plate sealed with parafilm to avoid excess evaporation. The next day, the cells were washed for 30 minutes 2 times in 15% formamide, SSC 1X buffer at 37°C. After, the cells underwent 2 washes in PBS for 5 minutes. Lastly, the coverslips were mounted using a mounting medium containing DAPI.

3.4.10 Flow Cytometry

HeLa cells were seeded on a plate and the transfection procedure was carried out as mentioned previously. For controls, unstained, propidium iodide only, and Histone H3 only conditions were used. Note, that the samples were spun down at 4°C at 7000rpm, all solutions were made using sterile PBS 1X, the supernatant was removed after each spin unless noted. When cells were ready for harvesting, they were detached by using 200μL trypsin and incubated for 5 minutes at 37°C. 800μL of media (DMEM + 10% FBS) was added to inactivate the trypsin and the samples were spun down at 1700rpm for 5 minutes at room temperature. 1mL of cold 70% ethanol was added to fix the cells. Next,

the samples were spun down for 5 minutes. After, the samples were suspended in 500μL of Krishan's solution (0.1% sodium citrate, 0.3% Nonidet, 0.02 mg/mL RNase A, and 0.05 mg/mL propidium iodide diluted in double distilled water). Samples underwent incubation on ice for 30 minutes and spun down. Next, the cells were resuspended in Krishan's solution and stained with propidium iodide. After Histone H3 staining was performed. Note that in the following steps, the solutions were made using cold PBS 1X. The cells were fixed with 1% formaldehyde for 15 minutes on ice. After samples were spun down and the cells were blocked using 0.5% BSA, 0.2% Triton-X for 15 minutes at room temperature. The cells were stained with primary antibody (Histone H3, 1:1000, rabbit) using the blocking solution and left on ice for 30 minutes. After, the cells were washed with blocking solution for 5 minutes twice on ice. Next, secondary antibody (FITC, 1:1000, rabbit) diluted in blocking solution was added to the sample and incubated for 30 minutes on ice. Cells were washed once with blocking solution and twice with PBS 1X for 5 minutes. Lastly, the cells were then ready to be processed using the FACSCalibur.

3.4.11 Microscopy

The samples were imaged on Leica DM5500B microscope, ZEISS spinning disc confocal microscope, or a Molecular Devices high content screening microscope.

3.4.12 Analysis of smiFISH-IF

Images were taken using the ZEISS spinning disc confocal microscope. The samples were analyzed using IMARIS software. A surface mask was created using the ASPM protein channel to identify the centrosomes, with an absolute intensity threshold was set to select them. This surface mask of ASPM protein was used to measure the mean voxel intensity of *ASPM* mRNA.

3.5 Results

3.5.1 RNA binding proteins show localization to mitotic apparatus structures.

While mRNAs have been shown to localize to mitotic structures, it is unclear which RBP machineries are involved in the localized regulation of such transcripts. To address this question, we conducted an imaging screen in HeLa cells to look for RBPs that show

localization to the mitotic apparatus structures. HeLa cells underwent a double thymidine block treatment to enrich for a population of mitotic cells and IF was performed against ~300 RBP antibodies (**Figure 3.1A**). Images were taken on the high content screening microscope and were analyzed. Analysis of the images revealed that a subset of these RBPs, 30 proteins were identified accounting for 10% of the screened RBPs [201] (**Figure 3.1A** and **Figure 3.1B**). Hits were scored as positive when they showed co-localization with either the α Tubulin or PCNT antibodies, markers for the spindle and centrosomes, respectively. Some RBPs including AKAP1, PPIL4, FXR2, and CCDC86 show localization exclusively to the centrosome whereas other RBPs such as SSB, CDC40, and ZNF622 were enriched solely to the spindle (**Figures 3.1B and 3.1C**). However, PUF60, SF1, and HNRNPUL1 exhibited dynamic localization to both the spindle and the centrosomes (**Figures 3.1B and 3.1C)**. Interestingly, a closer look at the candidate RBPs revealed that they exhibit a myriad of functions including alternative splicing (**Table 3.8**). The enrichment of RBPs to these mitotic apparatus structures suggests that there is post-transcriptional regulation occurring during mitosis.

3.5.2 Loss of RNA binding proteins results in mitotic defects.

To address the hypothesis of whether RBPs localized to the mitotic apparatus are involved in mitotic regulation, we next sought to investigate whether the depletion of these RBPs results in defects. Treatment with siRNA to silence the endogenous mRNA expression of the RBPs of interest was performed and the knockdown was validated by performing qRT-PCR (**Figure 3.2A and Supplemental Figure 3.1**). The mRNA expression levels of the target RBPs were less than 10% after siRNA treatment for all candidates (**Supplemental Figure 3.1**). Cells were stained with α Tubulin and PCNT antibodies and prometaphase/metaphase cells were imaged and analyzed. Defects in the spindle (multipolar/monopolar and morphological defects) and centrosome (abnormal number) were quantified microscopically. We found that depletion of 8 of the candidates: *CCDC86*, *PUF60*, *XPO1*, *WDR43*, *SF3A3*, *SF1*, *RPS3*, and *RBMX2* showed a higher incidence of mitotic defects (**Figure 3.2B** and **Figure 3.2C**). For instance, the loss of *PUF60* resulted in multiple centrosomes and aberrant spindle whereas the reduction of *CCDC86* resulted in an elongated spindle and multiple centrosomes (**Figure 3.2B)**. A

higher incidence of mitotic defects upon RBP depletion suggests that they are involved in the regulation of mitosis. XPO1 was removed from further downstream analyses due to its function as a nuclear export factor, which would make its role as a RBP to be indiscernible [382, 383]. Since the loss of RBPs resulted in mitotic defects, we wanted to assess whether the cells were cycling normally. There could be a possibility that the cells can be arrested due to the higher incidence of errors. After 48 hours of treatment with siRNA, the cells were harvested and stained with propidium iodide and Histone H3. The samples were subjected to flow cytometry to calculate the mitotic index. Treatment of siRNA against *RAD21*, a major player in maintaining sister chromatid cohesion was used as a positive control. As expected, loss of *RAD21* resulted in an increased mitotic index [384]. However, upon RBP depletion of the different candidates, the cells did not undergo a cell cycle arrest despite exhibiting errors (**Figure 3.2D**). In summary, these results suggest that RBPs are involved in mitosis but do not affect cell cycling.

3.5.3 Depletion of orthologs in fly embryos affects viability and mitosis.

As the knockdown of RBPs in the human model disrupted mitosis, we wanted to test if this was the case in the fly embryos of *D. melanogaster*. Utilizing DIOPT, an online tool to predict putative orthologs, the equivalent RBPs in the fly are identified [385]. From the 30 RBP hits found during the IF screen, we tested the fly ortholog of 10 RBPs. We used the *GAL4/UAS* system to perform knockdown using RNA interference (**Figure 3.3A**). The depletion targeted the female germline using the *nanos-Gal4-VP16* (*NGV)* driver (Figure 3.4A). These flies were crossed with ones carrying the Upstream Activating Sequence (UAS) that contained transgenes downstream expressing hairpin RNA (hpRNA) against the RBP of interest. Consequently, the cross resulted in RBP knockdown in the female germline resulting in RBP-depleted embryos (**Figure 3.3A**). First, we assessed the viabilities of the crosses that we performed. We found that loss of 4 of the RBPs, *CG7946 RNAi*, *CG7008 RNAi*, *CG31368 RNAi*, and *CG12085 RNAi* all resulted in impaired viability, suggesting a defect during embryonic development (**Figure 3.3B**). Next, we took a further look at the embryos by performing IF and FISH. Further analyses of *CG7946 RNAi* embryos revealed that they were developmentally blocked and displayed a loss of *centrocortin* (*cen*) localization (**Figure 3.3C**). *Cen* is a dynamic mRNA

that shows localization to both the centrosomes and astral microtubules, exhibiting high expression during early embryonic development of *D. melanogaster* and its downregulation leads to spindle defects [338, 386]. Furthermore, our preliminary data showed that the loss of 2 of the RBPs, *CG12085 RNAi* and *CG31386 RNAi* resulted in mitotic defects as they exhibited spindle abnormalities and free centrosomes (**Supplemental Figure 3.2**). Crosses performed using *CG13387 RNAi*, *CG10466 RNAi*, *CG6799 RNAi*, and *CG5808 RNAi* flies resulted in 4 of the RBP knockdown groups having sterile females that did not lay eggs, suggesting that these RBPs may be implicated during oogenesis (**Figure 3.3D**). In summary, 80% of the screened RBPs in *D. melanogaster* embryos showed defects, emphasizing the importance of RBPs in the regulation of development.

3.5.4 *ASPM* mRNA shows localization throughout mitosis and loss of RNA binding proteins disrupts *ASPM* localization at the centrosomes.

We wanted to assess how loss of RBPs affects the localization of mitotic mRNAs. We adapted the smiFISH protocol and combined it with IF (smiFISH-IF) to obtain co-staining of the protein and mRNA of interest [381]. To perform smiFISH, two types of probes were used: a primary and secondary probe. The primary probes contain a gene-specific sequence with a common FLAP sequence and the secondary probe contains two fluorophores that recognize the FLAP sequence. Hybridization of the fluorophores to the primary probes occurs through the shared FLAP sequence *in vitro* (**Figure 3.4A**). First, we tested the localization of *GFP* and β *ACTIN*, the negative and positive controls, respectively. As expected, *GFP* did not exhibit a specific localization whereas β *ACTIN* was enriched in the cytoplasm (**Figure 3.4B**). Next, we performed smiFISH-IF for *ASPM* mRNA and ASPM protein and found that both the mRNA and protein co-localize and exhibit localization to the centrosomes throughout mitosis as previously reported [123, 127, 387] (**Figure 3.4C**). Although a previous screen identified 8 mRNAs localized at the centrosomes in HeLa cells, we chose to focus primarily on *ASPM* due to its robust localization during metaphase, therefore making it serve as a good marker for readout when scoring phenotypes [127]. Earlier studies have shown that ASPM protein is involved

in spindle organization in human U2OS cells [388]. Similarly, the putative ortholog Asp also displays a related function in *D. melanogaster [389-391]*.

Next, we wanted to test if loss of RBPs affected the localization of the mitotic mRNA, *ASPM*, at the centrosomes. The localization *of ASPM* mRNA in knockdown of 7 of the RBP candidates that were identified in the siRNA screen was tested. Therefore, we performed smiFISH-IF and co-stained with *ASPM* mRNA, as well as ASPM and α Tubulin proteins. We found that the loss of *SF3A3*, *SF1*, *RBMX2*, *PUF60*, *RPS3*, and *WDR43* disrupted *ASPM* localization at the centrosomes (**Figure 3.5A**). The localization of *ASPM* transcripts either appeared diffused or there appeared to be more than two foci (**Figure 3.5A**). Despite the reduced amount of *ASPM* mRNA, its protein counterpart was still present and remained unaffected (**Figure 3.5A**). Next, we wanted to quantify the mRNA localization defects that existed in RBP depleted cells. Cells that had more than two foci at the centrosomes or had a diffused mRNA signal were scored as having a mRNA localization defect. We found that there was a general trend where the loss of RBPs exhibited a higher incidence of cells with mRNA localization defects (**Figure 3.5B**). Note, that the *siSF3A3* group (p-value: 0.0566) and *siCCDC86* group (p-value: 0.0786) was close to reaching significance. Lastly, we wanted to test if there was indeed reduced *ASPM* mRNA at the centrosomes. Therefore, quantitative image analysis was conducted using IMARIS software. ASPM protein was used as a mask and the amount of *ASPM* mRNA inside of the protein mask was measured. The mean pixel intensity was representative of the amount of *ASPM* mRNA. Indeed, we saw that in all cases of RBP depletion, there was reduced *ASPM,* with the exception of *siCCDC86* cells (**Figure 3.5C**). These results indicate that our candidate RBPs are involved in the recruitment of *ASPM* mRNA to the centrosomes, and loss of the RBPs disrupts mRNA localization.

3.6 Discussion

In this paper, we demonstrated that RBPs are involved in the regulation of mitosis, and the loss of some of these proteins results in mitotic defects. Moreover, we provide evidence for the first time that the loss of RBPs disrupts mRNA localization of the mitotic mRNA, *ASPM*. Similarly, orthologs in fly embryos experience developmental problems.

Importantly, these results support the notion that RBPs play a role during mitosis, and their interaction with mRNAs impact cell cycle fidelity.

Among the 300 RBPs, we observed that 30 of the RBPs exhibited localization to the mitotic apparatus structures (**Figure 3.1C**). In fact, there have been several examples in the literature supporting the association between the RBP and the centrosome/spindle [121-123, 127, 301]. Isolation of the mitotic spindle combined with mass spectrometry identified large number proteins co-purified association with the spindle in human cells [301]. Notably, 21% of proteins, were classified as nucleic acid binding proteins, including RBPs [301]. Similarly, a subset of proteins that were purified from the centrosomes in human cells were also RBPs [50]. Due to the high incidence of RBPs being associated with these structures, we decided to interrogate their functional attributes.

Although the localization of *ASPM* to the centrosome was disrupted, a question that still remains is whether the interaction between the RBP and mRNA is direct or not. It is quite possible that the phenotypes that have been observed were due to an indirect consequence of the loss of RBPs. The RBP can be interacting with other proteins and its removal can lead to a cascade of downstream events, affecting *ASPM* localization. To test this idea, RNA immunoprecipitation (RIP)-qRT-PCR could be conducted [392, 393]. Performing this procedure will allow us to unravel the RNA-protein interactions. If there is an increase in *ASPM* mRNA expression after performing the assay, it would support that there is a direct interaction between the RBP and mRNA. This would suggest that the observed mitotic defects are due to a disruption of the RBP-mRNA interaction. Furthermore, a smiFISH screening for mRNAs that includes other mitotic mRNAs as well as non-mitotic mRNAs can also be conducted in RBP depleted cells. A screening conducted in HeLa cells revealed that mRNAs exhibit localization to several compartments including the cell edge and protrusions [394]. These non-mitotic mRNAs can also be used to observe whether the interaction between the mRNA and RBP is direct. In conclusion, these experiments would further validate that recruitment of the mRNAs to the centrosomes is conducted by the RBP.

Typically, one of the purposes that localizing mRNAs serves is that it allows for local translation. It has been previously reported that *ASPM* undergoes local translation at the centrosomes [123, 127]. We expected that the loss of *ASPM* mRNA localization at the centrosomes would also lead to reduced levels of ASPM protein. However, it appears that the ASPM protein remains unaffected even at sites where there is reduced mRNA (**Figure 3.5A**). A technical caveat is that although we have validated that the endogenous mRNA levels of the RBPs were reduced, the protein levels were not tested. There could still be residual protein that is transporting *ASPM* mRNA. It could be that some of the RBPs have a slower turnover. Therefore, verifying the amount of endogenous RBP after siRNA knockdown by performing a Western blot would be essential. If the technical caveats are addressed and indeed we see RBP knockdown, it would hint that that there is something occurring in the cell. Perhaps, there are two populations of ASPM proteins, ones that come from local translation and the latter that are recruited by other proteins (**Figure 3.5A**). Since ASPM is a major player involved in spindle organization, it could be that the cell has multiple ways of recruiting the protein to ensure it gets to the centrosomes. For instance, *CTN-RNA* is retained in the nucleus [170]. However, upon stress the *CTN-RN*A is cleaved to form a version that is competent to code for protein [170]. Analogously, there could be a reserve of ASPM protein when one mode is withdrawn. In sum, our findings were unexpected in the sense that the distribution of the mRNA did not affect its counterpart protein.

Although mitotic defects were present upon knockdown of RBPs, it did not lead to a cell cycle arrest as shown by our flow cytometry data. These results suggest that the cells were continuing to cycle. A likely possibility is that the depletion of RBPs affects the surveillance systems during the cell cycle, consequently allowing the cells to surpass and progress. For instance, one study found that *siMAD2* treated HeLa cells continued to progress throughout mitosis despite exhibiting mitotic errors after microtubule depolymerization with colcemid treatment [395]. In line with this, it would be interesting to observe how the factors of the SAC impacted. Perhaps, there is aberrant expression of its components.

As knockdowns in *D. melanogaster* embryos interfered with viability, oogenesis, and embryogenesis, these results indicate that RBPs are a major player when it comes to the development of an organism (**Figure 3.3D**). It should come as no surprise considering that spatial and temporal resolution for mRNAs is required during embryogenesis and gametogenesis. RBPs have been implicated in development in a wide range of organisms including the fly, mouse, and zebrafish [396-398]. Since a great number of RBP knockdowns of our candidates led to sterile females, it made us question how these RBPs are involved in oogenesis (**Figure 3.3D**). A likely possibility is that these RBPs are involved in recruiting maternal mRNAs during oogenesis to different regions of the egg as in the case of Staufen [398, 399]. We speculate that the loss of the RBP candidates prevent the mRNAs required during oogenesis from being localized, consequently disrupting the process. Similarly, *CG7946 RNAi*, *CG31368 RNAi*, and *CG12085 RNAi* disrupted mitosis during embryogenesis (**Figures 3.3D and Supplementary Figure 3.2**). A likely possibility is that these RBPs are involved in recruiting mitotic mRNAs to ensure that the rapid nuclear divisions are occurring properly. For example, it has already been well-established that *cen* localization is required at the centrosomes during mitosis [386, 400]. Furthermore, in *CG7946 RNAi* embryos the *cen* exhibits a diffused signal. At earlier stages, the *cen* displays a perinuclear pattern. However, in *CG7946 RNAi* embryos, they are developmentally blocked, suggesting a high likelihood that the developmental block appears before *cen* recruitment. In conclusion, these results suggest that development is a highly intricate process requiring a choreography of dynamic interactions between protein and RNA. Disruption of this process can impede development.

Our current working model suggests that in a normal cell, RBPs are involved in the localization of *ASPM* mRNA to the centrosomes (**Figure 3.6**). This enrichment to the structure by the RBP is required for an error-free mitosis to occur. Whether the interaction is direct is to be further investigated. However, when there is a depletion of the RBP, it disrupts the localization of *ASPM* mRNA. Interestingly, the cells that have disrupted *ASPM* localization at the centrosomes also exhibit mitotic defects (**Figure 3.5A**). Furthermore, the reduced levels of *ASPM* at the centrosomes could potentially contribute

to mitotic defects (**Figure 3.5C**). This paper sheds light into the potential interactions among the components of the RNP complex during mitosis. Exploration of these interactions can possibly serve to understand the underlying mechanisms that lead to mitotic errors from an RNA angle.

3.7 Acknowledgments

We would like to thank the Bloomington *Drosophila* Stock Center. We thank Dominic Filion for his assistance in microscopy and image analysis. We would also like to thank Julie Lord and Eric Massicotte for their help in flow cytometry. We are grateful to Eunjeong Kwon and Farah Saad for helpful comments on the manuscript. E.L is a Senior FRQS research scholar. This work was supported by a grant to E.L. from the Canadian Institutes of Health Research (CIHR).

3.8 Declaration of Interests

The authors declare no competing interests.

3.9 Figures and Figure Legends

Figure 3.1

A.

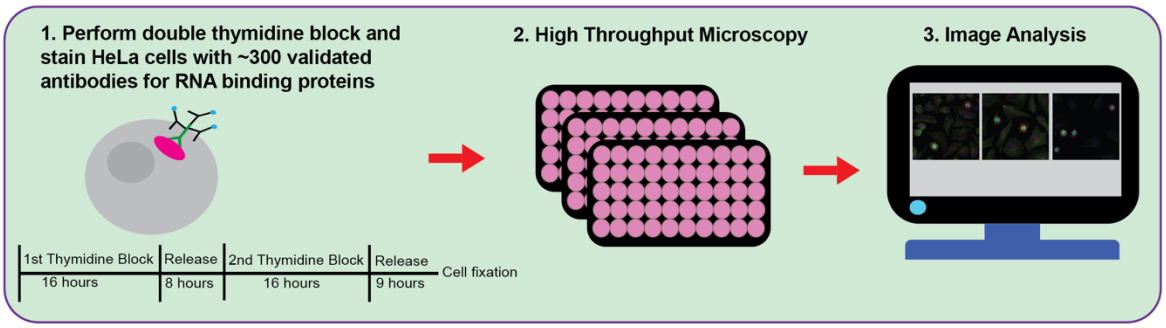

B.

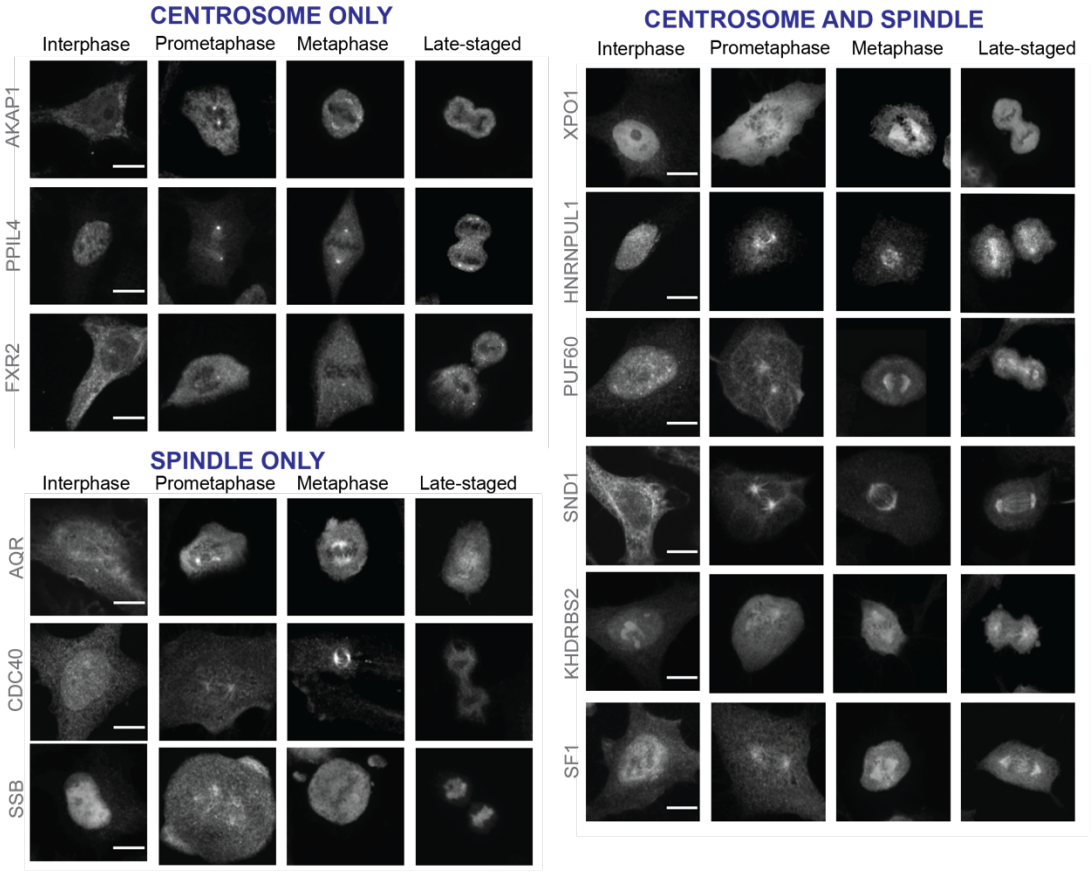

C.

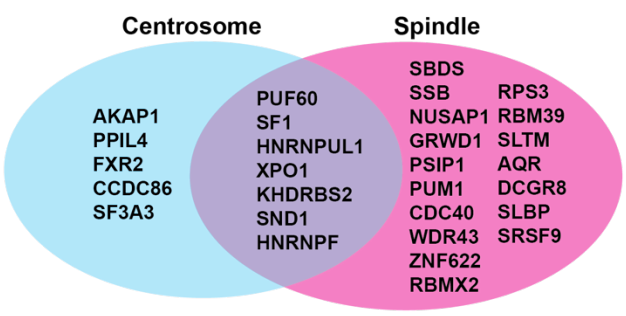

Figure 3.2

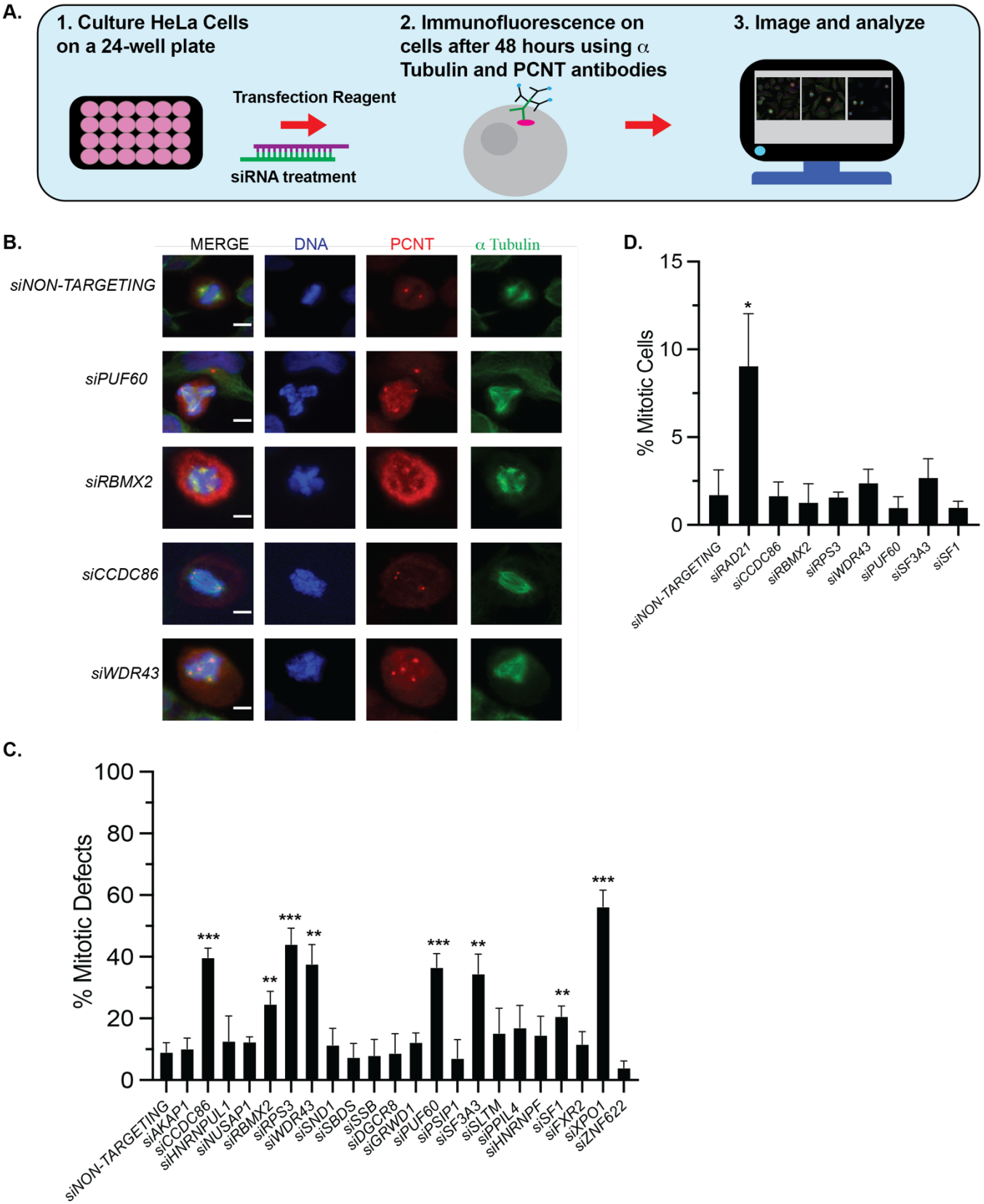
A.
1. Culture HeLa Cells on a 24-well plate
Transfection Reagent
siRNA treatment
2. Immunofluorescence on cells after 48 hours using α Tubulin and PCNT antibodies
3. Image and analyze
B.
MERGE
DNA
PCNT
α Tubulin
siNON-TARGETING
siPUF60
siRBMX2
siCCDC86
siWDR43
D.
% Mitotic Cells
15
10
5
0
siNON-TARGETING
siRAD21
siCCDC86
siRBMX2
siRPS3
siWDR43
siPUF60
siSF3A3
siSF1
C.
% Mitotic Defects
100
80
60
40
20
0
siNON-TARGETING
siAKAP1
siCCDC86
siHNRNPUL1
siNUSAP1
siRBMX2
siRPS3
siWDR43
siSND1
siSBDS
siSSB
siDGCR8
siGRWD1
siPUF60
siPSIP1
siSF3A3
siSLTM
siPPIL4
siHNRNPF
siSF1
siFXR2
siXPO1
siZNF622

Figure 3.3

A.

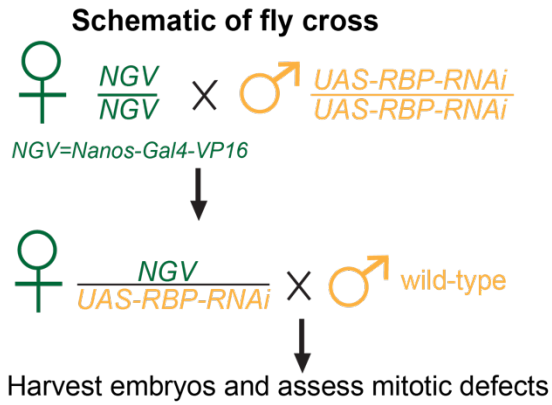

B.

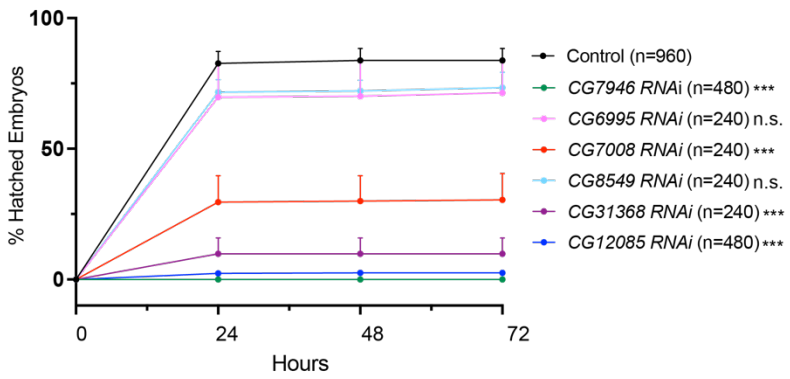

C.

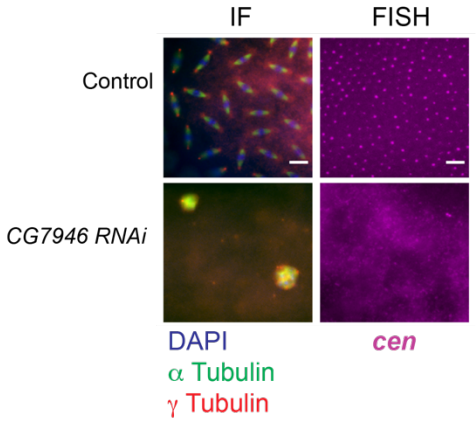

D.

RBP	HUMAN ORTHOLOG	PHENOTYPE
CG6995	SLTM	wild-type
CG8549	SBDS	wild-type
CG13387	XPO1	sterile females
CG10466	RBMX2	sterile females
CG6799	RPS3	sterile females
CG5808	PPIL4	sterile females
CG7008	SND1	reduced viability
CG7946	PSIP1	not viable, developmentally blocked
CG12085	PUF60	reduced viablity
CG31368	AQR	reduced viablity

Figure 3.4

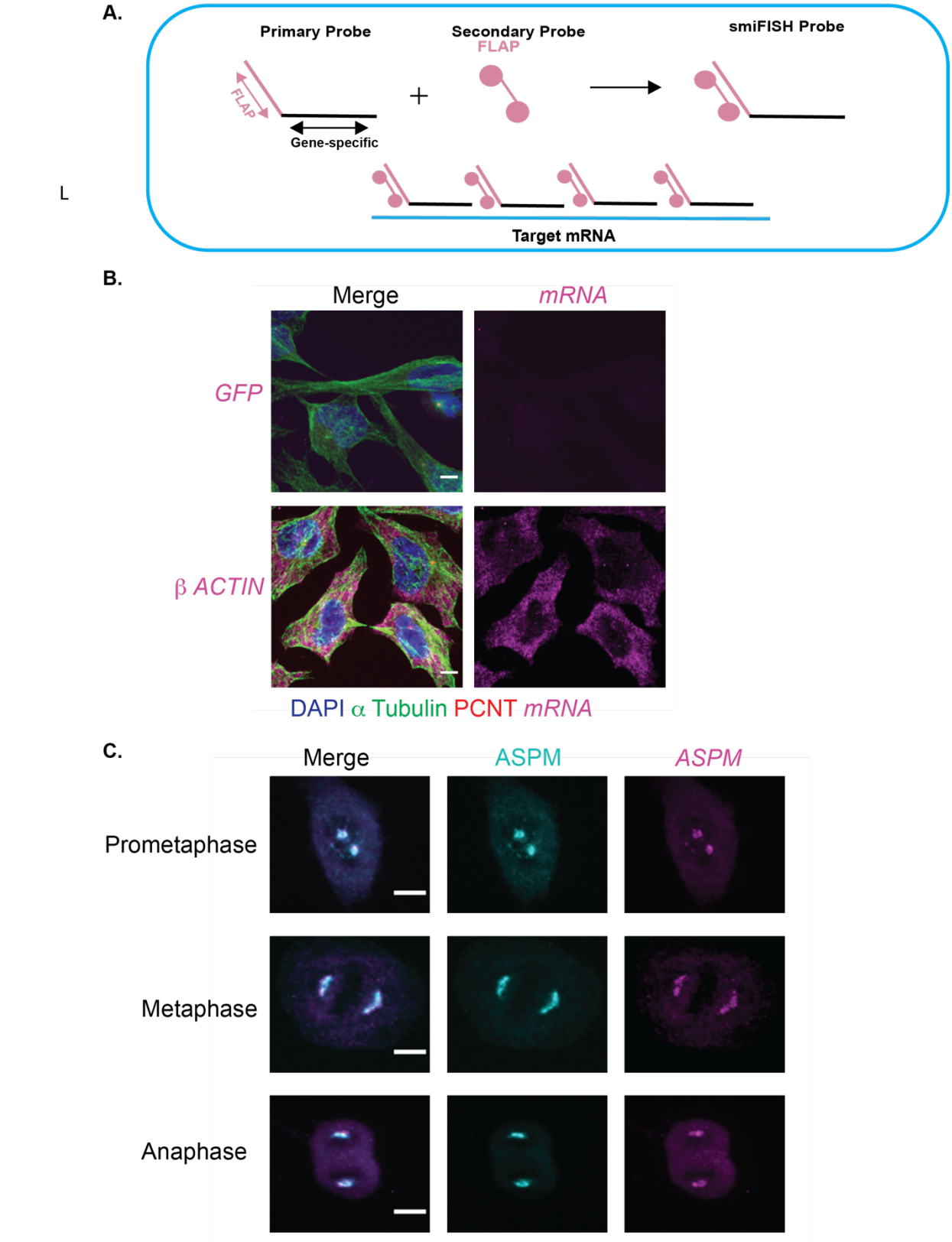
A.
Primary Probe
Secondary Probe
FLAP
smiFISH Probe
FLAP
Gene-specific
Target mRNA
B.
Merge
mRNA
GFP
β ACTIN
DAPI α Tubulin PCNT mRNA
C.
Merge
ASPM
ASPM
Prometaphase
Metaphase
Anaphase

Figure 3.5

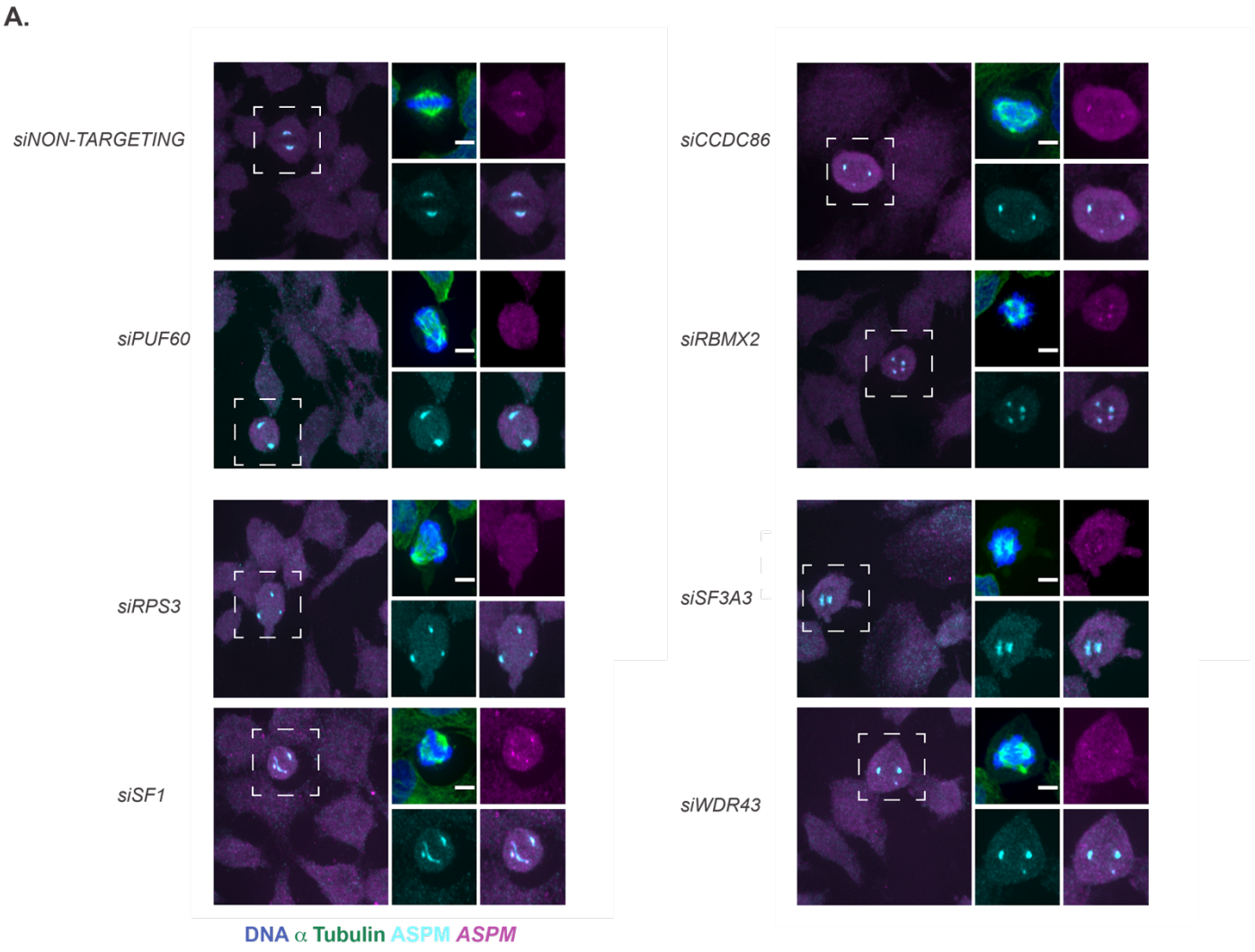
A.
siNON-TARGETING
siPUF60
siRPS3
siSF1
siCCDC86
siRBMX2
siSF3A3
siWDR43
DNA α Tubulin ASPM ASPM
B.
Normal
Multiple Foci
Diffused Signal
B'.
% mRNA localization defects
n.s.
Multiple Foci
Diffused
C.
Mean Intensity (a.u.)
n.s.
ASPM mRNA

Figure 3.6

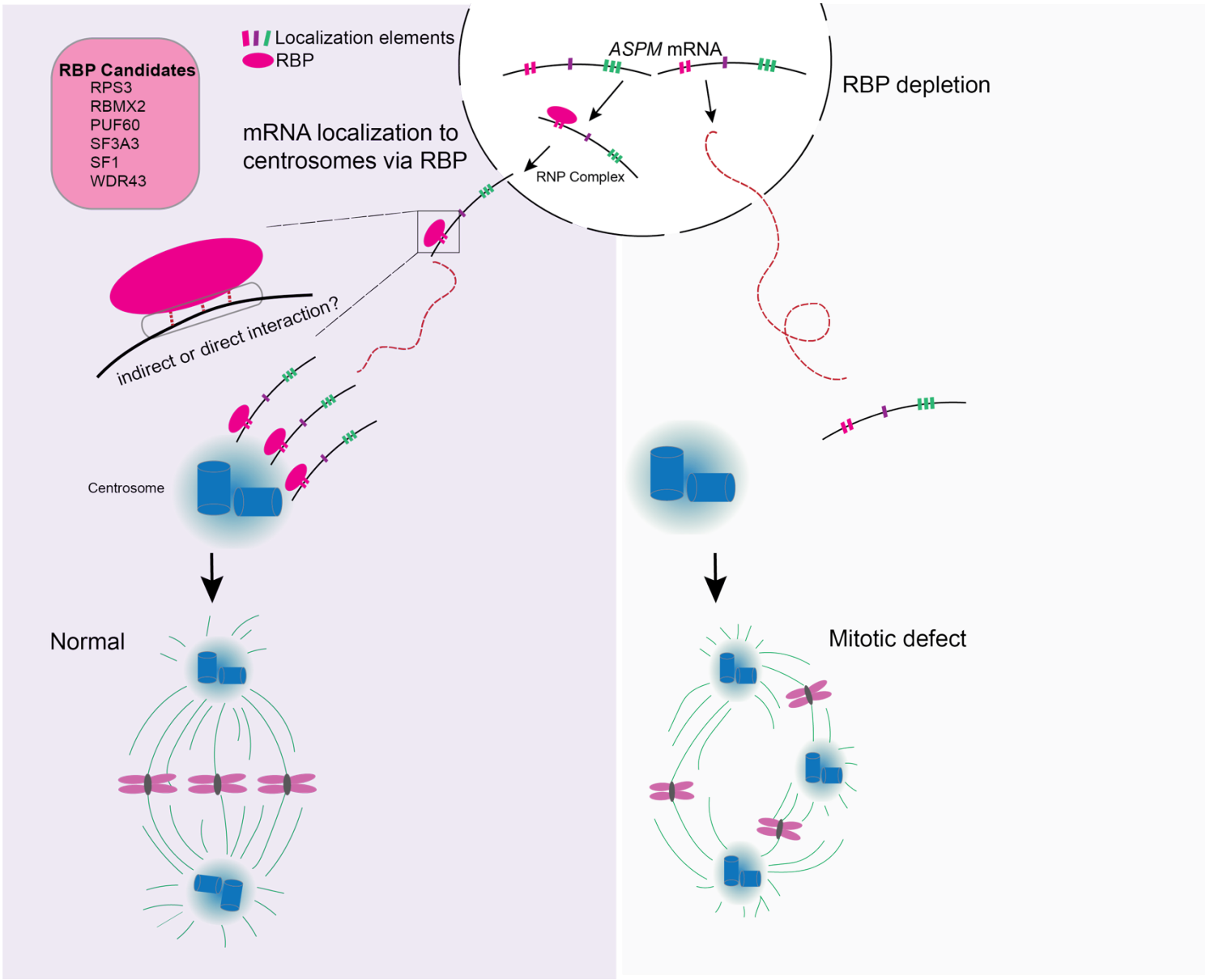
RBP Candidates
RPS3
RBMX2
PUF60
SF3A3
SF1
WDR43
Localization elements
RBP
mRNA localization to centrosomes via RBP
ASPM mRNA
RNP Complex
RBP depletion
indirect or direct interaction?
Centrosome
Normal
Mitotic defect

Figure 3.1: Screening reveals that approximately 10% of RBPs localize to the mitotic apparatus structures including the spindle and centrosomes.

(**A**) Schematic depicting the pipeline for the RBP screening. Hela cells were seeded onto 96 well plates and underwent a double thymidine block treatment to enrich for a mitotic cell population. To perform the double thymidine block, cells were treated with 2mM of thymidine followed by an 8-hour release in cell media. The 16-hour treatment was repeated once more and followed by a 9-hour release in cell media. After the second release, the cells were fixed and immunofluorescence was conducted for ~300 validated RBPs. A high content screening microscope was used for the initial screening to annotate RBPs that showed co-localization with the spindle and centrosome makers, α Tubulin and PCNT. (**B**) Immunofluorescence images taken on the spinning disc confocal microscope showing the localization of different RBPs during interphase, prometaphase, metaphase, and late-staged (telophase/cytokinesis). These results are representative of three independent experiments. Scale bar represents 10μm. (**C**) Venn diagram showing the different mitotic apparatus structures that the RBP localizes. Some RBPs are enriched to either the centrosome or spindle while others show dynamic localization to both structures.

Figure 3.2: RBP depletion leads to mitotic defects but does not compromise cell cycling. (**A**) Schematic showing the pipeline for RBP depletion in Hela cells. Cells were cultured on coverslips using 24-well plates. 50nM of siRNA was transfected using Lipofectamine RNAi Max transfection agent and the wells were replenished with fresh media after 24 hours. After 48 hours, the cells were fixed and stained with DAPI, α Tubulin, and PCNT. The cells were imaged, and mitotic defects were quantified on prometaphase and metaphase cells. (**B**) Representative images of metaphase-staged Hela cells treated with 50nM of siRNAs against the following RBP targets: *siNON-TARGETING*, *siPUF60*, *siRBMX2*, *siCCDC86*, and *siWDR43*. Scale bars represent 10μM. Blue, DAPI; Green, α Tubulin; Red, PCNT (**C**) A quantification of the percentage of Hela cells that exhibited mitotic defects against the indicated RBP targets. All groups were conducted in triplicates with the exception of the *siSBDS* group, which was

performed in a duplicate. A minimum of 150 cells were analyzed for each group. The data represent the mean ± SD of a minimum of two independent experiments. An unpaired two-tailed t test was performed to assess statistical significance (**p<0.01, ***p<0.001). (D) The mitotic index after treatment with the indicated siRNAs. The *siRAD21* was used as a positive control. This experiment was conducted in triplicates and the data represent mean ± SD of three independent experiments. An unpaired two-tailed t test was conducted to assess statistical significance (*p<0.05).

Figure 3.3: Loss of RBPs in fly orthologs leads to impaired viability and mitotic defects. (**A**) Schematic of fly cross in *D. melanogaster*. Virgin female (*NGV*) flies were crossed to males (*UAS-RBP*) and the result of this cross were flies with depletion of the RBP in the female germline. Virgin females were collected and crossed to wild-type (*Oregon R*) males and the embryos were harvested. (**B**) Hatching frequency of control and the indicated RBP RNAi embryos. The data indicate the mean ± SEM of a minimum of two independent experiments. The statistical significance was determined by an unpaired two-tailed t test at the 72-hour time point (n.s. not significant, ***p<0.001). (**C**) Immunofluorescence labeling of α/γ Tubulin and DAPI as well as FISH for *cen* mRNA in the indicated genotypes of embryos. These results are representative of two independent experiments. Scale bar represents 10μm. Blue, DAPI; Green, α TUBULIN; Red, γ TUBULIN; Magenta, *cen* (**D**) Summary table of observed phenotypes of the indicated RBP-RNAi crosses.

Figure 3.4: *ASPM* mRNA localizes to the centrosomes during mitosis. (**A**) Schematic of the smiFISH technique. Primary probes contain a gene-specific sequence and a shared FLAP sequence. The secondary probe contains two fluorophores that recognize the FLAP sequence when hybridized *in vitro*. This allows the detection of the mRNA in the cell. (**B**) smiFISH-IF was performed on HeLa cells to detect mRNA and protein. Negative (*GFP*) and positive (*β ACTIN*) controls for smiFISH-IF in HeLa cells. Scale bar represents 10μM. Blue, DAPI; Green, a Tubulin; Red, PCNT; Magenta, *ASPM* (**C**) Images of smiFISH-IF on *ASPM* mRNA and ASPM protein throughout different stages in mitosis. Scale bar represents 10μM. Magenta, *ASPM*; Cyan, ASPM

Figure 3.5: Loss of RBPs results in mRNA localization defects of *ASPM* at the centrosomes. (**A**) Representative confocal images of smiFISH-IF conducted on siRNA treated HeLa cells against the RBPs of interest. After treatment with 50nM of siRNAs, smiFISH was performed 48 hours later and imaged on a spinning disc confocal microscope. The zoom panels signify the merged and individual *ASPM* mRNA and ASPM protein channels in mitotic cells as well as the merged DAPI and α Tubulin protein channels. Scale bar represents 10μm. Blue, DAPI; Green, a Tubulin; Cyan, ASPM; Magenta, *ASPM* (**B**) Representative images of cells that are scored as normal or exhibiting a mRNA localization defect (diffused signal or multiple foci). **B'** Quantification of the percentage of cells exhibiting a mRNA localization defect in the indicated groups. Analysis was conducted on a minimum of 45 cells per group in two independent experiments. The data indicate the mean ± SEM of two independent experiments. An unpaired two-tailed t test was performed to assess statistical significance (n.s. not significant, *p<0.05, **p<0.01). (**C**) Quantification of the mean pixel intensity of *ASPM* mRNA on RBP depleted cells. Analysis was conducted with IMARIS software using the ASPM protein as a mask and then measuring the intensity of the *ASPM* mRNA. Analysis was conducted on a minimum of 100 centrosomes per group in two independent experiments. The data indicate the mean ± SEM of two independent experiments. An unpaired two-tailed t test was performed to assess the statistical significance (n.s. not significant, **p<0.01, ***p<0.001). a.u.- arbitrary units

Figure 3.6: Model for mRNA localization to the centrosomes. Our data identified 6 RBPs that are involved in the process of recruiting *ASPM* mRNA to the centrosomes. When RBPs are present in the cell, this allows *ASPM* to be appropriately localized, subsequently resulting in cell cycle fidelity. However, the loss of RBPs disrupts the localization of *ASPM* and impacts mitosis, consequently leading to mitotic defects. It remains unknown whether the RBP directly binds to the mRNA or if there are other factors involved. In conclusion, our data support that RBPs play a role in trafficking *ASPM* to the centrosomes during mitosis.

3.10 Supplemental Figures and Figure Legends

Supplemental Figure 3.1

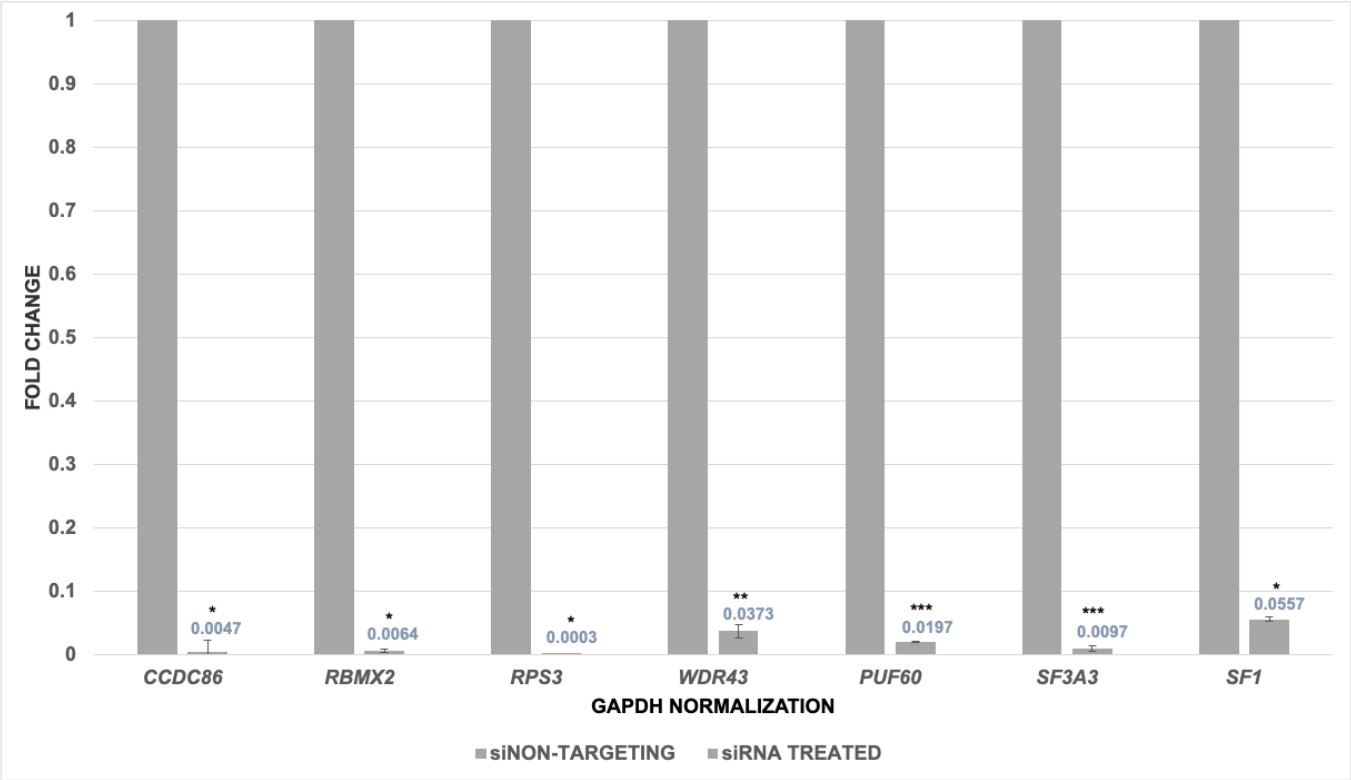

Supplemental Figure 3.2

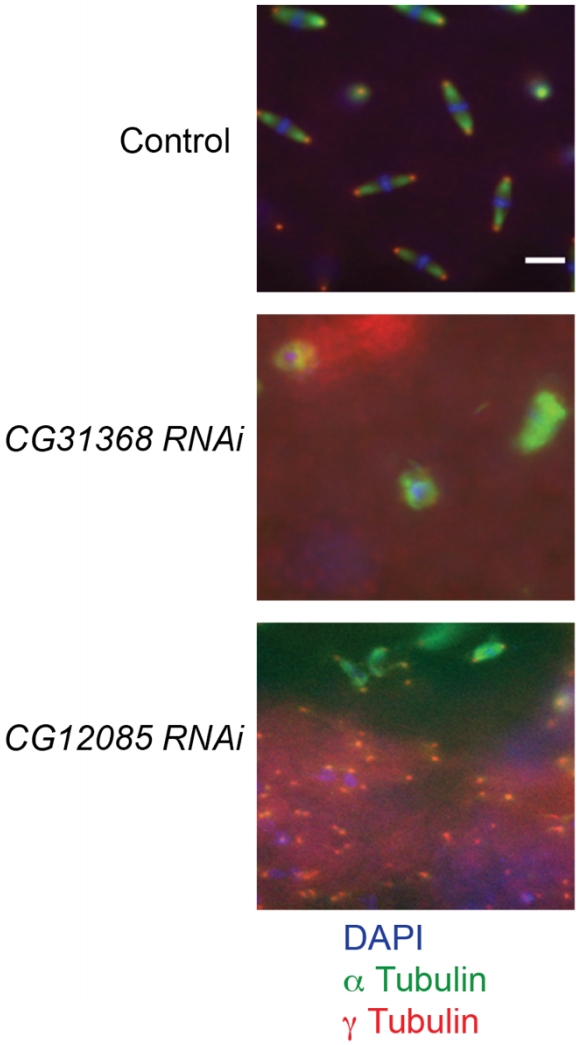

Supplemental Figure 3.1. Validation of mRNA expression levels after siRNA knockdown. Related to Figure 3.2. Relative expression levels of RBP candidates after treatment with 50nM siRNA for the respective RBP. The values above the bar indicate the mean. Data are normalized to *GAPDH* mRNA levels and represent the mean ± SEM from one experiment that was conducted in triplicates. An unpaired two-tailed t test was performed to assess the statistical significance (*p<0.05, **p<0.01, ***p<0.001).

Supplemental Figure 3.2. RBP depletion in fly embryos disrupts mitosis. Related to Figure 3.3. Immunofluorescence labeling of α/γ Tubulin and DAPI in the indicated genotypes of embryos. Scale bar represents 10μm. Blue, DAPI; Green, α Tubulin; Red, γ Tubulin

3.11 Tables

Table 3.3 Key Resources Table

REAGENT or RESOURCE	SOURCE	IDENTIFIER
Reagents		
Paraformaldehyde	Sigma-Aldrich	Cat#252549
Trizol	Invitrogen	Cat#15596026
Dextran Sulfate	Millipore Sigma	Cat#S4031
E. coli tRNA	Sigma	Cat#10109541001
FLAP Y CY5	IDT	Custom
FLAP X CY5	IDT	Custom
Lipofectamine RNAi Max	Invitrogen	Cat#13778150
OptiMEM 1X	Life Technologies	Cat#31985070
GlycoBlue Coprecipitatant	Invitrogen	Cat# AM9516
NEBuffer3	New England Biolabs	Cat#B7003S
RNAseOUT	ThermoFisher Scientific	Cat#10777019
ProLongGlassAntifa	Invitrogen	Cat#P36985
Albumin	BioShop	Cat#9048-46-8
Digoxigenin-11-UTP (DIG-	Roche	Cat#11209256910
Biotin-16-UTP	Roche	Cat#11388908910
Streptavidin-HRP	Sigma-Aldrich	Cat# S911
Propidum Iodide	Sigma-Aldrich	Cat#25535-16-4
NTPs	Promega	Cat#E601B, E602B, E603B, E604B
Thymidine	Sigma-Aldrich	Cat#50-89-5
RNase A	New England Biolabs	Cat#7013S
NonidetTM P-40	Sigma-Aldrich	Cat#9002-93-1
Fly Stocks		
CG6995 RNAi TRIP Stock	BDSC	Cat#51759
CG8549 RNAi TRIP Stock	BDSC	Cat#54466
CG13387 RNAi TRIP Stock	BDSC	Cat#34021
CG10466 RNAi TRIP Stock	BDSC	Cat#55263
CG6799 RNAi TRIP Stock	BDSC	Cat#35410
CG5808 RNAi TRIP Stock	BDSC	Cat#55208
CG7008 RNAi TRIP Stock	BDSC	Cat#34865
CG7946 RNAi TRIP Stock	BDSC	Cat#55274
CG12085 RNAi TRIP Stock	BDSC	Cat#34785
CG31368 RNAi TRIP Stock	BDSC	Cat#55172
Drosophila Oregon R	BDSC	n/a
Nanos-Gal4-VP16 (NGV)	BDSC	Cat#4937
Antibodies		
Rabbit Anti- γ Tubulin	Sigma-Aldrich	Cat#T0950
Rabbit Anti-ASPM	Bethyl	Cat#IHC-00058
Mouse Anti-PCNT	Abcam	Cat#ab28144

Rat Anti-α Tubulin	Bio-Rad	Cat#MCA78G
Anti-Rat-Alexa488	Invitrogen	Cat#A21208
Anti-Rabbit-Alexa647	Invitrogen	Cat#A31573
Anti-Rabbit-Alexa555	Jackson Immunoresearch	Cat#711-605-152
Rabbit Anti-AKAP1	Bethyl	Cat#A301-379A
Rabbit Anti-AKAP1	Genetex	Cat#GTX102578
Rabbit Anti-AQR	Bethyl	Cat#A302-547A
Rabbit Anti-CCDC86	Bethyl	Cat#A302-482A
Rabbit Anti-CDC40	Bethyl	Cat#A303-699A
Rabbit Anti-CPSF6	Bethyl	Cat#A301-356A
Rabbit Anti-CPSF6	Genetex	Cat# GTX115537
Rabbit Anti-CUGBP1	Genetex	Cat#GTX114129
Rabbit Anti-CUGBP1	MBL	Cat#RN034PW
Rabbit Anti-DDX1	Genetex	Cat#GTX105205
Rabbit Anti-DDX21	MBL	Cat#RN090PW
Rabbit Anti-DGCR8	Genetex	Cat#GTX130061
Rabbit Anti-DGCR8	Bethyl	Cat#A302-468A
Rabbit Anti-eIF4G2	MBL	Cat#RN003P
Rabbit Anti-FUBP1	Genetex	Cat#GTX115154
Rabbit Anti-FXR2	Bethyl	Cat#A303-894A
Rabbit Anti-FXR2	Genetex	Cat#GTX109465
Rabbit Anti-GPKOW	Genetex	Cat#GTX117716
Rabbit Anti-GRWD1	Bethyl	Cat#A301-576A
Rabbit Anti-HNRNPF	Genetex	Cat#GTX114476
Rabbit Anti-HNRNPUL1	Bethyl	Cat#A300-862A
Rabbit Anti-KHDRBS2	MBL	Cat#RN041P
Rabbit Anti-KRR1	Bethyl	Cat#A303-898A
Rabbit Anti-KRR1	Genetex	Cat#GTX105761
Rabbit Anti-LARP1	Bethyl	Cat#A302-089A
Rabbit Anti-MARK2	Bethyl	A303-135A
Rabbit Anti-NUSAP1	Bethyl	Cat#A302-596A
Rabbit Anti-PABPC4	Bethyl	Cat#A301-466A
Rabbit Anti-PPIL4	Genetex	Cat#GTX117014
Rabbit Anti-PRPF4	MBL	Cat#RN093PW
Rabbit Anti-PSIP1	Bethyl	Cat#A300-848A
Rabbit Anti-PUF60	Bethyl	Cat#A302-817A
Rabbit Anti-PUM1	Bethyl	Cat#A302-576A
Rabbit Anti-RBM27	Bethyl	Cat#A301-233A
Rabbit Anti-RBM39	Bethyl	Cat#A300-291A
Rabbit Anti-RBMX2	Bethyl	Cat#A302-222A
Rabbit Anti-RPS3	Bethyl	Cat#A303-840A
Rabbit Anti-SART3	Genetex	Cat#GTX107684
Rabbit Anti-SBDS	Genetex	Cat#GTX109168
Rabbit Anti-SF1	Genetex	Cat#GTX104540
Rabbit Anti-SF3A3	Genetex	Cat#GTX118225
Rabbit Anti-SF3A3	Bethyl	Cat#A302-506A
Rabbit Anti-SLBP	MBL	Cat#RN045P

Rabbit Anti-SLTM	Bethyl	Cat#A302-834A
Rabbit Anti-SND1	Bethyl	Cat#A302-883A
Rabbit Anti-SRSF5	MBL	Cat#RN082PW
Rabbit Anti-SRSF9	MBL	Cat#RN081PW
Rabbit Anti-SSB	MBL	Cat#RN074PW
Rabbit Anti-TIAL1	MBL	Cat#RN059PW
Rabbit Anti-WDR43	Bethyl	Cat#A302-478A
Rabbit Anti-XPO1	Bethyl	Cat#A300-469A
Rabbit Anti-ZNF622	Bethyl	Cat#A304-075A
Rabbit Anti-ZONAB	Bethyl	Cat#A303-070A
siRNAs		
siNON-TARGETING	Horizon Discovery Ltd	Cat#D-001810-10
siAKAP1	Horizon Discovery Ltd	Cat#L-011426-00
siCCDC86	Horizon Discovery Ltd	Cat#L-014304-02
siHNRNPUL1	Horizon Discovery Ltd	Cat#L-004132-00
siNUSAP1	Horizon Discovery Ltd	Cat#L-004754-00
siRBMX2	Horizon Discovery Ltd	Cat#L-020763-02
siRPS3	Horizon Discovery Ltd	Cat#L-013607-00
siWDR43	Horizon Discovery Ltd	Cat#L-022651-01
siSND1	Horizon Discovery Ltd	Cat#L-010657-01
siSBDS	Horizon Discovery Ltd	Cat#L-019217-00
siSSB	Horizon Discovery Ltd	Cat#L-006877-01
siDGCR8	Horizon Discovery Ltd	Cat#L-015713-00
siGRWD1	Horizon Discovery Ltd	Cat#L-027146-01
siPUF60	Horizon Discovery Ltd	Cat#L-012505-01
siPSIP1	Horizon Discovery Ltd	Cat#L-015209-00
siSF3A3	Horizon Discovery Ltd	Cat#L-019808-00
siSLTM	Horizon Discovery Ltd	Cat#L-014434-01
siPPIL4	Horizon Discovery Ltd	Cat#L-010401-01
siHNRNPF	Horizon Discovery Ltd	Cat#L-013449-01
siSF1	Horizon Discovery Ltd	Cat#L-012662-01
siFXR2	Horizon Discovery Ltd	Cat#L-011955-00
siXPO1	Horizon Discovery Ltd	Cat#L-003030-00
siZNF622	Horizon Discovery Ltd	Cat#L-015113-00
Sequence-Based Reagents		
Please see **Tables 3.4-3.6** for primer sequences of smiFISH probes.	This paper	n/a
Please see **Table 3.7** for qRT-PCR sequences.	This paper	n/a

Table 3.4 smiFISH: *GFP* Probe

Name	Sequence
GFP_FLAPY_1	CTTGTACAGCTCGTCCATGCCGAGAGTTTACACTCGGACCTCGTCGACATGCATT
GFP_FLAPY_2	CAGGACCATGTGATCGCGCTTCTCGTTTTACACTCGGACCTCGTCGACATGCATT
GFP_FLAPY_3	GGTCTTTGCTCAGGGCGGACTGGGTGTTACACTCGGACCTCGTCGACATGCATT
GFP_FLAPY_4	CAGGTAGTGGTTGTCGGGCAGCAGCACTTACACTCGGACCTCGTCGACATGCATT
GFP_FLAPY_5	GGCCGTCGCCGATGGGGGTGTTCTTTACACTCGGACCTCGTCGACATGCATT
GFP_FLAPY_6	TGGTAGTGGTCGGCGAGCTGCACGCTTACACTCGGACCTCGTCGACATGCATT
GFP_FLAPY_7	GTTCACCTTGATGCCGTTCTTCTGCTTTTACACTCGGACCTCGTCGACATGCATT
GFP_FLAPY_8	CGGCCATGATATAGACGTTGTGGCTGTTGTTTACACTCGGACCTCGTCGACATGCATT
GFP_FLAPY_9	TCAGCTCGATGCGGTTCACCAGGGTGTTACACTCGGACCTCGTCGACATGCATT
GFP_FLAPY_10	GTCTTGTAGTTGCCGTCGTCCTTGAAGAAGATTTACACTCGGACCTCGTCGACATGCATT
GFP_FLAPY_11	ATGGCGGACTTGAAGAAGTCGTGCTGCTTTACACTCGGACCTCGTCGACATGCATT
GFP_FLAPY_12	ATGTGGTCGGGGTAGCGGCTGAAGCACTTACACTCGGACCTCGTCGACATGCATT
GFP_FLAPY_13	TGGGCCAGGGCACGGGCAGCTTGTTACACTCGGACCTCGTCGACATGCATT
GFP_FLAPY_14	GGTGGTGCAGATGAACTTCAGGGTCAGCTTACACTCGGACCTCGTCGACATGCATT
GFP_FLAPY_15	TGTGGCCGTTTACGTCGCCGTCCAGTTACACTCGGACCTCGTCGACATGCATT
GFP_FLAPY_16	TCCCGGCGGCGGTCACGAACTCCTTACACTCGGACCTCGTCGACATGCATT
GFP_FLAPY_17	CCGTCCTCGATGTTGTGGCGGATCTTGTTACACTCGGACCTCGTCGACATGCATT
GFP_FLAPY_18	TTGTACTCCAGCTTGTGCCCCAGGATTACACTCGGACCTCGTCGACATGCATT
GFP_FLAPY_19	TTGCCGTCCTCCTTGAAGTCGATGCCTTACACTCGGACCTCGTCGACATGCATT
GFP_FLAPY_20	GCCCTCGAACTTCACCTCGGCGCTTACACTCGGACCTCGTCGACATGCATT
GFP_FLAPY_21	TGCGCTCCTGGACGTAGCCTTCGGTTACACTCGGACCTCGTCGACATGCATT
GFP_FLAPY_22	CACGCCGTAGGTCAGGGTGGTCACGAGTTACACTCGGACCTCGTCGACATGCATT
GFP_FLAPY_23	TCGCCCTCGCCGGACACGCTGAATTACACTCGGACCTCGTCGACATGCATT
GFP_FLAPY_24	CGACCAGGATGGGCACCACCCCGTTACACTCGGACCTCGTCGACATGCATT

Table 3.5 smiFISH: *β ACTIN* Probe

Name	Sequence
BACT_FLAPY_1	AAGGTGTGCACTTTTATTCAACTGGTCTCAAGTTACACTCGGACCTCGTCGACATGCATT
BACT _FLAPY_2	AGAAGCATTTGCGGTGGACGATGGAGGGGTTACACTCGGACCTCGTCGACATGCATT
BACT _FLAPY_3	GCTCAGGAGGAGCAATGATCTTGATCTTCTTACACTCGGACCTCGTCGACATGCATT
BACT _FLAPY_4	GGATGTCCACGTCACACTTCATGATGGAGTTACACTCGGACCTCGTCGACATGCATT
BACT _FLAPY_5	GAAGGTAGTTTCGTGGATGCCACAGGACTCTTACACTCGGACCTCGTCGACATGCATT
BACT _FLAPY_6	CAGCGGAACCGCTCATTGCCAATGGTTTACACTCGGACCTCGTCGACATGCATT
BACT _FLAPY_7	CAGCCTGGATAGCAACGTACATGGCTGTTACACTCGGACCTCGTCGACATGCATT
BACT _FLAPY_8	GTGTTGAAGGTCTCAAACATGATCTGGGTCATTTACACTCGGACCTCGTCGACATGCATT
BACT _FLAPY_9	TCGGGAGCCACACGCAGCTCATTGTATTACACTCGGACCTCGTCGACATGCATT
BACT_FLAPY_10	ACGAGCGCGGCGATATCATCATCCATTTACACTCGGACCTCGTCGACATGCATT
BACT_FLAPY_11	ACGAGCGCGGCGATATCATCATCCATTTACACTCGGACCTCGTCGACATGCATT
BACT_FLAPY_12	CATTGTGAACTTTGGGGGATGCTCGCTCTTACACTCGGACCTCGTCGACATGCATT
BACT_FLAPY_13	GACTGCTGTCACCTTCACCGTTCCAGTTACACTCGGACCTCGTCGACATGCATT
BACT_FLAPY_14	GGACTCGTCATACTCCTGCTTGCTGATTACACTCGGACCTCGTCGACATGCATT
BACT_FLAPY_15	CAGTGATCTCCTTCTGCATCCTGTCGTTACACTCGGACCTCGTCGACATGCATT
BACT_FLAPY_16	GACAGCACTGTGTTGGCGTACAGGTCTTTTTACACTCGGACCTCGTCGACATGCATT
BACT_FLAPY_17	CGTGGCCATCTCTTGCTCGAAGTCCATTACACTCGGACCTCGTCGACATGCATT
BACT_FLAPY_18	GCGACGTAGCACAGCTTCTCCTTAATGTTTACACTCGGACCTCGTCGACATGCATT
BACT_FLAPY_19	AGGTGTGGTGCCAGATTTTCTCCATGTCGTTACACTCGGACCTCGTCGACATGCATT
BACT_FLAPY_20	CCAGTTGGTGACGATGCCGTGCTCGATTTACACTCGGACCTCGTCGACATGCATT
BACT_FLAPY_21	GGTACTTCAGGGTGAGGATGCCTCTCTTTACACTCGGACCTCGTCGACATGCATT
BACT_FLAPY_22	CCTCGTCGCCCACATAGGAATCCTTCTTACACTCGGACCTCGTCGACATGCATT

Table 3.6 smiFISH: *ASPM* Probe

Name	Sequence
ASPM_FLAPX_1	TTCACTTCTGCCACCTCCTCGTTAGGCCTCCTAAGTTTCGAGCTGGACTCAGTG
ASPM _FLAPX_2	TCATAGCCAAGTTTTCACAAGCTTGTAGTGGGCCTCCTAAGTTTCGAGCTGGACTCAGTG
ASPM _FLAPX_3	AACGTTGGCACTGTGTACATTTAATAGTTCCCCCTCCTAAGTTTCGAGCTGGACTCAGTG
ASPM _FLAPX_4	ATAGCTTTGGGAGATTTTGAACCCTGACATTCCCTCCTAAGTTTCGAGCTGGACTCAGTG
ASPM _FLAPX_5	CAACTGAAGCTGTTGTCGAAGAGGGTGTTACCCCTCCTAAGTTTCGAGCTGGACTCAGTG
ASPM _FLAPX_6	TTTCTTAACAGCTGATGTTTTAGGCTCTGAGGCCTCCTAAGTTTCGAGCTGGACTCAGTG
ASPM _FLAPX_7	TCTGAGAGACATTTCCTCTTTTGTAGGTGCTCCTCCTAAGTTTCGAGCTGGACTCAGTG
ASPM _FLAPX_8	TCTATACAGGTGAGGAACAGTGGGGTGTCTACCTCCTAAGTTTCGAGCTGGACTCAGTG
ASPM_FLAPX_9	AGTTCTGTGTGAGAAGTTCCATGGTTCGCACCCTCCTAAGTTTCGAGCTGGACTCAGTG
ASPM_FLAPX_10	TTCCAAAGCAACCTGAGAGTTTTTTCTCTGTGCCTCCTAAGTTTCGAGCTGGACTCAGTG
ASPM_FLAPX_11	TTGTTCAAAGGAACCACTATCCCTTTTGCCCCTCCTAAGTTTCGAGCTGGACTCAGTG
ASPM_FLAPX_12	TTTCTCCATGTTGTTTGTATGAGTCGAGCAGCCCTCCTAAGTTTCGAGCTGGACTCAGTG
ASPM_FLAPX_13	GTAATTGAATGGCTGCAGCTCGTTTCTGCCCTCCTAAGTTTCGAGCTGGACTCAGTG
ASPM_FLAPX_14	TCTGTCGTTGTTGATGTTTTCTTACATGTGCCCCTCCTAAGTTTCGAGCTGGACTCAGTG
ASPM_FLAPX_15	GATGTGAGGATGTGAATATACATTTTCCTGGCCCTCCTAAGTTTCGAGCTGGACTCAGTG
ASPM_FLAPX_16	AGCTGCTTTTTTGACTTGCAAGAAGTTCTTCCCCTCCTAAGTTTCGAGCTGGACTCAGTG
ASPM_FLAPX_17	GCTCTGAAATTTTGCTGGATGACTAATGCTGCCTCCTAAGTTTCGAGCTGGACTCAGTG
ASPM_FLAPX_18	CATACATTGCTTCCTTCCTGCAGTCCCCTCCTAAGTTTCGAGCTGGACTCAGTG
ASPM_FLAPX_19	AATGAGTGTTGCTGCAGTCTGCATCTTTCCCTCCTAAGTTTCGAGCTGGACTCAGTG
ASPM_FLAPX_20	AATGAGTGTTGCTGCAGTCTGCATCTTTCCCTCCTAAGTTTCGAGCTGGACTCAGTG
ASPM_FLAPX_21	ATGAGAACTGCAGCCCTTTGCATTTCTTGCCTCCTAAGTTTCGAGCTGGACTCAGTG
ASPM_FLAPX_22	TTTACTTCTGTAACAGCAGAGTGCAGATTGGTCCTCCTAAGTTTCGAGCTGGACTCAGTG
ASPM_FLAPX_23	TGAATCCGTAGGGCAGCACATTTCTGTGTCCTCCTAAGTTTCGAGCTGGACTCAGTG
ASPM_FLAPX_24	ATCTATACCAGGCTTGAATCTTGCAGGCCCTCCTAAGTTTCGAGCTGGACTCAGTG
ASPM_FLAPX_25	TGTTCATGAGCTATCTTTGCAGGAAGTATAGCCCTCCTAAGTTTCGAGCTGGACTCAGTG
ASPM_FLAPX_26	CAGCCCTATTTCGCTGGCTCAGACATCCTCCTAAGTTTCGAGCTGGACTCAGTG
ASPM_FLAPX_27	AGCCCTATTTCGCTGGCTCAGACATCCTCCTAAGTTTCGAGCTGGACTCAGTG
ASPM_FLAPX_28	CACCATTTGAATAGCTTGCAGGGGATTTGTGACCTCCTAAGTTTCGAGCTGGACTCAGTG

Table 3.7 RT-qPCR Primers

GAPDH_RT _FW	ATGTTCGTCATGGGTGTG
GAPDH_RT_RV	GGTGCTAAGCAGTTGGTGG
CCDC86_RT_FW	AACGACAGGAGAGGAAGCTG
CCDC86_RT_RV	ATCACTTGGACGACCTCTGC
RBMX2_RT_FW	GGCCGTCGACAATTTTAATG
RBMX2_RT_FW	ACAGCCCTTCTCCTGGAG
RPS3_RT_FW	TGAGGTGCGAGTTACACC
RPS3_RT_RV	ACAGCAGTCAGTTCCCG
WDR43_RT_FW	CAGCCCAGATGGAAAGATG
WDR43_RT_RV	CAAAGGGCTGGCTCTC
PUF60_RT_FW	GCCTTTGGCAAGATCAAGTC
PUF60_RT_RV	TGGAAGACACAGCATCTTGG
SF3A3_RT_FW	GAAATGGGAGAATGGGACC
SF3A3_RT_RV	CTGTCCAAACCCAGAGAAGC
SF1_RT_FW	GTTGCCAGGAGAAGATGAGC
SF1_RT_RV	CATTTAAGCGAGCCAACTCC

Table 3.8 RBP Candidate Functions

Mitotic Apparatus Localized RBP	Description
AKAP1	Protein kinase A regulatory subunit [401]
CCDC86	RNA binding [205]
SND1	Transcriptional cofactor activity [402]
SF1	Transcriptional regulation [403]
HNRNPF	Pre-mRNA splicing [404]
PPIL4	Component of spliceosome [405]
FXR2	RNA binding [205]
CDC40	Pre-mRNA splicing [406]
HNRNPUL1	Alternative splicing and transcriptional regulation [407]
NUSAP1	Microtubule binding [408]
RBMX2	Pre-mRNA splicing [409]
ZNF622	Zinc ion binding [205]
SLTM	Negative regulation of gene expression [410]
AQR	Pre-mRNA splicing [411]
GRWD1	Chromatin regulator [412]
PUF60	Alternative splicing [413]
RBM39	RNA processing [414]
XPO1	Nuclear export [415]
SBDS	Ribosome and microtubule binding [416, 417]
RPS3	Involved in cytoplasmic translation [418]
WDR43	Ribosome biogenesis factor [419]
SF3A3	Pre-mRNA splicing [420]
SLBP	Histone pre-mRNA processing [421]
SRSF9	Pre-mRNA splicing [422]
DGCR8	Component of microprocessor complex [423]
PUM1	Post-transcriptional repressor [424]
PSIP1	Transcriptional coactivator [425]

Chapter 4 Discussion and Conclusion

4.1 Significant Findings

This section will compare our discoveries to what is known in the current literature, further decipher our results, and I will propose potential avenues to explore in the future.

4.1.1 Co-translational mechanism of mRNAs at the centrosomes

The treatment of embryos with harringtonine, a drug that inhibits translation initiation, consequently led to a disruption of *cen* (**Figure 2.6C**). These results led us to believe that the recruitment of *cen* to the centrosomes could be co-translational, where it requires the nascent polypeptide for its localization. Similarly, actively translating *PCNT* and *ASPM* mRNAs require intact polysomes in HeLa cells [123]. Additionally, it appears that the localization of both *PCNT* and *ASPM* mRNAs is microtubule dependent in HeLa cells [123, 127]. Treatment with the microtubule depolymerizing drug nocodazole resulted in a loss of *PCNT* and *ASPM* at the centrosomes [123, 127]. Furthermore, HeLa cells that were treated with ciliobrevin D, an inhibitor of dynein prevented the localization of *PCNT,* suggesting that the enrichment to the centrosomes was dynein dependent [123]. However, our results also support that RBPs are indeed indispensable when it comes to the recruitment of *ASPM* to the centrosomes, suggesting that there are many contributing factors when it comes to accurately trafficking mRNAs (**Figure 3.5A-C**). We think that transporting mRNAs to the centrosomes is a mechanism that depends on both RBPs and a co-translational mechanism. To sum up the results from **Chapters 2 and 3**, we propose a model for what we speculate is occurring in transporting centrosomal mRNAs (**Figure 4.1**). We think there could be a two-step mechanism that initially requires the RBP to transport the mRNA to the cytoskeletal networks during early mitosis. This would allow the mRNA to get closer to the centrosomes. Observation of the localization of candidate RBPs during early stages of mitosis reveals that several of them localize to the astral microtubules (**Figure 3.1B**). After, the mRNA uses a co-translational mechanism, relying on the nascent polypeptide chain for trafficking to the centrosomes as previously reported [123, 127]. Understanding how RBPs are involved in the co-translational mechanism would be an interesting avenue to explore.

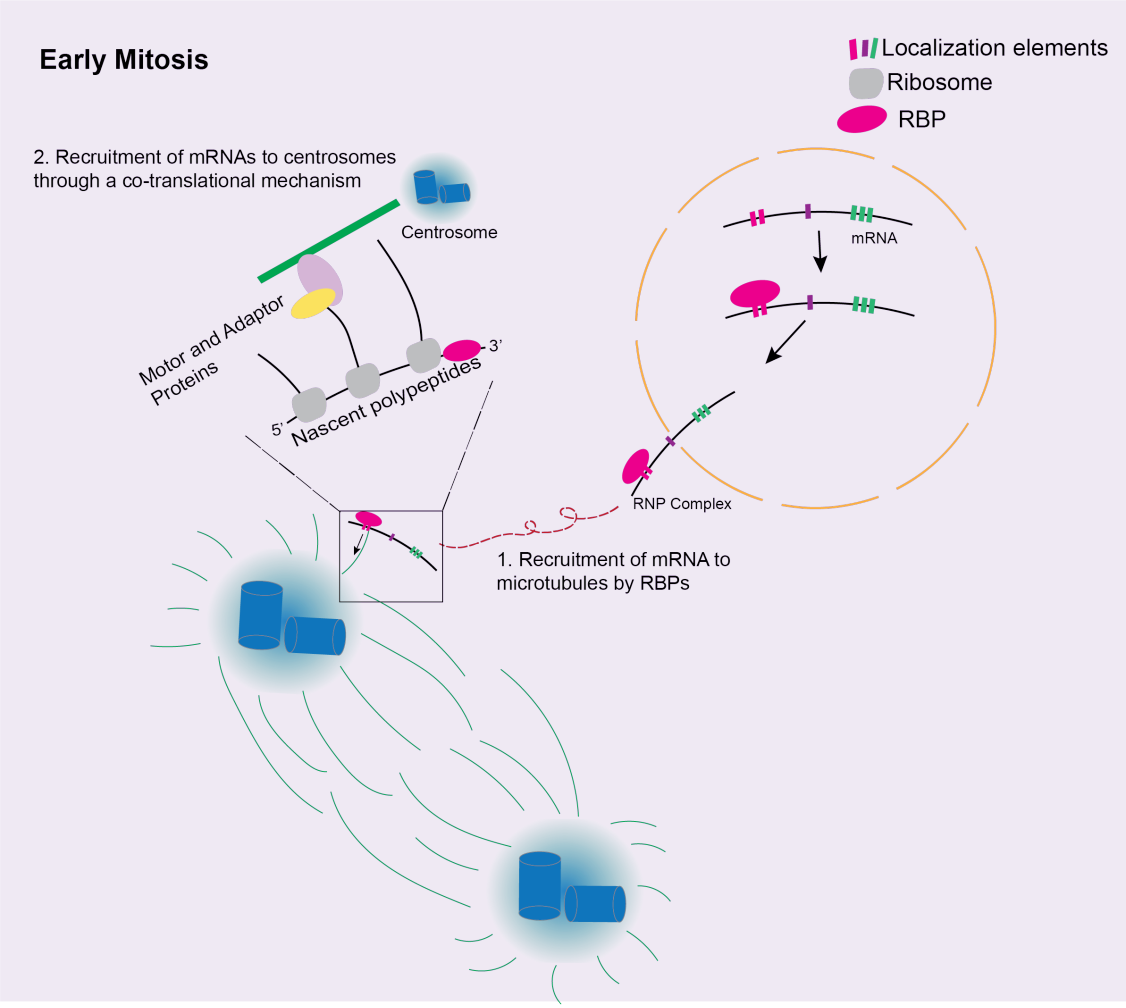

Figure 4.1: Model for targeting mRNAs to the centrosomes. Localizing mRNAs could be occurring in two steps. First, the RBP recruits centrosomal mRNAs to the microtubules during early mitosis. Second, a co-translational mechanism, as previously reported, that is dependent on the cytoskeletal network and motor proteins is required to bring the mRNA to its final destination [123, 127, 386].

4.1.2 Mitosis and RNA binding proteins

The main question we sought to answer was: Is mRNA localization at the mitotic apparatus structures required for the regulation of mitosis? My work and the work of others have supported this notion in both the centrosome and spindle, however, there have been very few examples cited in the literature [126, 400, 426, 427]. In **Chapter 2**, we show that *cen* and *ik2* localize to the centrosomes and loss of either of these mRNAs results in embryonic defects (**Figures 2.1 and 2.3A-C**). In a recent study, it was shown that the RBP FMRP is a negative regulator of *cen in D. melanogaster* embryos [400]. Null *fmr1* mutant embryos showed an increase in both *cen* mRNA and protein levels [400]. Notably, the *cen* mRNA granules also included CEN protein as well as the RBP, FMRP [400]. Observation of CEN protein at sites of *cen* mRNA is consistent with our findings that there is localized translation occurring. Similarly, in **Chapter 3** we show that loss of RBPs perturbs *ASPM* localization at the centrosomes (**Figures 3.5A-C**). Taken together, these results support that mRNA and RBPs, components of the RNP complex are needed for mitosis.

Interestingly, we found that a large number of candidate RBPs play a role in splicing, as revealed by closer examination of their protein function (**Table 3.8**). The downregulation of components of the exon junction complex impairs the localization of NIN mRNA and protein in RPE1 cells, hinting the involvement of the complex in centrosome organization [428]. Recent observations have supported that alternative splicing influences cytoplasmic mRNA destination [429]. For instance, analysis of RNA-seq across 13 cell lines identified thousands of transcripts exhibiting switches between the cytoplasm and nucleus, where isoforms had a preference for either of these compartments [430]. Additionally, in rat hippocampal neurons, isoforms containing different versions of the 3'UTR and 5'UTR influenced the localization of *Bdnf* within the neuron [431, 432]. Furthermore, enrichment of *oskar* to the posterior of *D. melanogaster* oocytes requires splicing at the first exon-exon junction [433].

It could be a possibility that the RBPs are involved in the splicing of *ASPM*, regulating its localization to the centrosomes. Because *ASPM* mRNA has four isoforms,

it would be interesting to see if a particular isoform is selected preferentially for recruitment to the centrosomes. To test this, *GFP* constructs containing different isoforms can be transfected into HeLa cells and the localization of each isoform can be assessed. If enrichment to the centrosome is selective to a certain isoform, it can suggest that alternative splicing is involved.

In **Chapter 3**, we showed that the depletion of RBPs results in a reduction of *ASPM* mRNA at the centrosomes and a higher incidence of mRNA localization defects (**Figures 3.5A-C**). Considering that RBDs serve as the functional unit for RBPs to bind to RNA, it would be necessary to observe how *ASPM* behaves with the loss of these domains. In line with this, truncations of different RBDs can be conducted to confirm that they indeed contribute to the centrosomal localization of *ASPM.* If removal of the RBDs results in the mis-localization of *ASPM*, it would solidify that there is a direct protein-mRNA protein interaction, thus requiring the RBD.

4.1.3 Behavior of other *cis-natural antisense transcrip*t pairs

In **Chapter 2**, we showed that genes encoding *cis-NATS* tend to colocalize to the same subcellular compartment in both human and fly cells as supported by our cell fractionation data (**Figure 2.7C**). Additionally, we showed the that the two mRNAs *cen* and *ik2* travel together for centrosomal targeting (**Figure 2.1A-C**). Our data made us wonder if other transcript pairs travel in a similar manner. To further investigate this, RNA pairs from isolated microtubules and centrosomes can be identified. Recently, there have been several high-throughput techniques that have been developed to detect RNA pairs: Psoralen Analysis of RNA Interactions and Structures (PARIS), Sequencing of Psoralen crosslinked, Ligated, and Selected Hybrids (SPLASH) and LIGation of interacting RNA followed by high throughput Sequencing (LIGR-seq) [353, 354, 356, 434]. In brief, these methods follow a similar approach where RNA pairs undergo crosslinking by utilizing the photocrosslinker psoralen, isolation, proximity ligation, reversing psoralen crosslinks, and sequencing followed by bioinformatics analyses [434]. Collectively, these data can reveal how common *cis-NATs* are in mitotic structures. Additionally, taking advantage of the FISH approach for other transcript pairs in fly and human models could be used to validate

the findings. Furthermore, *in vitro* pull-downs can be performed in a similar fashion where different versions of the mRNA either containing or lacking the coding region and UTRs could be used to assess whether it has the capacity to pull down the other mRNA (**Figure 2.5C**). Further insight into mRNAs travelling in pairs can open up a new perspective on how mRNAs are localized, considering there have been only a few examples cited in the literature of mRNA dimers being trafficked [193, 360].

4.1.4 Function of *ASPM* mRNA during mitosis

While *ASPM* mRNA and ASPM protein have both been previously shown to localize to the centrosomes it was interesting to see that the reduction of *ASPM* mRNA at the centrosomes did not prevent ASPM protein from being recruited [123, 127] (**Figure 3.5A**). Initially, one would expect that loss of protein would go hand in hand with the absence of mRNA. However, in the cells where mRNA localization was perturbed, they exhibited mitotic defects, even though the protein was present (**Figure 3.5A**). These results suggest that *ASPM* is implicated during mitosis, however, the mRNA may be playing a coding-independent role. For instance, in *Xenopus* oocytes, the loss of either long noncoding RNA, *xlsirts* and the mRNA, *vegt* interfere with the structural integrity of the cytokeratin cytoskeleton network [169]. A similar event may be taking place in the case of *ASPM*. Perhaps the loss of the RBPs prevents *ASPM* from being recruited to the centrosomes, hence compromising the structural integrity of the centrosome. This disturbance could be causing the observed mitotic phenotypes. It would be interesting to see if other mitotic mRNAs exhibit a similar pattern. As proteins have been known to serve molecular scaffold or decoy, there has been emerging evidence that RNAs can serve the same function [435]. They can influence the interactions with other proteins [435].

4.1.5 Exploration of the role that RNA binding proteins play in *Drosophila melanogaster* development

In **Chapter 3**, I showed that 80% of the RBP knockdowns that were conducted in *D. melanogaster* embryos resulted in a phenotype (**Figure 3.3D**). We observed a variety of phenotypes including mitotic defects, reduced viability, and sterile females (**Figures 3.3 B-D** and **Supplemental Figure 3.2**). Strikingly, 40% of RBP knockdowns resulted in

sterile females, suggesting a problem during oogenesis (**Figure 3.3D**). These results highlight that RBPs play a big part during development of the fly. In fact, a previous study to identify RBPs bound to polyadenylated transcript during early embryogenesis found in *D. melanogaster* embryos found 476 RBPs, emphasizing its importance in post-transcriptional regulation during development [436]. However, not much is known about the RBPs that were found in the screen. Further examination of these RBPs could potentially give more insight of their roles during development and could be potentially applied to the human model. An essential experiment to perform on candidates that showed reduced viability is to perform a screen using mRNAs that showed enrichment to mitotic apparatus structures on RNAi RBP embryos [125]. Since protein synthesis occurs during embryogenesis, it could be the case that the newly synthesized protein product of mitotic mRNAs is required [437]. For instance, blocking protein synthesis with inhibitors such as puromycin, cycloheximide, and pactamycin results in a mitotic arrest in *D. melanogaster* embryos [437]. If there is perturbed localization of these mRNAs, it can account for a block in development. It could be possible that the RBPs are involved in recruiting mitotic mRNAs during the rapid divisions. However, the loss of these RBPs prevents the mRNAs from being involved in this process, leading to a block in development. Additionally, a similar screen can be performed on candidates that resulted in sterile females. In this case, FISH can be performed on mRNAs that have been shown to be found to be enriched at the pole cells, a precursor of germ cells [125]. These experiments would give more insight into how RBPs are involved in regulating mRNAs during the development of the embryo and reproductive organs.

4.1.6 Testing the impact of spindle-associated mRNAs upon RNA binding protein depletion

The localization of a centrosome-associated mRNA was further investigated upon RBP depletion, albeit having RBPs localize to both the spindle and centrosome (**Figure 3.5B,C**). It would be interesting to test how mRNAs that have been enriched to the mitotic spindle would behave with the loss of RBPs. There have been several examples in the literature of mRNAs localizing to the spindle including *tpx2*, *xpat*, *xdia*, and *cyclin b1*, *incenp*, and *xrhamm, and bub3* [121, 122, 126]. Among these mRNAs, a majority of the

protein products of these mRNAs have been found to be localized to the spindle in the human model [438-441]. Additionally, loss of CPEB1 consequently disrupted C*CNB1* and *BUB3* localization at the spindle in U2OS cells [126]. While there have been very few examples on spindle-associated mRNAs, further details pertaining to their functional purpose would be interesting to unravel. As the formation of a proper spindle is a highly intricate process involving many factors, understanding how mRNAs factor in its assembly would be important to explore.

4.1.7 PUF60, a potential candidate to explore

The RBP screening conducted in **Chapter 3** narrowed down to 6 candidates to potentially investigate. A particular one to focus on in the future would be the splicing factor, PUF60 [413]. Our observations in HeLa cells show that PUF60 has a strong enrichment to both the centrosome and spindle, and its depletion leads to mitotic and mRNA localization defects (**Figures 3.1B,C**, **3.2B,C**, and **3.5A-C**). In *D. melanogaster* embryos, its loss results in reduced viability and mitotic defects (**Figure 3.3B** and **Supplemental Figure 3.2**). Further examination of patients with developmental problems identified deletions in the PUF60 gene [442]. In parallel, injection of morpholinos against PUF60 in zebrafish embryos resulted in short stature and microcephaly [442]. In comparison, we found that viability was impaired in *D. melanogaster* embryos suggesting there was a developmental defect. Additionally, *PUF60* is implicated in cancer where it has a higher expression in tissue from breast and bladder cancer as opposed to normal tissue [443, 444]. As such, one study found that higher expression of *PUF60* was correlated with poor survival in bladder cancer patients, hinting that PUF60 could potentially serve as a biomarker for bladder cancer [444]. With its involvement in both development and cancer, Puf60 serves to be an excellent candidate to explore and dissect its mechanism.

4.1.8 Broader Implication of Findings: mRNA localization and cancer

As uncontrolled cell division occurs during cancer, a better understanding on the implication of mRNA localization during mitosis can aid in finding treatments. Currently there are antimitotic drugs targeting the microtubules, different kinases, motor proteins,

and multiprotein complexes [445]. Although several drugs targeting different components of mitosis exist, there are undesirable consequences [445]. More recently, light has been shed on understanding the implication of mRNA localization on cancer. For example, LARP6 is involved in the recruitment of several ribosomal protein-coding mRNAs to the cell protrusions [446]. As such, this leads to an increase of local translation and ribosome biogenesis at the cell protrusions [446]. As aforementioned in **Section 1.7.3**, the *NET1* and *RAB13* RNAs localize to the front in invasive breast cancer cells in a microtubule-dependent manner [147]. A question that remains is how the localization of mitotic mRNAs is affected in cancer cells. One approach to tackle this question is to perform a screening for microtubule and centrosome-associated mRNAs in a normal cell line (MCF10A) versus a cancer cell line (MDA-MB-231 or MCF7). It would be quite interesting to see the behavior of these transcripts and whether having a particular localization profile can determine a cell's invasive capabilities. Furthermore, RBP knockdowns can be performed in cancerous cells and the localization of these mRNA can be assessed. Exploring this aspect when deciphering the mechanisms that lead to cancer could be interesting. These studies will help to further define how targeting RBPs could allow for a novel therapeutic approach for cancer.

4.2 Limitations

The work that I have presented for my thesis adds insight into understanding how mRNA localization is implicated during mitosis. Yet, there are potential limitations that need to be addressed.

4.2.1 Antibody screening to search for RNA binding proteins enriched at mitotic structures

The screening conducted in **Chapter 3** resulted in finding RBPs that colocalized with mitotic markers (α TUBULIN and PCNT) (**Figures 3.1A-C**). However, the classification was more qualitative and scoring was based on candidates that exhibited protein patterns that were similar to the centrosome and spindle. If there was a lower abundance of protein at either of these structures, it made it more difficult to make the call if a protein would be considered a hit. To circumvent misclassification of the RBPs, I

used both the high content screening microscope as well as the spinning disc confocal. The spinning disc confocal microscope allowed for higher resolution images, leading to more certainty during classification. For future studies, transfecting fluorescently tagged versions that are overexpressing these RBPs can be used for further validation.

4.2.2 HeLa cell line as a model for mRNA localization

HeLa cells serve to be a classic model for human studies in research. Most of the results in **Chapter 3** utilized HeLa cells. However, it is important to note that since they are a cancer cell line, and they might not resemble a normal cell. They are genetically unstable and contain multiple gene copies [447]. An alternative to HeLa cells would be to use the human mammary epithelial cell line, MCF10A. It would be important to observe if the RBPs and mRNAs localize in a more normal cell line. Moreover, mRNA localization has been observed frequently in development and in neurons and has not been extensively studied in the context of cancer [448]. Therefore, our complementary studies in the *D. melanogaster* embryos further validated our observations.

4.2.3 Depletion of RNA binding protein candidates

To assess if the RBP candidates had functional roles, loss of function experiments were performed by utilizing siRNAs. Although some knockdowns did not result in a higher incidence of mitotic defects, it does not necessarily mean that these RBPs are not involved in mitosis. It is a possibility that the proteins have a homolog that play a compensatory role. One candidate that comes to mind is FXR2, a candidate for which we did not observe a phenotype (Figure 3.2). For instance, it has been previously shown that FXR2 has tight interactions with both FXR1 and FMR1, having the ability to form heteromers with the other proteins [449]. Therefore, the depletion of just one protein might not be sufficient to see an effect due to a likelihood of functional redundancy among the proteins.

4.3 Conclusion

The primary goal of the research presented in this thesis aimed to answer the following question: Is the localization of mRNAs to mitotic apparatus involved in the

regulation of mitosis? To date, there have been only a few papers that have looked at the enrichment of mRNAs to the mitotic apparatus structures, and even fewer papers shedding light on the dynamic interaction between the components of the ribonucleoprotein complex. The role of trafficking mRNAs to cell division machineries remained largely unknown.

In **Chapter 2**, my colleagues and I provided compelling evidence that the *cis-natural antisense transcripts*, *cen* and *ik2*, physically interact via the 3'UTR to localize to the centrosomes. Perturbation of either of these genes resulted in mitotic and morphology defects as well as impaired viability in *D. melanogaster* embryos. Furthermore, we found localization determinants within the *cen* coding region and the 3'UTR of *ik2*. Interestingly, comparative analyses among different Drosophilid species revealed that the *D. melanogaster* and *D. simulans* had *cen* and *ik2* genes arranged in an overlapping configuration and both showed localization to the centrosomes. Whereas in *D. virilis* and *D. mojavensis*, where the genes are not physically linked, only *cen* was enriched at the centrosomes. Moreover, *cen* was found to be locally translated and required intact polysomes. To further investigate whether *cis-natural antisense transcripts* tend to be enriched in the same subcellular compartment, transcriptomic datasets revealed that overlapping genes that have a 3'UTR overlap, or full overlap have a trend of being localized to the same compartment in both human and fly models. In conclusion, these data highlight the importance of the post-transcriptional interactions that occur between mRNAs for localization to the centrosomes.

In **Chapter 3**, a screening conducted by my colleagues and I showed that a large number of RBPs are indeed localized to the mitotic apparatus structures. Loss of these RBPs in HeLa cells resulted in mitotic defects including centrosome and spindle abnormalities, suggesting that post-transcriptional regulation is involved during cell division. Interestingly, loss of RBPs did not affect the mitotic index, suggesting that the cells are cycling normally. In parallel, RNAi against the RBP orthologs in *D. melanogaster* embryos led to developmental defects during oogenesis and embryogenesis, as well as mitotic defects. Lastly, we wanted to see how the depletion of RBPs would affect the

localization of *ASPM*, which has been previously shown to be localized to the centrosomes throughout mitosis. The loss of RBPs disrupted localization of *ASPM* at the centrosomes and mitosis, thus reflecting that localized mRNAs. In conclusion, these results show that RBPs are implicated in mitosis and their disruption can lead to catastrophic consequences.

Collectively, my research presents evidence that the localization of mRNAs and RBPs play a role in the regulation of mitosis. We revealed a mechanism where the post-transcriptional interaction between two mRNAs mediates the localization of mRNAs to the centrosomes. Importantly, a functional purpose for localizing RBPs to the centrosomes was unraveled, where the loss of the RBPs altered mRNA localization.

Chapter 5 References

1. Schafer, K. A. (1998) The cell cycle: a review, *Vet Pathol.* **35**, 461-78.
2. Vermeulen, K., Van Bockstaele, D. R. & Berneman, Z. N. (2003) The cell cycle: a review of regulation, deregulation and therapeutic targets in cancer, *Cell Prolif.* **36**, 131-49.
3. Ho, A. & Dowdy, S. F. (2002) Regulation of G(1) cell-cycle progression by oncogenes and tumor suppressor genes, *Curr Opin Genet Dev.* **12**, 47-52.
4. Norbury, C. & Nurse, P. (1992) Animal cell cycles and their control, *Annu Rev Biochem.* **61**, 441-70.
5. McIntosh, J. R. (2016) Mitosis, *Cold Spring Harb Perspect Biol.* **8**.
6. Malumbres, M. (2014) Cyclin-dependent kinases, *Genome Biol.* **15**, 122.
7. Malumbres, M. & Barbacid, M. (2009) Cell cycle, CDKs and cancer: a changing paradigm, *Nat Rev Cancer.* **9**, 153-66.
8. Satyanarayana, A. & Kaldis, P. (2009) Mammalian cell-cycle regulation: several Cdks, numerous cyclins and diverse compensatory mechanisms, *Oncogene.* **28**, 2925-39.
9. Malumbres, M. & Barbacid, M. (2005) Mammalian cyclin-dependent kinases, *Trends Biochem Sci.* **30**, 630-41.
10. Ortega, S., Prieto, I., Odajima, J., Martin, A., Dubus, P., Sotillo, R., Barbero, J. L., Malumbres, M. & Barbacid, M. (2003) Cyclin-dependent kinase 2 is essential for meiosis but not for mitotic cell division in mice, *Nat Genet.* **35**, 25-31.
11. Santamaria, D., Barriere, C., Cerqueira, A., Hunt, S., Tardy, C., Newton, K., Caceres, J. F., Dubus, P., Malumbres, M. & Barbacid, M. (2007) Cdk1 is sufficient to drive the mammalian cell cycle, *Nature.* **448**, 811-5.
12. Jeffrey, P. D., Russo, A. A., Polyak, K., Gibbs, E., Hurwitz, J., Massague, J. & Pavletich, N. P. (1995) Mechanism of CDK activation revealed by the structure of a cyclinA-CDK2 complex, *Nature.* **376**, 313-20.
13. Irniger, S. (2002) Cyclin destruction in mitosis: a crucial task of Cdc20, *FEBS Lett.* **532**, 7-11.
14. Irniger, S., Piatti, S., Michaelis, C. & Nasmyth, K. (1995) Genes involved in sister chromatid separation are needed for B-type cyclin proteolysis in budding yeast, *Cell.* **81**, 269-78.
15. King, R. W., Peters, J. M., Tugendreich, S., Rolfe, M., Hieter, P. & Kirschner, M. W. (1995) A 20S complex containing CDC27 and CDC16 catalyzes the mitosis-specific conjugation of ubiquitin to cyclin B, *Cell.* **81**, 279-88.
16. Murray, A. W. & Kirschner, M. W. (1989) Cyclin synthesis drives the early embryonic cell cycle, *Nature.* **339**, 275-80.
17. Dominguez-Brauer, C., Thu, K. L., Mason, J. M., Blaser, H., Bray, M. R. & Mak, T. W. (2015) Targeting Mitosis in Cancer: Emerging Strategies, *Mol Cell.* **60**, 524-36.
18. Hume, S., Dianov, G. L. & Ramadan, K. (2020) A unified model for the G1/S cell cycle transition, *Nucleic Acids Res.* **48**, 12483-12501.
19. Blagosklonny, M. V. & Pardee, A. B. (2002) The restriction point of the cell cycle, *Cell Cycle.* **1**, 103-10.
20. Kastan, M. B. & Bartek, J. (2004) Cell-cycle checkpoints and cancer, *Nature.* **432**, 316-23.
21. Peters, J. M. & Nishiyama, T. (2012) Sister chromatid cohesion, *Cold Spring Harb Perspect Biol.* **4**.

22. Hirano, T., Kobayashi, R. & Hirano, M. (1997) Condensins, chromosome condensation protein complexes containing XCAP-C, XCAP-E and a Xenopus homolog of the Drosophila Barren protein, *Cell.* **89**, 511-21.
23. Freeman, L., Aragon-Alcaide, L. & Strunnikov, A. (2000) The condensin complex governs chromosome condensation and mitotic transmission of rDNA, *J Cell Biol.* **149**, 811-24.
24. Martinez-Balbas, M. A., Dey, A., Rabindran, S. K., Ozato, K. & Wu, C. (1995) Displacement of sequence-specific transcription factors from mitotic chromatin, *Cell.* **83**, 29-38.
25. Meraldi, P. & Nigg, E. A. (2002) The centrosome cycle, *FEBS Lett.* **521**, 9-13.
26. Ferreira, L. T. & Maiato, H. (2021) Prometaphase, *Semin Cell Dev Biol.* **117**, 52-61.
27. Tauchman, E. C., Boehm, F. J. & DeLuca, J. G. (2015) Stable kinetochore-microtubule attachment is sufficient to silence the spindle assembly checkpoint in human cells, *Nat Commun.* **6**, 10036.
28. Musacchio, A. & Desai, A. (2017) A Molecular View of Kinetochore Assembly and Function, *Biology (Basel).* **6**.
29. Fukagawa, T. & Earnshaw, W. C. (2014) The centromere: chromatin foundation for the kinetochore machinery, *Dev Cell.* **30**, 496-508.
30. Barr, F. A. & Gruneberg, U. (2007) Cytokinesis: placing and making the final cut, *Cell.* **131**, 847-60.
31. Haase, J., Bonner, M. K., Halas, H. & Kelly, A. E. (2017) Distinct Roles of the Chromosomal Passenger Complex in the Detection of and Response to Errors in Kinetochore-Microtubule Attachment, *Dev Cell.* **42**, 640-654 e5.
32. Kitagawa, M. & Lee, S. H. (2015) The chromosomal passenger complex (CPC) as a key orchestrator of orderly mitotic exit and cytokinesis, *Front Cell Dev Biol.* **3**, 14.
33. Musacchio, A. (2015) The Molecular Biology of Spindle Assembly Checkpoint Signaling Dynamics, *Curr Biol.* **25**, R1002-18.
34. Vader, G., Maia, A. F. & Lens, S. M. (2008) The chromosomal passenger complex and the spindle assembly checkpoint: kinetochore-microtubule error correction and beyond, *Cell Div.* **3**, 10.
35. Levine, M. S. & Holland, A. J. (2018) The impact of mitotic errors on cell proliferation and tumorigenesis, *Genes Dev.* **32**, 620-638.
36. Carmena, M., Wheelock, M., Funabiki, H. & Earnshaw, W. C. (2012) The chromosomal passenger complex (CPC): from easy rider to the godfather of mitosis, *Nat Rev Mol Cell Biol.* **13**, 789-803.
37. Duijf, P. H., Schultz, N. & Benezra, R. (2013) Cancer cells preferentially lose small chromosomes, *Int J Cancer.* **132**, 2316-26.
38. Thompson, S. L., Bakhoum, S. F. & Compton, D. A. (2010) Mechanisms of chromosomal instability, *Curr Biol.* **20**, R285-95.
39. Komlodi-Pasztor, E., Sackett, D. L. & Fojo, A. T. (2012) Inhibitors targeting mitosis: tales of how great drugs against a promising target were brought down by a flawed rationale, *Clin Cancer Res.* **18**, 51-63.
40. Qi, C., Wang, X., Shen, Z., Chen, S., Yu, H., Williams, N. & Wang, G. (2018) Anti-mitotic chemotherapeutics promote apoptosis through TL1A-activated death receptor 3 in cancer cells, *Cell Res.* **28**, 544-555.

41. Wunderlich, V. (2002) JMM---past and present. Chromosomes and cancer: Theodor Boveri's predictions 100 years later, *J Mol Med (Berl).* **80**, 545-8.
42. Graf, R. (2018) Comparative Biology of Centrosomal Structures in Eukaryotes, *Cells.* **7**.
43. Boveri, T. (2008) Concerning the origin of malignant tumours by Theodor Boveri. Translated and annotated by Henry Harris, *J Cell Sci.* **121 Suppl 1**, 1-84.
44. Godinho, S. A. & Pellman, D. (2014) Causes and consequences of centrosome abnormalities in cancer, *Philos Trans R Soc Lond B Biol Sci.* **369**.
45. Bettencourt-Dias, M. & Glover, D. M. (2007) Centrosome biogenesis and function: centrosomics brings new understanding, *Nat Rev Mol Cell Biol.* **8**, 451-63.
46. Doxsey, S., McCollum, D. & Theurkauf, W. (2005) Centrosomes in cellular regulation, *Annu Rev Cell Dev Biol.* **21**, 411-34.
47. Rivera-Rivera, Y. & Saavedra, H. I. (2016) Centrosome - a promising anti-cancer target, *Biologics.* **10**, 167-176.
48. Winey, M. & O'Toole, E. (2014) Centriole structure, *Philos Trans R Soc Lond B Biol Sci.* **369**.
49. Mennella, V., Keszthelyi, B., McDonald, K. L., Chhun, B., Kan, F., Rogers, G. C., Huang, B. & Agard, D. A. (2012) Subdiffraction-resolution fluorescence microscopy reveals a domain of the centrosome critical for pericentriolar material organization, *Nat Cell Biol.* **14**, 1159-68.
50. Andersen, J. S., Wilkinson, C. J., Mayor, T., Mortensen, P., Nigg, E. A. & Mann, M. (2003) Proteomic characterization of the human centrosome by protein correlation profiling, *Nature.* **426**, 570-4.
51. Alves-Cruzeiro, J. M., Nogales-Cadenas, R. & Pascual-Montano, A. D. (2014) CentrosomeDB: a new generation of the centrosomal proteins database for Human and Drosophila melanogaster, *Nucleic Acids Res.* **42**, D430-6.
52. Moritz, M. & Agard, D. A. (2001) Gamma-tubulin complexes and microtubule nucleation, *Curr Opin Struct Biol.* **11**, 174-81.
53. Zheng, Y., Wong, M. L., Alberts, B. & Mitchison, T. (1995) Nucleation of microtubule assembly by a gamma-tubulin-containing ring complex, *Nature.* **378**, 578-83.
54. Basto, R., Lau, J., Vinogradova, T., Gardiol, A., Woods, C. G., Khodjakov, A. & Raff, J. W. (2006) Flies without centrioles, *Cell.* **125**, 1375-86.
55. Hinchcliffe, E. H., Miller, F. J., Cham, M., Khodjakov, A. & Sluder, G. (2001) Requirement of a centrosomal activity for cell cycle progression through G1 into S phase, *Science.* **291**, 1547-50.
56. Khodjakov, A., Cole, R. W., Oakley, B. R. & Rieder, C. L. (2000) Centrosome-independent mitotic spindle formation in vertebrates, *Curr Biol.* **10**, 59-67.
57. Calarco-Gillam, P. D., Siebert, M. C., Hubble, R., Mitchison, T. & Kirschner, M. (1983) Centrosome development in early mouse embryos as defined by an autoantibody against pericentriolar material, *Cell.* **35**, 621-9.
58. Heald, R., Tournebize, R., Blank, T., Sandaltzopoulos, R., Becker, P., Hyman, A. & Karsenti, E. (1996) Self-organization of microtubules into bipolar spindles around artificial chromosomes in Xenopus egg extracts, *Nature.* **382**, 420-5.
59. Matthies, H. J., McDonald, H. B., Goldstein, L. S. & Theurkauf, W. E. (1996) Anastral meiotic spindle morphogenesis: role of the non-claret disjunctional kinesin-like protein, *J Cell Biol.* **134**, 455-64.

60. Namgoong, S. & Kim, N. H. (2018) Meiotic spindle formation in mammalian oocytes: implications for human infertility, *Biol Reprod.* **98**, 153-161.
61. Fu, J., Hagan, I. M. & Glover, D. M. (2015) The centrosome and its duplication cycle, *Cold Spring Harb Perspect Biol.* **7**, a015800.
62. Fujita, H., Yoshino, Y. & Chiba, N. (2016) Regulation of the centrosome cycle, *Mol Cell Oncol.* **3**, e1075643.
63. Tsou, M. F., Wang, W. J., George, K. A., Uryu, K., Stearns, T. & Jallepalli, P. V. (2009) Polo kinase and separase regulate the mitotic licensing of centriole duplication in human cells, *Dev Cell.* **17**, 344-54.
64. Graser, S., Stierhof, Y. D. & Nigg, E. A. (2007) Cep68 and Cep215 (Cdk5rap2) are required for centrosome cohesion, *J Cell Sci.* **120**, 4321-31.
65. Mardin, B. R. & Schiebel, E. (2012) Breaking the ties that bind: new advances in centrosome biology, *J Cell Biol.* **197**, 11-8.
66. Bettencourt-Dias, M., Rodrigues-Martins, A., Carpenter, L., Riparbelli, M., Lehmann, L., Gatt, M. K., Carmo, N., Balloux, F., Callaini, G. & Glover, D. M. (2005) SAK/PLK4 is required for centriole duplication and flagella development, *Curr Biol.* **15**, 2199-207.
67. Habedanck, R., Stierhof, Y. D., Wilkinson, C. J. & Nigg, E. A. (2005) The Polo kinase Plk4 functions in centriole duplication, *Nat Cell Biol.* **7**, 1140-6.
68. Kleylein-Sohn, J., Westendorf, J., Le Clech, M., Habedanck, R., Stierhof, Y. D. & Nigg, E. A. (2007) Plk4-induced centriole biogenesis in human cells, *Dev Cell.* **13**, 190-202.
69. Kim, T. S., Park, J. E., Shukla, A., Choi, S., Murugan, R. N., Lee, J. H., Ahn, M., Rhee, K., Bang, J. K., Kim, B. Y., Loncarek, J., Erikson, R. L. & Lee, K. S. (2013) Hierarchical recruitment of Plk4 and regulation of centriole biogenesis by two centrosomal scaffolds, Cep192 and Cep152, *Proc Natl Acad Sci U S A.* **110**, E4849-57.
70. Sonnen, K. F., Gabryjonczyk, A. M., Anselm, E., Stierhof, Y. D. & Nigg, E. A. (2013) Human Cep192 and Cep152 cooperate in Plk4 recruitment and centriole duplication, *J Cell Sci.* **126**, 3223-33.
71. Dammermann, A., Muller-Reichert, T., Pelletier, L., Habermann, B., Desai, A. & Oegema, K. (2004) Centriole assembly requires both centriolar and pericentriolar material proteins, *Dev Cell.* **7**, 815-29.
72. Leidel, S., Delattre, M., Cerutti, L., Baumer, K. & Gonczy, P. (2005) SAS-6 defines a protein family required for centrosome duplication in C. elegans and in human cells, *Nat Cell Biol.* **7**, 115-25.
73. Vulprecht, J., David, A., Tibelius, A., Castiel, A., Konotop, G., Liu, F., Bestvater, F., Raab, M. S., Zentgraf, H., Izraeli, S. & Kramer, A. (2012) STIL is required for centriole duplication in human cells, *J Cell Sci.* **125**, 1353-62.
74. Tang, C. J., Lin, S. Y., Hsu, W. B., Lin, Y. N., Wu, C. T., Lin, Y. C., Chang, C. W., Wu, K. S. & Tang, T. K. (2011) The human microcephaly protein STIL interacts with CPAP and is required for procentriole formation, *EMBO J.* **30**, 4790-804.
75. Guichard, P., Desfosses, A., Maheshwari, A., Hachet, V., Dietrich, C., Brune, A., Ishikawa, T., Sachse, C. & Gonczy, P. (2012) Cartwheel architecture of Trichonympha basal body, *Science.* **337**, 553.
76. Guichard, P., Hachet, V., Majubu, N., Neves, A., Demurtas, D., Olieric, N., Fluckiger, I., Yamada, A., Kihara, K., Nishida, Y., Moriya, S., Steinmetz, M. O., Hongoh, Y. &

Gonczy, P. (2013) Native architecture of the centriole proximal region reveals features underlying its 9-fold radial symmetry, *Curr Biol.* **23**, 1620-8.
77. Jana, S. C., Marteil, G. & Bettencourt-Dias, M. (2014) Mapping molecules to structure: unveiling secrets of centriole and cilia assembly with near-atomic resolution, *Curr Opin Cell Biol.* **26**, 96-106.
78. Kohlmaier, G., Loncarek, J., Meng, X., McEwen, B. F., Mogensen, M. M., Spektor, A., Dynlacht, B. D., Khodjakov, A. & Gonczy, P. (2009) Overly long centrioles and defective cell division upon excess of the SAS-4-related protein CPAP, *Curr Biol.* **19**, 1012-8.
79. Schmidt, T. I., Kleylein-Sohn, J., Westendorf, J., Le Clech, M., Lavoie, S. B., Stierhof, Y. D. & Nigg, E. A. (2009) Control of centriole length by CPAP and CP110, *Curr Biol.* **19**, 1005-11.
80. Tang, C. J., Fu, R. H., Wu, K. S., Hsu, W. B. & Tang, T. K. (2009) CPAP is a cell-cycle regulated protein that controls centriole length, *Nat Cell Biol.* **11**, 825-31.
81. Cottee, M. A., Muschalik, N., Wong, Y. L., Johnson, C. M., Johnson, S., Andreeva, A., Oegema, K., Lea, S. M., Raff, J. W. & van Breugel, M. (2013) Crystal structures of the CPAP/STIL complex reveal its role in centriole assembly and human microcephaly, *Elife.* **2**, e01071.
82. Hatzopoulos, G. N., Erat, M. C., Cutts, E., Rogala, K. B., Slater, L. M., Stansfeld, P. J. & Vakonakis, I. (2013) Structural analysis of the G-box domain of the microcephaly protein CPAP suggests a role in centriole architecture, *Structure.* **21**, 2069-77.
83. Chang, J., Cizmecioglu, O., Hoffmann, I. & Rhee, K. (2010) PLK2 phosphorylation is critical for CPAP function in procentriole formation during the centrosome cycle, *EMBO J.* **29**, 2395-406.
84. Azimzadeh, J., Hergert, P., Delouvee, A., Euteneuer, U., Formstecher, E., Khodjakov, A. & Bornens, M. (2009) hPOC5 is a centrin-binding protein required for assembly of full-length centrioles, *J Cell Biol.* **185**, 101-14.
85. Singla, V., Romaguera-Ros, M., Garcia-Verdugo, J. M. & Reiter, J. F. (2010) Ofd1, a human disease gene, regulates the length and distal structure of centrioles, *Dev Cell.* **18**, 410-24.
86. Piehl, M., Tulu, U. S., Wadsworth, P. & Cassimeris, L. (2004) Centrosome maturation: measurement of microtubule nucleation throughout the cell cycle by using GFP-tagged EB1, *Proc Natl Acad Sci U S A.* **101**, 1584-8.
87. Gopalakrishnan, J., Mennella, V., Blachon, S., Zhai, B., Smith, A. H., Megraw, T. L., Nicastro, D., Gygi, S. P., Agard, D. A. & Avidor-Reiss, T. (2011) Sas-4 provides a scaffold for cytoplasmic complexes and tethers them in a centrosome, *Nat Commun.* **2**, 359.
88. Zheng, X., Gooi, L. M., Wason, A., Gabriel, E., Mehrjardi, N. Z., Yang, Q., Zhang, X., Debec, A., Basiri, M. L., Avidor-Reiss, T., Pozniakovsky, A., Poser, I., Saric, T., Hyman, A. A., Li, H. & Gopalakrishnan, J. (2014) Conserved TCP domain of Sas-4/CPAP is essential for pericentriolar material tethering during centrosome biogenesis, *Proc Natl Acad Sci U S A.* **111**, E354-63.
89. Santamaria, A., Wang, B., Elowe, S., Malik, R., Zhang, F., Bauer, M., Schmidt, A., Sillje, H. H., Korner, R. & Nigg, E. A. (2011) The Plk1-dependent phosphoproteome of the early mitotic spindle, *Mol Cell Proteomics.* **10**, M110 004457.

90. Mahen, R., Jeyasekharan, A. D., Barry, N. P. & Venkitaraman, A. R. (2011) Continuous polo-like kinase 1 activity regulates diffusion to maintain centrosome self-organization during mitosis, *Proc Natl Acad Sci U S A.* **108**, 9310-5.
91. Schatten, H. & Sun, Q. Y. (2018) Functions and dysfunctions of the mammalian centrosome in health, disorders, disease, and aging, *Histochem Cell Biol.* **150**, 303-325.
92. Chan, J. Y. (2011) A clinical overview of centrosome amplification in human cancers, *Int J Biol Sci.* **7**, 1122-44.
93. Vitre, B. D. & Cleveland, D. W. (2012) Centrosomes, chromosome instability (CIN) and aneuploidy, *Curr Opin Cell Biol.* **24**, 809-15.
94. Duensing, S. (2005) A tentative classification of centrosome abnormalities in cancer, *Cell Biol Int.* **29**, 352-9.
95. Kwon, M., Godinho, S. A., Chandhok, N. S., Ganem, N. J., Azioune, A., Thery, M. & Pellman, D. (2008) Mechanisms to suppress multipolar divisions in cancer cells with extra centrosomes, *Genes Dev.* **22**, 2189-203.
96. Ring, D., Hubble, R. & Kirschner, M. (1982) Mitosis in a cell with multiple centrioles, *J Cell Biol.* **94**, 549-56.
97. Sharp, G. A., Osborn, M. & Weber, K. (1981) Ultrastructure of multiple microtubule initiation sites in mouse neuroblastoma cells, *J Cell Sci.* **47**, 1-24.
98. Kawamura, E., Fielding, A. B., Kannan, N., Balgi, A., Eaves, C. J., Roberge, M. & Dedhar, S. (2013) Identification of novel small molecule inhibitors of centrosome clustering in cancer cells, *Oncotarget.* **4**, 1763-76.
99. Nigg, E. A. (2002) Centrosome aberrations: cause or consequence of cancer progression?, *Nat Rev Cancer.* **2**, 815-25.
100. Pihan, G. A. (2013) Centrosome dysfunction contributes to chromosome instability, chromoanagenesis, and genome reprograming in cancer, *Front Oncol.* **3**, 277.
101. Storchova, Z. & Pellman, D. (2004) From polyploidy to aneuploidy, genome instability and cancer, *Nat Rev Mol Cell Biol.* **5**, 45-54.
102. Basto, R., Brunk, K., Vinadogrova, T., Peel, N., Franz, A., Khodjakov, A. & Raff, J. W. (2008) Centrosome amplification can initiate tumorigenesis in flies, *Cell.* **133**, 1032-42.
103. Waters, A. M. & Beales, P. L. (2011) Ciliopathies: an expanding disease spectrum, *Pediatr Nephrol.* **26**, 1039-56.
104. Nigg, E. A. & Raff, J. W. (2009) Centrioles, centrosomes, and cilia in health and disease, *Cell.* **139**, 663-78.
105. Satir, P. & Christensen, S. T. (2007) Overview of structure and function of mammalian cilia, *Annu Rev Physiol.* **69**, 377-400.
106. Sathananthan, A. H. (1994) Functional competence of abnormal spermatozoa, *Baillieres Clin Obstet Gynaecol.* **8**, 141-56.
107. Avidor-Reiss, T., Mazur, M., Fishman, E. L. & Sindhwani, P. (2019) The Role of Sperm Centrioles in Human Reproduction - The Known and the Unknown, *Front Cell Dev Biol.* **7**, 188.
108. Prosser, S. L. & Pelletier, L. (2017) Mitotic spindle assembly in animal cells: a fine balancing act, *Nat Rev Mol Cell Biol.* **18**, 187-201.
109. Tillement, V., Remy, M. H., Raynaud-Messina, B., Mazzolini, L., Haren, L. & Merdes, A. (2009) Spindle assembly defects leading to the formation of a monopolar mitotic apparatus, *Biol Cell.* **101**, 1-11.

110. Bodakuntla, S., Jijumon, A. S., Villablanca, C., Gonzalez-Billault, C. & Janke, C. (2019) Microtubule-Associated Proteins: Structuring the Cytoskeleton, *Trends Cell Biol.* **29**, 804-819.
111. Horio, T. & Murata, T. (2014) The role of dynamic instability in microtubule organization, *Front Plant Sci.* **5**, 511.
112. Akhmanova, A. & Steinmetz, M. O. (2019) Microtubule minus-end regulation at a glance, *J Cell Sci.* **132**.
113. Maiato, H. & Logarinho, E. (2014) Mitotic spindle multipolarity without centrosome amplification, *Nat Cell Biol.* **16**, 386-94.
114. Mayer, T. U., Kapoor, T. M., Haggarty, S. J., King, R. W., Schreiber, S. L. & Mitchison, T. J. (1999) Small molecule inhibitor of mitotic spindle bipolarity identified in a phenotype-based screen, *Science.* **286**, 971-4.
115. Kline-Smith, S. L. & Walczak, C. E. (2002) The microtubule-destabilizing kinesin XKCM1 regulates microtubule dynamic instability in cells, *Mol Biol Cell.* **13**, 2718-31.
116. Petretti, C., Savoian, M., Montembault, E., Glover, D. M., Prigent, C. & Giet, R. (2006) The PITSLRE/CDK11p58 protein kinase promotes centrosome maturation and bipolar spindle formation, *EMBO Rep.* **7**, 418-24.
117. Goldman, R. D. & Rebhun, L. I. (1969) The structure and some properties of the isolated mitotic apparatus, *J Cell Sci.* **4**, 179-209.
118. Ferri, F., Bouzinba-Segard, H., Velasco, G., Hube, F. & Francastel, C. (2009) Non-coding murine centromeric transcripts associate with and potentiate Aurora B kinase, *Nucleic Acids Res.* **37**, 5071-80.
119. Jambhekar, A., Emerman, A. B., Schweidenback, C. T. & Blower, M. D. (2014) RNA stimulates Aurora B kinase activity during mitosis, *PLoS One.* **9**, e100748.
120. Wong, L. H., Brettingham-Moore, K. H., Chan, L., Quach, J. M., Anderson, M. A., Northrop, E. L., Hannan, R., Saffery, R., Shaw, M. L., Williams, E. & Choo, K. H. (2007) Centromere RNA is a key component for the assembly of nucleoproteins at the nucleolus and centromere, *Genome Res.* **17**, 1146-60.
121. Blower, M. D., Feric, E., Weis, K. & Heald, R. (2007) Genome-wide analysis demonstrates conserved localization of messenger RNAs to mitotic microtubules, *J Cell Biol.* **179**, 1365-73.
122. Sharp, J. A., Plant, J. J., Ohsumi, T. K., Borowsky, M. & Blower, M. D. (2011) Functional analysis of the microtubule-interacting transcriptome, *Mol Biol Cell.* **22**, 4312-23.
123. Sepulveda, G., Antkowiak, M., Brust-Mascher, I., Mahe, K., Ou, T., Castro, N. M., Christensen, L. N., Cheung, L., Jiang, X., Yoon, D., Huang, B. & Jao, L. E. (2018) Co-translational protein targeting facilitates centrosomal recruitment of PCNT during centrosome maturation in vertebrates, *Elife.* **7**.
124. Groisman, I., Huang, Y. S., Mendez, R., Cao, Q., Theurkauf, W. & Richter, J. D. (2000) CPEB, maskin, and cyclin B1 mRNA at the mitotic apparatus: implications for local translational control of cell division, *Cell.* **103**, 435-47.
125. Lecuyer, E., Yoshida, H., Parthasarathy, N., Alm, C., Babak, T., Cerovina, T., Hughes, T. R., Tomancak, P. & Krause, H. M. (2007) Global analysis of mRNA localization reveals a prominent role in organizing cellular architecture and function, *Cell.* **131**, 174-87.

126. Pascual, R., Segura-Morales, C., Omerzu, M., Bellora, N., Belloc, E., Castellazzi, C. L., Reina, O., Eyras, E., Maurice, M. M., Millanes-Romero, A. & Mendez, R. (2020) mRNA spindle localization and mitotic translational regulation by CPEB1 and CPEB4, *RNA*.
127. Safieddine, A., Coleno, E., Salloum, S., Imbert, A., Traboulsi, A. M., Kwon, O. S., Lionneton, F., Georget, V., Robert, M. C., Gostan, T., Lecellier, C. H., Chouaib, R., Pichon, X., Le Hir, H., Zibara, K., Mueller, F., Walter, T., Peter, M. & Bertrand, E. (2021) A choreography of centrosomal mRNAs reveals a conserved localization mechanism involving active polysome transport, *Nat Commun.* **12**, 1352.
128. Raff, J. W., Whitfield, W. G. & Glover, D. M. (1990) Two distinct mechanisms localise cyclin B transcripts in syncytial Drosophila embryos, *Development.* **110**, 1249-61.
129. Kalthoff, K. (1971) Position of targets and period of competence for UV-induction of the malformation "Double Abdomen" in the egg ofSmittia spec. (Diptera, Chironomidae), *Wilhelm Roux Arch Entwickl Mech Org.* **168**, 63-84.
130. Kandler-Singer, I. & Kalthoff, K. (1976) RNase sensitivity of an anterior morphogenetic determinant in an insect egg (Smittia sp., Chironomidae, Diptera), *Proc Natl Acad Sci U S A.* **73**, 3739-43.
131. Jeffery, W. R., Tomlinson, C. R. & Brodeur, R. D. (1983) Localization of actin messenger RNA during early ascidian development, *Dev Biol.* **99**, 408-17.
132. Berleth, T., Burri, M., Thoma, G., Bopp, D., Richstein, S., Frigerio, G., Noll, M. & Nusslein-Volhard, C. (1988) The role of localization of bicoid RNA in organizing the anterior pattern of the Drosophila embryo, *EMBO J.* **7**, 1749-56.
133. Ephrussi, A., Dickinson, L. K. & Lehmann, R. (1991) Oskar organizes the germ plasm and directs localization of the posterior determinant nanos, *Cell.* **66**, 37-50.
134. Kim-Ha, J., Smith, J. L. & Macdonald, P. M. (1991) oskar mRNA is localized to the posterior pole of the Drosophila oocyte, *Cell.* **66**, 23-35.
135. Lawrence, J. B. & Singer, R. H. (1986) Intracellular localization of messenger RNAs for cytoskeletal proteins, *Cell.* **45**, 407-15.
136. Long, R. M., Singer, R. H., Meng, X., Gonzalez, I., Nasmyth, K. & Jansen, R. P. (1997) Mating type switching in yeast controlled by asymmetric localization of ASH1 mRNA, *Science.* **277**, 383-7.
137. Melton, D. A. (1987) Translocation of a localized maternal mRNA to the vegetal pole of Xenopus oocytes, *Nature.* **328**, 80-2.
138. Neuman-Silberberg, F. S. & Schupbach, T. (1996) The Drosophila TGF-alpha-like protein Gurken: expression and cellular localization during Drosophila oogenesis, *Mech Dev.* **59**, 105-13.
139. Takizawa, P. A., Sil, A., Swedlow, J. R., Herskowitz, I. & Vale, R. D. (1997) Actin-dependent localization of an RNA encoding a cell-fate determinant in yeast, *Nature.* **389**, 90-3.
140. Fei, J. & Sharma, C. M. (2018) RNA Localization in Bacteria, *Microbiol Spectr.* **6**.
141. Han, J. W., Park, J. H., Kim, M. & Lee, J. (1997) mRNAs for microtubule proteins are specifically colocalized during the sequential formation of basal body, flagella, and cytoskeletal microtubules in the differentiation of Naegleria gruberi, *J Cell Biol.* **137**, 871-9.
142. Keiler, K. C. (2011) RNA localization in bacteria, *Curr Opin Microbiol.* **14**, 155-9.

143. Li, X., Franceschi, V. R. & Okita, T. W. (1993) Segregation of storage protein mRNAs on the rough endoplasmic reticulum membranes of rice endosperm cells, *Cell.* **72**, 869-79.
144. Montero Llopis, P., Jackson, A. F., Sliusarenko, O., Surovtsev, I., Heinritz, J., Emonet, T. & Jacobs-Wagner, C. (2010) Spatial organization of the flow of genetic information in bacteria, *Nature.* **466**, 77-81.
145. Tian, L., Chou, H. L., Fukuda, M., Kumamaru, T. & Okita, T. W. (2020) mRNA Localization in Plant Cells, *Plant Physiol.* **182**, 97-109.
146. Moffitt, J. R., Pandey, S., Boettiger, A. N., Wang, S. & Zhuang, X. (2016) Spatial organization shapes the turnover of a bacterial transcriptome, *Elife.* **5**.
147. Chrisafis, G., Wang, T., Moissoglu, K., Gasparski, A. N., Ng, Y., Weigert, R., Lockett, S. J. & Mili, S. (2020) Collective cancer cell invasion requires RNA accumulation at the invasive front, *Proc Natl Acad Sci U S A.* **117**, 27423-27434.
148. Jansova, D., Tetkova, A., Koncicka, M., Kubelka, M. & Susor, A. (2018) Localization of RNA and translation in the mammalian oocyte and embryo, *PLoS One.* **13**, e0192544.
149. Ma, L., Shelness, G. S., Snipes, J. A., Murea, M., Antinozzi, P. A., Cheng, D., Saleem, M. A., Satchell, S. C., Banas, B., Mathieson, P. W., Kretzler, M., Hemal, A. K., Rudel, L. L., Petrovic, S., Weckerle, A., Pollak, M. R., Ross, M. D., Parks, J. S. & Freedman, B. I. (2015) Localization of APOL1 protein and mRNA in the human kidney: nondiseased tissue, primary cells, and immortalized cell lines, *J Am Soc Nephrol.* **26**, 339-48.
150. Mofatteh, M. (2020) mRNA localization and local translation in neurons, *AIMS Neurosci.* **7**, 299-310.
151. Eberwine, J., Miyashiro, K., Kacharmina, J. E. & Job, C. (2001) Local translation of classes of mRNAs that are targeted to neuronal dendrites, *Proc Natl Acad Sci U S A.* **98**, 7080-5.
152. Gonzalez-Reyes, A., Elliott, H. & St Johnston, D. (1995) Polarization of both major body axes in Drosophila by gurken-torpedo signalling, *Nature.* **375**, 654-8.
153. Garcia, M., Darzacq, X., Delaveau, T., Jourdren, L., Singer, R. H. & Jacq, C. (2007) Mitochondria-associated yeast mRNAs and the biogenesis of molecular complexes, *Mol Biol Cell.* **18**, 362-8.
154. Kopczynski, C. C., Noordermeer, J. N., Serano, T. L., Chen, W. Y., Pendleton, J. D., Lewis, S., Goodman, C. S. & Rubin, G. M. (1998) A high throughput screen to identify secreted and transmembrane proteins involved in Drosophila embryogenesis, *Proc Natl Acad Sci U S A.* **95**, 9973-8.
155. Mili, S., Moissoglu, K. & Macara, I. G. (2008) Genome-wide screen reveals APC-associated RNAs enriched in cell protrusions, *Nature.* **453**, 115-9.
156. Derby, M. C. & Gleeson, P. A. (2007) New insights into membrane trafficking and protein sorting, *Int Rev Cytol.* **261**, 47-116.
157. Martin, K. C. & Ephrussi, A. (2009) mRNA localization: gene expression in the spatial dimension, *Cell.* **136**, 719-30.
158. Holt, C. E. & Schuman, E. M. (2013) The central dogma decentralized: new perspectives on RNA function and local translation in neurons, *Neuron.* **80**, 648-57.
159. Lin, A. C. & Holt, C. E. (2007) Local translation and directional steering in axons, *EMBO J.* **26**, 3729-36.

160. Ouyang, Y., Rosenstein, A., Kreiman, G., Schuman, E. M. & Kennedy, M. B. (1999) Tetanic stimulation leads to increased accumulation of Ca(2+)/calmodulin-dependent protein kinase II via dendritic protein synthesis in hippocampal neurons, *J Neurosci.* **19**, 7823-33.
161. Willis, D. E., van Niekerk, E. A., Sasaki, Y., Mesngon, M., Merianda, T. T., Williams, G. G., Kendall, M., Smith, D. S., Bassell, G. J. & Twiss, J. L. (2007) Extracellular stimuli specifically regulate localized levels of individual neuronal mRNAs, *J Cell Biol.* **178**, 965-80.
162. Wu, L., Wells, D., Tay, J., Mendis, D., Abbott, M. A., Barnitt, A., Quinlan, E., Heynen, A., Fallon, J. R. & Richter, J. D. (1998) CPEB-mediated cytoplasmic polyadenylation and the regulation of experience-dependent translation of alpha-CaMKII mRNA at synapses, *Neuron.* **21**, 1129-39.
163. Yan, X., Hoek, T. A., Vale, R. D. & Tanenbaum, M. E. (2016) Dynamics of Translation of Single mRNA Molecules In Vivo, *Cell.* **165**, 976-89.
164. Jansen, R. P. (2001) mRNA localization: message on the move, *Nat Rev Mol Cell Biol.* **2**, 247-56.
165. Smith, R. (2004) Moving molecules: mRNA trafficking in Mammalian oligodendrocytes and neurons, *Neuroscientist.* **10**, 495-500.
166. Gavis, E. R. & Lehmann, R. (1992) Localization of nanos RNA controls embryonic polarity, *Cell.* **71**, 301-13.
167. Batada, N. N., Shepp, L. A. & Siegmund, D. O. (2004) Stochastic model of protein-protein interaction: why signaling proteins need to be colocalized, *Proc Natl Acad Sci U S A.* **101**, 6445-9.
168. Mingle, L. A., Okuhama, N. N., Shi, J., Singer, R. H., Condeelis, J. & Liu, G. (2005) Localization of all seven messenger RNAs for the actin-polymerization nucleator Arp2/3 complex in the protrusions of fibroblasts, *J Cell Sci.* **118**, 2425-33.
169. Kloc, M., Wilk, K., Vargas, D., Shirato, Y., Bilinski, S. & Etkin, L. D. (2005) Potential structural role of non-coding and coding RNAs in the organization of the cytoskeleton at the vegetal cortex of Xenopus oocytes, *Development.* **132**, 3445-57.
170. Prasanth, K. V., Prasanth, S. G., Xuan, Z., Hearn, S., Freier, S. M., Bennett, C. F., Zhang, M. Q. & Spector, D. L. (2005) Regulating gene expression through RNA nuclear retention, *Cell.* **123**, 249-63.
171. Iampietro, C., Bergalet, J., Wang, X., Cody, N. A., Chin, A., Lefebvre, F. A., Douziech, M., Krause, H. M. & Lecuyer, E. (2014) Developmentally regulated elimination of damaged nuclei involves a Chk2-dependent mechanism of mRNA nuclear retention, *Dev Cell.* **29**, 468-81.
172. Valluy, J., Bicker, S., Aksoy-Aksel, A., Lackinger, M., Sumer, S., Fiore, R., Wust, T., Seffer, D., Metge, F., Dieterich, C., Wohr, M., Schwarting, R. & Schratt, G. (2015) A coding-independent function of an alternative Ube3a transcript during neuronal development, *Nat Neurosci.* **18**, 666-73.
173. Cody, N. A., Iampietro, C. & Lecuyer, E. (2013) The many functions of mRNA localization during normal development and disease: from pillar to post, *Wiley Interdiscip Rev Dev Biol.* **2**, 781-96.
174. Lipshitz, H. D. & Smibert, C. A. (2000) Mechanisms of RNA localization and translational regulation, *Curr Opin Genet Dev.* **10**, 476-88.

175. Kloc, M., Zearfoss, N. R. & Etkin, L. D. (2002) Mechanisms of subcellular mRNA localization, *Cell.* **108**, 533-44.
176. Yisraeli, J. K., Sokol, S. & Melton, D. A. (1990) A two-step model for the localization of maternal mRNA in Xenopus oocytes: involvement of microtubules and microfilaments in the translocation and anchoring of Vg1 mRNA, *Development.* **108**, 289-98.
177. Sundell, C. L. & Singer, R. H. (1991) Requirement of microfilaments in sorting of actin messenger RNA, *Science.* **253**, 1275-7.
178. Wilkie, G. S. & Davis, I. (2001) Drosophila wingless and pair-rule transcripts localize apically by dynein-mediated transport of RNA particles, *Cell.* **105**, 209-19.
179. Shulman, J. M., Benton, R. & St Johnston, D. (2000) The Drosophila homolog of C. elegans PAR-1 organizes the oocyte cytoskeleton and directs oskar mRNA localization to the posterior pole, *Cell.* **101**, 377-88.
180. Jankovics, F., Sinka, R. & Erdelyi, M. (2001) An interaction type of genetic screen reveals a role of the Rab11 gene in oskar mRNA localization in the developing Drosophila melanogaster oocyte, *Genetics.* **158**, 1177-88.
181. Erdelyi, M., Michon, A. M., Guichet, A., Glotzer, J. B. & Ephrussi, A. (1995) Requirement for Drosophila cytoplasmic tropomyosin in oskar mRNA localization, *Nature.* **377**, 524-7.
182. Bally-Cuif, L., Schatz, W. J. & Ho, R. K. (1998) Characterization of the zebrafish Orb/CPEB-related RNA binding protein and localization of maternal components in the zebrafish oocyte, *Mech Dev.* **77**, 31-47.
183. Forrest, K. M. & Gavis, E. R. (2003) Live imaging of endogenous RNA reveals a diffusion and entrapment mechanism for nanos mRNA localization in Drosophila, *Curr Biol.* **13**, 1159-68.
184. Kloc, M., Larabell, C., Chan, A. P. & Etkin, L. D. (1998) Contribution of METRO pathway localized molecules to the organization of the germ cell lineage, *Mech Dev.* **75**, 81-93.
185. MacArthur, H., Bubunenko, M., Houston, D. W. & King, M. L. (1999) Xcat2 RNA is a translationally sequestered germ plasm component in Xenopus, *Mech Dev.* **84**, 75-88.
186. Ding, D., Parkhurst, S. M., Halsell, S. R. & Lipshitz, H. D. (1993) Dynamic Hsp83 RNA localization during Drosophila oogenesis and embryogenesis, *Mol Cell Biol.* **13**, 3773-81.
187. Bashirullah, A., Cooperstock, R. L. & Lipshitz, H. D. (2001) Spatial and temporal control of RNA stability, *Proc Natl Acad Sci U S A.* **98**, 7025-8.
188. Bashirullah, A., Halsell, S. R., Cooperstock, R. L., Kloc, M., Karaiskakis, A., Fisher, W. W., Fu, W., Hamilton, J. K., Etkin, L. D. & Lipshitz, H. D. (1999) Joint action of two RNA degradation pathways controls the timing of maternal transcript elimination at the midblastula transition in Drosophila melanogaster, *EMBO J.* **18**, 2610-20.
189. Zaessinger, S., Busseau, I. & Simonelig, M. (2006) Oskar allows nanos mRNA translation in Drosophila embryos by preventing its deadenylation by Smaug/CCR4, *Development.* **133**, 4573-83.
190. Jambhekar, A. & Derisi, J. L. (2007) Cis-acting determinants of asymmetric, cytoplasmic RNA transport, *RNA.* **13**, 625-42.
191. Kislauskis, E. H., Zhu, X. & Singer, R. H. (1994) Sequences responsible for intracellular localization of beta-actin messenger RNA also affect cell phenotype, *J Cell Biol.* **127**, 441-51.

192. Macdonald, P. M., Kerr, K., Smith, J. L. & Leask, A. (1993) RNA regulatory element BLE1 directs the early steps of bicoid mRNA localization, *Development.* **118**, 1233-43.
193. Ferrandon, D., Koch, I., Westhof, E. & Nusslein-Volhard, C. (1997) RNA-RNA interaction is required for the formation of specific bicoid mRNA 3' UTR-STAUFEN ribonucleoprotein particles, *EMBO J.* **16**, 1751-8.
194. Chartrand, P., Meng, X. H., Singer, R. H. & Long, R. M. (1999) Structural elements required for the localization of ASH1 mRNA and of a green fluorescent protein reporter particle in vivo, *Curr Biol.* **9**, 333-6.
195. Gonzalez, I., Buonomo, S. B., Nasmyth, K. & von Ahsen, U. (1999) ASH1 mRNA localization in yeast involves multiple secondary structural elements and Ash1 protein translation, *Curr Biol.* **9**, 337-40.
196. Mowry, K. L. & Melton, D. A. (1992) Vegetal messenger RNA localization directed by a 340-nt RNA sequence element in Xenopus oocytes, *Science.* **255**, 991-4.
197. Chan, A. P., Kloc, M. & Etkin, L. D. (1999) fatvg encodes a new localized RNA that uses a 25-nucleotide element (FVLE1) to localize to the vegetal cortex of Xenopus oocytes, *Development.* **126**, 4943-53.
198. Kim-Ha, J., Webster, P. J., Smith, J. L. & Macdonald, P. M. (1993) Multiple RNA regulatory elements mediate distinct steps in localization of oskar mRNA, *Development.* **119**, 169-78.
199. Gavis, E. R., Curtis, D. & Lehmann, R. (1996) Identification of cis-acting sequences that control nanos RNA localization, *Dev Biol.* **176**, 36-50.
200. Glisovic, T., Bachorik, J. L., Yong, J. & Dreyfuss, G. (2008) RNA-binding proteins and post-transcriptional gene regulation, *FEBS Lett.* **582**, 1977-86.
201. Sundararaman, B., Zhan, L., Blue, S. M., Stanton, R., Elkins, K., Olson, S., Wei, X., Van Nostrand, E. L., Pratt, G. A., Huelga, S. C., Smalec, B. M., Wang, X., Hong, E. L., Davidson, J. M., Lecuyer, E., Graveley, B. R. & Yeo, G. W. (2016) Resources for the Comprehensive Discovery of Functional RNA Elements, *Mol Cell.* **61**, 903-13.
202. Anantharaman, V., Koonin, E. V. & Aravind, L. (2002) Comparative genomics and evolution of proteins involved in RNA metabolism, *Nucleic Acids Res.* **30**, 1427-64.
203. Harvey, R. F., Smith, T. S., Mulroney, T., Queiroz, R. M. L., Pizzinga, M., Dezi, V., Villenueva, E., Ramakrishna, M., Lilley, K. S. & Willis, A. E. (2018) Trans-acting translational regulatory RNA binding proteins, *Wiley Interdiscip Rev RNA.* **9**, e1465.
204. Baltz, A. G., Munschauer, M., Schwanhausser, B., Vasile, A., Murakawa, Y., Schueler, M., Youngs, N., Penfold-Brown, D., Drew, K., Milek, M., Wyler, E., Bonneau, R., Selbach, M., Dieterich, C. & Landthaler, M. (2012) The mRNA-bound proteome and its global occupancy profile on protein-coding transcripts, *Mol Cell.* **46**, 674-90.
205. Castello, A., Fischer, B., Eichelbaum, K., Horos, R., Beckmann, B. M., Strein, C., Davey, N. E., Humphreys, D. T., Preiss, T., Steinmetz, L. M., Krijgsveld, J. & Hentze, M. W. (2012) Insights into RNA biology from an atlas of mammalian mRNA-binding proteins, *Cell.* **149**, 1393-406.
206. Mitchell, S. F., Jain, S., She, M. & Parker, R. (2013) Global analysis of yeast mRNPs, *Nat Struct Mol Biol.* **20**, 127-33.
207. Gerstberger, S., Hafner, M. & Tuschl, T. (2014) A census of human RNA-binding proteins, *Nat Rev Genet.* **15**, 829-45.

208. Sysoev, V. O., Fischer, B., Frese, C. K., Gupta, I., Krijgsveld, J., Hentze, M. W., Castello, A. & Ephrussi, A. (2016) Global changes of the RNA-bound proteome during the maternal-to-zygotic transition in Drosophila, *Nat Commun.* **7**, 12128.
209. Lunde, B. M., Moore, C. & Varani, G. (2007) RNA-binding proteins: modular design for efficient function, *Nat Rev Mol Cell Biol.* **8**, 479-90.
210. Auweter, S. D., Oberstrass, F. C. & Allain, F. H. (2006) Sequence-specific binding of single-stranded RNA: is there a code for recognition?, *Nucleic Acids Res.* **34**, 4943-59.
211. Ryter, J. M. & Schultz, S. C. (1998) Molecular basis of double-stranded RNA-protein interactions: structure of a dsRNA-binding domain complexed with dsRNA, *EMBO J.* **17**, 7505-13.
212. Gebauer, F., Schwarzl, T., Valcarcel, J. & Hentze, M. W. (2021) RNA-binding proteins in human genetic disease, *Nat Rev Genet.* **22**, 185-198.
213. Shukla, S. & Parker, R. (2016) Hypo- and Hyper-Assembly Diseases of RNA-Protein Complexes, *Trends Mol Med.* **22**, 615-628.
214. Tauber, D., Tauber, G. & Parker, R. (2020) Mechanisms and Regulation of RNA Condensation in RNP Granule Formation, *Trends Biochem Sci.* **45**, 764-778.
215. Protter, D. S. W. & Parker, R. (2016) Principles and Properties of Stress Granules, *Trends Cell Biol.* **26**, 668-679.
216. An, H., de Meritens, C. R. & Shelkovnikova, T. A. (2021) Connecting the "dots": RNP granule network in health and disease, *Biochim Biophys Acta Mol Cell Res.* **1868**, 119058.
217. Anderson, P. & Kedersha, N. (2006) RNA granules, *J Cell Biol.* **172**, 803-8.
218. Cioce, M., Boulon, S., Matera, A. G. & Lamond, A. I. (2006) UV-induced fragmentation of Cajal bodies, *J Cell Biol.* **175**, 401-13.
219. Ramaswami, M., Taylor, J. P. & Parker, R. (2013) Altered ribostasis: RNA-protein granules in degenerative disorders, *Cell.* **154**, 727-36.
220. Song, M. S. & Grabocka, E. (2020) Stress Granules in Cancer, *Rev Physiol Biochem Pharmacol*.
221. Markmiller, S., Soltanieh, S., Server, K. L., Mak, R., Jin, W., Fang, M. Y., Luo, E. C., Krach, F., Yang, D., Sen, A., Fulzele, A., Wozniak, J. M., Gonzalez, D. J., Kankel, M. W., Gao, F. B., Bennett, E. J., Lécuyer, E. & Yeo, G. W. (2018) Context-Dependent and Disease-Specific Diversity in Protein Interactions within Stress Granules, *Cell.* **172**, 590-604.e13.
222. Buchan, J. R. & Parker, R. (2009) Eukaryotic stress granules: the ins and outs of translation, *Mol Cell.* **36**, 932-41.
223. Hofmann, S., Kedersha, N., Anderson, P. & Ivanov, P. (2021) Molecular mechanisms of stress granule assembly and disassembly, *Biochim Biophys Acta Mol Cell Res.* **1868**, 118876.
224. Chen-Plotkin, A. S., Lee, V. M.-Y. & Trojanowski, J. Q. (2010) TAR DNA-binding protein 43 in neurodegenerative disease, *Nature Reviews Neurology.* **6**, 211-220.
225. Jakobsen, K. R., Sorensen, E., Brondum, K. K., Daugaard, T. F., Thomsen, R. & Nielsen, A. L. (2013) Direct RNA sequencing mediated identification of mRNA localized in protrusions of human MDA-MB-231 metastatic breast cancer cells, *J Mol Signal.* **8**, 9.
226. DeJesus-Hernandez, M., Mackenzie, I. R., Boeve, B. F., Boxer, A. L., Baker, M., Rutherford, N. J., Nicholson, A. M., Finch, N. A., Flynn, H., Adamson, J., Kouri, N., Wojtas, A., Sengdy, P., Hsiung, G. Y., Karydas, A., Seeley, W. W., Josephs, K. A., Coppola, G.,

Geschwind, D. H., Wszolek, Z. K., Feldman, H., Knopman, D. S., Petersen, R. C., Miller, B. L., Dickson, D. W., Boylan, K. B., Graff-Radford, N. R. & Rademakers, R. (2011) Expanded GGGGCC hexanucleotide repeat in noncoding region of C9ORF72 causes chromosome 9p-linked FTD and ALS, *Neuron.* **72**, 245-56.
227. Renton, A. E., Majounie, E., Waite, A., Simon-Sanchez, J., Rollinson, S., Gibbs, J. R., Schymick, J. C., Laaksovirta, H., van Swieten, J. C., Myllykangas, L., Kalimo, H., Paetau, A., Abramzon, Y., Remes, A. M., Kaganovich, A., Scholz, S. W., Duckworth, J., Ding, J., Harmer, D. W., Hernandez, D. G., Johnson, J. O., Mok, K., Ryten, M., Trabzuni, D., Guerreiro, R. J., Orrell, R. W., Neal, J., Murray, A., Pearson, J., Jansen, I. E., Sondervan, D., Seelaar, H., Blake, D., Young, K., Halliwell, N., Callister, J. B., Toulson, G., Richardson, A., Gerhard, A., Snowden, J., Mann, D., Neary, D., Nalls, M. A., Peuralinna, T., Jansson, L., Isoviita, V. M., Kaivorinne, A. L., Holtta-Vuori, M., Ikonen, E., Sulkava, R., Benatar, M., Wuu, J., Chio, A., Restagno, G., Borghero, G., Sabatelli, M., Consortium, I., Heckerman, D., Rogaeva, E., Zinman, L., Rothstein, J. D., Sendtner, M., Drepper, C., Eichler, E. E., Alkan, C., Abdullaev, Z., Pack, S. D., Dutra, A., Pak, E., Hardy, J., Singleton, A., Williams, N. M., Heutink, P., Pickering-Brown, S., Morris, H. R., Tienari, P. J. & Traynor, B. J. (2011) A hexanucleotide repeat expansion in C9ORF72 is the cause of chromosome 9p21-linked ALS-FTD, *Neuron.* **72**, 257-68.
228. Weil, T. T. (2014) mRNA localization in the Drosophila germline, *RNA Biol.* **11**, 1010-8.
229. Lasko, P. (2012) mRNA localization and translational control in Drosophila oogenesis, *Cold Spring Harb Perspect Biol.* **4**.
230. Tomancak, P., Berman, B. P., Beaton, A., Weiszmann, R., Kwan, E., Hartenstein, V., Celniker, S. E. & Rubin, G. M. (2007) Global analysis of patterns of gene expression during Drosophila embryogenesis, *Genome Biol.* **8**, R145.
231. Kenney, D. E. & Borisy, G. G. (2009) Thomas Hunt Morgan at the marine biological laboratory: naturalist and experimentalist, *Genetics.* **181**, 841-6.
232. Chintapalli, V. R., Wang, J. & Dow, J. A. (2007) Using FlyAtlas to identify better Drosophila melanogaster models of human disease, *Nat Genet.* **39**, 715-20.
233. Ugur, B., Chen, K. & Bellen, H. J. (2016) Drosophila tools and assays for the study of human diseases, *Dis Model Mech.* **9**, 235-44.
234. Eberl, D. F., Duyk, G. M. & Perrimon, N. (1997) A genetic screen for mutations that disrupt an auditory response in Drosophila melanogaster, *Proc Natl Acad Sci U S A.* **94**, 14837-42.
235. Guichard, A., Srinivasan, S., Zimm, G. & Bier, E. (2002) A screen for dominant mutations applied to components in the Drosophila EGF-R pathway, *Proc Natl Acad Sci U S A.* **99**, 3752-7.
236. Nusslein-Volhard, C. & Wieschaus, E. (1980) Mutations affecting segment number and polarity in Drosophila, *Nature.* **287**, 795-801.
237. Pagliarini, R. A. & Xu, T. (2003) A genetic screen in Drosophila for metastatic behavior, *Science.* **302**, 1227-31.
238. Port, F., Strein, C., Stricker, M., Rauscher, B., Heigwer, F., Zhou, J., Beyersdorffer, C., Frei, J., Hess, A., Kern, K., Lange, L., Langner, N., Malamud, R., Pavlovic, B., Radecke, K., Schmitt, L., Voos, L., Valentini, E. & Boutros, M. (2020) A large-scale resource for tissue-specific CRISPR mutagenesis in Drosophila, *Elife.* **9**.

239. Staller, M. V., Yan, D., Randklev, S., Bragdon, M. D., Wunderlich, Z. B., Tao, R., Perkins, L. A., Depace, A. H. & Perrimon, N. (2013) Depleting gene activities in early Drosophila embryos with the "maternal-Gal4-shRNA" system, *Genetics.* **193**, 51-61.
240. Rotelli, M. D., Bolling, A. M., Killion, A. W., Weinberg, A. J., Dixon, M. J. & Calvi, B. R. (2019) An RNAi Screen for Genes Required for Growth of Drosophila Wing Tissue, *G3 (Bethesda).* **9**, 3087-3100.
241. Mummery-Widmer, J. L., Yamazaki, M., Stoeger, T., Novatchkova, M., Bhalerao, S., Chen, D., Dietzl, G., Dickson, B. J. & Knoblich, J. A. (2009) Genome-wide analysis of Notch signalling in Drosophila by transgenic RNAi, *Nature.* **458**, 987-92.
242. Yamamoto-Hino, M. & Goto, S. (2013) In Vivo RNAi-Based Screens: Studies in Model Organisms, *Genes (Basel).* **4**, 646-65.
243. Cronin, S. J., Nehme, N. T., Limmer, S., Liegeois, S., Pospisilik, J. A., Schramek, D., Leibbrandt, A., Simoes Rde, M., Gruber, S., Puc, U., Ebersberger, I., Zoranovic, T., Neely, G. G., von Haeseler, A., Ferrandon, D. & Penninger, J. M. (2009) Genome-wide RNAi screen identifies genes involved in intestinal pathogenic bacterial infection, *Science.* **325**, 340-3.
244. Neely, G. G., Kuba, K., Cammarato, A., Isobe, K., Amann, S., Zhang, L., Murata, M., Elmen, L., Gupta, V., Arora, S., Sarangi, R., Dan, D., Fujisawa, S., Usami, T., Xia, C. P., Keene, A. C., Alayari, N. N., Yamakawa, H., Elling, U., Berger, C., Novatchkova, M., Koglgruber, R., Fukuda, K., Nishina, H., Isobe, M., Pospisilik, J. A., Imai, Y., Pfeufer, A., Hicks, A. A., Pramstaller, P. P., Subramaniam, S., Kimura, A., Ocorr, K., Bodmer, R. & Penninger, J. M. (2010) A global in vivo Drosophila RNAi screen identifies NOT3 as a conserved regulator of heart function, *Cell.* **141**, 142-53.
245. Neely, G. G., Hess, A., Costigan, M., Keene, A. C., Goulas, S., Langeslag, M., Griffin, R. S., Belfer, I., Dai, F., Smith, S. B., Diatchenko, L., Gupta, V., Xia, C. P., Amann, S., Kreitz, S., Heindl-Erdmann, C., Wolz, S., Ly, C. V., Arora, S., Sarangi, R., Dan, D., Novatchkova, M., Rosenzweig, M., Gibson, D. G., Truong, D., Schramek, D., Zoranovic, T., Cronin, S. J., Angjeli, B., Brune, K., Dietzl, G., Maixner, W., Meixner, A., Thomas, W., Pospisilik, J. A., Alenius, M., Kress, M., Subramaniam, S., Garrity, P. A., Bellen, H. J., Woolf, C. J. & Penninger, J. M. (2010) A genome-wide Drosophila screen for heat nociception identifies alpha2delta3 as an evolutionarily conserved pain gene, *Cell.* **143**, 628-38.
246. Zoranovic, T., Manent, J., Willoughby, L., Matos de Simoes, R., La Marca, J. E., Golenkina, S., Cuiping, X., Gruber, S., Angjeli, B., Kanitz, E. E., Cronin, S. J. F., Neely, G. G., Wernitznig, A., Humbert, P. O., Simpson, K. J., Mitsiades, C. S., Richardson, H. E. & Penninger, J. M. (2018) A genome-wide Drosophila epithelial tumorigenesis screen identifies Tetraspanin 29Fb as an evolutionarily conserved suppressor of Ras-driven cancer, *PLoS Genet.* **14**, e1007688.
247. David, J. R. & Capy, P. (1988) Genetic variation of Drosophila melanogaster natural populations, *Trends Genet.* **4**, 106-11.
248. Markow, T. A. & O'Grady, P. M. (2007) Drosophila biology in the genomic age, *Genetics.* **177**, 1269-76.
249. Hales, K. G., Korey, C. A., Larracuente, A. M. & Roberts, D. M. (2015) Genetics on the Fly: A Primer on the Drosophila Model System, *Genetics.* **201**, 815-42.
250. Brand, A. H. & Perrimon, N. (1993) Targeted gene expression as a means of altering cell fates and generating dominant phenotypes, *Development.* **118**, 401-15.

251. Petersen, N. S. (1990) Effects of heat and chemical stress on development, *Adv Genet.* **28**, 275-96.
252. Petersen, N. S. & Mitchell, H. K. (1987) The induction of a multiple wing hair phenocopy by heat shock in mutant heterozygotes, *Dev Biol.* **121**, 335-41.
253. Parkhurst, S. M., Bopp, D. & Ish-Horowicz, D. (1990) X:A ratio, the primary sex-determining signal in Drosophila, is transduced by helix-loop-helix proteins, *Cell.* **63**, 1179-91.
254. Parkhurst, S. M. & Ish-Horowicz, D. (1991) Mis-regulating segmentation gene expression in Drosophila, *Development.* **111**, 1121-35.
255. Zuker, C. S., Mismer, D., Hardy, R. & Rubin, G. M. (1988) Ectopic expression of a minor Drosophila opsin in the major photoreceptor cell class: distinguishing the role of primary receptor and cellular context, *Cell.* **53**, 475-82.
256. Fischer, J. A., Giniger, E., Maniatis, T. & Ptashne, M. (1988) GAL4 activates transcription in Drosophila, *Nature.* **332**, 853-6.
257. Giniger, E., Varnum, S. M. & Ptashne, M. (1985) Specific DNA binding of GAL4, a positive regulatory protein of yeast, *Cell.* **40**, 767-74.
258. Ptashne, M. (1988) How eukaryotic transcriptional activators work, *Nature.* **335**, 683-9.
259. Napoli, C., Lemieux, C. & Jorgensen, R. (1990) Introduction of a Chimeric Chalcone Synthase Gene into Petunia Results in Reversible Co-Suppression of Homologous Genes in trans, *Plant Cell.* **2**, 279-289.
260. Fire, A., Xu, S., Montgomery, M. K., Kostas, S. A., Driver, S. E. & Mello, C. C. (1998) Potent and specific genetic interference by double-stranded RNA in Caenorhabditis elegans, *Nature.* **391**, 806-11.
261. Heigwer, F., Port, F. & Boutros, M. (2018) RNA Interference (RNAi) Screening in Drosophila, *Genetics.* **208**, 853-874.
262. Iwasaki, S., Kobayashi, M., Yoda, M., Sakaguchi, Y., Katsuma, S., Suzuki, T. & Tomari, Y. (2010) Hsc70/Hsp90 chaperone machinery mediates ATP-dependent RISC loading of small RNA duplexes, *Mol Cell.* **39**, 292-9.
263. Leuschner, P. J., Ameres, S. L., Kueng, S. & Martinez, J. (2006) Cleavage of the siRNA passenger strand during RISC assembly in human cells, *EMBO Rep.* **7**, 314-20.
264. Bastock, R. & St Johnston, D. (2008) Drosophila oogenesis, *Curr Biol.* **18**, R1082-7.
265. Dai, W., Peterson, A., Kenney, T., Burrous, H. & Montell, D. J. (2017) Quantitative microscopy of the Drosophila ovary shows multiple niche signals specify progenitor cell fate, *Nat Commun.* **8**, 1244.
266. Fadiga, J. & Nystul, T. G. (2019) The follicle epithelium in the Drosophila ovary is maintained by a small number of stem cells, *Elife.* **8**.
267. Horne-Badovinac, S. (2014) The Drosophila egg chamber-a new spin on how tissues elongate, *Integr Comp Biol.* **54**, 667-76.
268. Koch, E. A. & King, R. C. (1966) The origin and early differentiation of the egg chamber of Drosophila melanogaster, *J Morphol.* **119**, 283-303.
269. Antel, M. & Inaba, M. (2020) Modulation of Cell-Cell Interactions in Drosophila Oocyte Development, *Cells.* **9**.
270. de Cuevas, M. Drosophila Oogenesis in *eLS* pp. 1-7.

271. Ali-Murthy, Z., Fetter, R. D., Wang, W., Yang, B., Royer, L. A. & Kornberg, T. B. (2021) Elimination of nurse cell nuclei that shuttle into oocytes during oogenesis, *J Cell Biol.* **220**.
272. Buszczak, M. & Cooley, L. (2000) Eggs to die for: cell death during Drosophila oogenesis, *Cell Death Differ.* **7**, 1071-4.
273. Riechmann, V. & Ephrussi, A. (2001) Axis formation during Drosophila oogenesis, *Curr Opin Genet Dev.* **11**, 374-83.
274. Riparbelli, M. G., Persico, V. & Callaini, G. (2021) Early Drosophila Oogenesis: A Tale of Centriolar Asymmetry, *Cells.* **10**.
275. de Cuevas, M. & Spradling, A. C. (1998) Morphogenesis of the Drosophila fusome and its implications for oocyte specification, *Development.* **125**, 2781-9.
276. Huynh, J. R. & St Johnston, D. (2000) The role of BicD, Egl, Orb and the microtubules in the restriction of meiosis to the Drosophila oocyte, *Development.* **127**, 2785-94.
277. McGrail, M. & Hays, T. S. (1997) The microtubule motor cytoplasmic dynein is required for spindle orientation during germline cell divisions and oocyte differentiation in Drosophila, *Development.* **124**, 2409-19.
278. Liu, Z., Xie, T. & Steward, R. (1999) Lis1, the Drosophila homolog of a human lissencephaly disease gene, is required for germline cell division and oocyte differentiation, *Development.* **126**, 4477-88.
279. Swan, A., Nguyen, T. & Suter, B. (1999) Drosophila Lissencephaly-1 functions with Bic-D and dynein in oocyte determination and nuclear positioning, *Nat Cell Biol.* **1**, 444-9.
280. Bolivar, J., Huynh, J. R., Lopez-Schier, H., Gonzalez, C., St Johnston, D. & Gonzalez-Reyes, A. (2001) Centrosome migration into the Drosophila oocyte is independent of BicD and egl, and of the organisation of the microtubule cytoskeleton, *Development.* **128**, 1889-97.
281. Grieder, N. C., de Cuevas, M. & Spradling, A. C. (2000) The fusome organizes the microtubule network during oocyte differentiation in Drosophila, *Development.* **127**, 4253-64.
282. Mahowald, A. P. & Strassheim, J. M. (1970) Intercellular migration of centrioles in the germarium of Drosophila melanogaster. An electron microscopic study, *J Cell Biol.* **45**, 306-20.
283. Fabian, L. & Brill, J. A. (2012) Drosophila spermiogenesis: Big things come from little packages, *Spermatogenesis.* **2**, 197-212.
284. Demarco, R. S., Eikenes, A. H., Haglund, K. & Jones, D. L. (2014) Investigating spermatogenesis in Drosophila melanogaster, *Methods.* **68**, 218-27.
285. Foe, V. E. & Alberts, B. M. (1983) Studies of nuclear and cytoplasmic behaviour during the five mitotic cycles that precede gastrulation in Drosophila embryogenesis, *J Cell Sci.* **61**, 31-70.
286. Vergassola, M., Deneke, V. E. & Di Talia, S. (2018) Mitotic waves in the early embryogenesis of Drosophila: Bistability traded for speed, *Proc Natl Acad Sci U S A.* **115**, E2165-E2174.
287. Hamm, D. C. & Harrison, M. M. (2018) Regulatory principles governing the maternal-to-zygotic transition: insights from Drosophila melanogaster, *Open Biol.* **8**, 180183.

288. Ferree, P. L., Deneke, V. E. & Di Talia, S. (2016) Measuring time during early embryonic development, *Semin Cell Dev Biol.* **55**, 80-8.
289. Mahowald, A. P. & Hardy, P. A. (1985) Genetics of Drosophila embryogenesis, *Annu Rev Genet.* **19**, 149-77.
290. Tadros, W. & Lipshitz, H. D. (2009) The maternal-to-zygotic transition: a play in two acts, *Development.* **136**, 3033-42.
291. O'Farrell, P. H. (2015) Growing an Embryo from a Single Cell: A Hurdle in Animal Life, *Cold Spring Harb Perspect Biol.* **7**.
292. Schier, A. F. (2007) The maternal-zygotic transition: death and birth of RNAs, *Science.* **316**, 406-7.
293. Langley, A. R., Smith, J. C., Stemple, D. L. & Harvey, S. A. (2014) New insights into the maternal to zygotic transition, *Development.* **141**, 3834-41.
294. Tadros, W., Houston, S. A., Bashirullah, A., Cooperstock, R. L., Semotok, J. L., Reed, B. H. & Lipshitz, H. D. (2003) Regulation of maternal transcript destabilization during egg activation in Drosophila, *Genetics.* **164**, 989-1001.
295. De Renzis, S., Elemento, O., Tavazoie, S. & Wieschaus, E. F. (2007) Unmasking activation of the zygotic genome using chromosomal deletions in the Drosophila embryo, *PLoS Biol.* **5**, e117.
296. King, R. W., Jackson, P. K. & Kirschner, M. W. (1994) Mitosis in transition, *Cell.* **79**, 563-71.
297. Rustad, R. C. (1959) An interference microscopical and cytochemical analysis of local mass changes in the mitotic apparatus during mitosis, *Exp Cell Res.* **16**, 575-83.
298. Van Nostrand, E. L., Freese, P., Pratt, G. A., Wang, X., Wei, X., Xiao, R., Blue, S. M., Chen, J. Y., Cody, N. A. L., Dominguez, D., Olson, S., Sundararaman, B., Zhan, L., Bazile, C., Bouvrette, L. P. B., Bergalet, J., Duff, M. O., Garcia, K. E., Gelboin-Burkhart, C., Hochman, M., Lambert, N. J., Li, H., McGurk, M. P., Nguyen, T. B., Palden, T., Rabano, I., Sathe, S., Stanton, R., Su, A., Wang, R., Yee, B. A., Zhou, B., Louie, A. L., Aigner, S., Fu, X. D., Lecuyer, E., Burge, C. B., Graveley, B. R. & Yeo, G. W. (2020) A large-scale binding and functional map of human RNA-binding proteins, *Nature.* **583**, 711-719.
299. Muller, H., Schmidt, D., Steinbrink, S., Mirgorodskaya, E., Lehmann, V., Habermann, K., Dreher, F., Gustavsson, N., Kessler, T., Lehrach, H., Herwig, R., Gobom, J., Ploubidou, A., Boutros, M. & Lange, B. M. (2010) Proteomic and functional analysis of the mitotic Drosophila centrosome, *EMBO J.* **29**, 3344-57.
300. Alliegro, M. C., Alliegro, M. A. & Palazzo, R. E. (2006) Centrosome-associated RNA in surf clam oocytes, *Proc Natl Acad Sci U S A.* **103**, 9034-8.
301. Sauer, G., Korner, R., Hanisch, A., Ries, A., Nigg, E. A. & Sillje, H. H. (2005) Proteome analysis of the human mitotic spindle, *Mol Cell Proteomics.* **4**, 35-43.
302. Pelechano, V. & Steinmetz, L. M. (2013) Gene regulation by antisense transcription, *Nat Rev Genet.* **14**, 880-93.
303. Makalowska, I., Lin, C. F. & Makalowski, W. (2005) Overlapping genes in vertebrate genomes, *Comput Biol Chem.* **29**, 1-12.
304. He, Y., Vogelstein, B., Velculescu, V. E., Papadopoulos, N. & Kinzler, K. W. (2008) The antisense transcriptomes of human cells, *Science.* **322**, 1855-7.

305. Hillier, L. W., Coulson, A., Murray, J. I., Bao, Z., Sulston, J. E. & Waterston, R. H. (2005) Genomics in C. elegans: so many genes, such a little worm, *Genome Res.* **15**, 1651-60.
306. Jen, C. H., Michalopoulos, I., Westhead, D. R. & Meyer, P. (2005) Natural antisense transcripts with coding capacity in Arabidopsis may have a regulatory role that is not linked to double-stranded RNA degradation, *Genome Biol.* **6**, R51.
307. Katayama, S., Tomaru, Y., Kasukawa, T., Waki, K., Nakanishi, M., Nakamura, M., Nishida, H., Yap, C. C., Suzuki, M., Kawai, J., Suzuki, H., Carninci, P., Hayashizaki, Y., Wells, C., Frith, M., Ravasi, T., Pang, K. C., Hallinan, J., Mattick, J., Hume, D. A., Lipovich, L., Batalov, S., Engstrom, P. G., Mizuno, Y., Faghihi, M. A., Sandelin, A., Chalk, A. M., Mottagui-Tabar, S., Liang, Z., Lenhard, B., Wahlestedt, C., Group, R. G. E. R., Genome Science, G. & Consortium, F. (2005) Antisense transcription in the mammalian transcriptome, *Science.* **309**, 1564-6.
308. Kim, D. S., Cho, C. Y., Huh, J. W., Kim, H. S. & Cho, H. G. (2009) EVOG: a database for evolutionary analysis of overlapping genes, *Nucleic Acids Res.* **37**, D698-702.
309. Zhang, Y., Liu, X. S., Liu, Q. R. & Wei, L. (2006) Genome-wide in silico identification and analysis of cis natural antisense transcripts (cis-NATs) in ten species, *Nucleic Acids Res.* **34**, 3465-75.
310. Balbin, O. A., Malik, R., Dhanasekaran, S. M., Prensner, J. R., Cao, X., Wu, Y. M., Robinson, D., Wang, R., Chen, G., Beer, D. G., Nesvizhskii, A. I. & Chinnaiyan, A. M. (2015) The landscape of antisense gene expression in human cancers, *Genome Res.* **25**, 1068-79.
311. Ozsolak, F., Kapranov, P., Foissac, S., Kim, S. W., Fishilevich, E., Monaghan, A. P., John, B. & Milos, P. M. (2010) Comprehensive polyadenylation site maps in yeast and human reveal pervasive alternative polyadenylation, *Cell.* **143**, 1018-29.
312. Chen, J., Sun, M., Hurst, L. D., Carmichael, G. G. & Rowley, J. D. (2005) Genome-wide analysis of coordinate expression and evolution of human cis-encoded sense-antisense transcripts, *Trends Genet.* **21**, 326-9.
313. Faghihi, M. A. & Wahlestedt, C. (2009) Regulatory roles of natural antisense transcripts, *Nat Rev Mol Cell Biol.* **10**, 637-43.
314. Rougeulle, C. & Heard, E. (2002) Antisense RNA in imprinting: spreading silence through Air, *Trends Genet.* **18**, 434-7.
315. Camblong, J., Iglesias, N., Fickentscher, C., Dieppois, G. & Stutz, F. (2007) Antisense RNA stabilization induces transcriptional gene silencing via histone deacetylation in S. cerevisiae, *Cell.* **131**, 706-17.
316. Camblong, J., Beyrouthy, N., Guffanti, E., Schlaepfer, G., Steinmetz, L. M. & Stutz, F. (2009) Trans-acting antisense RNAs mediate transcriptional gene cosuppression in S. cerevisiae, *Genes Dev.* **23**, 1534-45.
317. Castelnuovo, M., Rahman, S., Guffanti, E., Infantino, V., Stutz, F. & Zenklusen, D. (2013) Bimodal expression of PHO84 is modulated by early termination of antisense transcription, *Nat Struct Mol Biol.* **20**, 851-8.
318. Hongay, C. F., Grisafi, P. L., Galitski, T. & Fink, G. R. (2006) Antisense transcription controls cell fate in Saccharomyces cerevisiae, *Cell.* **127**, 735-45.
319. Prescott, E. M. & Proudfoot, N. J. (2002) Transcriptional collision between convergent genes in budding yeast, *Proc Natl Acad Sci U S A.* **99**, 8796-801.

320. Wang, L., Jiang, N., Wang, L., Fang, O., Leach, L. J., Hu, X. & Luo, Z. (2014) 3' Untranslated regions mediate transcriptional interference between convergent genes both locally and ectopically in Saccharomyces cerevisiae, *PLoS Genet.* **10**, e1004021.
321. Gu, R., Zhang, Z., DeCerbo, J. N. & Carmichael, G. G. (2009) Gene regulation by sense-antisense overlap of polyadenylation signals, *RNA.* **15**, 1154-63.
322. Kimelman, D. & Kirschner, M. W. (1989) An antisense mRNA directs the covalent modification of the transcript encoding fibroblast growth factor in Xenopus oocytes, *Cell.* **59**, 687-96.
323. Peters, N. T., Rohrbach, J. A., Zalewski, B. A., Byrkett, C. M. & Vaughn, J. C. (2003) RNA editing and regulation of Drosophila 4f-rnp expression by sas-10 antisense readthrough mRNA transcripts, *RNA.* **9**, 698-710.
324. Faghihi, M. A., Modarresi, F., Khalil, A. M., Wood, D. E., Sahagan, B. G., Morgan, T. E., Finch, C. E., St Laurent, G., 3rd, Kenny, P. J. & Wahlestedt, C. (2008) Expression of a noncoding RNA is elevated in Alzheimer's disease and drives rapid feed-forward regulation of beta-secretase, *Nat Med.* **14**, 723-30.
325. Faghihi, M. A., Zhang, M., Huang, J., Modarresi, F., Van der Brug, M. P., Nalls, M. A., Cookson, M. R., St-Laurent, G., 3rd & Wahlestedt, C. (2010) Evidence for natural antisense transcript-mediated inhibition of microRNA function, *Genome Biol.* **11**, R56.
326. Sinturel, F., Navickas, A., Wery, M., Descrimes, M., Morillon, A., Torchet, C. & Benard, L. (2015) Cytoplasmic Control of Sense-Antisense mRNA Pairs, *Cell Rep.* **12**, 1853-64.
327. Carrieri, C., Cimatti, L., Biagioli, M., Beugnet, A., Zucchelli, S., Fedele, S., Pesce, E., Ferrer, I., Collavin, L., Santoro, C., Forrest, A. R., Carninci, P., Biffo, S., Stupka, E. & Gustincich, S. (2012) Long non-coding antisense RNA controls Uchl1 translation through an embedded SINEB2 repeat, *Nature.* **491**, 454-7.
328. Kawano, M., Aravind, L. & Storz, G. (2007) An antisense RNA controls synthesis of an SOS-induced toxin evolved from an antitoxin, *Mol Microbiol.* **64**, 738-54.
329. Bergalet, J. & Lecuyer, E. (2014) The functions and regulatory principles of mRNA intracellular trafficking, *Adv Exp Med Biol.* **825**, 57-96.
330. Chin, A. & Lecuyer, E. (2017) RNA localization: Making its way to the center stage, *Biochim Biophys Acta Gen Subj.* **1861**, 2956-2970.
331. Benoit Bouvrette, L. P., Cody, N. A. L., Bergalet, J., Lefebvre, F. A., Diot, C., Wang, X., Blanchette, M. & Lecuyer, E. (2018) CeFra-seq reveals broad asymmetric mRNA and noncoding RNA distribution profiles in Drosophila and human cells, *RNA.* **24**, 98-113.
332. Fazal, F. M., Han, S., Parker, K. R., Kaewsapsak, P., Xu, J., Boettiger, A. N., Chang, H. Y. & Ting, A. Y. (2019) Atlas of Subcellular RNA Localization Revealed by APEX-Seq, *Cell.* **178**, 473-490 e26.
333. Wilk, R., Hu, J., Blotsky, D. & Krause, H. M. (2016) Diverse and pervasive subcellular distributions for both coding and long noncoding RNAs, *Genes Dev.* **30**, 594-609.
334. Van Doren, M., Williamson, A. L. & Lehmann, R. (1998) Regulation of zygotic gene expression in Drosophila primordial germ cells, *Curr Biol.* **8**, 243-6.
335. Trcek, T., Lionnet, T., Shroff, H. & Lehmann, R. (2017) mRNA quantification using single-molecule FISH in Drosophila embryos, *Nat Protoc.* **12**, 1326-1348.

336. Zimmerman, S. G., Peters, N. C., Altaras, A. E. & Berg, C. A. (2013) Optimized RNA ISH, RNA FISH and protein-RNA double labeling (IF/FISH) in Drosophila ovaries, *Nat Protoc.* **8**, 2158-79.
337. tom Dieck, S., Kochen, L., Hanus, C., Heumuller, M., Bartnik, I., Nassim-Assir, B., Merk, K., Mosler, T., Garg, S., Bunse, S., Tirrell, D. A. & Schuman, E. M. (2015) Direct visualization of newly synthesized target proteins in situ, *Nat Methods.* **12**, 411-4.
338. Kao, L. R. & Megraw, T. L. (2009) Centrocortin cooperates with centrosomin to organize Drosophila embryonic cleavage furrows, *Curr Biol.* **19**, 937-42.
339. Lefebvre, F. A., Cody, N. A. L., Bouvrette, L. P. B., Bergalet, J., Wang, X. & Lecuyer, E. (2017) CeFra-seq: Systematic mapping of RNA subcellular distribution properties through cell fractionation coupled to deep-sequencing, *Methods.* **126**, 138-148.
340. Sutton, I. (2002) Paraneoplastic neurological syndromes, *Curr Opin Neurol.* **15**, 685-90.
341. Oshima, K., Takeda, M., Kuranaga, E., Ueda, R., Aigaki, T., Miura, M. & Hayashi, S. (2006) IKK epsilon regulates F actin assembly and interacts with Drosophila IAP1 in cellular morphogenesis, *Curr Biol.* **16**, 1531-7.
342. Otani, T., Oshima, K., Onishi, S., Takeda, M., Shinmyozu, K., Yonemura, S. & Hayashi, S. (2011) IKKepsilon regulates cell elongation through recycling endosome shuttling, *Dev Cell.* **20**, 219-32.
343. Cox, R. T. & Spradling, A. C. (2009) Clueless, a conserved Drosophila gene required for mitochondrial subcellular localization, interacts genetically with parkin, *Dis Model Mech.* **2**, 490-9.
344. Kong, J., Han, H., Bergalet, J., Bouvrette, L. P. B., Hernandez, G., Moon, N. S., Vali, H., Lecuyer, E. & Lasko, P. (2019) A ribosomal protein S5 isoform is essential for oogenesis and interacts with distinct RNAs in Drosophila melanogaster, *Sci Rep.* **9**, 13779.
345. Shapiro, R. S. & Anderson, K. V. (2006) Drosophila Ik2, a member of the I kappa B kinase family, is required for mRNA localization during oogenesis, *Development.* **133**, 1467-75.
346. Bischof, J., Maeda, R. K., Hediger, M., Karch, F. & Basler, K. (2007) An optimized transgenesis system for Drosophila using germ-line-specific phiC31 integrases, *Proc Natl Acad Sci U S A.* **104**, 3312-7.
347. Zappulo, A., van den Bruck, D., Ciolli Mattioli, C., Franke, V., Imami, K., McShane, E., Moreno-Estelles, M., Calviello, L., Filipchyk, A., Peguero-Sanchez, E., Muller, T., Woehler, A., Birchmeier, C., Merino, E., Rajewsky, N., Ohler, U., Mazzoni, E. O., Selbach, M., Akalin, A. & Chekulaeva, M. (2017) RNA localization is a key determinant of neurite-enriched proteome, *Nat Commun.* **8**, 583.
348. Fresno, M., Jimenez, A. & Vazquez, D. (1977) Inhibition of translation in eukaryotic systems by harringtonine, *Eur J Biochem.* **72**, 323-30.
349. Celton, J. M., Gaillard, S., Bruneau, M., Pelletier, S., Aubourg, S., Martin-Magniette, M. L., Navarro, L., Laurens, F. & Renou, J. P. (2014) Widespread anti-sense transcription in apple is correlated with siRNA production and indicates a large potential for transcriptional and/or post-transcriptional control, *New Phytol.* **203**, 287-99.
350. Lu, T., Zhu, C., Lu, G., Guo, Y., Zhou, Y., Zhang, Z., Zhao, Y., Li, W., Lu, Y., Tang, W., Feng, Q. & Han, B. (2012) Strand-specific RNA-seq reveals widespread occurrence of novel cis-natural antisense transcripts in rice, *BMC Genomics.* **13**, 721.

351. Rosikiewicz, W. & Makalowska, I. (2016) Biological functions of natural antisense transcripts, *Acta Biochim Pol.* **63**, 665-673.
352. Hobson, D. J., Wei, W., Steinmetz, L. M. & Svejstrup, J. Q. (2012) RNA polymerase II collision interrupts convergent transcription, *Mol Cell.* **48**, 365-74.
353. Aw, J. G., Shen, Y., Wilm, A., Sun, M., Lim, X. N., Boon, K. L., Tapsin, S., Chan, Y. S., Tan, C. P., Sim, A. Y., Zhang, T., Susanto, T. T., Fu, Z., Nagarajan, N. & Wan, Y. (2016) In Vivo Mapping of Eukaryotic RNA Interactomes Reveals Principles of Higher-Order Organization and Regulation, *Mol Cell.* **62**, 603-17.
354. Lu, Z., Zhang, Q. C., Lee, B., Flynn, R. A., Smith, M. A., Robinson, J. T., Davidovich, C., Gooding, A. R., Goodrich, K. J., Mattick, J. S., Mesirov, J. P., Cech, T. R. & Chang, H. Y. (2016) RNA Duplex Map in Living Cells Reveals Higher-Order Transcriptome Structure, *Cell.* **165**, 1267-1279.
355. Nguyen, T. C., Cao, X., Yu, P., Xiao, S., Lu, J., Biase, F. H., Sridhar, B., Huang, N., Zhang, K. & Zhong, S. (2016) Mapping RNA-RNA interactome and RNA structure in vivo by MARIO, *Nat Commun.* **7**, 12023.
356. Sharma, E., Sterne-Weiler, T., O'Hanlon, D. & Blencowe, B. J. (2016) Global Mapping of Human RNA-RNA Interactions, *Mol Cell.* **62**, 618-26.
357. Batish, M., van den Bogaard, P., Kramer, F. R. & Tyagi, S. (2012) Neuronal mRNAs travel singly into dendrites, *Proc Natl Acad Sci U S A.* **109**, 4645-50.
358. Little, S. C., Sinsimer, K. S., Lee, J. J., Wieschaus, E. F. & Gavis, E. R. (2015) Independent and coordinate trafficking of single Drosophila germ plasm mRNAs, *Nat Cell Biol.* **17**, 558-68.
359. Antar, L. N., Dictenberg, J. B., Plociniak, M., Afroz, R. & Bassell, G. J. (2005) Localization of FMRP-associated mRNA granules and requirement of microtubules for activity-dependent trafficking in hippocampal neurons, *Genes Brain Behav.* **4**, 350-9.
360. Jambor, H., Brunel, C. & Ephrussi, A. (2011) Dimerization of oskar 3' UTRs promotes hitchhiking for RNA localization in the Drosophila oocyte, *RNA.* **17**, 2049-57.
361. Alliegro, M. C. (2008) The implications of centrosomal RNA, *RNA Biol.* **5**, 198-200.
362. Alliegro, M. C. & Alliegro, M. A. (2008) Centrosomal RNA correlates with intron-poor nuclear genes in Spisula oocytes, *Proc Natl Acad Sci U S A.* **105**, 6993-7.
363. Kingsley, E. P., Chan, X. Y., Duan, Y. & Lambert, J. D. (2007) Widespread RNA segregation in a spiralian embryo, *Evol Dev.* **9**, 527-39.
364. Kowanda, M., Bergalet, J., Wieczorek, M., Brouhard, G., Lecuyer, E. & Lasko, P. (2016) Loss of function of the Drosophila Ninein-related centrosomal protein Bsg25D causes mitotic defects and impairs embryonic development, *Biol Open.* **5**, 1040-51.
365. Lambert, J. D. & Nagy, L. M. (2002) Asymmetric inheritance of centrosomally localized mRNAs during embryonic cleavages, *Nature.* **420**, 682-6.
366. Lerit, D. A. & Gavis, E. R. (2011) Transport of germ plasm on astral microtubules directs germ cell development in Drosophila, *Curr Biol.* **21**, 439-48.
367. Salmon, E. D. & Segall, R. R. (1980) Calcium-labile mitotic spindles isolated from sea urchin eggs (Lytechinus variegatus), *J Cell Biol.* **86**, 355-65.
368. Gupta, G. D., Coyaud, E., Goncalves, J., Mojarad, B. A., Liu, Y., Wu, Q., Gheiratmand, L., Comartin, D., Tkach, J. M., Cheung, S. W., Bashkurov, M., Hasegan, M., Knight, J. D., Lin, Z. Y., Schueler, M., Hildebrandt, F., Moffat, J., Gingras, A. C., Raught, B. & Pelletier, L. (2015) A Dynamic Protein Interaction Landscape of the Human Centrosome-Cilium Interface, *Cell.* **163**, 1484-99.

369. Lee, H. H., Jan, L. Y. & Jan, Y. N. (2009) Drosophila IKK-related kinase Ik2 and Katanin p60-like 1 regulate dendrite pruning of sensory neuron during metamorphosis, *Proc Natl Acad Sci U S A.* **106**, 6363-8.
370. Lin, T., Pan, P. Y., Lai, Y. T., Chiang, K. W., Hsieh, H. L., Wu, Y. P., Ke, J. M., Lee, M. C., Liao, S. S., Shih, H. T., Tang, C. Y., Yang, S. B., Cheng, H. C., Wu, J. T., Jan, Y. N. & Lee, H. H. (2015) Spindle-F Is the Central Mediator of Ik2 Kinase-Dependent Dendrite Pruning in Drosophila Sensory Neurons, *PLoS Genet.* **11**, e1005642.
371. Julio, A. R. & Backus, K. M. (2021) New approaches to target RNA binding proteins, *Curr Opin Chem Biol.* **62**, 13-23.
372. Kelaini, S., Chan, C., Cornelius, V. A. & Margariti, A. (2021) RNA-Binding Proteins Hold Key Roles in Function, Dysfunction, and Disease, *Biology (Basel).* **10**.
373. Hentze, M. W., Castello, A., Schwarzl, T. & Preiss, T. (2018) A brave new world of RNA-binding proteins, *Nat Rev Mol Cell Biol.* **19**, 327-341.
374. Driever, W. & Nusslein-Volhard, C. (1988) The bicoid protein determines position in the Drosophila embryo in a concentration-dependent manner, *Cell.* **54**, 95-104.
375. Broadus, J., Fuerstenberg, S. & Doe, C. Q. (1998) Staufen-dependent localization of prospero mRNA contributes to neuroblast daughter-cell fate, *Nature.* **391**, 792-5.
376. Gore, A. V., Maegawa, S., Cheong, A., Gilligan, P. C., Weinberg, E. S. & Sampath, K. (2005) The zebrafish dorsal axis is apparent at the four-cell stage, *Nature.* **438**, 1030-5.
377. Hughes, J. R., Bullock, S. L. & Ish-Horowicz, D. (2004) Inscuteable mRNA localization is dynein-dependent and regulates apicobasal polarity and spindle length in Drosophila neuroblasts, *Curr Biol.* **14**, 1950-6.
378. Li, P., Yang, X., Wasser, M., Cai, Y. & Chia, W. (1997) Inscuteable and Staufen mediate asymmetric localization and segregation of prospero RNA during Drosophila neuroblast cell divisions, *Cell.* **90**, 437-47.
379. Zhang, J., Houston, D. W., King, M. L., Payne, C., Wylie, C. & Heasman, J. (1998) The role of maternal VegT in establishing the primary germ layers in Xenopus embryos, *Cell.* **94**, 515-24.
380. Burrows, C., Abd Latip, N., Lam, S. J., Carpenter, L., Sawicka, K., Tzolovsky, G., Gabra, H., Bushell, M., Glover, D. M., Willis, A. E. & Blagden, S. P. (2010) The RNA binding protein Larp1 regulates cell division, apoptosis and cell migration, *Nucleic Acids Res.* **38**, 5542-53.
381. Tsanov, N., Samacoits, A., Chouaib, R., Traboulsi, A. M., Gostan, T., Weber, C., Zimmer, C., Zibara, K., Walter, T., Peter, M., Bertrand, E. & Mueller, F. (2016) smiFISH and FISH-quant - a flexible single RNA detection approach with super-resolution capability, *Nucleic Acids Res.* **44**, e165.
382. Stade, K., Ford, C. S., Guthrie, C. & Weis, K. (1997) Exportin 1 (Crm1p) is an essential nuclear export factor, *Cell.* **90**, 1041-50.
383. Azizian, N. G. & Li, Y. (2020) XPO1-dependent nuclear export as a target for cancer therapy, *J Hematol Oncol.* **13**, 61.
384. Xia, L., Wang, M., Li, H., Tang, X., Chen, F. & Cui, J. (2018) The effect of aberrant expression and genetic polymorphisms of Rad21 on cervical cancer biology, *Cancer Med.* **7**, 3393-405.

385. Hu, Y., Flockhart, I., Vinayagam, A., Bergwitz, C., Berger, B., Perrimon, N. & Mohr, S. E. (2011) An integrative approach to ortholog prediction for disease-focused and other functional studies, *BMC Bioinformatics.* **12**, 357.
386. Bergalet, J., Patel, D., Legendre, F., Lapointe, C., Benoit Bouvrette, L. P., Chin, A., Blanchette, M., Kwon, E. & Lecuyer, E. (2020) Inter-dependent Centrosomal Co-localization of the cen and ik2 cis-Natural Antisense mRNAs in Drosophila, *Cell Rep.* **30**, 3339-3352 e6.
387. Zhong, X., Liu, L., Zhao, A., Pfeifer, G. P. & Xu, X. (2005) The abnormal spindle-like, microcephaly-associated (ASPM) gene encodes a centrosomal protein, *Cell Cycle.* **4**, 1227-9.
388. Higgins, J., Midgley, C., Bergh, A. M., Bell, S. M., Askham, J. M., Roberts, E., Binns, R. K., Sharif, S. M., Bennett, C., Glover, D. M., Woods, C. G., Morrison, E. E. & Bond, J. (2010) Human ASPM participates in spindle organisation, spindle orientation and cytokinesis, *BMC Cell Biol.* **11**, 85.
389. do Carmo Avides, M. & Glover, D. M. (1999) Abnormal spindle protein, Asp, and the integrity of mitotic centrosomal microtubule organizing centers, *Science.* **283**, 1733-5.
390. Saunders, R. D., Avides, M. C., Howard, T., Gonzalez, C. & Glover, D. M. (1997) The Drosophila gene abnormal spindle encodes a novel microtubule-associated protein that associates with the polar regions of the mitotic spindle, *J Cell Biol.* **137**, 881-90.
391. Wakefield, J. G., Bonaccorsi, S. & Gatti, M. (2001) The drosophila protein asp is involved in microtubule organization during spindle formation and cytokinesis, *J Cell Biol.* **153**, 637-48.
392. Gagliardi, M. & Matarazzo, M. R. (2016) RIP: RNA Immunoprecipitation, *Methods Mol Biol.* **1480**, 73-86.
393. Martindale, J. L., Gorospe, M. & Idda, M. L. (2020) Ribonucleoprotein Immunoprecipitation (RIP) Analysis, *Bio Protoc.* **10**, e3488.
394. Chouaib, R., Safieddine, A., Pichon, X., Imbert, A., Kwon, O. S., Samacoits, A., Traboulsi, A. M., Robert, M. C., Tsanov, N., Coleno, E., Poser, I., Zimmer, C., Hyman, A., Le Hir, H., Zibara, K., Peter, M., Mueller, F., Walter, T. & Bertrand, E. (2020) A Dual Protein-mRNA Localization Screen Reveals Compartmentalized Translation and Widespread Co-translational RNA Targeting, *Dev Cell.* **54**, 773-791 e5.
395. Kops, G. J., Foltz, D. R. & Cleveland, D. W. (2004) Lethality to human cancer cells through massive chromosome loss by inhibition of the mitotic checkpoint, *Proc Natl Acad Sci U S A.* **101**, 8699-704.
396. Vong, Y. H., Sivashanmugam, L., Leech, R., Zaucker, A., Jones, A. & Sampath, K. (2021) The RNA-binding protein Igf2bp3 is critical for embryonic and germline development in zebrafish, *PLoS Genet.* **17**, e1009667.
397. Mak, W., Fang, C., Holden, T., Dratver, M. B. & Lin, H. (2016) An Important Role of Pumilio 1 in Regulating the Development of the Mammalian Female Germline, *Biol Reprod.* **94**, 134.
398. St Johnston, D., Beuchle, D. & Nusslein-Volhard, C. (1991) Staufen, a gene required to localize maternal RNAs in the Drosophila egg, *Cell.* **66**, 51-63.
399. Ferrandon, D., Elphick, L., Nusslein-Volhard, C. & St Johnston, D. (1994) Staufen protein associates with the 3'UTR of bicoid mRNA to form particles that move in a microtubule-dependent manner, *Cell.* **79**, 1221-32.

400. Ryder, P. V., Fang, J. & Lerit, D. A. (2020) centrocortin RNA localization to centrosomes is regulated by FMRP and facilitates error-free mitosis, *J Cell Biol.* **219**.
401. Affaitati, A., Cardone, L., de Cristofaro, T., Carlucci, A., Ginsberg, M. D., Varrone, S., Gottesman, M. E., Avvedimento, E. V. & Feliciello, A. (2003) Essential role of A-kinase anchor protein 121 for cAMP signaling to mitochondria, *J Biol Chem.* **278**, 4286-94.
402. Paukku, K., Yang, J. & Silvennoinen, O. (2003) Tudor and nuclease-like domains containing protein p100 function as coactivators for signal transducer and activator of transcription 5, *Mol Endocrinol.* **17**, 1805-14.
403. Jacob, A. L., Lund, J., Martinez, P. & Hedin, L. (2001) Acetylation of steroidogenic factor 1 protein regulates its transcriptional activity and recruits the coactivator GCN5, *J Biol Chem.* **276**, 37659-64.
404. Martinez-Contreras, R., Fisette, J. F., Nasim, F. U., Madden, R., Cordeau, M. & Chabot, B. (2006) Intronic binding sites for hnRNP A/B and hnRNP F/H proteins stimulate pre-mRNA splicing, *PLoS Biol.* **4**, e21.
405. Thapar, R. (2015) Roles of Prolyl Isomerases in RNA-Mediated Gene Expression, *Biomolecules.* **5**, 974-99.
406. Kaplan, Y. & Kupiec, M. (2007) A role for the yeast cell cycle/splicing factor Cdc40 in the G1/S transition, *Curr Genet.* **51**, 123-40.
407. Blackwell, D. L., Fraser, S. D., Caluseriu, O., Vivori, C., Tyndall, A. V., Lamont, R. E., Parboosingh, J. S., Innes, A. M., Bernier, F. P. & Childs, S. J. (2022) Hnrnpul1 controls transcription, splicing, and modulates skeletal and limb development in vivo, *G3 (Bethesda).* **12**.
408. Ribbeck, K., Raemaekers, T., Carmeliet, G. & Mattaj, I. W. (2007) A role for NuSAP in linking microtubules to mitotic chromosomes, *Curr Biol.* **17**, 230-6.
409. Laine, P., Rowell, W. J., Paulin, L., Kujawa, S., Raterman, D., Mayhew, G., Wendt, J., Burgess, D. L., Partonen, T., Paunio, T., Auvinen, P. & Ekholm, J. M. (2021) Alu element in the RNA binding motif protein, X-linked 2 (RBMX2) gene found to be linked to bipolar disorder, *PLoS One.* **16**, e0261170.
410. Chan, C. W., Lee, Y. B., Uney, J., Flynn, A., Tobias, J. H. & Norman, M. (2007) A novel member of the SAF (scaffold attachment factor)-box protein family inhibits gene expression and induces apoptosis, *Biochem J.* **407**, 355-62.
411. Hirose, T., Ideue, T., Nagai, M., Hagiwara, M., Shu, M. D. & Steitz, J. A. (2006) A spliceosomal intron binding protein, IBP160, links position-dependent assembly of intron-encoded box C/D snoRNP to pre-mRNA splicing, *Mol Cell.* **23**, 673-84.
412. Sugimoto, N., Maehara, K., Yoshida, K., Yasukouchi, S., Osano, S., Watanabe, S., Aizawa, M., Yugawa, T., Kiyono, T., Kurumizaka, H., Ohkawa, Y. & Fujita, M. (2015) Cdt1-binding protein GRWD1 is a novel histone-binding protein that facilitates MCM loading through its influence on chromatin architecture, *Nucleic Acids Res.* **43**, 5898-911.
413. Hastings, M. L., Allemand, E., Duelli, D. M., Myers, M. P. & Krainer, A. R. (2007) Control of pre-mRNA splicing by the general splicing factors PUF60 and U2AF(65), *PLoS One.* **2**, e538.
414. Han, T., Goralski, M., Gaskill, N., Capota, E., Kim, J., Ting, T. C., Xie, Y., Williams, N. S. & Nijhawan, D. (2017) Anticancer sulfonamides target splicing by inducing RBM39 degradation via recruitment to DCAF15, *Science.* **356**.
415. Thomas, F. & Kutay, U. (2003) Biogenesis and nuclear export of ribosomal subunits in higher eukaryotes depend on the CRM1 export pathway, *J Cell Sci.* **116**, 2409-19.

416. Austin, K. M., Gupta, M. L., Jr., Coats, S. A., Tulpule, A., Mostoslavsky, G., Balazs, A. B., Mulligan, R. C., Daley, G., Pellman, D. & Shimamura, A. (2008) Mitotic spindle destabilization and genomic instability in Shwachman-Diamond syndrome, *J Clin Invest.* **118**, 1511-8.
417. Finch, A. J., Hilcenko, C., Basse, N., Drynan, L. F., Goyenechea, B., Menne, T. F., Gonzalez Fernandez, A., Simpson, P., D'Santos, C. S., Arends, M. J., Donadieu, J., Bellanne-Chantelot, C., Costanzo, M., Boone, C., McKenzie, A. N., Freund, S. M. & Warren, A. J. (2011) Uncoupling of GTP hydrolysis from eIF6 release on the ribosome causes Shwachman-Diamond syndrome, *Genes Dev.* **25**, 917-29.
418. Anger, A. M., Armache, J. P., Berninghausen, O., Habeck, M., Subklewe, M., Wilson, D. N. & Beckmann, R. (2013) Structures of the human and Drosophila 80S ribosome, *Nature.* **497**, 80-5.
419. Prieto, J. L. & McStay, B. (2007) Recruitment of factors linking transcription and processing of pre-rRNA to NOR chromatin is UBF-dependent and occurs independent of transcription in human cells, *Genes Dev.* **21**, 2041-54.
420. Zhan, X., Yan, C., Zhang, X., Lei, J. & Shi, Y. (2018) Structures of the human pre-catalytic spliceosome and its precursor spliceosome, *Cell Res.* **28**, 1129-1140.
421. Martin, F., Schaller, A., Eglite, S., Schumperli, D. & Muller, B. (1997) The gene for histone RNA hairpin binding protein is located on human chromosome 4 and encodes a novel type of RNA binding protein, *EMBO J.* **16**, 769-78.
422. Screaton, G. R., Caceres, J. F., Mayeda, A., Bell, M. V., Plebanski, M., Jackson, D. G., Bell, J. I. & Krainer, A. R. (1995) Identification and characterization of three members of the human SR family of pre-mRNA splicing factors, *EMBO J.* **14**, 4336-49.
423. Nguyen, T. A., Jo, M. H., Choi, Y. G., Park, J., Kwon, S. C., Hohng, S., Kim, V. N. & Woo, J. S. (2015) Functional Anatomy of the Human Microprocessor, *Cell.* **161**, 1374-87.
424. Wickens, M., Bernstein, D. S., Kimble, J. & Parker, R. (2002) A PUF family portrait: 3'UTR regulation as a way of life, *Trends Genet.* **18**, 150-7.
425. Ge, H., Si, Y. & Roeder, R. G. (1998) Isolation of cDNAs encoding novel transcription coactivators p52 and p75 reveals an alternate regulatory mechanism of transcriptional activation, *EMBO J.* **17**, 6723-9.
426. Hassine, S., Bonnet-Magnaval, F., Benoit Bouvrette, L. P., Doran, B., Ghram, M., Bouthillette, M., Lecuyer, E. & DesGroseillers, L. (2020) Staufen1 localizes to the mitotic spindle and controls the localization of RNA populations to the spindle, *J Cell Sci.* **133**.
427. Waldron, A. & Yajima, M. (2020) Localized translation on the mitotic apparatus: A history and perspective, *Dev Biol.* **468**, 55-58.
428. Kwon, O. S., Mishra, R., Safieddine, A., Coleno, E., Alasseur, Q., Faucourt, M., Barbosa, I., Bertrand, E., Spassky, N. & Le Hir, H. (2021) Exon junction complex dependent mRNA localization is linked to centrosome organization during ciliogenesis, *Nat Commun.* **12**, 1351.
429. Titus, M. B., Chang, A. W. & Olesnicky, E. C. (2021) Exploring the Diverse Functional and Regulatory Consequences of Alternative Splicing in Development and Disease, *Front Genet.* **12**, 775395.
430. Zeng, C. & Hamada, M. (2020) RNA-Seq Analysis Reveals Localization-Associated Alternative Splicing across 13 Cell Lines, *Genes (Basel).* **11**.

431. Baj, G., Leone, E., Chao, M. V. & Tongiorgi, E. (2011) Spatial segregation of BDNF transcripts enables BDNF to differentially shape distinct dendritic compartments, *Proc Natl Acad Sci U S A.* **108**, 16813-8.
432. An, J. J., Gharami, K., Liao, G. Y., Woo, N. H., Lau, A. G., Vanevski, F., Torre, E. R., Jones, K. R., Feng, Y., Lu, B. & Xu, B. (2008) Distinct role of long 3' UTR BDNF mRNA in spine morphology and synaptic plasticity in hippocampal neurons, *Cell.* **134**, 175-87.
433. Hachet, O. & Ephrussi, A. (2004) Splicing of oskar RNA in the nucleus is coupled to its cytoplasmic localization, *Nature.* **428**, 959-63.
434. Graveley, B. R. (2016) RNA Matchmaking: Finding Cellular Pairing Partners, *Mol Cell.* **63**, 186-189.
435. Fernandes, N. & Buchan, J. R. (2021) RNAs as Regulators of Cellular Matchmaking, *Front Mol Biosci.* **8**, 634146.
436. Wessels, H. H., Imami, K., Baltz, A. G., Kolinski, M., Beldovskaya, A., Selbach, M., Small, S., Ohler, U. & Landthaler, M. (2016) The mRNA-bound proteome of the early fly embryo, *Genome Res.* **26**, 1000-9.
437. Qin, X., Ahn, S., Speed, T. P. & Rubin, G. M. (2007) Global analyses of mRNA translational control during early Drosophila embryogenesis, *Genome Biol.* **8**, R63.
438. Groen, A. C., Cameron, L. A., Coughlin, M., Miyamoto, D. T., Mitchison, T. J. & Ohi, R. (2004) XRHAMM functions in ran-dependent microtubule nucleation and pole formation during anastral spindle assembly, *Curr Biol.* **14**, 1801-11.
439. Gruss, O. J., Wittmann, M., Yokoyama, H., Pepperkok, R., Kufer, T., Sillje, H., Karsenti, E., Mattaj, I. W. & Vernos, I. (2002) Chromosome-induced microtubule assembly mediated by TPX2 is required for spindle formation in HeLa cells, *Nat Cell Biol.* **4**, 871-9.
440. Chen, Q., Zhang, X., Jiang, Q., Clarke, P. R. & Zhang, C. (2008) Cyclin B1 is localized to unattached kinetochores and contributes to efficient microtubule attachment and proper chromosome alignment during mitosis, *Cell Res.* **18**, 268-80.
441. Samejima, K., Platani, M., Wolny, M., Ogawa, H., Vargiu, G., Knight, P. J., Peckham, M. & Earnshaw, W. C. (2015) The Inner Centromere Protein (INCENP) Coil Is a Single alpha-Helix (SAH) Domain That Binds Directly to Microtubules and Is Important for Chromosome Passenger Complex (CPC) Localization and Function in Mitosis, *J Biol Chem.* **290**, 21460-72.
442. Dauber, A., Golzio, C., Guenot, C., Jodelka, F. M., Kibaek, M., Kjaergaard, S., Leheup, B., Martinet, D., Nowaczyk, M. J., Rosenfeld, J. A., Zeesman, S., Zunich, J., Beckmann, J. S., Hirschhorn, J. N., Hastings, M. L., Jacquemont, S. & Katsanis, N. (2013) SCRIB and PUF60 are primary drivers of the multisystemic phenotypes of the 8q24.3 copy-number variant, *Am J Hum Genet.* **93**, 798-811.
443. Sun, D., Lei, W., Hou, X., Li, H. & Ni, W. (2019) PUF60 accelerates the progression of breast cancer through downregulation of PTEN expression, *Cancer Manag Res.* **11**, 821-830.
444. Long, Q., An, X., Chen, M., Wang, N., Sui, S., Li, Y., Zhang, C., Lee, K., Wang, X., Tian, T., Pan, Y., Qiu, H., Xie, F., Deng, W., Zheng, F. & He, L. (2020) PUF60/AURKA Axis Contributes to Tumor Progression and Malignant Phenotypes in Bladder Cancer, *Front Oncol.* **10**, 568015.
445. Chan, K. S., Koh, C. G. & Li, H. Y. (2012) Mitosis-targeted anti-cancer therapies: where they stand, *Cell Death Dis.* **3**, e411.

446. Dermit, M., Dodel, M., Lee, F. C. Y., Azman, M. S., Schwenzer, H., Jones, J. L., Blagden, S. P., Ule, J. & Mardakheh, F. K. (2020) Subcellular mRNA Localization Regulates Ribosome Biogenesis in Migrating Cells, *Dev Cell.* **55**, 298-313 e10.
447. Landry, J. J., Pyl, P. T., Rausch, T., Zichner, T., Tekkedil, M. M., Stutz, A. M., Jauch, A., Aiyar, R. S., Pau, G., Delhomme, N., Gagneur, J., Korbel, J. O., Huber, W. & Steinmetz, L. M. (2013) The genomic and transcriptomic landscape of a HeLa cell line, *G3 (Bethesda).* **3**, 1213-24.
448. Qu, Y., Han, B., Yu, Y., Yao, W., Bose, S., Karlan, B. Y., Giuliano, A. E. & Cui, X. (2015) Evaluation of MCF10A as a Reliable Model for Normal Human Mammary Epithelial Cells, *PLoS One.* **10**, e0131285.
449. Zhang, Y., O'Connor, J. P., Siomi, M. C., Srinivasan, S., Dutra, A., Nussbaum, R. L. & Dreyfuss, G. (1995) The fragile X mental retardation syndrome protein interacts with novel homologs FXR1 and FXR2, *EMBO J.* **14**, 5358-66.

THE END.